Universitat Politècnica de Catalunya
BarcelonaTech

Departament d'Enginyeria Hidràulica, Marítima i Ambiental
Laboratori d'Enginyeria Marítima

Programa de Doctorat en Ciències del Mar

Coastal Vulnerability to Storms at Different Time Scales. Application to the Catalan Coast

PhD Thesis presented by

Eva BOSOM

for the degree of DOCTOR

Supervisor:

Dr. José A. JIMÉNEZ

Barcelona, May 2014

Cover photo by Eva Bosom

And you have your choices
And these are what make man great.
His ladder to the stars

Mumford & Sons "Timshel"

Als meus pares,
Albert i Eva

To my parents,
Albert and Eva

Acknowledgements
Agraïments

La realització d'aquesta tesi ha estat possible gràcies al finançament de dues beques predoctorals: (i) la beca de Formació de personal Investigador (FI) de la Generalitat de Catalunya, des de gener fins a juliol de 2009, i (ii) la beca de Formación de Profesorado Universitario (FPU) del Ministerio de Educación, Cultura y Deporte, des d'agost de 2009 fins a gener de 2013. A més, cal remarcar que part del treball desenvolupat durant el transcurs de la tesi està vinculat a tres projectes d'investigació: (i) El projecte VuCoMa "Vulnerabilidad Costera a Múltiples Agentes. Aplicación al litoral Catalán" (CTM2008-05597/MAR), (ii) el projecte PaiRisC-M "El Paisaje del Riesgo Costero en el Litoral Catalán" (CTM2011-29808) i (iii) el projecte RISC-KIT EU "Resilience-Increasing Strategies for Coasts - toolKIT" (Grant No 603458). Els dos primers són d'àmbit nacional, finançats pel Ministerio de Ciencia e Innovación del Gobierno de España, mentre que el segon és d'àmbit europeu. El finançament addicional proporcionat per aquest tres projectes m'ha permés participar en diversos seminaris i congressos internacionals. Pel que fa als dos darrers projectes, també han finançat la darrera etapa de redacció de la tesi.

D'altra banda, durant el transcurs de la tesi he tingut l'oportunitat de realitzar dues estades de recerca internacionals finançades també pel Ministerio de Educación, Cultura y Deporte, dins del programa FPU. La primera va tenir lloc de setembre a desembre de 2010 al US Geological Survey St. Petersburg Science Center, a Florida (Estats Units), mentre que la segona es va dur a terme de gener a abril de 2012 a la School of Civil Engineering and the Environment, de la University of Southampton (Regne Unit).

Pel que fa a aspectes més pràctics, aquesta tesi no hagués estat possible sense les dades que diferents persones i organismes m'han facilitat. En aquest sentit, vull agrair a Puertos del Estado, del Ministerio de Obras Públicas del Gobierno de España, la

cessió de les dades d'onatge referents tant al projecte HIPOCAS com a una de les boies de la zona d'estudi. Gràcies també a la XIOM, la Xarxa d'Instruments Oceanogràfics i Meteorològics de la Generalitat de Catalunya, per facilitar-me les dades d'onatge de la resta de boies de la costa catalana. Gràcies a l'Instituto de Hidráulica Ambietal "IH Cantabria", per proporcionar-me les dades de retroanàlisi (hindcast) d'onatge (GOW) i de nivell del mar (GOS) per a diferents punts del litoral català. Finalment, gràcies també a la Dra. Herminia I. Valdemoro per facilitar-me les dades d'evolució costanera a mitjà termini referents a la zona d'estudi.

Al llarg dels darrers anys, moltes han estat les persones que, d'una manera o una altra, han influït en aquesta tesi. És per això que vull aprofitar aquesta ocasió per agrair la seva contribució tant a nivell intel·lectual com afectiu.

En primer lugar, quiero dar las gracias al Dr. José Antonio Jiménez, mi director de tesis, por haberme dado la oportunidad de realizar este doctorado y por todo lo que he aprendido a su lado. Gracias por tu implicación, tus consejos y tu entusiasmo. Durante estos años has respondido pacientemente a todas mis preguntas y me has enseñado mucho más de lo que seguramente te imaginas. Gracias por tener siempre la puerta abierta.

Al tot el personal del Laboratori d'Enginyeria Marítima, on he estat treballant durant el transcurs de la tesi, per la vostra amabilitat i per fer-me sentir com a casa durant tots aquests anys. Ha estat un plaer gaudir de la vostra companyia al llarg d'aquest viatge. Gràcies també al personal administratiu, per fer dels tràmits burocràtics una càrrega menys feixuga.

Als que han estat o són els meus companys de despatx, amb qui he compartit molt més que un bon ambient de treball. Mercè Casas, Marta Alomar, Tiago Castro, Manel Grifoll, Tona Mendoza, Dago Alvarado, Jordi Cateura, Joan Puigdefàbregues, Jaime López, Federico Jeréz, Raimon Tolosana, Jacqueline Albino, Checco Sole, Eduard Ariza, Claudia Guilovança, Marcela Cunha, Cari Ballesteros, Mónica Valeria, Rosigleyse Sousa, Alina Pascual, Marc Mestres, Marc Sanuy... gràcies per fer d'aquests anys un camí ple de somriures, dinars al solet, sopars, concerts, debats i, darrerament, bufandes. Gràcies també per escoltar les meves cabòries i aconsellar-me en els moments més difícils. Sincerament, no m'imagino una millor companyia. En especial gràcies a la Mercè, que va començar aquesta aventura al mateix temps que jo i amb qui he compartit incomptables hores de música, gastronomia, viatges i una molt bona amistat.

No em puc oblidar d'altres membres de la UPC que, tot i no formar part del meu

entorn laboral més pròxim, han estat sempre presents: Niels Van den Berg, Corrado Altomare, Andrea Marzzedu, Elena Pallarès, Pablo Cerralbo, Arnel German... gràcies pels cafès, els dinars a la Barceloneta, i totes les estones que hem compartit dins i fora de la UPC.

The international research stays gave me the opportunity to work with two leading teams in terms of coastal vulnerability to extreme storms and to relative sea-level rise. The experiences that I went through during my stays in St. Petersburg and Southampton have allowed me to grow not only intellectually but also personally. I am extremely grateful for having had the opportunity to meet such talented scientists and to share my work with them.

Regarding to my stay in Florida, I want to thank late Dr. Asbury H. Sallenger and Dr. Hillary F. Stockdon for their attention, kindness and implication. I would also like to thank the rest of colleagues at the USGS: Kristin Sopkin, Kara Doran, Ann Marie Ascough, Karen L.M. Morgan, Nathaniel Plant, David Thompson, Peter Howd, Joe Long, Mark Hansen, Kristy Guy, Marilyn Montgomery, Janice Subiño... for making me feel like home with your warm welcome. I have learned a lot from you. On top, you become part of one of the most special and exciting experiences of my life, which includes, among many others, my first "Trick-or-treating" and an amazing kayak trip surrounded by gators. Special thanks to Kristin, who kindly took good care of me from the second I met her and became a good friend. Lastly, I also want to thank Kimberly Freed for the good times that I spent with her.

When I arrived to Southampton, I was not less fortunate. In this sense, I would like to thank Dr Robert J. Nicholls for his kindness, enthusiasm and guidance. To my other colleagues: Sally Brown, Susan Hanson, Olwen Rowlands, Sid Narayan, Natasha Carpenter, Abiy Kebede, Andy Stevens, Matthew Wadey and many others, thank you for your friendly welcome and attention. I really enjoyed your lovely working atmosphere and our coffee break conversations. It was a pleasure to share those three months with you. Special thanks to Sally for her comments and advices. Dr. Robert J. Nicholls also gave me the opportunity to assist to many seminars that were held at the University of Southampton and the NOC, in which I got to meet and share points of view with other scientists that worked on similar subjects. I would also thank Dave Harlow and Clive Moon for giving me a tour of the key areas of Bournemouth and Hayling Island respectively, introducing me to the main challenges of the coastal management in these areas. For all this I am sincerely grateful.

I would also like to thank Emily Shrosbree, my lovely flatmate in Southampton, for being so helpful and thoughtful. Gràcies també a la colla de Catalans-Valencians-

Balears a Southampton, per rebre'ns amb els braços oberts i per les nits de pintes i Barça.

Fora de l'àmbit acadèmic, moltes són les persones a qui he d'agrair el suport i els bons moments compartits en els darrers anys. A la colla d'ambientals: Jessi, Àlex, Xavi, Dani, Ceci, Irene i respectius, gràcies pel vostre optimisme i per estar sempre aquí, malgrat la distància que en alguns moments ens ha separat. Gràcies també a la Bene i la Cris, pels moments irrepetibles que hem viscut juntes. La vostra energia positiva ha il·luminat fins i tot els dies més ennuvolats. A la Marga i a la Inés, les meves artistes preferides, gràcies per encomanar-me una mica de la vostra dolçor i la vostra creativitat. A la Lucia, la Marta, la Laura, la Mireia, la Sandra el Joanet i respectius, per fer-me sentir com una més de la colla des del primer dia que us vaig conèixer. A la Marta Cayetano, amb qui he compartit estones molt agradables fora i dins de l'aigua.

També a la Gemma, en Pere, l'Unai, l'Anna, l'Aniol i en Blai, per fer-me sentir una més de la família i per les bones estones que hem passat junts durant aquest temps.

Arribats a aquest punt, m'agradaria donar les gràcies a la família a la qual em sento afortunada de pertànyer. Als meus germans i cunyades Jordi, Bea, David i Simone, pels llargs dinars de diumenge i per ensenyar-me que la vida és molt més simple del que de vegades ens sembla. Jordi i David, la vostra tenacitat i el vostre enginy són inspiradors. Als meus nebots Pol i Laia, gràcies per arrancar-me els millors somriures en els pitjors moments. Molt especialment, vull agrair als meus pares, Albert i Eva, la seva paciència infinita i el seu amor incondicional. Algú em va dir una vegada que si Mendel ens hagués conegut no li haurien calgut els pèsols. Aquest ha estat, de lluny, el millor compliment que m'ha fet mai ningú. Res de tot això hagués estat possible sense el vostre suport. Aquesta és també la vostra tesi.

Per últim, però no menys important, gràcies a en Marc, el millor company de viatge. Junts hem viscut per duplicat totes les aventures que suposa fer una tesi, n'hem celebrat les petites victòries i hem après de les derrotes. Gràcies per fer-me riure cada dia i per donar suport a les meves decisions, per molt caòtiques que resultin. Allà on la vida ens porti, serà un plaer seguir viatjant amb tu, Dr. Abrisqueta.

Abstract

Storm-induced impacts are known to cause important economic and environmental damages to coastal systems worldwide. As a consequence, the relevance of including hazards and vulnerability assessments in coastal policies has been highlighted during the last years, so that coastal managers can make informed decision to apply mitigation and/or adaptation plans.

The main purpose of this thesis is to develop a methodology to quantitatively assess coastal vulnerability to storms at different time scales, considering the two main storm-induced hazards separately (inundation and erosion). In this work, vulnerability is defined as the potential of a coastal system to be harmed by the impact of a storm. Thus, it has been quantified by comparing the magnitude of the hazards with the adaptation ability of the coast. To do so, a combination of storm and beach geomorphology data has been used to assess hazards' intensity, whereas beach morphology has been used to determine its resilience.

The proposed methodology is based on a probabilistic approach where hazard time series are fitted to an extreme value distribution. Consequently, hazard magnitudes and vulnerability are related to a probability of occurrence instead of to a determined storm event, which allows a robust comparison of the results along different spatial scales at the same level of occurrence. The coastal manager has to decide the probability of occurrence to be accepted in the analysis, which will determine the return period (Tr) to be considered. Vulnerability indicators that compare the magnitude of each hazard to the response capability of the beach are built for erosion and inundation independently. Final vulnerability is formulated in terms of these two intermediate variables by means of a linear function that ranges from a minimum value of 0 (optimum state) to a maximum of 1 (failure state), defining 5 qualitative categories. The safety level of the analysis depends, not only on the probability of occurrence, but also on the selected value of the intermediate variables at the end of the range. In this particular case, these thresholds have been defined for each

hazard in terms of the protection function provided by the beach. To optimise the application of the method at regional scale, a definition of different coastal sectors with homogeneous storm climate together with a beach classification has been carried out. As a consequence, hazards' intensity has been calculated for a combination of 6 sectors and 8 beach types instead of for each beach. In spite of this, vulnerability is assessed considering the local resilience by using local values of beach parameters.

In order to evaluate changes in vulnerability at different time scales, variations in the adaptation ability of the coast due to the effects of other medium and long-term processes have also been considered. Taking into account the characteristics of the study area, erosion due to longshore sediment transport (LST) gradients and erosion and inundation caused by relative sea-level rise (RSLR) have been selected as the main medium and long-term coastal processes, respectively, to be analysed. In this sense, shoreline evolution rates have been used as representative of accretion/erosion due to LST, whereas different combinations of sea-level and subsidence scenarios have been used to determine erosion and inundation due to RSLR.

The developed methodology has been applied to most of the sedimentary coastline (219 km) of the Catalonia (NW Mediterranean). Results obtained considering the integrated contribution of LST and the medium RSLR scenario (3.8 mm/yr + subsidence) indicate that, for a Tr=50-yr, 28% of the coastline results highly or very highly vulnerable to erosion under current conditions, increasing up to 46%, 63% and 75% for the 10-yr, 25-yr and 50-yr projections respectively. In the case of inundation, such increment is smaller, ranging from 31% at the baseline to 34%, 48% and 67% for the same projections. Changes in vulnerability due to the contribution of RSLR are generally lower than those obtained when only LST is accounted. As expected, RSLR contribution is detected at longer time scales and results significantly higher in the southern part of the Catalan coast. The presence of dissipative beaches with very mild slopes, together with the potentially significant subsidence of the Ebre delta, contribute to increase RSLR-induced erosion in this area. On the opposite, LST contribution does not seem to target any specific beach type. Vulnerability has also been interpreted at different spatial and administrative scales.

To conclude, the method presented in this thesis permits to identify the most vulnerable spots of a coastal area considering the dynamic response of the system along different time scales. This information is relevant for coastal managers when it comes to efficiently allocate the available resources. Moreover, the versatility of this methodology permits, not only to update the results according to the available information on hazards magnitude and beach geomorphology, but also to easily apply it to other coastal regions.

Resum

L'impacte de temporals pot causar danys rellevants, tant a nivell econòmic com ambiental, a les zones costaners d'arreu del món. Com a conseqüència, durant els últims anys s'ha destacat la importància d'incloure anàlisis de la magnitud dels processos i de la vulnerabilitat en les polítiques costaneres, de manera que els gestors puguin prendre decisions informades per aplicar plans de mitigació i/o adaptació.

L'objectiu principal d'aquesta tesi és desenvolupar una metodologia que permeti avaluar, quantitativament, la vulnerabilitat de la costa a l'impacte de temporals per a diferents escales de temps, considerant per separat els principals processos induïts pels temporals (inundació i erosió). En aquest treball, la vulnerabilitat es defineix com el potencial d'un sistema costaner de ser danyat. Per quantificar-la es compara la magnitud dels processos amb la capacitat d'adaptació de la costa. Per tal d'avaluar la intensitat d'aquests processos, s'han combinat dades referents tant a l'onatge com a la geomorfologia costanera, mentre que la resiliència del sistema s'ha determinat a partir de les característiques morfològiques de cada platja.

La metodologia proposada es basa en una aproximació probabilística en la qual les sèries temporals de la intensitat dels processos s'ajusten a una distribució de valors extrems. En conseqüència, tant la magnitud dels processos com la vulnerabilitat s'obtenen en relació a una probabilitat d'ocurrència en comptes de per a un temporal determinat. Aquesta aproximació permet comparar els resultats de forma robusta al llarg de diferents escales espacials per a un mateix nivell d'ocurrència. El gestor de la zona costanera ha de decidir la probabilitat d'ocurrència a tenir en compte en l'anàlisi, la qual determinarà el període de retorn (Tr). Un cop seleccionat el període de retorn, es creen uns indicadors de vulnerabilitat que comparen la magnitud del procés amb la capacitat de resposta de la platja de forma independent per a erosió i inundació. La vulnerabilitat final es formula en termes d'aquestes dues variables intermèdies per mitjà d'una funció lineal que va des d'un valor mínim de 0 (estat òptim) a un màxim d'1 (estat de fallida), definint 5 categories qualitatives.

El nivell de seguretat de l'anàlisi depèn, no només de la probabilitat d'ocurrència, sinó també del valor seleccionat de les variables intermèdies als extrems de la funció. En aquest cas en particular, els llindars màxims i mínims s'han definit per a cada procés tenint en compte la funció de protecció proporcionada per la platja. Per tal d'optimitzar l'aplicació del mètode a escala regional, s'ha divit la costa en diferents sectors amb definit diferents sectors de la costa amb un clima d'onatge homogeni i s'ha dut a terme una classificació de les platges. En conseqüència, la intensitat dels processos d'erosió i inundació ha estat calculada per a una combinació de 6 sectors i 8 tipus de platja en comptes de per a cada platja. Tot i això, la vulnerabilitat s'ha avaluat a nivell local tenint en compte les característiques específiques de cada platja que en determinen la resiliència.

Amb l'objectiu d'avaluar com canvia la vulnerabilitat al llarg de diferents escales temporals, s'ha analitzat com varia la capacitat d'adaptació de la costa enfront de l'impacte de temporals degut als efectes d'altres processos. Tenint en compte les característiques de l'àrea d'estudi, l'erosió deguda als gradients en el transport longitudinal de sediments (LST) i l'erosió i la inundació degudes a la pujada relativa del nivell del mar (RSLR) han estat seleccionats com els principals processos costaners que actuen a mitjà i llarg termini respectivament. En aquest sentit, l'erosió/acreció deguda al LST s'ha determinat mitjançant l'ús de taxes d'evolució costanera, mentre que per caracteritzar l'erosió i la inundació degudes a la RSLR s'ha utilitzat una combinació de diferents escenaris de nivell del mar i subsidència.

La metodologia desenvolupada s'ha aplicat a la major part de la costa sedimentaria (219 km) de Catalunya (Mediterrani nord-oest). Els resultats obtinguts considerant la contribució integrada del LST juntament amb l'escenari mitjà de RSLR (3.8 mm/any + subsidència) indiquen que, per a un Tr=50 anys, el 28% de la costa presenta una vulnerabilitat alta o molt alta a l'erosió induïda per l'impacte de temporals sota les condicions actuals, un percentatge que augmenta fins al 46%, 63% i 75% per a les projeccions de 10, 25 i 50 anys respectivament. En el cas de la inundació, els increments de vulnerabilitat són menors, variant des del 31% sota les condicions actuals, fins al 34%, 48% i 67% per a les esmentades projeccions. En general, les variacions de vulnerabilitat degudes a la contribució de la RSLR són menors que les obtingudes quan només es té en compte el LST. Com era d'esperar, la contribució de la RSLR es detecta a escales de temps més llargues i resulta significativament major a la part sud de la costa catalana. La presència de platges dissipatives amb pendents molt suaus, juntament amb la potencialment significativa subsidència del Delta de l'Ebre, contribueixen a incrementar l'erosió induïda per la RSLR en aquesta zona. Per contra, la contribució del LST no sembla estar focalitzada en cap tipus de

platja concret. Els resultats de vulnerabilitat també han estat interpretats a diferents escales espacials i administratives.

Finalment, la metodologia presentada en aquesta tesi permet identificar els punts més vulnerables d'una àrea costanera considerant la resposta dinàmica del sistema al llarg de diferents escales de temps. Aquest tipus d'informació és rellevant per als gestors de la zona costanera quant a l'organització dels recursos disponibles. A més, la versatilitat d'aquest mètode permet, no només actualitzar els resultats en funció de la informació disponible sobre la magnitud dels processos y la geomorfologia costanera, sinó també aplicar-lo fàcilment a d'altres regions.

Resumen

El impacto de temporales puede producir importantes daños tanto a nivel económico como ambiental en los sistemas costeros de todo el mundo. En consecuencia, durante los últimos años se ha destacado la importancia de incluir estimaciones de la magnitud de los procesos costeros y de la vulnerabilidad en las políticas costeras, de forma que los gestores puedan tomar decisiones informadas para aplicar planes de mitigación y/o adaptación.

El principal objetivo de esta tesis es desarrollar una metodología que permita evaluar, cuantitativamente, la vulnerabilidad de la costa al impacto de temporales para diferentes escalas de tiempo, considerando por separado los dos procesos principales inducidos por los temporales (inundacón y erosión). En este trabajo, la vulnerabilidad se define como el potencial de un sistema costero a ser dañado, por lo que se ha cuantificado comparando la magnitud de los procesos con la capacidad de adaptación de la costa. Para evaluar la intensidad de dichos procesos, se han combinado datos tanto de oleaje como de la geomorfología costera, mientras que la resiliencia del sistema se ha determinado a partir de las características morfológicas de cada playa.

La metodología propuesta se basa en una aproximación probabilística en la que las series temporales de intensidad de los procesos se ajustan a una distribución de valores extremos. En consecuencia, tanto la magnitud de los procesos como la vulnerabilidad se asocian a una probabilidad de ocurrencia en vez de a un evento determinado, lo que permite una comparación robusta de los resultados a lo largo de diferentes escalas espaciales, para el mismo nivel de ocurrencia. El gestor de la zona costera debe decidir la probabilidad de ocurrencia a tener en cuenta en el análisis, la cual determinará el periodo de retorno (Tr). Una vez seleccionado el periodo de retorno, se crean indicadores de vulnerabilidad que comparan la magnitud del proceso con la capacidad de respuesta de la playa de forma independiente para erosión e inundación. La vulnerabilidad final se formula en términos de estas dos variables intermedias por medio de una función lineal que va desde un valor mínimo de 0 (estado óptimo) a

un máximo de 1 (estado de fallida), definiendo 5 categorías cualitativas. El nivel de seguridad del análisis depende, no sólo de la probabilidad de ocurrencia, sino también del valor seleccionado de las variables intermedias en los extremos de la función. En este caso en particular, los umbrales máximos y mínimos de vulnerabilidad se han definido para cada proceso teniendo en cuenta la función de protección proporcionada por la playa. Para optimizar la aplicación del método a escala regional, se han definido diferentes sectores costeros con un clima de oleaje homogéneo y se ha llevado a cabo una clasificación de las playas. Como consecuencia, la intensidad de los procesos de erosión e inundación ha sido calculada para una combinación de 6 sectores y 8 tipos de playa en vez de para cada playa. A pesar de esto, la vulnerabilidad se ha evaluado a nivel local considerando las características específicas de cada playa que determinan su resiliencia.

Con el objetivo de evaluar los cambios en la vulnerabilidad a lo largo de distintas escalas temporales, se han analizado las variaciones de la capacidad de adaptación de la costa frente al impacto de temporales causadas por los efectos de otros procesos costeros. Teniendo en cuenta las características de la zona de estudio, la erosión debida a los gradientes en el transporte longitudinal de sedimentos (LST) y la erosión y e inundación causadas por la subida relativa del nivel del mar (RSLR) han sido seleccionados como los principales procesos que actúan en la costa a medio y largo plazo respectivamente. En este sentido, la erosión/acreción debida al LST se ha determinado mediante el uso de tasas de evolución costera, mientras que para caracterizar la erosión e inundación debidas a la RSLR se ha utilizado una combinación de distintos escenarios de nivel del mar y subsidencia.

La metodología desarrollada se ha aplicado a la mayor parte de la costa sedimentaria (219 km) de Cataluña (Mediterráneo noroeste). Los resultados obtenidos considerando la contribución integrada del LST junto con el escenario medio de RSLR (3.8 mm/año + subsidencia) indican que, para un Tr=50 años, el 28% de la costa presenta alta o muy alta vulnerabilidad a erosión inducida por temporales bajo las condiciones actuales, un porcentaje que aumenta hasta el 46%, 63% y 75% para las proyecciones de 10, 25 y 50 años respectivamente. En el caso de la inundación, los incrementos de vulnerabilidad son menores, variando desde el 31% bajo las condiciones actuales, hasta el 34%, 48% y 67% para las citadas proyecciones. En general, las variaciones de vulnerabilidad debidas a la contribución de la RSLR son menores que las obtenidas cuando sólo se tiene en consideración el LST. Como cabía esperar, la contribución de la RSLR se detecta a escalas de tiempo mayores y resulta significativamente mayor en la parte sur de la costa catalana. La presencia de playas disipativas con pendientes muy suaves, junto con la potencialmente significativa subsidencia del

Delta del Ebro, contribuyen a incrementar la erosión inducida por la RSLR en esta zona. En cambio, la contribución del LST no parece estar focalizada en ningún tipo concreto de playa. Los resultados de vulnerabilidad también han sido interpretados a diferentes escalas espaciales y administrativas.

Finalmente, la metodología presentada en esta tesis permite identificar los puntos más vulnerables de un área costera considerando la respuesta dinámica del sistema a lo largo de diferentes escalas temporales. Este tipo de información es relevante para los gestores de la zona costera en cuanto a la organización de los recursos disponibles. Además, la versatilidad de este método permite, no sólo actualizar los resultados en función de la información disponible sobre la magnitud de los procesos y la geomorfología costera, sino también aplicarlo fácilmente a otras regiones.

Contents

List of Figures

List of Tables

Chapter 1

Introduction

1.1 Generalities

The coastal zone has always resulted of high interest for human settlements due to the social, economic and ecological services that it offers. According to Small and Nicholls (2003), 23% of the worldwide population (1.2 billion people) lived within 100 km of the coastline in 1990, increasing up to 41% (2.5 billion people) in 2003 (Martínez et al., 2007). More recent estimates indicate that this trend has remained similar until present, with 44% of the world population living within 150 km of the coastline, as reported by the United Nations (UN) Atlas of the Oceans (2010). On the other hand, coastal areas are subjected to different natural hazards that can produce important economic and environmental damages (e.g. Pérez-Maqueo et al., 2007). As a result of this high population density, a wide range of activities and infrastructures are concentrated in these areas, progressively increasing the existing value along the coastal zone.

With respect to the Catalan coast, Jiménez et al. (2012) suggests that the damages caused by storm impacts have increased at an approximated rate of 40% per decade during the last 50 years. In spite of this, the same study indicates that storm-induced hazards show no trend during the same period and points at other factors such as coastal development and generalized coastal retreat, among others, as the main cause of this increase. An example of the relevance of storm-induced damages in the Catalan coast is presented in figure 1.1. The top map is an extract from a Catalan newspaper that highlights the coastal locations that resulted affected by the impact of a storm occurred on 2001. The bottom picture shows damages on the facilities of a desalination

plant located at the central coast, caused by a storm that took place on 2007.

Because storms are one of the most frequent and important coastal hazards, it should be relevant to develop tools to assess the vulnerability of coastal systems to storm impacts. These tools would become of crucial importance to develop coastal management plans, permitting to identify the uses and resources potentially vulnerable and providing decision-makers information about the potential consequences of storm impacts in order to apply mitigation and/or adaptation strategies (e.g. Godschalk et al., 1989).

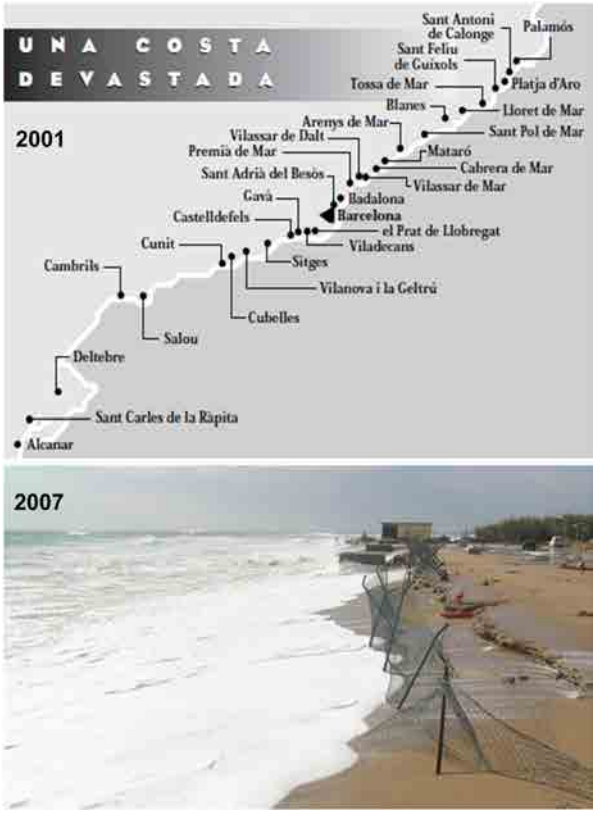

Figure 1.1: Top: Locations reporting damages along the Catalan coast produced by a storm on 2001 (Avui, November 13th 2001); Bottom: Facilities of a desalination plant damaged by a storm on 2007. Blanes, central coast (LIM, UPC).

In this work, vulnerability is understood as the potential of a coastal system to be harmed. During the last years, the importance of including hazards and vulnerability assessments in coastal zone policies has become a growing concern. A clear example of it is the Protocol on Integrated Coastal Zone Management in the Mediterranean

(PAP/RAC 2007), signed in January 2008, which specifically recommends countries to undertake vulnerability and hazard assessments to address the effects of natural disasters in coastal zones.

1.2 Objective

The **main objective** of this study is to *develop a methodology to quantitatively assess the vulnerability of sedimentary coasts to the impact of storms at different time scales for Mediterranean conditions and to apply it to the Catalan coast.* In order to achieve it, **3 partial objectives** have been defined:

1. To develop a methodology to assess storm-induced vulnerability considering inundation and erosion separately.
2. To develop a methodology to include medium and long-term coastal processes into the storm-induced vulnerability assessment.
3. To assess storm-induced vulnerability at different time scales for the Catalan coast considering different scenarios.

1.3 Outline

The document has been divided into 6 main chapters and 3 annexes with the following contents:

Chapter 2 provides an overview of previous works on coastal vulnerability as well as a summary of the proposed methodology.

Chapter 3 describes the main characteristics of the study area (Catalan coast) and the used datasets.

Chapter 4 focuses on the detailed description of the methodology developed to assess coastal vulnerability to storm-induced erosion and inundation. The results obtained from its application to the Catalan coast at different spatial scales are also presented in this chapter.

Chapter 5 analyses the contribution of medium and long-term coastal processes to storm-induced vulnerability. The obtained results are evaluated considering

both contributions separately as well as their integration into a final vulnerability index.

Chapter 6 gives an overview of the main conclusions of this study and its implications for coastal managers. Finally, some suggestions for further research about the studied topics are given.

Bibliography presents a list of the references cited in this work.

Annex A contains a series of final storm-induced vulnerability maps at beach scale considering different processes contribution.

Annex B contains a brief summary of the GOW wave height calibration process corresponding to three different nodes along the Catalan coast.

Annex C contains a list of the different scientific contributions resulting from the development of this thesis.

Chapter 2

Coastal Vulnerability

2.1 Previous works

The complexity of coastal systems has lead to different definitions of the term vulnerability in the existent literature, specially when socio-economic aspects are included (Green and McFadden, 2007). Often, such definitions result ambiguous and imprecise, which complicates its application to obtain quantitative assessments (Hinkel and Klein, 2007). Thus, a lot of effort has been put into defining conceptual frameworks of vulnerability in the last decades (e.g. Brooks, 2003; Füssel, 2007). As before mentioned, in this work coastal vulnerability is understood as the potential of a coastal system to be harmed by the impact of a storm (see e.g. Gouldby and Samuels, 2005).

During the last decades, the concept of coastal vulnerability has emerged as an important piece to understand and manage coastal risks. It has been mainly associated to disaster situations, because of the growing concern about their rising intensity and consequences (e.g. Alcántara-Araya, 2002; Gaddis et al., 2007). Furthermore, many authors have highlighted the relevance of developing tools to integrate vulnerability into coastal management frameworks during the last years (e.g. McFadden et al., 2007; McFadden and Green, 2007; Meur-Férec et al., 2008).

Based on the study of the evolution of vulnerability assessments to climate change, Füssel and Klein (2006) suggests an increase of their complexity towards interdisciplinary analysis, including policy option recommendations. An exhaustive assessment

of the different approaches to define vulnerability from a practical and theoretical point of view, as well as their implications, can be found in McFadden et al. (2007). This book collects the contribution of several worldwide experts on the matter and points out the need to perform regional studies of vulnerability that can result useful to coastal managers at small scales.

One of the first applications of the vulnerability concept to coastal systems corresponds to the analysis of the relative sea-level rise effects on coastal zones, performed by the *Intergovernmental Panel on Climate Change* (IPCC CZMS, 1992). However, the lack of discussion about practical aspects of its application –such as information collection and post-implementation– entails some difficulties when it comes to implement it (Klein et al., 1999).

From this point, different methodologies to assess vulnerability at large-scale focussed on climate change effects were developed. In this sense, the *European Topic Centre on Climate Change Impacts, Vulnerability and Adaptation*, under contract of the *European Environment Agency*, recently presented a compilation of different vulnerability assessment methods related to climate change impacts as well as the existing visualisation tools (Ramieri et al., 2011).

One of the most relevant methodologies is the Coastal Vulnerability Index (CVI) developed in the United States (Gornitz, 1991; Gornitz et al., 1994, 1997), which was subsequently adapted by the *United States Geological Survey* (USGS) to apply it at national scale (Thieler and Hammar-Klose, 1999, 2000a,b). With respect to the European contribution, the Dynamic and Interactive Vulnerability Assessment (DIVA) tool to evaluate coastal vulnerability to relative sea-level rise, developed within the framework of the DINAS-COAST European project, has to be highlighted (Hinkel, 2005; Hinkel and Klein, 2009). At the same time, Harvey and Woodroffe (2008) presents a review of the different approaches to asses coastal vulnerability to climate change in Australia at national and regional scale. Lastly, a recent evaluation of coastal vulnerability to climate change of Latin America and the Caribbean has been performed by the *Environmental Hydraulics Institute "IH Cantabria"* of the University of Cantabria in collaboration with the *Economic Commission for Latin America and the Caribbean* (CEPAL) and the *Spanish Office for Climate Change* (OECC) (CEPAL, 2012).

The application of vulnerability assessments at smaller scales is generally more limited, often focussing rather in damages and risk than in vulnerability. In some cases, the replication of the methodologies developed for global-scale assessments

implies that vulnerability analysis are carried out without considering the current knowledge about coastal processes at small scales (e.g. De Pippo et al., 2008).

In spite of this, a wide range of approaches to evaluate vulnerability to relative sea-level rise at regional/local scale have been developed during the last years (e.g. Gutierrez et al., 2011; Abuodha and Woodroffe, 2010; Khouakhi et al., 2013; Sahin and Mohamed, 2013). In some studies, different methodologies are applied to the same coastal stretch so that differences between them can be identified (e.g. Di Paola et al., 2011). In the case of the Spanish coast, a study to determine its vulnerability to climate change that proposes a series of tools to support the establishment of action strategies can be found in GIOC (2004).

With respect to recent vulnerability assessments considering other or more agents than climate change, a large variability of approaches and methods is also found depending on different aspects such as the driving process, the scale of the analysis and the type of considered vulnerability (e.g. Sanchez-Arcilla et al., 1998; Pethick and Crooks, 2000; Boruff et al., 2005; Youssef et al., 2009; Furlan et al., 2011; Alves et al., 2011; Mahendra et al., 2011; Martins et al., 2012; Torresan et al., 2012).

In Spain, García-Mora et al. (2000, 2001) presented a vulnerability assessment of dune environments based on ecological indicators as well as geomorphology and human pressure aspects. In terms of erosion, Málvarez García et al. (2000) proposed several qualitative indicators to characterize coastal sensitivity. After this, Domínguez et al. (2005) combined the potential coastal retreat with land-use information in order to evaluate the erosion vulnerability of the SW coast of Spain. A few years later, this approach was adopted by Anfuso and Martínez Del Pozo (2009) and Rangel-Buitrago and Anfuso (2009) to evaluate the vulnerability of a coastal zone in Italy and Colombia respectively.

Because vulnerability is often related to disasters, storm-induced impact results the most analysed small-scale coastal process, specially in terms of beach and/or dune erosion. In this sense, many conceptual and methodological approaches to characterise storm-induced vulnerability at different spatial scales have been developed in the last decades.

Sallenger (2000) defined a storm impact scale that categorizes tropical and extra-tropical storm impacts on natural barrier islands into 4 different regimes. Such classification is obtained through the comparison of water levels against dune morphology. Bearing this approach in mind, Stockdon et al. (2009) developed an algorithm to accurately determine dune morphology from LIDAR (Light Detecting And Ranging)

data. Focussing on coastal dunes, Judge et al. (2003) created a parameter that provides information on their vulnerability to storms, based on a revision of the existent ones.

At a national scale, the *Federal Emergency Management Agency* (FEMA) and the USGS developed the HAZUS (HAZard US) tool to estimate potential losses from hurricanes among other natural disasters in the United States (Vickery et al., 2006b,a).

Concerning to Mediterranean conditions, the methodology developed by Mendoza (2008) and subsequently published in Mendoza and Jiménez (2008, 2009) has to be highlighted. It consists of a couple of indicators that separately evaluates flood an erosion vulnerability to different storm classes, considering physical variables. The results from these partial indicators are integrated to obtain the final categories of the storm-induced vulnerability index. This methodology was applied at regional scale to evaluate the vulnerability of the Catalan coast, which required a previous storm classification of the studied area.

Finally, one of the most recent storm vulnerability studies can be found in Santos et al. (2013). In this case, the authors developed a methodology that considers physical and socio-economic variables separately to create two partial indexes, which are lastly combined into a final index. In the same work, the method is applied to a mesotidal coastal environment of the South of Spain.

2.2 Proposed framework

The methodological framework presented in this study permits to evaluate coastal vulnerability to storms at different time scales and to identify the most vulnerable spots of a determined region. At this point, it is necessary to stand out that the purpose of this study is not to describe in detail the behaviour of each beach in front of storm-impacts, but to obtain a first approach of the order of magnitude of such impacts to estimate vulnerability at a regional scale.

According to the definition of vulnerability adopted in this work, it can be described as:

$$\textbf{vulnerability} = \textbf{impact - adaptation} \tag{2.1}$$

Therefore, vulnerability can be quantified by characterising the magnitude of the impact as well as the ability of the coast to cope with it. Considering that here we have entirely focussed on the physical aspects of the coastal system, the impact

is determined by the intensity of the storm-induced coastal processes, whereas the adaptation ability is defined by the beach physical properties determining its capacity to cope with the considered impacts.

A simplified diagram of the proposed methodological framework is shown in 2.1. Since the main objective of this work is to determine the coastal vulnerability to storms at different time scales, other coastal processes than the storm-induced ones have also been considered. In this case, longshore sediment transport gradients and relative sea-level rise have been selected as the main medium and long-term agents taking place in the study area that can affect coastal vulnerability to storms. As a result, a total of 5 different processes are considered in this study:

- storm-induced erosion
- storm-induced inundation
- erosion/accretion due to longshore sediment transport gradients
- erosion due to relative sea-level rise
- inundation due to relative sea-level rise

The situation of such processes within the diagram is based on whether they are relevant to determine the impact of the storm or the adaptation ability of the coast. The magnitude of storm-induced erosion and inundation is used to characterize the impact of the storm, whereas the ability of the coastal system to cope with such impact is defined by the beach geomorphology (beach width and maximum berm height for erosion and inundation respectively). Given that longshore sediment transport and relative sea-level rise can modify such geomorphology, their effects on the coastal system at different time scales are estimated, so that the adaptation ability of the coast can be properly described. As a result, vulnerability to storms can be assessed for current and future beach configurations. Besides this, the contribution of these agents can also be assessed separately, which permits to identify the relevance of each process at different time scales.

The proposed method consists of three main steps: (i) forcing definition, (ii) hazard assessment and (iii) vulnerability assessment. First of all, the variables that define the forcing are evaluated. In this sense, waves and water levels are used to define storms, shoreline evolution rates are used as a proxy to characterise medium-term erosion and accretion due to longshore sediment transport and sea-level and subsidence rates are used to define relative sea-level rise. Once these variables are obtained,

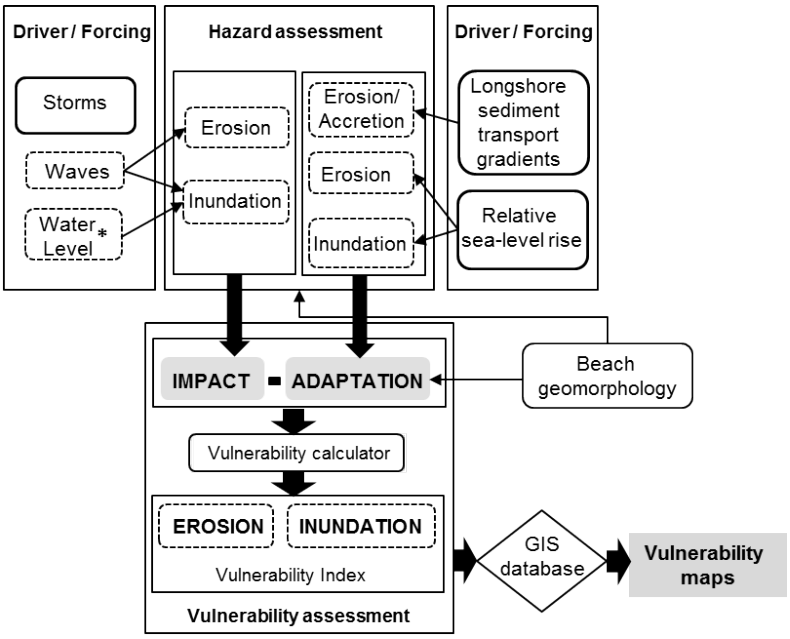

Figure 2.1: Methodological framework to assess coastal vulnerability to storms at different time scales. (*) Due to the low magnitude of storm surges in the study area, the water level, yet used in some of the analysis, is not considered to obtain the final results.

the magnitude of each process –also considered a hazard due to its potential to cause damages– is calculated. After this, changes in beach morphology due to the effects of medium and long-term coastal processes are evaluated. Lastly, the magnitude of the storm-induced processes is compared to the morphological characteristics that confer the adaptation ability of the beach. As a result, two vulnerability indicators are obtained separately for erosion and inundation. Such indicators are posteriorly fit into a vulnerability function that ranges from 0 to 1 and defines 5 different categories. The thresholds of the functions describe the maximum and minimum vulnerability situations for each of the storm-induced processes, which can vary depending on the considered beach function and safety level of the analysis.

One of the key aspects of this methodology lies in its probabilistic approach. Here, vulnerability is not assessed for a determined storm, but for a given probability of occurrence. Thus, differences in vulnerability under the same forcing conditions can be assessed. One relevant aspect of this method is the role of the coastal manager to define the safety level of the analysis and, consequently, the return period to be considered. To "objectively" make such decision, the characteristics of the hinterland have to be also taken into account.

As a result of the application of this methodology, storm-induced erosion and inundation vulnerability indexes are obtained separately. The fact that these two hazards are independently assessed permits to identify which is the most relevant. The obtained results are represented by means of a Geographic Information System (GIS), so that vulnerability can be compared to any other relevant spatial information.

To conclude with the general description of the proposed methodology, its versatility to be applied to different coastal regions must be mentioned as another key aspect. Although in this study it has been applied to the Catalan coast, the same procedure could be implemented to other coastal areas. Moreover, the framework could be employed with other processes/hazards depending on the characteristics of the study sites.

Chapter 3

Study area and data

3.1 Study area

Catalonia is an autonomous region located at the NE of Spain (NW Mediterranean) (see Figure 3.1). It is divided into 4 provinces (first-level administrative subdivision), 41 *comarcas* units (second-level administrative subdivision) and 946 municipalities (third-level administrative subdivision). According to data from IDESCAT (2014), the 12 coastal *comarcas* units comprise about 63.3% of the total population, yet they only account for 22.8% of the territory. As a consequence, the average population density in these areas is of about 509.7 people/km^2, without considering Barcelonès (see Figure 3.1), where it reaches 1906.6 people/km^2. These values are significantly higher than the Catalan average, which is 235.3 people/km^2.

The socio-economic structure is based on typical coastal activities such as commerce, agriculture and residential developments, being tourism the dominant one (Sardá et al., 2005). Despite the fact that they only represent about 0.1% of the region surface, beaches are one of the main reasons of the elevated tourism demand. In this sense, Catalonia was the most important destination of the country on 2012, attracting 25% of the total foreign tourism. Of this percentage, 45.7% was concentrated in coastal zones, without considering the city of Barcelona, which held about 50% (Generalitat de Catalunya, 2012). Furthermore, in 2010 tourism contributed to around 11.1% of the autonomous region Gross Domestic Product (GDP) (Duro and Rodríguez, 2011). At the same time, coastal *comarcas* units support 68.3% of the region hotel, camping and rural accommodation capacity, excluding Barcelonès, which

supports 12.5% of the capacity (IDESCAT, 2014). These facts state the importance of beaches in the economic development of the area. Nonetheless, protection and natural functions of beaches are also relevant. The first one is essential to maintain the beach resources available for the bathing season and to protect public and private properties and infrastructures located near the coast. On the other hand, the second one not only contributes to maintain the ecosystems –some of them endemics–, but also attract another kind of tourism mainly concerned about environment and natural spaces. In fact, there are several natural protected areas within coastal areas in Catalonia, located in the northern region (Alt and Baix Empordà), the Llobregat delta and the Ebre delta.

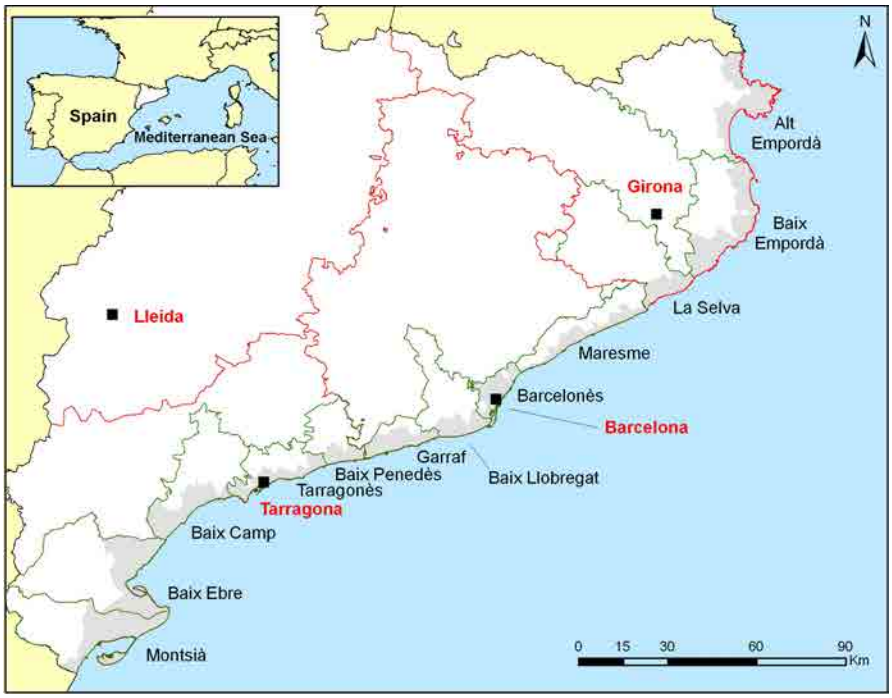

Figure 3.1: Administrative map of the stud area. Catalan provinces and their capitals in red. Coastal *comarca* limits in green and names in black. Coastal municipalities in grey.

The total length of the Catalan coast is about 699 km (CADS, 2005). It is characterized by comprising a large diversity of coastal types such as cliffs and bay beaches in the northern province of Girona, or long straight beaches and deltas in Tarragona (see Figures 3.1 and 3.2). In terms of different coastal environments, the Catalan coast can be divided into 7 areas:

- *Costa Brava:* Located at the North and mainly composed of rocky coast, cliffs

and the presence of bay beaches composed of coarse sand. (Alt Empordà, Baix Empordà and La Selva)

- *Maresme:* From the Costa Brava (Tordera river) to the North of Barcelona, originally characterized by an almost continuous coarse sand beach, now divided into different coastal cells due to the construction of several marinas and ports. (Maresme)

- *Barcelona:* From the Besos river to the Llobregat river, a highly engineered coast that contains artificial beaches of medium size sand and coastal structures such as Barcelona's port and airport. (Barcelonès).

- *South Barcelona:* Containing the Llobregat delta and the adjoining fine sandy beaches. (Baix Llobregat).

- *Costa del Garraf:* From the Baix Llobregat to the Costa Daurada, it is mainly formed by low cliffs and pocket beaches with fine sands. (Garraf).

- *Costa Daurada:* From the Garraf coast to the Ebre Delta, mainly dominated by straight, long and open beaches, composed of fine sediment and mild slope. (Baix Pendès, Tarragonès and Baix Camp).

- *Ebre Delta:* The southernmost area, a very low lying coast presenting sediment depositions from the Ebre river. It is formed by fine sand beaches with very mild slopes. (Baix Ebre and Montsià).

The main direction of the coast is North East to South West, with the exception of the Costa Brava area, which direction is North to South. An example of different beaches existing within each of these areas is presented in Figure 3.2.

Table 3.1: Number of beaches and length by coastal provinces.

Province	Num. of beaches	Km	% beaches	% Km
Girona	103	49.13	29.89	22.47
Barcelona	104	73.76	29.8	33.73
Tarragona	141	95.76	40.4	43.80
TOTAL	348	218.65	100	100

Among all the existing geomorphological environments, this work focusses on non-consolidated sedimentary material areas: beaches. They represent approximately 270 km of the total coastline, of which around 220 km are considered in this study. This

Figure 3.2: Examples of beaches representative of the different coastal environments present in the study area. Source: CIIRC (2010).

coastal length is divided into 348 beaches, which delimitation has been done considering the existing natural and artificial features that may alter their behaviour in terms of sediment transport. Thus, there might be cases in which the same administratively defined beach has been divided into different stretches due to the existence of structures like breakwaters. In these cases, every one of these stretches is considered separately as a beach. Note that the total coastal length will be henceforth understood as the total length occupied by the 348 beaches of the study (218.65 km).

Despite the different coastal environments present within the study area, the mean Catalan beach defined in CIIRC (2010) is 37 meters width, presents a quite thick sediment grain size of 0.7 mm and a rather elevated beach slope (higher than 1/10). This hypothetical situation represents the averaged values obtained considering all beaches, but does not necessarily describe the most frequent type of beach. The same study determines that, when comparing beach characteristics by provinces, Girona contains the narrower beaches whilst the widest ones are located in Barcelona. On the other hand, the location of the Ebre delta in Tarragona (see Figure 3.1) turns this province into the one with lowest sediment grain sizes and beach slopes.

Table 3.1 shows the number of beaches and its corresponding length by coastal provinces. As it can be observed, Tarragona is the province with a longest coastline, corresponding to about 44% of the total length considered in this study. Despite the fact that Girona and Barcelona hold almost the same number of beaches, in the case of Barcelona they represent a slightly longer coastal length (33.73% of the total in front 22.47% in Girona).

3.2 Wave data

The primary data to characterize coastal storms are waves. Two types of wave data are available in the study area: (i) instrumental data recorded by nearshore wave buoys deployed at specific locations along the coast, at depths between 40m and 90m, that have been operating since the end of the 1980s and (ii) hindcast data obtained in different studies. Referring to the second one, the most relevant are: (a) the SIMAR-44 database obtained in the framework of the HIPOCAS project, which extends from 1958 to 2001 (Guedes Soares et al., 2002), and (b) the GOW database, obtained in the framework of a global ocean wave reanalysis performed by the Environmental Hydraulics Institute "IH Cantabria", which extends from 1948 to 2009 (Reguero et al., 2012).

In order to process wave data in such a way that the study zone heterogeneity is not compromised, areas that present uniform wave characteristics along the Catalan coast have been grouped to define different coastal sectors. Such zoning is based on the previously presented by Mendoza et al. (2011) for the same area and results into 5 or 6 coastal sectors depending on the considered wave dataset (see Figure 3.3).

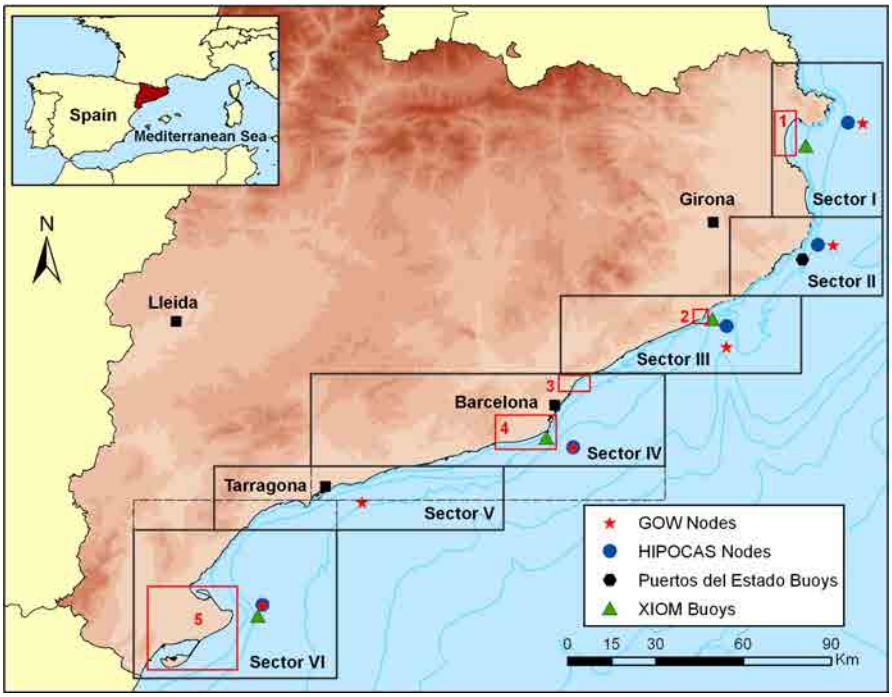

Figure 3.3: Map of the study area. Coastal sector limits and position of buoys and HIPOCAS/GOW nodes. Dashed line represents the 5-sector division corresponding to buoy, and HIPOCAS wave data series. Province capitals in black. Red squares indicate areas potentially subjected to subsidence.

Figure 3.3 shows the location of the buoys and Hipocas and GOW nodes used in this study. A total of 5 coastal wave buoys located along the Catalan littoral are available. Four of them belong to the XIOM network for oceanographic and coastal meteorological measurements (Xarxa d'Instrumentaci Oceanogrfica i Meteorologics), an organism that depends on the Catalan government (Generalitat de Catalunya). The last one belongs to Puertos del Estado (http://www.puertos.es), a public organism of the Spanish Government. Table 3.2 summarizes main data for each buoy.

As it can be seen in this table, the buoys located within sectors III and IV are the ones that have been recording for a longer period of time (about 29 years). Neverthe-

Table 3.2: Coastal buoys in the study area, location and operational period.

Sector	Location	Operational period	Organisation
I	Roses Bay 45 m depth	September 1992 August 2011	XIOM
II	Palamós 90 m depth	April 1988 April 2012	Puertos del Estado
III	Llobregat Delta 45 m depth	May 1984 February 2013	XIOM
IV	Blanes 65 m depth	May 1984 July 2013	XIOM
V	Cap Tortosa 45 m depth	June 1990 February 2013	XIOM

less, it has to be considered that buoy registers are not regular in time and contain data gaps that not only might coincide with storm periods but that in some occasions last several years. Furthermore, buoys in sectors III and IV were originally operating at a frequency of 12 hours until March 1991, which complicates the estimation of storm parameters during these years.

The SIMAR-44 database, obtained within the HIPOCAS project (Guedes Soares et al., 2002), consists of a 40-year hindcast of wave climatology for European waters including the Mediterranean region. The wave fields were obtained from numerical modelling, using the WAM model (WAMDI Group, 1988), with an approximated resolution of 12.5 km by 12.5 km. One of the potential problems of using hindcast wave data without previous validation is their reliability. This is especially important in the NW Mediterranean, that presents short fetches and where storm events are of limited duration, which could lead to model errors in comparison to open ocean predictions (Ponce de León and Guedes Soares, 2008; Bolaños et al., 2007; Cavaleri and Bertotti, 2004). Thus, although a general calibration of the HIPOCAS data has already been performed, since measured data for different coastal sectors are available, a specific calibration for storm conditions has been carried out in this work. To do so, data from five nodes close to the buoys location (see Figure 3.3) have been selected to determine storm characteristics. After this, HIPOCAS values have been compared to measured ones to obtain a calibration function that allows to transform simulated values and to reconstruct new data series. As a consequence, 5 coastal sectors are considered when using buoy, HIPOCAS and reconstructed data (see dashed line on Figure 3.3). Calibration and reconstructed series obtaining are explained in detail in section 4.2.2.

The last available wave dataset corresponds to a global ocean wave (GOW) calibrated reanalysis (Reguero et al., 2012). In this case, the WaveWatch-III model (Tolman, 2002) was used to obtain the wave fields, with a spatial resolution of 1/16° by 1/16°. This simulation covers the period from 1948 onwards. In order to properly cover the spatial heterogeneity of the coast, an additional node has been considered when this dataset is used (see Figure 3.3).

3.3 Water level data

With the objective to characterize storm surge, data from the Global Ocean Surge (GOW) reanalysis (Abascal et al., 2010) has been used. It consists of a meteorological tide reanalysis of 60 years performed by the Environmental Hydraulics Institute "IH Cantabria", covering the period from 1948 to 2009. The dataset was obtained using the ROMS model (Shchepetkin and McWilliams, 2005), with a spatial resolution of 1/8° by 1/8°.

3.4 Relative sea level rise data

To characterize relative sea-level rise (RSLR), two components have been considered: eustatic and subsidence. Since there are no long-term water level data that allow reliable estimations of actual RSLR rates, for the eustatic component, three different future scenarios estimations have been taken into account according to the Fourth Assessment Report (AR4) of the *Intergovernmental Panel on Climate Change* (IPCC) (Meehl et al., 2007). These scenarios correspond to the minimum and maximum estimates for the B1 scenario and the maximum for the A1FI. Both scenarios describe a convergent world defined by a rapid economic and population growth, yet B1 considers the implementation of green technologies whilst A1FI represents a fossil fuel intensive scenario in terms of energy sources. Apart from the IPCC estimates, an additional one has been adopted as the worst possible scenario. It corresponds to the Vermeer and Rahmstorf (2009) maximum sea-level estimate, obtained for the IPCC B1 temperature scenario and based on a semi-empirical method that links global sea-level variations to global mean temperature.

In terms of subsidence, according to the RISKCAT report about natural risks in Catalonia (CADS, 2008), 5 different areas that are highly susceptible to suffer collapse and subsidence have been defined, corresponding to the existing deltaic zones (see

red squares in Figure 3.3). For the most important one (the Ebre delta), several subsidence rate estimations exist. They have been obtained using different methods and spatial scales (e.g. Ibáñez et al., 1997; Jiménez et al., 1997b; Sornoza et al., 1998; Ibáñez et al., 2010), leading to results that range from 1 to 6 mm/yr. Considering the difficulty to obtain a reliable value, a representative subsidence of 3 mm/year has been used for the Ebro delta, corresponding to the largest deltaic deposit, whereas a value of 1.5 mm/yr has been assumed for the rest and considerably smaller sediment deposits.

Table 3.3: Considered RSLR scenarios.

RSLR scenario		low	medium	high	worst
Sea-level rise (mm/yr)		1.8	3.8	5.9	13
Subsidence (mm/yr)	(low/high) subs.	1.5/3	1.5/3	1.5/3	1.5/3
	no subs.	0	0	0	0
RSLR (mm/yr)	(low/high) subs.	3.3/4.8	5.3/6.8	7.4/8.9	14.5/16
	no subs.	1.8	3.8	5.9	13

Table 3.4: Subsidence areas location, length and rates.

Subsidence area	length (km)	sector	subsidence rate (mm/yr)
1: Empordà	14.32	I	1.5
2: Tordera	6.11	III	1.5
3: Besòs	4.43	IV	1.5
4: Llobregat	15.78	IV	1.5
5: Ebre	33.99	V	3
TOTAL	74.63	–	–

The combination of 4 projected sea-level rates with and without considering subsidence result in 8 possible RSLR scenarios (see Table 3.3). Values range from 1.8 mm/yr for the low sea-level rates and no subsidence to 16 mm/yr when the worst sea-level and highest subsidence rates are considered.

Table 3.4 shows the length of all the areas that are potentially subject to subsidence, their correspondent subsidence rates and the coastal sector to which they belong. In total, these areas represent about 34% of the studied coastline, 15.55% if only the Ebre delta area, which is associated to the highest subsidence rate, is considered.

3.5 Beach geomorphology data

To account for the contribution of beach geomorphology to vulnerability, dimensions and basic characteristics of each of the considered beaches along the Catalan coast have been included in a GIS database, together with information about existing uses and resources. The most part of the variables have been collected from the aforementioned CIIRC (2010) study to characterise the state of the Catalan coast, in which beach width, length, surface and orientation were calculated from a collection of colour orthophotos at a 1:5000 scale, taken at 2004 and supplied by the "Institut Cartogràfic de Catalunya" (ICC). Within the same study, beach elevation, beach-face slope, internal slope and sediment grain size data were acquired for all beaches during different profiling and sediment sampling field campaigns, that were carried out during 2008.

Apart from these variables, the submerged slope (sl), understood as the slope of the internal platform down to closure depth d, has also been obtained from the analysis of bathymetric maps provided by the Departament de Territory i Sostenibilitat" of the Generalitat de Catalunya. This slope is used to determine beach retreat due to RSLR according to the Bruun rule (Bruun, 1962), which is explained in detail further on. Taking into account the study area characteristics and the uncertainty involved in the closure depth selection (see Ranasinghe et al., 2011), a representative value of 10 meters has been contemplated for all beaches, assuming that resulting submerged slopes can be considered as reliable approximations.

3.6 Shoreline evolution rates

Beach evolution rates for the period from 1995 to 2010 have been used to determine the magnitude of medium-term erosion/accretion caused by longshore sediment transport (LST). They were obtained through the analysis of orthophotomaps from the "Institut Cartogràfic de Catalunya" (ICC) (www.icc.cat). This analysis was carried out by Jiménez and Valdemoro (2013) to update the previous one performed within the framework of the CIIRC (2010) study. Since no major alterations of the Catalan coastline in terms of engineering were carried out within this period, these evolution rates can be considered the result of littoral dynamic effects under actual conditions.

Chapter 4

Vulnerability to storms: a probabilistic approach*

4.1 Introduction

The methodology developed to assess coastal vulnerability to storm-induced erosion and inundation is presented in this chapter. Furthermore, the results obtained from its application to the Catalan coast are explained in detail. The practical goal of the methodology is to provide information to managers to plan on resources allocation to manage/mitigate damages induced by storm impacts at regional scale. In this work, this regional scale corresponds to a length of several hundreds of km. From the management standpoint, it has been selected because it comprises an administrative unit with its own legal competences, in this case the autonomous region of Catalonia, which should be equivalent to a state in a federal republic.

When referring to storms, vulnerability is quantified by comparing the magnitude of the impact of the storm with the adaptation capacity of the coastal system. Considering this, the methodology presented here is divided into three main steps: (i) forcing definition, (ii) hazard assessment and (iii) vulnerability assessment (see Figure 4.1). In the first step, storms are defined in terms of the significant wave height at the

*This chapter is largely based on Bosom and Jiménez (2010, 2011): Storm-induced coastal hazard assessment at regional scale: application to Catalonia (NW Mediterranean). Advances in Geosciences, 8:1-5; Probabilistic coastal vulnerability assessment to storm at regional scale – application to Catalan beaches (NW Mediterranean). Natural Hazards and Earth System Science, 11(2):475-484

peak of the storm (H_s), peak period (T_p) and duration. In the second step, time series of storms are used, together with information of basic characteristics of beaches, to assess the magnitude of the two considered processes: inundation and erosion. Time series of hazard magnitudes are fit to extreme value distributions so that magnitudes are related to a probability of occurrence. Finally, the last step consist on assessing vulnerability. To do so, hazard magnitudes are compared to the physical properties of the beach determining its capacity to cope with considered impacts. Each one of these steps is thoroughly described within the following sections.

In this work we have adopted a probabilistic approach where, the probability of occurrence of induced hazards along the coast are estimated and, once a risk level is defined by the manager, the spatial distribution of the expected magnitude of the impact is compared to identify the potentially most endangered areas. Thus, instead of assessing the vulnerability for all beaches induced by a given (single) storm, the objective is to calculate the vulnerability associated with a given probability of occurrence at each site. In this approach, the decision-maker selects the acceptable probability of occurrence. This can vary along the coast, depending on the importance of the hinterland. In the case of selecting spatially varying risk levels, this should result in comparing vulnerabilities associated with different probabilities.

Lastly it must be considered that, although this methodology can be applied to any coastal zone, some variations of the specific procedures used here may be needed depending on the characteristics of the study area.

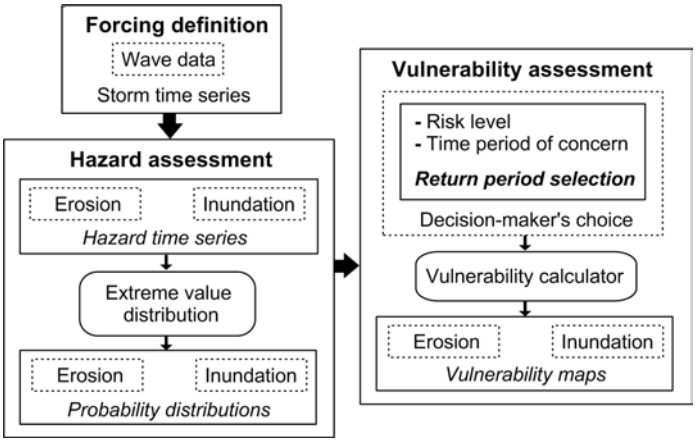

Figure 4.1: Methodological framework for coastal vulnerability assessment to storms.

4.2 Forcing definition

4.2.1 Storm definition

Since the objective of this work is to analyse coastal vulnerability to storms, used wave data will be restricted to those corresponding to such conditions. A storm can be defined in a simple manner as a violent atmospheric perturbation that when occurs at the sea, the most immediate effects are the increase in wave height and sometimes sea level (storm surge). Mendoza and Jiménez (2006) and Mendoza et al. (2011), define a storm as an event in which significant wave height, H_s, exceeds a value of 2 meters during a minimum period of 6 hours. This criterion was proposed as the minimum conditions required to generate a significant morphodynamic impact along the Catalan coast, and has also been followed in this work. In addition, events where H_s exceeds 2 meters during less than 6 hours but are separated less than 6 hours from major storms, are also included as part of the same storm. Furthermore, as also discussed in Mendoza (2008), the existence of double peak events in the study area must be contemplated. To do so, storm peaks separated less that 72 hours from each other are considered the same storm. Unlike in Mendoza (2008), and due to the characteristics of the datasets used in this study, no restriction of minimum wave height between peaks is considered. Nevertheless, a maximum of two peaks per storm has been allowed in order to restrict storm extent. Figure 4.2 describes in simple terms criteria used to define annual maximum storms through the representation of GOW data in sector IV.

The availability of long time series of wave data (>40 years) permits to define storms according to the annual maximum method without compromising the robustness of the statistical analysis. Thus, representative time series of annual maximum storms have been built for each sector. They have been defined in terms of significant wave height at the peak of the storm ($H_s\ max$), associated peak period ($T_p\ max$), direction and storm duration. The annual maximum storms have been calculated for climatic years (period from September to August). Very exceptionally, time series of all the storms have also been built. In those very few cases, which will be explained in detail further on, no maximum number of peaks yet a minimum wave height value of 1.5 meters between them has been set. This has been done in order to guarantee independence among storms. Full details about coastal storms and forcing meteorological conditions along the Catalan coast can be seen in Mendoza et al. (2011).

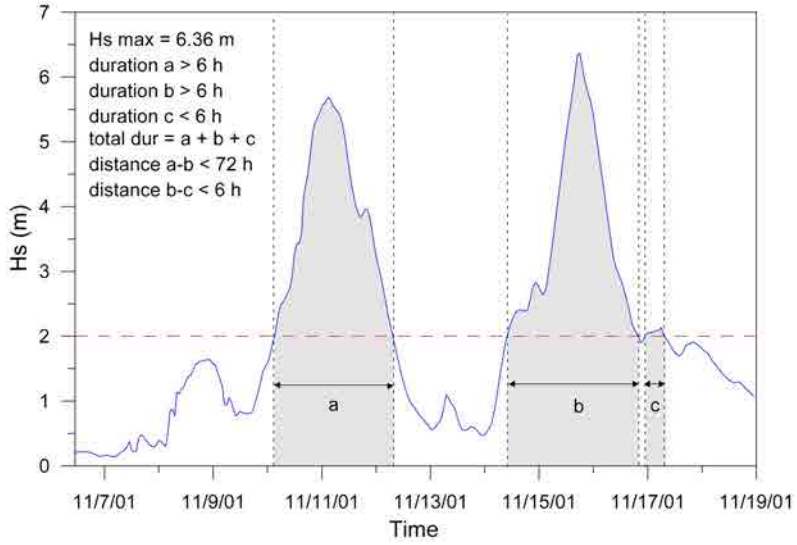

Figure 4.2: Annual maximum storm definition parameters for the 2001 storm in sector IV (wave data from GOW reanalysis).

4.2.2 Wave dataset selection

Previous to the application of the methodology, and considering the availability of three different wave datasets for the study area, a simple analysis has been performed to determine which is the most suitable for the purposes of this work. To do so, all the available datasets have been compared between them. In addition, a calibration of HIPOCAS values has been performed to obtain a reconstructed dataset that combines measured and calibrated values.

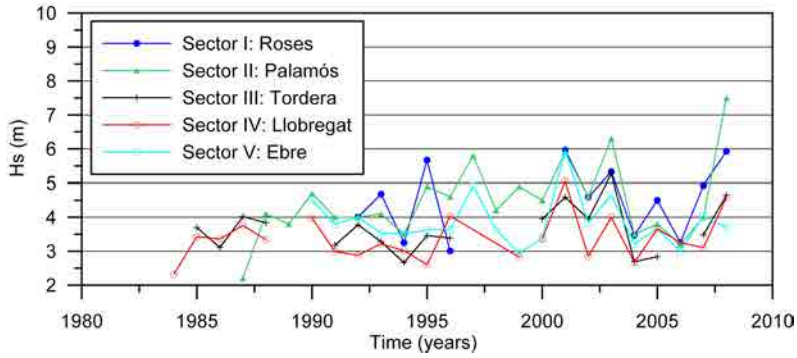

Figure 4.3: Wave height (m) corresponding to the annual maximum storm at each coastal buoy.

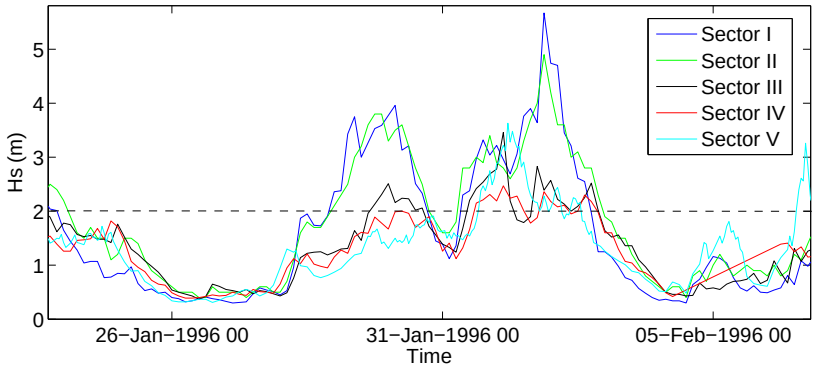

Figure 4.4: Wave height (m) corresponding to the annual maximum storm at each coastal buoy.

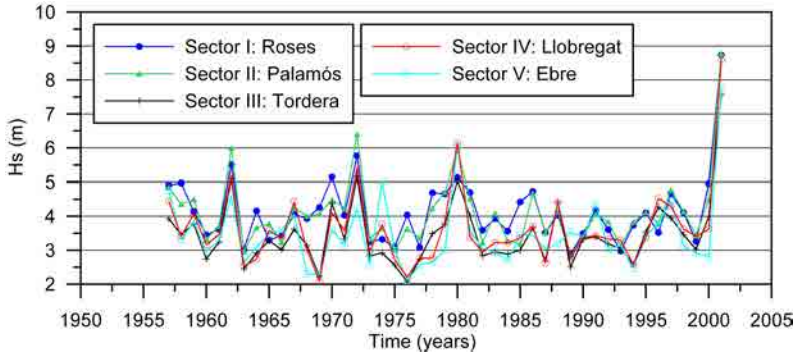

Figure 4.5: Wave height (m) corresponding to the annual maximum storm at each 5 HIPOCAS nodes.

To obtain a first characterisation of recorded storm data, Figure 4.3 shows annual maximum recorded storms for each buoy. As it can be observed, only sectors II and V have complete data series and some of the existent storms contain data gaps or are incomplete. In spite of this, in general, maximum H_s values are found in the two northernmost sectors (Roses and Palamós) followed by the southernmost sector (Ebre). Although higher wave heights may have occurred —yet not registered— within the same or different storms, the highest recorded value in all series corresponds to the 2008 event in sector II (7.5 m). When comparing mean values of all series, sector I and II are the only ones where these values exceed 4 meters (4.51 m and 4.46 m respectively). For further details on measured storm characteristics along the Catalan coast, see the work of Mendoza et al. (2011).

In order to highlight spatial differences in storm properties, Figure 4.4 compares

a given storm event in all sectors in terms of H_s. Here, significant differences among the same storm magnitude along the coast can be detected. It corresponds to the 1995 climatic year maximum storm for sectors I, II, III and V, but not for sector IV, were its magnitude is clearly lower. Again, the two northern sectors register higher storm peaks, followed by the southernmost one. Duration is also significantly longer in sectors I and II, and it corresponds to a double peak storm except in the southern part of the coast (sectors IV and V), where it is a single peak one.

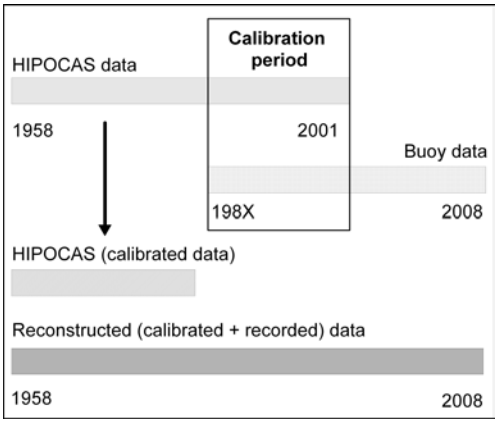

Figure 4.6: Diagram of the calibration and obtaining process of reconstructed series.

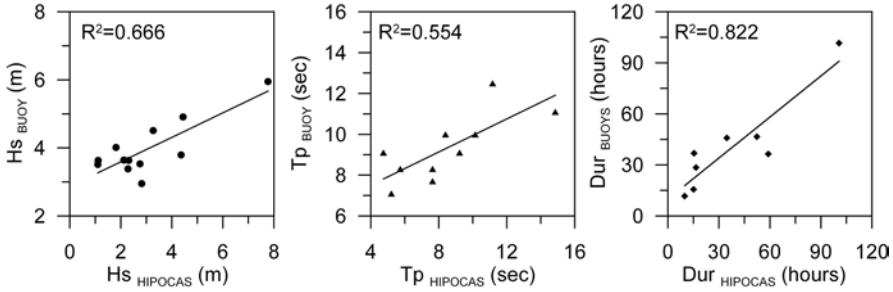

Figure 4.7: HIPOCAS and buoy storm parameters comparison and linear regression for sector V and associated determination coefficient (r^2).

Recorded series are the most reliable yet they are too short to become a suitable source of information to obtain extreme probability distributions. In spite of this, they can be used to determine spatial differences between coastal sectors in terms of wave climate as well as to calibrate other kind of data. Unfortunately, none of the buoys of the XIOM network are currently functioning (at the time this thesis has been written – February 2014), which supposes a break in data series that should difficult

future scientific studies related to wave climate.

Table 4.1: Equations obtained through linear regression analysis comparing recorded and simulated wave data at the storm peak ($y = mx + b$). Correspondent determination coefficients. All storm parameters and coastal sectors are considered.

Sector	Parameter	Equation	r^2
I	H_s	$y = 1.14m + 0.76$	0.541
	T_p	$y = 0.22m + 9.52$	0.010
	duration	$y = 1.51m - 17.02$	0.421
II	H_s	$y = 0.53m + 2.87$	0.412
	T_p	$y = 0.34m + 7.02$	0.122
	duration	$y = 0.02m + 59.64$	0.0003
III	H_s	$y = 0.25m + 2.77$	0.709
	T_p	$y = 0.83m + 3.09$	0.595
	duration	$y = 0.55m + 21.34$	0.75
IV	H_s	$y = 0.32m + 2.35$	0.778
	T_p	$y = 0.6m + 3.56$	0.279
	duration	$y = 0.52m + 20.69$	0.617
V	H_s	$y = 0.36m + 2.87$	0.666
	T_p	$y = 0.41m + 5.89$	0.0.554
	duration	$y = 0.8m + 9.85$	0.822

With respect to the HIPOCAS wave dataset, Figure 4.5 represents the 45-yr annual maximum H_s series for each node, corresponding to each coastal sector. Once again, the highest wave height values are generally found at the two northernmost sectors, yet they are not always followed by the southernmost one. On the other hand, the lowest H_s values correspond to different sectors depending on the year. Regarding the annual maximum storm, the highest wave height value of all series correspond to 2001.

As before mentioned, considering the availability of measured wave data in the study area, a local calibration of HIPOCAS hindcast data has been carried out. As a result, reconstructed series that combine measured and simulated data have been built up. To do so, data within the same period has been compared and a regression analysis has been performed in order to obtain a calibration function. This equation has been used to convert each storm parameter of the HIPOCAS series into calibrated data to finally obtain reconstructed series by adding calibrated values to recorded ones. A simple diagram of this process is presented in Figure 4.6. Resulting 50-yr long wave time series are composed by calibrated hindcast data from 1958 to 1989

(when no instrumental data did exist) and recorded data from 1990 until 2008 (when available). Note that this is applicable to storm data only.

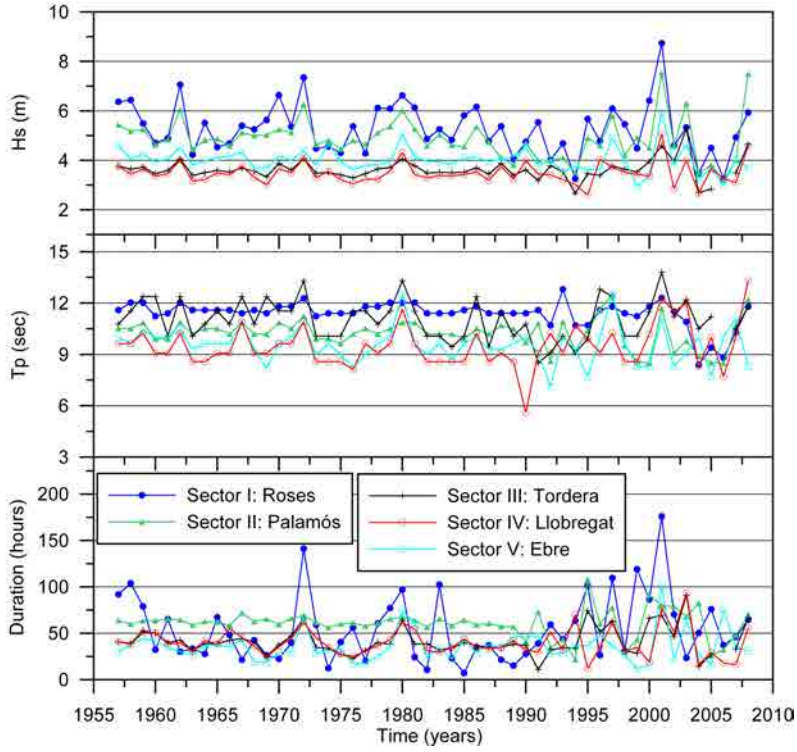

Figure 4.8: Time series of the annual maximum storm conditions of reconstructed data.

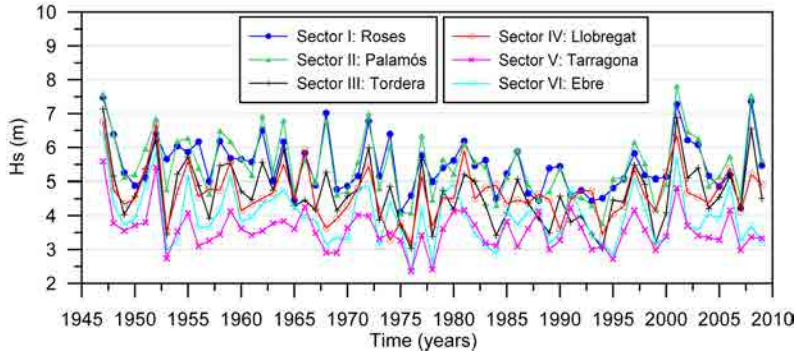

Figure 4.9: Wave height (m) corresponding to the annual maximum storm at each sector considering GOW data.

Figure 4.7 shows the comparison between recorded and simulated values of all storm parameters (H_s, T_p and duration) at the storm peak for simultaneous events at sector V (Ebre). This is one of the sectors where a better fit between both kind of data was obtained. However, some of the results corresponding to other sectors show a large dispersion of data around the fitted model (see Table 4.1), being Sector II the most extreme in this sense. In addition, and as it appears to happen with data from sector V, HIPOCAS values are frequently higher than recorded values. These results confirm our suspicions that the use of simulated wave data without previous validation might lead to little reliable results. Equations from Table 4.1 have been used to transform simulated wave data and, thus, to obtain longer wave time series. Final reconstructed series of H_s, T_p and duration for all sectors are exposed in Figure 4.8. As seen in previous datasets, highest values of wave height are found in sectors I and II, followed in general by sector V, which seems to properly reproduce the behaviour observed in real data.

This approach solves the inadequate length and data gaps of buoy series, at the same time that allows to calibrate simulated data considering real measurements. Nevertheless, it might entail some shortcomings. If we look at the lowest determination coefficients in Table 4.1 (T_p at sector I; duration and T_p at sector II), we can observe how their correspondent reconstructed series in Figure 4.8 show very little variation for the years in which only simulated data is available. Since these series are not realistic, original HIPOCAS data should replace reconstructed data in these three specific cases.

Finally, Figure 4.9 shows series of H_s at the peak of the annual maximum storm for each sector considering GOW data. As this dataset has already been calibrated and validated with satellite altimetry data, no calibration has been performed in this case. Thus, 6 coastal sectors instead o 5 are considered to better define spatial heterogeneity in terms of wave climate. As observed in the other datasets, the highest values correspond to sector I and II. On the other side, the lowest values are associated to the new sector (Tarragona), located between former sectors IV (Llobregat) and V (Ebre). Unlike in the case of reconstructed series, values corresponding to sector VI (former sector V) are generally lower than the ones obtained at sectors III and IV.

After considering all the available wave datasets, GOW seems to be the most suitable for the purposes of this work. This is due to the fact that it covers the longest period of time and has been thoroughly calibrated and validated (see Annex B). Thus, using this dataset we can avoid problems that arise in the case of reconstructed series when the fit between real and simulated data is not consistent enough.

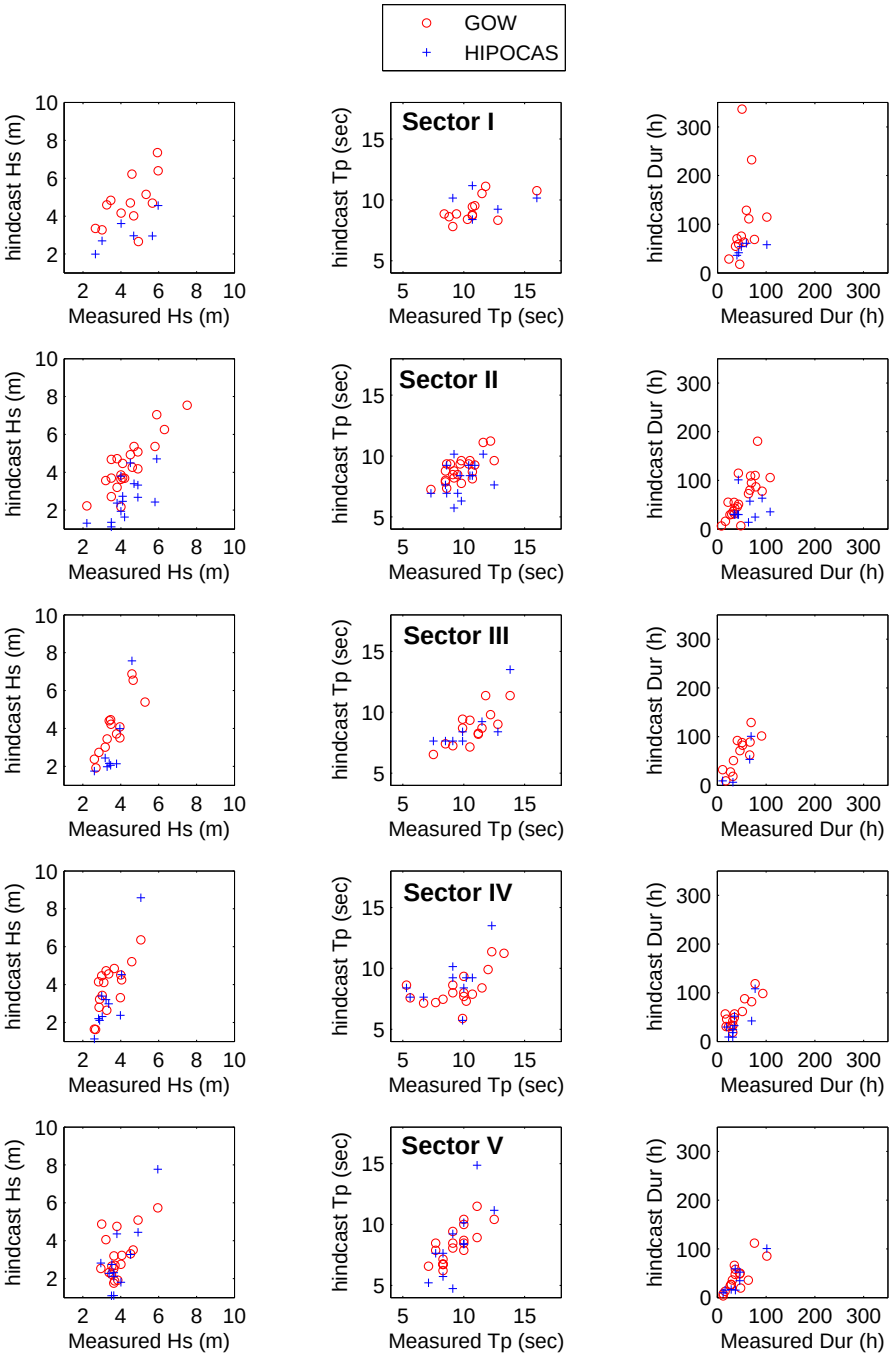

Figure 4.10: Comparison of same storm parameters between recorded (buoys) and simulated datasets (GOW and HIPOCAS).

To put in context the consequences of the database selection, Figure 4.10 compares simulated and real data considering the same storm. Results indicate that GOW seems to better reproduce real wave height data in all sectors, whereas peak period is slightly underestimated in all cases, specially at northern sectors. In terms of storm duration, both simulated data seem to properly reproduce recorded values, with the exception of two GOW data points that show a clear overestimation at sector I. The fact that GOW data reasonably reproduce measured values support the selection of this dataset to perform the analysis. Besides this, the slight overestimation of parameter values in some cases is accepted, meaning that the worst situation is considered.

Finally, to better represent the wave climate characteristics of the study area, 6 coastal sectors that present relatively homogeneous wave conditions during storms have been defined in this case. As a result, GOW data from 6 nodes representative of each sector have been considered. In this sense, Table 4.2 shows the number of beaches and length of each sector. As observed, sector V results the most extensive and sector II the least one.

Table 4.2: Number of beaches and total length within each coastal sector.

Coastal sector	Num. of beaches	Km
Sector I	46	31.01
Sector II	42	10.96
Sector III	64	46.01
Sector IV	55	34.91
Sector V	83	51.84
Sector VI	58	43.92
TOTAL	348	218.65

4.3 Hazard assessment

When an extreme storm impacts on a sandy coast, it produces different morphodynamic responses which rapidly and significantly modify the coastal landscape. These processes and changes are controlled by a combination of different factors that essentially are storm characteristics and the coastal geomorphology (e.g., Morton, 2002; Morton and Sallenger, 2003). Having adopted a regional scale approach, we simplify the analysis by retaining the two most important storm-induced coastal processes, inundation and erosion (see Figure 4.11). As these processes are potentially harmful for

coastal stability and they should affect existing uses and resources, they are usually considered as hazards.

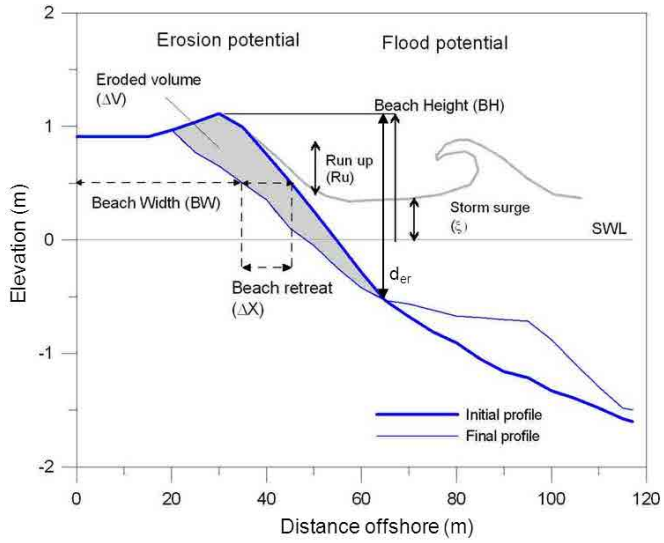

Figure 4.11: Diagram of the two studied storm-induced hazards, modified from Mendoza and Jiménez (2009).

Because the intensity of each of these coastal hazards depends on different storm properties and beach characteristics, they will not necessarily be equally important during a given storm event. Moreover, their induced damages in the coastal zone are also different and, in consequence, managers should be interested to know which is the dominant hazard during a given event. Therefore, the developed methodology allows the evaluation of the coastal vulnerability to these two processes separately. Their magnitude has been parametrized by selecting a representative indicator including information on storm properties (forcing) and beach characteristics (receptor).

Some examples of the damages caused by the impact of coastal storms at different locations of the Catalan coast are shown in Figures 4.12 and 4.13. More precisely, the first one refers to damages caused by storm-induced erosion, whereas the second one refers to inundation.

In order to work at regional scale in an efficient but robust way, we have grouped beaches into different classes, in such a way that hazard magnitude is calculated for each beach class instead of for each single beach in the study area.

Figure 4.12: Examples of damages caused by storm-induced erosion in the Catalan coast (Location, date and image property). 1: Blanes promenade (La Selva), 2008, LIM; 2: Cubelles (Garraf), June 2009, *La Vanguardia* newspaper; 3: Blanes (La Selva), December 2008, *La Vanguardia* newspaper.

Figure 4.13: Examples of damages caused by storm-induced inundation in the Catalan coast (Location, date and image property). 1: Lloret de Mar (La Selva), November 2001, Lloret de Mar Council; 2: Blanes, December 2008, *La Vanguardia* newspaper; 3:L'Escala (Alt Empordà), December 2008, Lloret de Mar Council; 4: Ebre delta (Montsià), November 2001, D.G. Costas Tarragona.

4.3.1 Beach classification

Beaches have been classified from a morphodynamic standpoint according to its sediment mean grain size and beach-face slope. There is a strong relation between these two characteristics since the material of the beach is one of the main variables determining its morphology. In the Catalan coast, this relation has been described

by CIIRC (2010). In general terms, an increase in sediment size entails bigger slopes and berm heights. Nevertheless, this relation is not uniform along all sizes. Considering this and the high variability of coastal environments in the study zone, a hierarchical cluster analysis has been performed to determine different beach groups according to its d_{50} and beach-face slope. To do so, both variables have been standardised and a Ward's clustering method considering euclidean distances has been applied. As a result, the dendrogram showed in Figure 4.14 has been obtained. A cut-off distance of 5 has been selected to obtain 8 different beach groups. Figure 4.15 shows the distribution of each of the beaches within its final category according to the two selected variables.

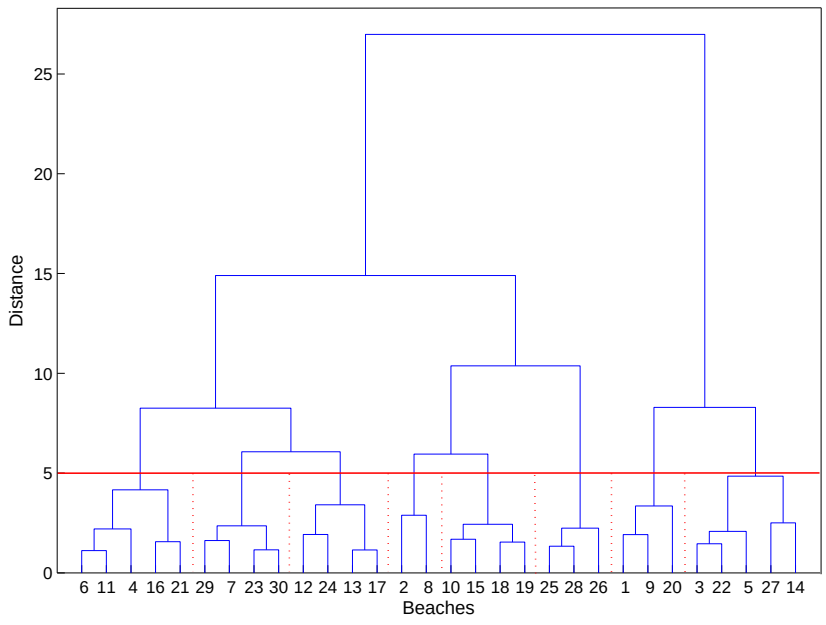

Figure 4.14: Dendrogram obtained from the hierarchical clustering analysis performed to classify beaches in terms of its sediment grain size and beach-face slope.

For each class, representative d_{50} and slope values have been calculated by averaging actual d_{50} and slope values of all beaches within the group. In addition, sediment fall velocity for each beach type has been determined with the settling velocity equations defined by Jiménez and Madsen (2003).

Table 4.3: Reference values of d_{50}(mm), slope (tanβ) and fall velocity (m/s) corresponding to each of the beach types.

Beach type	d_{50} range (mm)	ref. d_{50} (mm)	slope range (tanβ)	ref. slope (tanβ)	ref. fall vel (m/s)
Type 1	0.23 - 1.21	0.70	0.21 - 0.30	0.24	0.09
Type 2	1.33 - 1.84	1.57	0.18 - 0.27	0.21	0.16
Type 3	1.15 - 1.93	1.60	0.05 - 0.17	0.11	0.16
Type 4	0.14 - 0.52	0.23	0.02 - 0.09	0.06	0.03
Type 5	1.15 - 1.86	1.42	0.29 - 0.40	0.33	0.15
Type 6	0.20 - 0.80	0.47	0.14 - 0.20	0.17	0.06
Type 7	0.85 - 1.46	1.13	0.12 - 0.22	0.16	0.13
Type 8	0.16 - 1.02	0.45	0.06 - 0.12	0.11	0.06

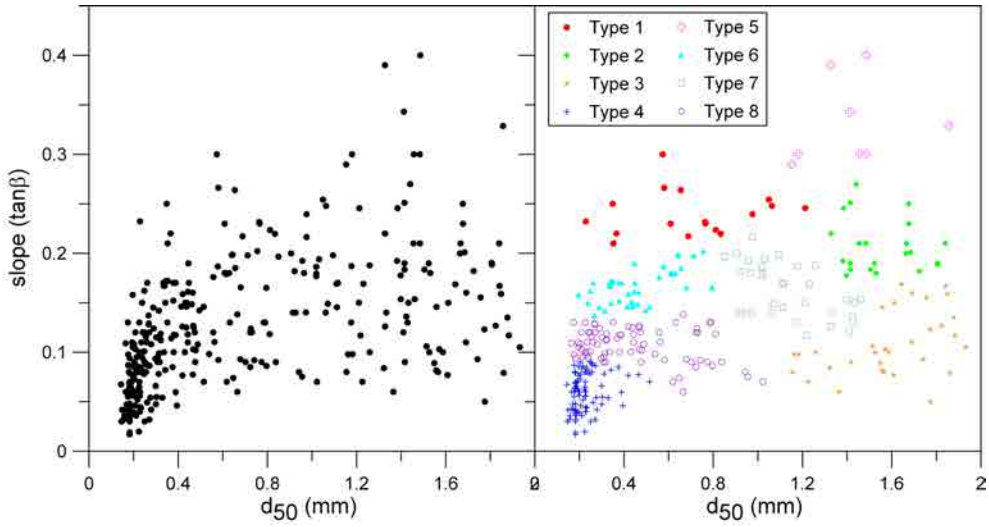

Figure 4.15: Left: d_{50} and slope values for the Catalan coast beaches. Right: Beach type final classification.

Table 4.3 shows final range and reference values of slope, sediment mean size and sediment fall velocity for each beach type. Notice that this classification is specific for the study area and that the application of the method to other geographical zones would require applying the same procedure to characterize the corresponding representative beaches. As it can be seen in this table, reference slope values range

from 0.06 to 0.33, sediment mean size from 0.23 to 1.60 mm and fall velocity form 0.03 to 0.16 m/s. This reflects once more the before mentioned high variability in coastal environments. Dissipative profiles are characterized by very mild slopes and fine sand. They are present in areas such as the Costa Daurada and Ebre delta and mainly represented by beach type 4. On the other side, beaches composed of steep slope and coarse sediment are classified as reflective and they are typically found in the Costa Brava and Maresme areas. Beach type 5 represents the most reflective beaches of the Catalan coast. As showed in Table 4.3, this study comprehends several intermediate situations between these two extreme beach morphologies.

Table 4.4: Total number of beaches and corresponding length within each beach type for the Catalan coast.

Beach type	Num. of beaches	Km
Type 1	17	18.03
Type 2	25	10.22
Type 3	36	10.64
Type 4	100	76.31
Type 5	8	4.32
Type 6	42	21.94
Type 7	35	19.28
Type 8	85	57.91
TOTAL	348	218.65

Even though 8 beach types have been described, their frequency and spatial distribution vary along the study area. Table 4.4 reveals type 4 as the most common beach type along all the coast occupying a total of 76.31 km (about 35% of the total coastline). Nevertheless, a major number of beaches within a determined beach type does not necessarily mean that they are equally distributed along the study area. In this sense, Figure 4.16 shows the coastal length corresponding to each beach type for the three coastal provinces.

Agreeing with the previous definition of the Catalan coast, the most frequent beach type, which is also the most dissipative one, is mainly found at the southern province (Tarragona), where it occupies about 58% of the studied coastline. However, this beach type is one of the less frequent in the northern province (Girona), contributing only to about 6% of the coast. On the opposite end, type 5 beaches are defined by major slopes and grain sizes. It is the least common beach type and it is only and exclusively found at the northern province, where it occupies less than a 5% of the total coastline (slightly above 8.5% of the province's coastline).

Despite the fact that some beach types follow a clear spatial pattern in terms of their distribution, there are others such as type 8, the second most common, which even though it is the most important in Girona, its presence is also significant in the other two provinces. Type 6 can be found in all provinces as well, although it represents a minor number of km in all of them. Finally, Barcelona is the province where beach types (except type 3) are distributed more homogeneously, being type 4 the one occupying a slightly major part of its coastline.

Finally, 4.17 shows beach type spatial distribution in terms of coastal length considering each sector separately, which allows a more accurate description of spatial differences:

Sector I Includes the northern area of the *Costa Brava*. Although it comprises all the beach types present along the whole study area, it is mainly composed of medium to high grain size and slope beaches (types 8, 6 and 1). The most dissipative beach type (4) is also present but less frequent (only 4 yet large beaches).

Sector II This coastal sector comprises the southern part of the *Costa Brava* and it is also characterized by the presence of reflective beaches (types 7 and 5). Medium grain size and slope beaches are also present (type 8), whereas type 4, representative of the most dissipative beaches along the Catalan coast, is not present in this sector.

Sector III Encompasses the *Maresme* area and a bit of the lower *Costa Brava*. Again, all the beach types can be found in this sector but those representing reflective beaches are more frequent. On the contrary, types 4 and 8, the ones with the lowest representative values of grain size and slope, are less important.

Sector IV *Barcelona*, *South Barcelona* and the *Costa del Garraf* are included in this sector, where the majority of the coastline is composed of dissipative (type 4) and intermediate (type 8) beaches. The beach type representing the highest values of slope and sediment main size is not present (type 5). Nevertheless, other reflective beach types are present (type 1).

Sector V Includes the majority of the *Costa Daurada* and its coastline is clearly dominated by dissipative beaches (type 4). Beaches within types 1, 2 and 5 are not present in this sector

Sector VI The southernmost sector contains the *Ebre Delta* and the southern part of the *Costa Daurada*. The beaches of this sector belong mainly to the three

types combining lower values of slope and sediment size, whereas beaches corresponding to types 5 and 7 are not present.

Figure 4.16: Length of coastline per province corresponding to each beach type.

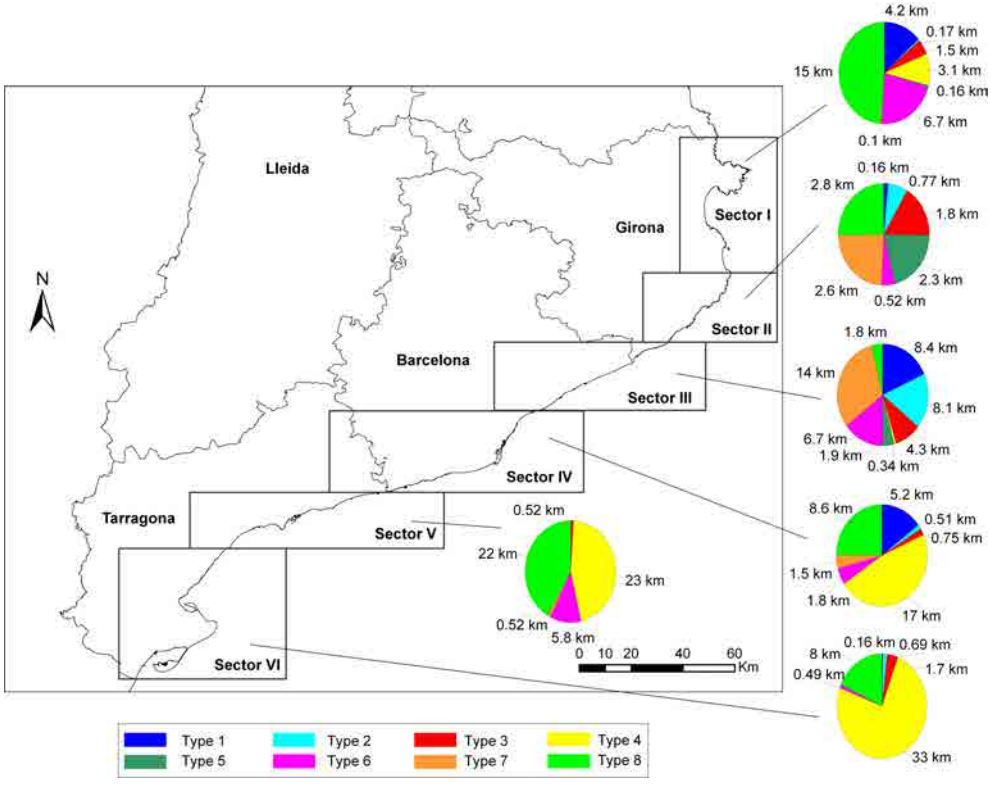

Figure 4.17: Length of coastline per sector corresponding to each beach type.

In general terms, low-lying coasts comprising sandy beaches with mild slopes are mainly located at the south, opposite to the most reflective profiles, which are more frequent in the northern and central coastal sectors.

4.3.2 Hazard time series

In order to characterise the magnitude of the storm-induced processes, erosion and inundation have been parametrized separately.

Erosion magnitude has been calculated by using the parametric model proposed by Mendoza and Jiménez (2006). In their work, numerical simulations of the impact of typical storm conditions and beach characteristics along the Catalan coast, obtained using SBEACH model, were compared to eroded volumes obtained through the use of a simple predictor JAτ (Jiménez et al., 1993, 1997a). After this, a linear regression analysis was performed to obtain a simple parametrization of storm-induced eroded volumes, specific for the Catalan coast. Based on this approach, we have used the equation:

$$\Delta V = 2.9(JA\tau) + 6.73 = [2.9(|Deq - D)|^{0.5} tan\beta)\tau] + 6.73 \tag{4.1}$$

where τ is the storm duration, JA is a parameter characterising beach profile changes proposed by Jiménez et al. (1993), $D = (H/T * wf)$ is the dimensionless fall velocity parameter (Dean, 1973), *Deq* is its value at equilibrium (2.7 when wave conditions are specified at deep waters), tanβ is the beach slope, H is the wave height (here taken as H_s), *wf* is the sediment fall velocity and T is the wave period (here taken as T_p).

This equation coefficients (2.9 and 6.73) correspond to the ones obtained when JAτ values are calculated using maximum values of H_s and T_p. Moreover, when working with JAτ predictor it is important to bear in mind that the sign of $Deq - D$ indicates the type of change of the profile, where negative values indicate profile erosion. Due to this, the equation is only valid for storm and beach combinations resulting in erosive conditions.

It has to be considered that the pre-storm beach morphology, among other factors, will modulate the induced beach erosion (e.g. Morton, 2002). As a consequence, the approach adopted here is a simplification of the real beach response to wave action. However, the objective is not to reproduce the full response of the beach to the impact of a storm but to estimate an order of magnitude of the expected erosion. In consequence, equation 4.1 has been used to parametrize the eroded volume resulting

from the impact of storms at 6 different sectors and for 8 different beach types in each one of them.

Since the difference between *Deq* and *D* indicates whether or not erosive processes are occurring, special attention has been paid to identify cases in which annual maximum storms do not produce erosive changes in the profile according to JAτ predictor. In this sense, beach types 2, 3, 5 and 7 are the most affected ones. This is due to the fact that they represent the most reflective beaches (higher d_{50} and tanβ values), in which only higher storm intensities can mobilise sediment. However, these beach types are not present in all sectors (see Figure 4.17), in such a way that the coastal length corresponding to beaches in which not all the annual storms produce erosion is of little significance compared to the total length (only about 17%). Furthermore, the frequency of these type of events within the 63-yr series of annual storms differs highly depending on the selected sector and beach type, being types 2 and 3 the most affected. An example of *Deq-D* values obtained for all series in sector II, as well as their correspondent erosion potential series, are shown in Figure 4.18. In this case, only 10 years are considered (1947-1967). As it can be seen, three events without erosive storms have been identified (grey areas). The first and the last one, corresponding to 1949 and 1957, affect beach types 2 and 3, whereas in the second one, corresponding to 1953, types 5 and 7 are also included. When translated into erosion magnitudes, the eroded volume has been considered zero in all these cases.

Despite the fact that *Deq-D* is used to identify the type of morphological change that a certain storm can produce, to quantitatively evaluate erosion magnitude, additional variables such as beach slope and storm duration are considered. Consequently, when comparing both graphs in Figure 4.18, the series with lowest values of *Deq-D* does not necessarily correspond to the highest eroded volumes. Results indicate that the lowest values of *Deq-D* correspond to type 4 beaches, which is mainly explained by the fact lower grain sizes facilitate erosion. Despite this, when the eroded volume is analysed, the time series corresponding to type 4 beaches present medium values with respect to the other beach types. This highlights the important role of beach slope and storm duration to assess erosion magnitude. In this sense, as previously commented by Jiménez et al. (1993) and Mendoza and Jiménez (2006), the consideration of these two parameters significantly improve quantitative prediction of storm-induced eroded volume.

Coastal inundation is generally caused by a combination of high water levels (storm surges plus high tides) and wave action. To properly determine the total water level in probabilistic terms, a joint probability analysis of storm surges and wave run-up

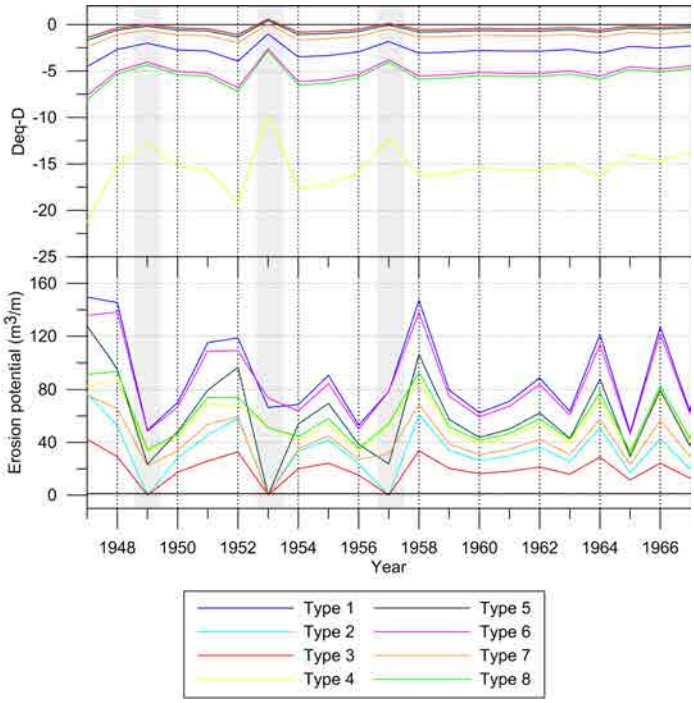

Figure 4.18: Representation of (Deq-D) and erosion potential for all beach types in sector III from 1947 to 1967. Grey zones identify cases in which annual maximum storm does not lead to erosive profiles.

should be needed. In spite of this, in this work we have only considered the wave-induced run-up to characterize inundation magnitude, because although storm-surges are not infrequent during Eastern storms in the Catalan coast (e.g. Jiménez et al., 1997b), their magnitude is much lower than wave-induced run-up (Mendoza, 2008).

Formally, this represents that the vulnerability to inundation here characterised will refer to the storm wave-induced component. Thus, the inundation hazard has been parametrized by using the wave-induced run-up at the storm peak by using the Stockdon et al. (2006) model, which is given by

$$Ru_{2\%} = 1.1 \left(0.35 tan\beta (H_s Lo)^{1/2} + \frac{[H_s Lo(0.563 tan\beta^2 + 0.004]^{1/2}}{2} \right) \tag{4.2}$$

where H_s is the deep water significant wave height, Lo is the deep water wave length associated to the wave peak period, T_p, and $tan\beta$ is the beach-face slope. This formula has been selected because it was derived specifically for beaches and it was adjusted by using only field data.

Because beach profiles usually present a change in the slope, with an inner part of the profile ($tan\alpha$) being milder than the one at the beach-face ($tan\beta$), a correction factor for the run-up following Van der Meer and Janseen (1995) has been considered. This correction factor, γ , accounts for the expected modification in the run-up as waves propagate over the inner part of the profile and it is given by

$$\gamma = tan\alpha/tan\beta \tag{4.3}$$

which is truncated to values within the interval [0.6, 1]. The final run-up magnitude is obtained by multiplying the value obtained for the beach-face slope (Equation 4.2) and the gamma coefficient (4.3).

Once the equations to parametrize both hazards are selected, inundation and erosion hazard time series, corresponding to the annual maximum storms, are built for each coastal sector and beach type. This will permit to directly assess spatial and temporal variations of storm-induced hazards over a period of about 60 years for different regions. As an example, Figure 4.19 shows obtained hazard time series for each representative beach type along sectors II and VI. As it can be observed, erosion magnitude varies significantly between these two sectors, being higher in the northern one, were at the same time variations between types of beaches are also larger than in sector VI. With respect to the events in which erosion magnitude corresponds to zero, a larger number of them are found in sector VI. In the case of inundation, these differences of magnitude between sectors and beach types are also present, yet much lower. Besides this, beach types 5 and 7 are not present in sector VI.

One of the aspects to be considered is that this analysis follows a conservative approach where a normal wave incidence is assumed. This means that in some cases, erosion and inundation will be overestimated, specially in beaches oriented towards the south or when they are partially sheltered from E-NE directions, which are the most important for storm waves.

Obtained inundation and erosion time series show a different temporal pattern. This highlights the importance of evaluating both processes in a separate manner so that, for a given storm event, the dominant one can be identified. Moreover, the relative variation in the hazard magnitude in function of beach morphology is also different. In this sense, run-up values are directly related to the beach-face slope of the beach, in such a way that reflective beaches (types 5, 1 and 2) present higher values of run-up. On the contrary, because erosion potential depends both on beach-face slope and sediment fall velocity, differences between beach types are not that simple

and depend on the combination of both properties.

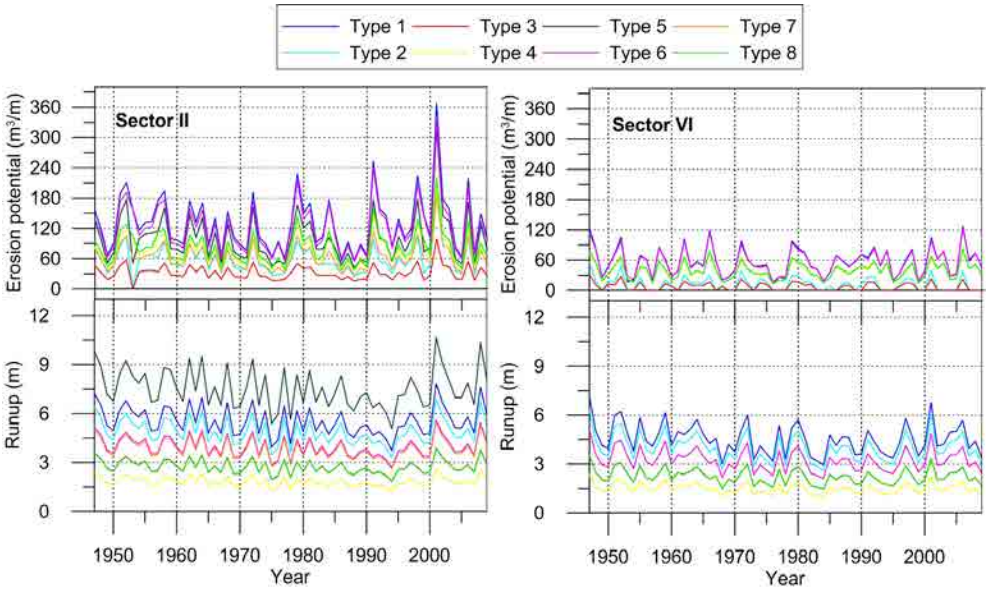

Figure 4.19: Hazards time series for each beach type at sectors II and VI.

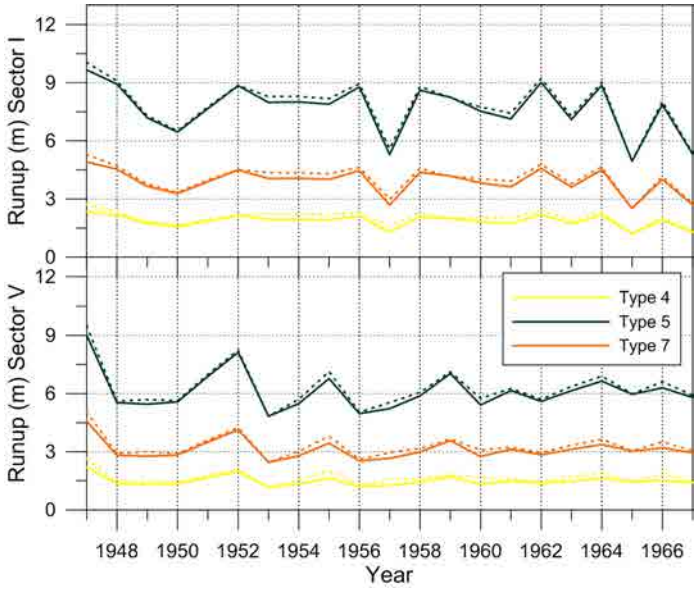

Figure 4.20: Run-up time series for three significantly different beach types with (dashed line) and without considering storm surge.

Even though run-up has been considered to quantify inundation magnitude, the assessment of storm surge contribution to this process has also been carried out. To this end, the aforementioned GOS dataset has been used to obtain series of maximum water level within each annual maximum storm and for each coastal sector. These values have been added to the run-up ones in order to evaluate the relative contribution of storm surge to inundation. Within this context, Figure 4.20 shows three 10-yr series of run-up and run-up plus storm surge (dashed line) corresponding to different beach types. As it can be clearly seen, storm surge magnitude results of little relevance compared to run-up values, and no differences between beach types are detected. At this point it has to be stressed out that this kind of approach does not reflect real conditions because maximum water levels are added to maximum wave heights, yet they do not always occur simultaneously. Although this approach results appropriate to the end of this analysis, a more detailed joint probability assessment should be considered in order to obtain more accurate quantitative estimations. This result is in agreement with the previous assumption on the quasi-negligible role of storm surge versus the run-up.

4.3.3 Hazard extreme probability distribution

Once hazards time series have been obtained, they are characterized in probabilistic terms. This has been done following the response approach (see e.g. Divoky and Mcdougal, 2006) in which the probabilities are directly assigned to the processes (hazards) and not to the drivers that generate them (storm). Such approach results especially appropriated when processes depend on more than one variable (H_s, T_p, duration) and particularly when this dependence differs between considered processes (e.g., see Figure 4.19). There exist several functions to define extreme probability distributions (see e.g. Prinos and Sanchez-Arcilla, 2008). Since in most cases we are working with series of annual maxima, the Generalized Extreme Value (GEV) distribution has been used, which at the same time encompasses three families of distributions: (i)Gumbell, (ii)Frechet and (iii)Weibull (see e.g. Coles, 2001; Doherty et al., 2011). As a result of fitting GEV distribution to the data, different hazard extreme probability distributions are obtained for each sector and beach type. This permits to assess the spatial variations in hazards intensity along different geographical regions and to compare them in a robust manner (see e.g. Jiménez et al., 2009).

However, a different methodology has been used to obtain extreme probability distributions of the aforementioned erosion series in which not all the annual maximum storms lead to erosive profiles. In these cases, a Peak-Over Threshold method has

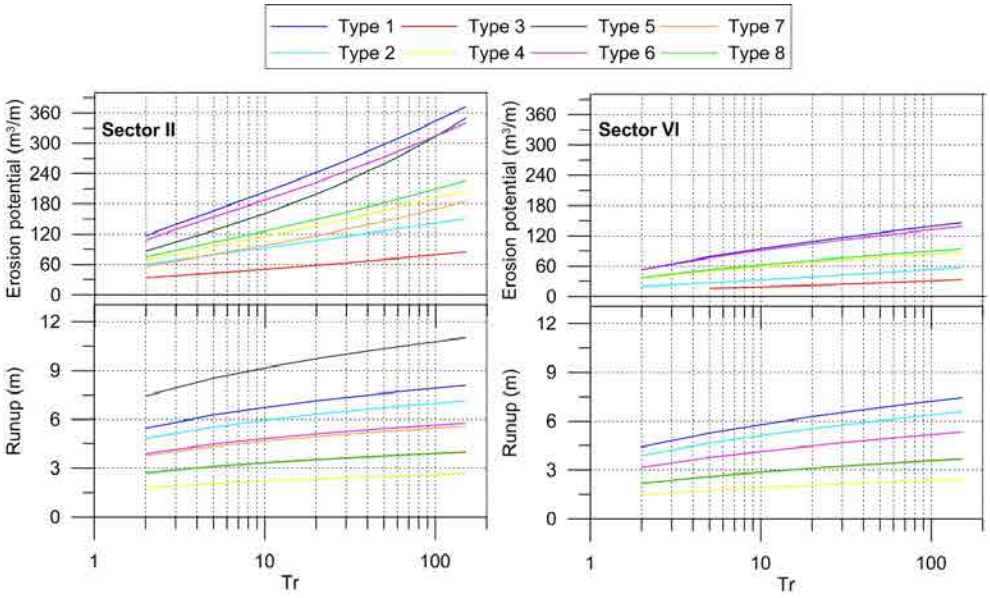

Figure 4.21: Erosion and inundation extreme probability distributions obtained at sectors II and VI, corresponding to each beach type .

been applied to obtain series that not only include the annual maximum storms but all of them. After this, they have been fitted into a Generalised Pareto distribution (GPD), which requires a threshold level definition (see Doherty et al., 2011). In this case, this threshold has been set to an eroded volume of 15 m^3, considering that in all the hazard series it represents at least the percentile 70. In addition, this volume would be translated into a beach retreat of 3 meters in about 60% of the studied coastline, which can already be considered significant. This approach, yet applied to very few cases, improves the fitting of the data by solving the inadequate number of erosive events obtained in some series when solely annual maximum storms are considered.

Figure 4.21 shows the extreme probability distributions obtained for each hazard at sectors II and VI. Results suggest again that the highest inundation intensity will potentially verify for the higher representative beach-face slope types (5, 1 and 2). On the other hand, the largest erosion for a given return period is related to beach types 1 and 6, being representative of intermediate to reflective beaches.

According to these results, beach type 1 seems to be one of the most affected in terms of erosion and inundation magnitudes. In spite of this, the beaches represented by this type only correspond to about 8% of the total considered coastline (18 km) and are not equally distributed within all sectors. Something similar happens with

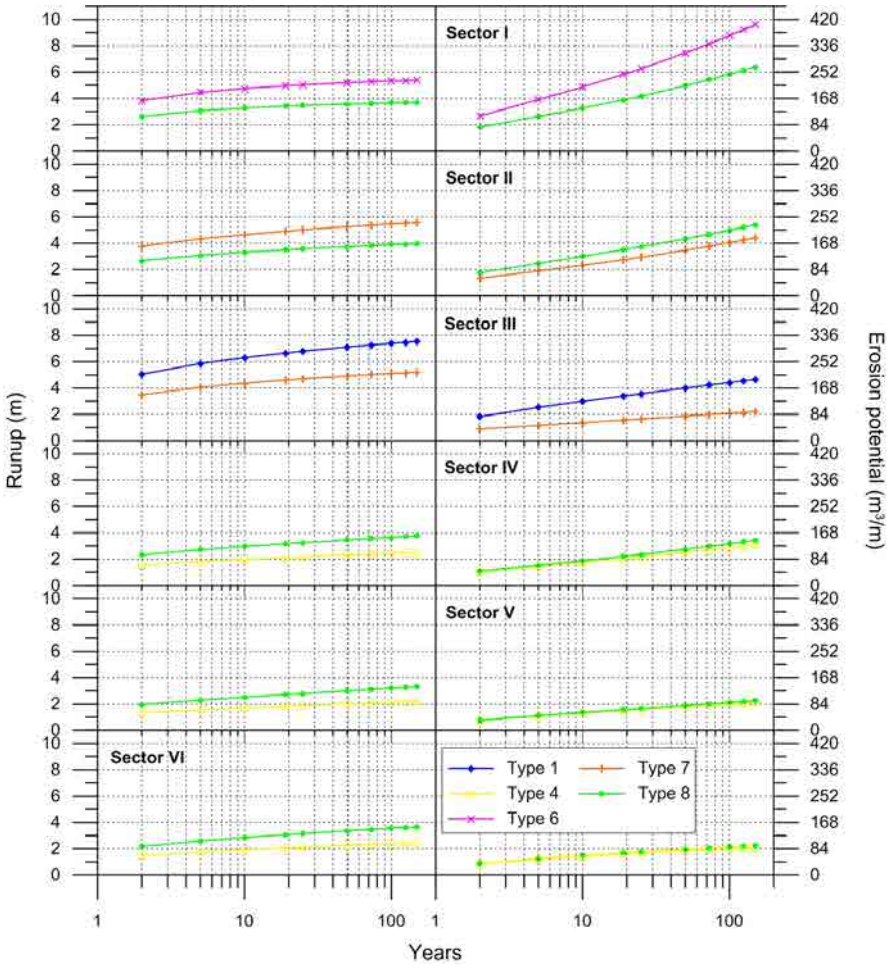

Figure 4.22: Erosion and inundation extreme probability distributions for each coastal sector corresponding to the two most frequent beach types in terms of coastal length.

type 5, for which the highest values of run-up are obtained. In this case it corresponds to about 2% (4 km) of the coastal length, and it is not present in sectors IV, V and VI. The lowest erosion magnitudes correspond to beach types 3 and 2, which represent 21% of the coastal length. In the case of inundation, the lowest run-up values are related to types 4 and 8, which are the most frequent (about 61% of the total length).

Figure 4.22 shows extreme probability distributions corresponding to the two most frequent beach types of all sectors. As observed, the highest magnitudes of erosion are found in the northern sector and correspond to beach type 6, whereas the southern sector is where the lowest values are obtained. In terms of inundation, the highest values are obtained in sector III and correspond to beach type 1, whereas again,

lowest values are found in the two southernmost sectors. It is important to stand out that the differences in magnitude between sectors are significantly higher for erosion, ranging from more than 300 m^3/m of erosion potential for a return period event of 50 years in sector I, to little less than 80 m^3/m in Sectors V and VI.

In summary, the obtained results reflect the ability of this method to quantify differences in hazards intensity –associated to a given return period– due to wave climate (coastal sector) and geomorphology (beach characteristics) contribution. At this point it has to be stressed out that higher values of hazard intensity do not necessarily imply higher vulnerability values. To obtain the last ones, the capacity of the coastal system to cope with hazards has to be taken into consideration. Despite this, such assessment provides the decision-maker with information about spatial variations of potential problems related to the magnitude of these two processes.

4.4 Vulnerability assessment

4.4.1 Introduction

The final step of the methodology consists of including the ability of the coastal system to cope with the induced impacts to quantify vulnerability. To do so, intermediate variables that compare the magnitude of the processes to beach characteristics that confer the ability to cope with them are evaluated. Once this is done, a vulnerability function is defined for each process resulting into a 5-category vulnerability index. Before arriving to this point, and considering the probabilistic approach of this methodology, a return period for the analysis needs to be selected.

4.4.2 Erosion and inundation vulnerability indexes

To finally assess coastal vulnerability to storm-induced inundation and erosion, the beach response capability has to be characterized. In the case of erosion, the parameter used as an indicator of the resilience of the beach is the beach width (W_{av}). Hence, the wider the beach is, smaller the probability to be fully eroded (and, in consequence, infrastructures in the hinterland to be exposed) will be. This is formulated in terms of the intermediate variable:

$$EV = \Delta x / W_{av} \tag{4.4}$$

in which Δx is the storm induced beach retreat and W_{av} is the average beach width. The beach retreat parameter has been obtained by dividing the eroded volume (Equation 4.1) by the depth of the eroded part of the profile (d_{er} in Figure 4.11), although a similar relationship to Equation 4.1 formulated for storm-induced shoreline retreat can also be applied (see Mendoza and Jiménez, 2006).

In this case, the sub-aerial depth of the eroded part of the profile is considered equal to 3 meters for all beaches. This criterion has been selected after performing an assessment using the beach profile numerical model SBEACH (Larson and Kraus, 1989; Wise et al., 1996) to reproduce beach behaviour in front of real storms. To do so, the model was fed with data from two different profiles of the Catalan coast: (i) a profile corresponding to sector III, with beach-face slope equal to 0.14 and 0.6 mm of d_{50}, and (ii) a very dissipative profile corresponding to the Ebre delta with a becah-face slope equal to 0.02 and 0.2 mm of d_{50}. These two profiles correspond to beaches within types 8 and 4 respectively (see Figure 4.15), which are the two most common in the study area. Moreover, wave data from 16 recorded storms corresponding to sector III and 19 corresponding to sector VI were used to run the model.

Figure 4.23 shows an example of the two pre and post storm profiles corresponding to the impact of the same storm (H_s= 4 meters). Despite differences between profiles, in both cases the depth of the eroded profile approaches 3 meters. As revealed by Figure 4.24, were all the obtained heights of the eroded part of the profiles are represented, this behaviour is similarly repeated in all SBEACH simulations. In fact, the averaged depth value considering all cases is 2.97 metres.

When considering inundation, the parameter used as a proxy of the resilience of the beach is the dune height or, if absent, the berm height. Thus, as higher the beach is the smaller the inundation will be. Consequently, the intermediate variable is expressed as:

$$IV = Ru/B_{max} \tag{4.5}$$

in which Ru is the run-up and B_{max} is the maximum of berm or dune heights.

It has to be mentioned that, even in the context of a steady forcing (storm climate), beach vulnerability could change due to a change in beach morphology (width and elevation). To account this potential variation, the coastal database needs to be updated (periodically and/or after the impact of a significant event) to properly reflect real beach characteristics.

Final vulnerability is formulated in terms of these two intermediate variables by

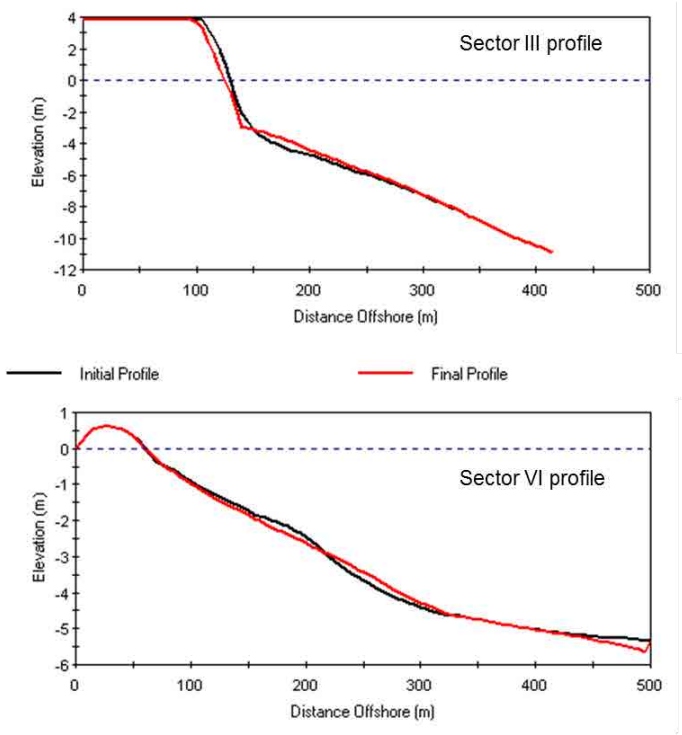

Figure 4.23: Pre and post storm profiles obtained using SBEACH and corresponding to an approximately 4m wave height storm.

means of the functional relationship shown in Figure 4.25. As it can be see, it is scaled in a range from a minimum 0 value (optimum state) to a maximum of 1 (failure state), and divided into 5 qualitative classes (very low, low, medium, high, very high). Here, we assume that vulnerability linearly depends on the intermediate variables with the slope of the curve being a function of the safety level of the analysis. Thus, more conservative analyses (indicating larger vulnerabilities for the same hazard conditions) will have steeper curves and vice versa.

The safety level of the analysis depends on the selected value of the intermediate variables at the end of the range. These vulnerability maximum and minimum threshold can be defined in terms of the three main beach functions: protection, recreational and natural. Because storms mainly occur during winter and fall seasons, and their impact can produce personal and public properties damage as well as human losses, the protection function of the beach has been considered in this work.

Table 4.5 defines the selected minimum and maximum vulnerability thresholds for both processes. In the case of erosion, the maximum vulnerability value (1) has been

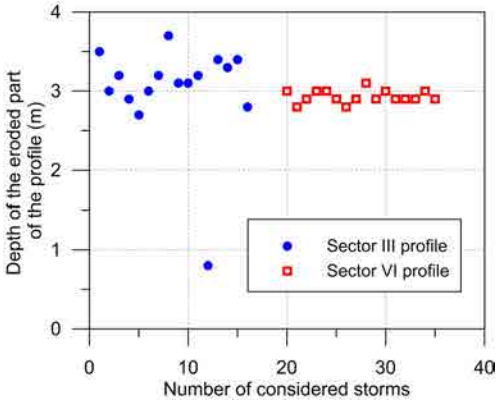

Figure 4.24: Depth of the eroded part of the profiles corresponding to all SBEACH simulations.

fixed as the situation in which the beach width equals the minimum beach width (W_{Vm}) plus the storm-induced beach retreat (Δx). The minimum beach width is defined in this case as the required minimum value to maintain the beach operative and/or to avoid the direct exposure of the hinterland to the wave action. This value can be used as a safety margin to guarantee a minimum width to face the impact of multiple storms or, as assumed in this work, it can be set to the minimum width to let machinery work along the beach to repair damages in infrastructures in the hinterland (e.g., to repair promenades). According to this, we have selected a value of 5m to let trucks and bulldozers operate after storm-induced damages.

Regarding to the function thresholds, the minimum vulnerability (0) will occur when the beach width equals the minimum beach width (W_{Vm}) plus the induced beach retreat (Δx) plus two times the beach retreat associated to a 75% probability of occurrence storm ($\Delta x_{0.75p}$). In other words, the maximum threshold represents the situation in which, when a storm-induced hazard corresponding to the selected return period occurs, the beach disappears almost completely, being unable to protect the hinterland from any other possible storm. On the contrary, the minimum threshold defines a situation in which, even though a hazard corresponding to the selected return period occurs, beach width is still large enough to face two times the beach retreat associated to a more probable hazard (75% of occurrence probability).

Figure 4.26 shows an example of erosion vulnerability thresholds that define failure and optimum beach configurations. The optimum configuration is the one that leads to vulnerability lower or equal to zero for a determined storm, whereas the failure configuration corresponds to vulnerability values equal or higher than 1.

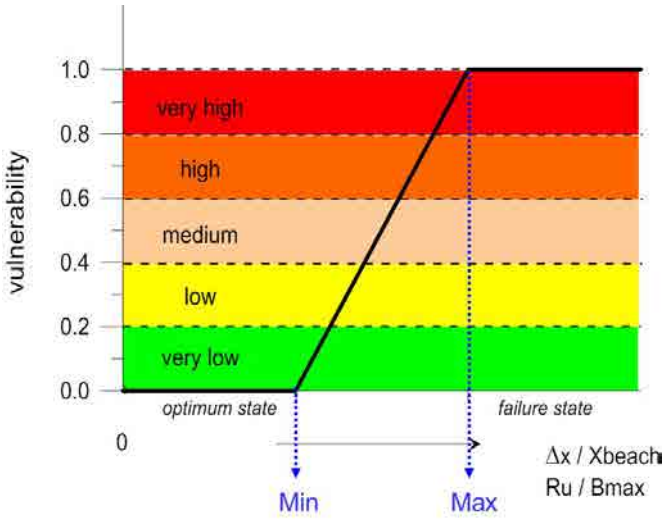

Figure 4.25: Vulnerability function.

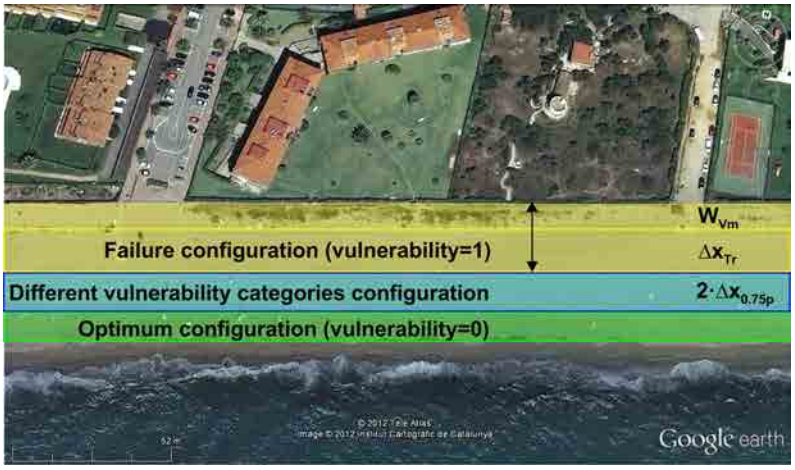

Figure 4.26: Example of erosion vulnerability thresholds and definition of optimum and failure states.

Table 4.5: Erosion and inundation vulnerability function limits (thresholds).

Process	Minimum threshold	Maximum threshold
Inundation	$B_{max} = 2Ru$	$B_{max} = Ru - 2$
Erosion	$W_{av} = W_{min} + \Delta x_{Tr} + (2 * \Delta x_{0.75p})$	$W_{av} = W_{min} + \Delta x_{Tr}$

In terms of inundation, the minimum value (0) is defined by the situation in which the run-up magnitude equals half of the actual berm height, whereas the maximum value (1) will occur when the run-up exceeds by two meters the maximum berm height. These values have been selected arbitrarily as a function of the characteristics of the study area and, for the maximum case, they represent overtopping conditions with significant water volumes flowing to the hinterland. To apply this methodology in other areas or for other objectives, these values should be adapted to specific conditions and/or requirements of the area or function to be analysed.

4.4.3 Return period selection

The selection of the return period (Tr) used in the vulnerability assessment depends on the level of safety required by the decision-maker, which at the same time depends on the importance of the hinterland. According to this importance, a probability of occurrence, R, is selected and then the corresponding return period is estimated for a given time period of concern, L. The relationship between these three variables can be expressed by (Borgman, 1963):

$$R = 1 - \left(1 - \frac{1}{Tr}\right)^{L} \tag{4.6}$$

As an example of the criteria to determine the variables involved in this equation, the Spanish Ministry of Public Works recommends a minimum period of concern, L, of 25 years for coastal protection and nourishment works. This value has been considered appropriate for this analysis assuming that beaches are protecting the hinterland from storm impacts and, therefore, they are behaving as coastal protection works. The same study remarks that, at most of the Mediterranean beaches, the failure of the beach regarding its protection function will not likely cause human losses and it will have an economic repercussion ranging from low to medium, which correspond to maximum admissible probabilities, R, of 0.5 and 0.3, respectively.

The substitution of these values in Equation 4.6 results in return periods between 37 and 71 years respectively. As a consequence, an approximated mean return period of 50 years has been selected as the main one to assess storm induced vulnerability .

4.5 Results

4.5.1 Current vulnerability of the Catalan coast

Once the return period of the analysis is selected and vulnerability functions are defined, values of vulnerability to storm-induced erosion and inundation for each beach can be obtained. To do so, information about beach geomorphology and vulnerability has been introduced into a GIS database in such a way that results can be better interpreted. Moreover, this information can be easily combined with other territorial information such as land use in case that further investigation on issues as, for instance, land risk has to be conducted.

Figure 4.27 shows each beach vulnerability considering both hazards, providing a general vision of how vulnerability is spatially distributed. In general, an important spatial variability can be appreciated in both cases, specially for inundation. However, in the case of erosion, results suggest that the two extreme categories are the most frequent. Despite the fact that the number of beaches that fall into the highest erosion vulnerability category (red) is higher, in terms of coastal extension, the most part of the coastline corresponds to the lowest category (blue). Note that empty spaces represent rocky coast, gravel beaches, engineered areas such as ports and marinas and a few other beaches that have not been considered due to lack of data. Although beaches represent about 270 km of the Catalan coastline, hereinafter vulnerability results expressed in terms of percentage of (Catalan/sector/province/*comarca*) coastline will always refer to the total length of sedimentary coastline considered in this work: 218.65 km.

With respect to global results, Figure 4.28 shows the number of beaches and percentage of coastline corresponding to each erosion vulnerability category for the Catalan coast, associated to a 50-yr return period. Here, two different beach widths have been used to obtain the intermediate variable: (i) the average (W_{av} in Equation 4.4) and (ii) the minimum (W_{min}). The last one must not be mistaken for the before mentioned minimum beach width, W_{Vm}, which was used to determine erosion vulnerability thresholds. In this case, it does not refer to an arbitrary value, but to real beach dimensions.

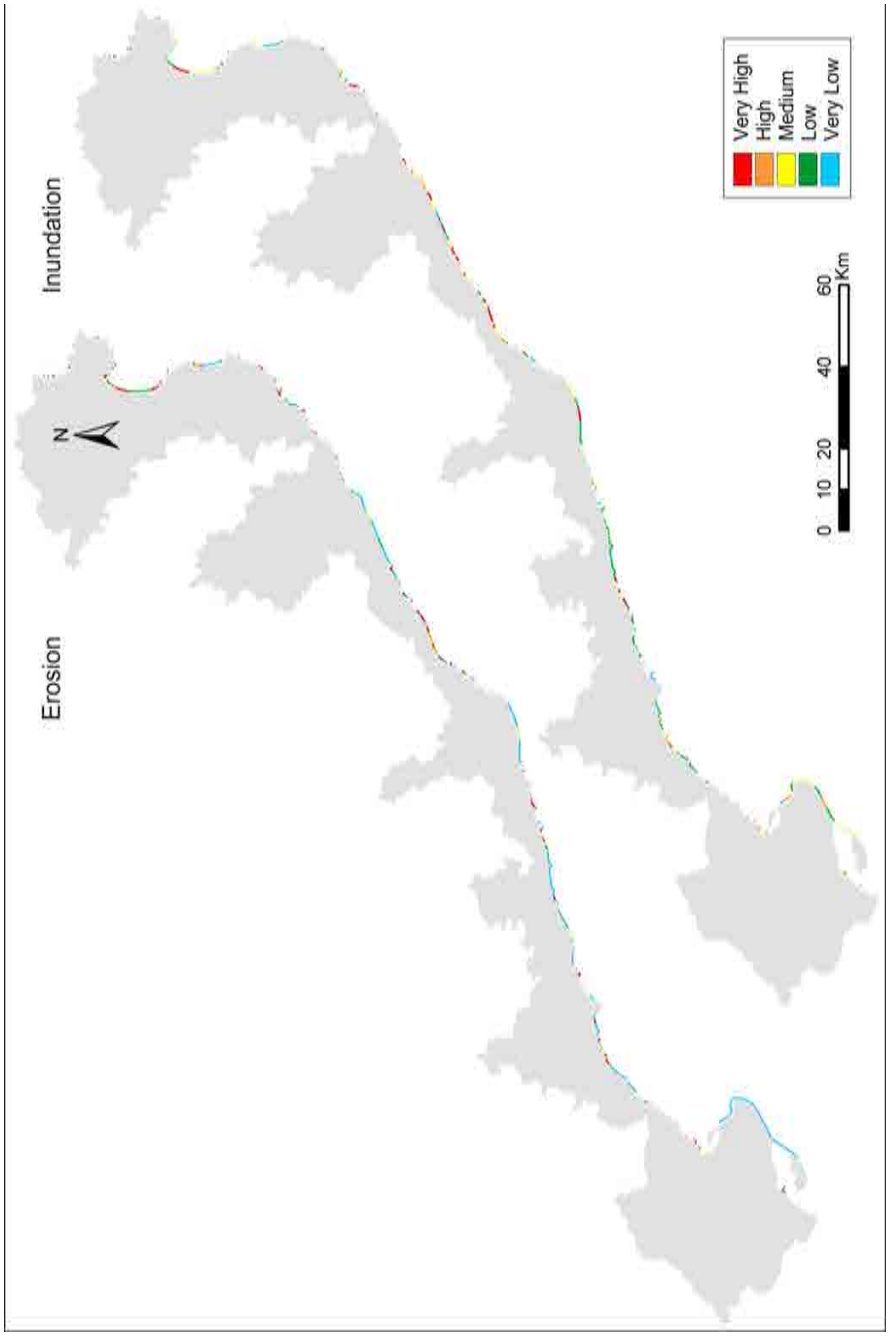

Figure 4.27: Vulnerability to storm-induced erosion and inundation of all the beaches within the study area. Tr= 50 years.

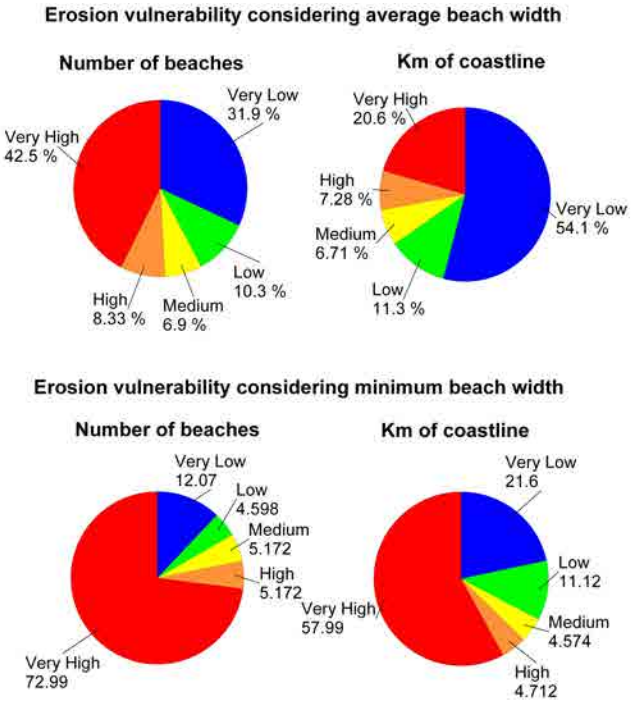

Figure 4.28: Percentage of beaches and coastline corresponding to each category of vulnerability to erosion for a 50-yr return period. Upper results have been calculated considering the average beach width (W_{av}) to define the intermediate variable, whereas the minimum (W_{min}) has been used to obtain the bottom ones.

In this sense, the minimum beach width, W_{min}, is used to detect all beaches in which punctual and very local problems related to erosion may arise due to irregular beach configurations. On the other side, when the average beach width is used, some vulnerable points within beaches that in general present low or medium vulnerability may be unnoticed. In spite of this, the use of the averaged parameter will serve to assess the "representative" vulnerability of the beach. Therefore, this parameter will be used in most cases, unless otherwise specified.

As expected for coasts where beaches present an alongshore difference in beach width, significant differences in erosion vulnerability are found. When the average width is considered, results indicate that 51% of the beaches fall into high or very high vulnerability categories, although they only represent about 28% of the studied coastline. In terms of coastal extension, the lowest vulnerability category results the most important (54.1%). When the minimum beach width is considered, the percentage of beaches corresponding to the two most vulnerable categories increases up to 78% and represent about 63% of the coastline. This could be interpreted as

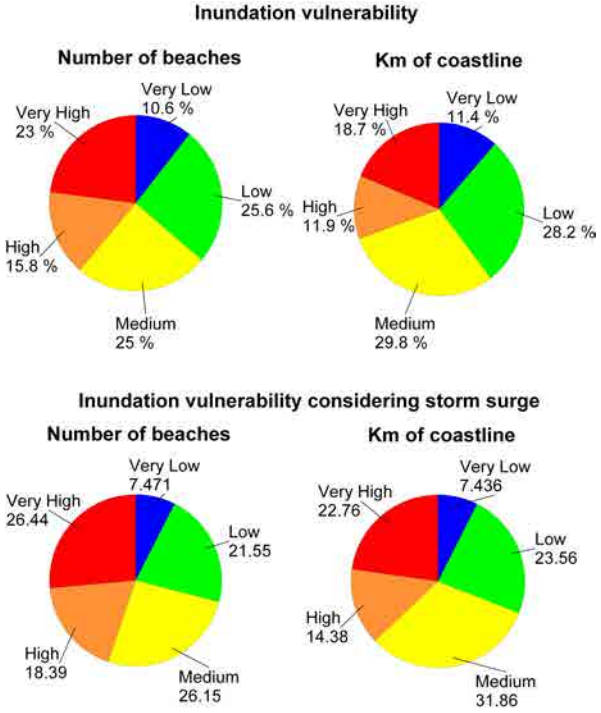

Figure 4.29: Percentage of beaches and coastline corresponding to each category of vulnerability to inundation for a 50-yr return period. Upper results have been calculated considering only run-up to define inundation magnitude, whereas bottom ones include also storm surge contribution to inundation magnitude.

that although beaches are, in general terms, able to cope with induced erosion, they have weak points susceptible to be significantly impacted.

Vulnerability results obtained for inundation under the same conditions are shown in Figure 4.29. Again, two different approaches have been adopted to define the hazard magnitude. The first one only considers run-up, whereas in the second one the storm surge contribution is also accounted. As expected due to the small differences in hazard magnitude, very little differences between both results can be appreciated. Therefore, as in the case of erosion, the second approach will not be considered unless otherwise specified. When the first approach is considered, about 39% of the beaches fall into the two worst vulnerability categories, representing approximately 31% of the coastline. Obtained results also indicate a more heterogeneous distribution of the vulnerability categories in the case of inundation, although the total coastal length corresponding to the most vulnerable category is similar in both cases (45 km and 41 km for erosion and inundation respectively).

In order to better assess the wave climate contribution to vulnerability, results have also been grouped for each sector (see Figure 4.30). In the case of erosion, sector I presents the largest length of beach corresponding to high and very high vulnerable beaches, opposite to what can be observed in sector VI (16 km and 4 km respectively). The same results assessed in terms of percentage of coastline reveal a clear decrease in vulnerability from northern to southern sectors.

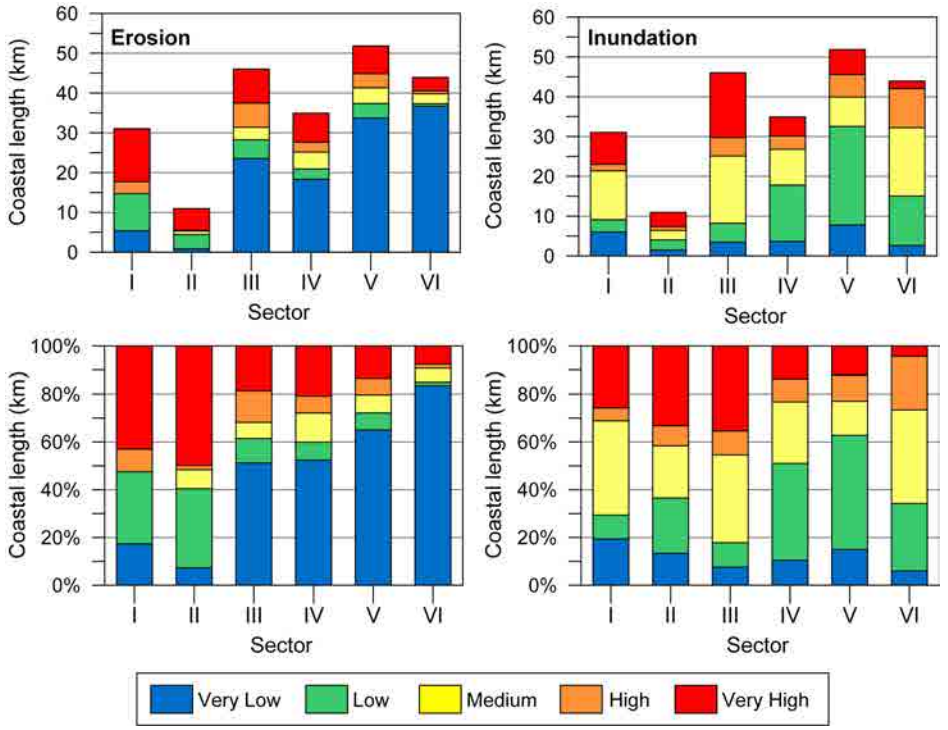

Figure 4.30: Length (top) and percentage (bottom) of coastline per sector corresponding to each category of vulnerability to storm-induced erosion and inundation for a 50-yr return period.

The fact that northern sectors result more vulnerable to storm induced erosion than southern ones has to do with the combination of wave climate and beach characteristics of each sector. In this specific case, sectors I and VI (the most and least vulnerable ones) present similar average beach widths of 40 and 42 meters respectively, which reveals little contribution of this variable to the overall vulnerability. This occurs for extremely high values of erosion magnitude (44.6 meters of mean beach retreat in sector I compared to 18.5 meters in sector VI), in which case the role of beach width as a measure of the system ability co cope with the impact results little significant.

Referring to inundation, results point at sector III as the most vulnerable, with a total of 21 km of coast falling into the two highest vulnerability categories (52% of its coastline). On the other hand, the three southernmost sectors result the least vulnerable, being sector V the one presenting the largest coastal length corresponding to the two lowest vulnerability categories. In addition, and corresponding to what has been previously observed in global results, intermediate categories result much more frequent than in the case of erosion.

Another interesting interpretation of the vulnerability results is in terms of the different beach types existing in the study area. In this sense, beach types 6 and 1 result the most vulnerable to erosion. Of the total coastal length occupied by those beach types, 83% and 55% result high or very high vulnerable to erosion respectively, which represent 18.2 km and 9.9 km of coastline. On the other hand, the highest percentages of coastline corresponding to the lowest vulnerability class correspond to types 3 and 4, with 71% and 78% respectively. These percentages are also significant in the case of types 2, 7 and 8 with values of 61%, 57% and 51% respectively. Considering that beach types 4 and 8 are the most common along the Catalan cost, these results corroborate the ones presented in Figure 4.28, where the coastal length corresponding to very low vulnerable beaches is clearly superior to the one representing very high vulnerability.

When referring to inundation, beach types 5 and 1 clearly stand out. All beaches classified within type 5 fall into the highest vulnerability category. Nevertheless, its impact on global vulnerability is low because it is the most unusual beach type in terms of coastal extension. At the same time, 96% of the coastline occupied by type 1 beaches results very high vulnerable to erosion. This is due to the fact that these two beach types are the ones with major beach slopes, being therefore related to elevated run-up levels.

Finally, although the results presented to this point are obtained for a 50-yr return period, an analysis of vulnerability related to other occurrence probabilities has also been performed (see Figure 4.31). Thus, 10-yr, 25-yr, 50-yr and 100-yr return periods have been considered. As expected, results indicate that the length of coastline corresponding to the two most vulnerable categories increases as the return period does so. The increasing rate appears to be similar for both hazards, being the difference between 50-yr and 100-yr return periods the least significant. Furthermore, the coastal length corresponding to the two worst categories is always larger for inundation than for erosion.

Figure 4.32 presents vulnerability results for different return periods in terms of percentage of coastline corresponding to each vulnerability category. At first sight, the same pattern is detected for both hazards: vulnerability increases for major return periods while the percentage of coastline corresponding to the lowest vulnerability category decreases. If the highest return period is considered (100 years), about 35% of the coastline results high or very high vulnerable to erosion, whereas these same categories represent about 30% of the total coastal length in the case of inundation. Finally, it has to be pointed out that vulnerability associated to the lowest return period event (10 years) can already be considered significant as it results in 15% to 20% of the coastline classified as high or very high vulnerable to storm-induced inundation and erosion respectively.

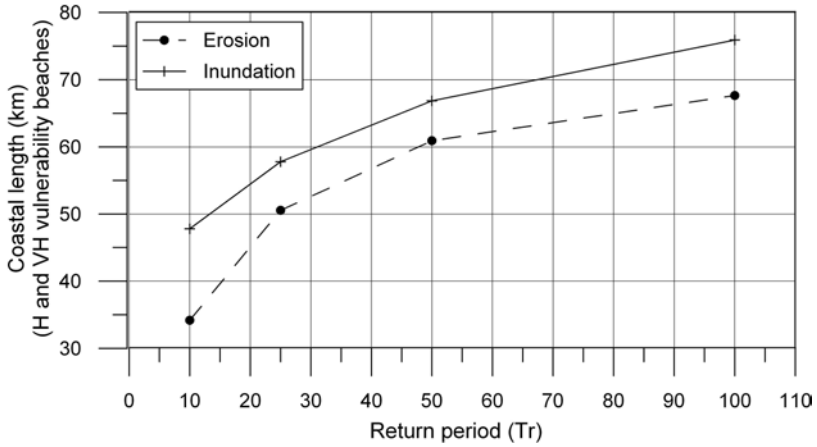

Figure 4.31: Length of coastline classified as high or very high vulnerable to storm-induced erosion and inundation for different return periods. Total coastal length: 218.65 km.

4.5.2 Vulnerability at different administrative scales

Although global results at beach scale determine the overall state of the coast in terms of its vulnerability to inundation and erosion, an analysis considering the existent administrative coastal units permits to identify the potentially most affected ones. Within this context, vulnerability results have been interpreted considering two administrative territorial units: provinces and *comarcas*. Providing this kind of information to decision-makers can help them organize the available resources to adopt adaptation or mitigation strategies in an effective way.

Erosion vulnerability results at province scale are presented in Table 4.6. As in

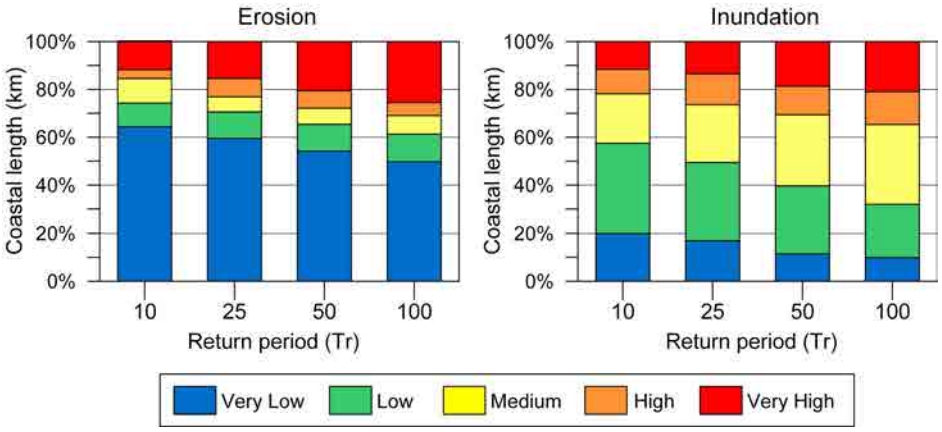

Figure 4.32: Percentage of coastline corresponding to each category of vulnerability to storm-induced erosion and inundation for different return periods.

the previous section, unless specified otherwise, result are always associated to a 50-yr return period. If only the two extreme vulnerability categories are considered, Tarragona is the least vulnerable province, with 73% of its coastline classified as very low vulnerable (70.38 km). This can be explained by the fact that long and wide dissipative beaches are very frequent within this province, specially in the Ebre delta region (see Figure 4.17). On the opposite end, Girona stands out as the most vulnerable province with 39% of its coastline corresponding to very high vulnerable beaches (19.31 km). An interesting fact is observed in the case of Barcelona, where the number of beaches belonging to the highest and lowest vulnerability categories is identical, yet in the second case it corresponds to twice the coastal length.

With respect to inundation (see Table 4.7), results suggest that Barcelona has the largest length of coastline occupied by very high vulnerable beaches. In spite of this, when assessed in relative terms, the percentage of coastline classified within the highest category is slightly higher in Girona, with 28% in front of 26% obtained in Barcelona. In the case of Tarragona, this percentage results much lower (9%). To conclude, results point at Girona as the province that is potentially most vulnerable to both hazards, with Barcelona presenting similar results in the case of inundation.

Figures 4.33, 4.34 and 4.35 show the coastal length corresponding to each vulnerability category for each *comarca* located within the northern, central and southern coastal provinces respectively. In order to simplify the representation, each *comarca* has been enumerated from North (1) to South (12). In addition, vulnerability results expressed in relative terms with respect to each *comarca* coastal length are also shown in Figure 4.36.

Table 4.6: Erosion vulnerability results obtained for each coastal province considering the average beach width.

	Number of beaches			Km of coastline		
Vulnerability	Girona	Barcelona	Tarragona	Girona	Barcelona	Tarragona
Very Low	14	38	59	10.21	37.81	70.38
Low	10	12	14	13.62	6.71	4.33
Medium	5	5	14	1.30	6.95	6.43
High	8	11	10	4.69	6.93	4.30
Very High	66	38	44	19.31	15.36	10.33
TOTAL	103	104	141	49.13	73.76	95.76

Table 4.7: Inundation vulnerability results obtained for each coastal province without considering storm surge.

	Number of beaches			Km of coastline		
Vulnerability	Girona	Barcelona	Tarragona	Girona	Barcelona	Tarragona
Very Low	10	13	14	7.47	7.09	10.35
Low	19	22	48	6.04	18.51	37.21
Medium	27	28	32	19.16	21.38	24.59
High	14	18	23	2.86	7.63	15.44
Very High	33	23	24	13.60	19.15	8.17
TOTAL	103	104	141	49.13	73.76	95.76

In terms of erosion, results suggest that the northernmost *comarca* (Alt Empordà (1)) is the most vulnerable, with more than 50% of its coastline falling into the highest vulnerability category (12 km). Furthermore, medium and very low vulnerability categories are not present in this *comarca*. On the contrary, Baix Llobregat (6), which is only composed by 3 beaches, is the only one in which the two highest vulnerability categories are not present. The highest values of coastal length corresponding to low and very low vulnerable beaches are found in Maresme (4) and Montsià (12), with 20 km and 23 km respectively. The same results evaluated in terms of percentage of coastline clearly point at Baix Penedès (8) and Montsià (12) as the least vulnerable *comarcas*, with 94% and 79% of its coastline corresponding to the two lowest categories.

With respect to inundation, Maresme (4) appears to be the most vulnerable *comarca* with a total of 14 km of very high vulnerable coastline (37% of its total length). In this sense, Alt Empordà (1) also stands out with 8 km of coastline classified into the same category, opposite to Montsià (12) and Garraf (7), in which this value decreases to 0.3 km and 0.5 km respectively. Results expressed in percentage of coastline

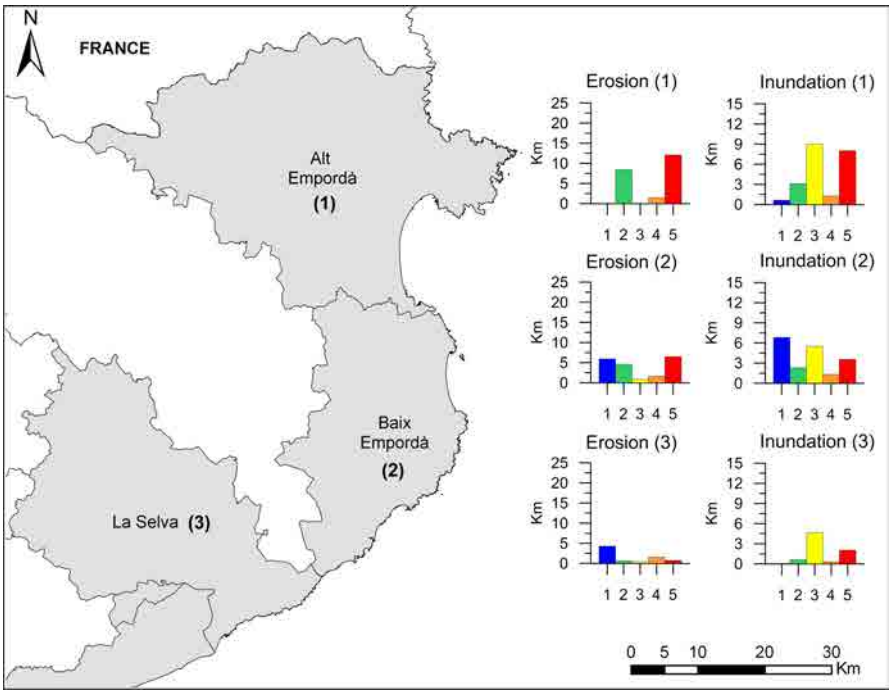

Figure 4.33: Length of coastline per *comarca* corresponding to each category of vulnerability to storm-induced erosion and inundation for a 50-yr return period. Results referred to the *comarcas* located within Girona province. Vulnerability categories range from 1 (very low) to 5 (very high).

also highlight Baix Llobregat (6) and Baix Penedès (8) as low vulnerable *comarcas*, since they present the highest percentages of coastline classified within the two lowest categories (67% and 81% respectively).

To conclude with the assessment at *comarca* scale, Table 4.8 shows the percentage of coastline corresponding to the two highest erosion and inundation vulnerability categories. At first sight, a much higher spatial variability is observed than when results are assessed at sector scale, so that the previously detected uniform and clear decrease in erosion vulnerability from North to South is not observed here. As observed, it can be concluded that Alt Empordà (1) and Garraf (7) are the most vulnerable *comarcas* in terms of erosion, opposite to Baix Llobregat (6) and Montsià (12). With respect to inundation, Maresme (4) and Baix Ebre (11) are the most vulnerable *comarcas*, opposite to Garraf (7), Baix Penedès (8) and Montsià (12). Furthermore, it has to be mentioned that in this study we are not considering additional coastal processes such as overtopping, which results specially important in low-lying areas.

Figure 4.37 shows a detailed example of erosion vulnerability at beach scale corre-

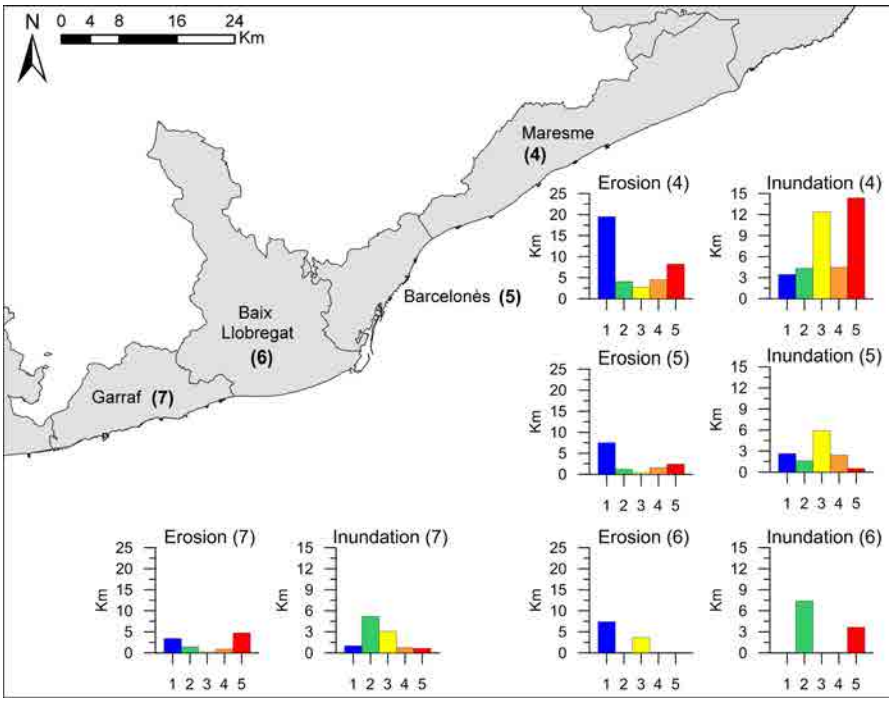

Figure 4.34: Length of coastline per *comarca* corresponding to each category of vulnerability to storm-induced erosion and inundation for a 50-yr return period. Results referred to the *comarcas* located within Barcelona province. Vulnerability categories range from 1 (very low) to 5 (very high)

sponding to three *comarcas* that belong to different coastal provinces: Alt Empordà (1), Garraf (7) and Baix Penedès (8). The last one, which belongs to the southernmost coastal province, results the second less vulnerable *comarca* to erosion, after Montsià (12). Note that the very low vulnerability observed in the southernmost *comarca* is mainly due to the use of the average beach width to calculate vulnerability. In fact, there are specific points in the Ebre delta in which barrier breaching usually occurs as a consequence of storm impacts. However, to take into account these situations, the vulnerability assessment should be performed considering the minimum beach width. On the other side, an important number of high and very high vulnerable beaches can be observed in Alt Empordà (1), which is also the most vulnerable *comarca* in terms of percentage of coastline corresponding to the two worst categories. Lastly, although Garraf (7) is the second most vulnerable *comarca*, it presents a higher spatial variability, stressing again the important contribution of beach geomorphology to the overall vulnerability.

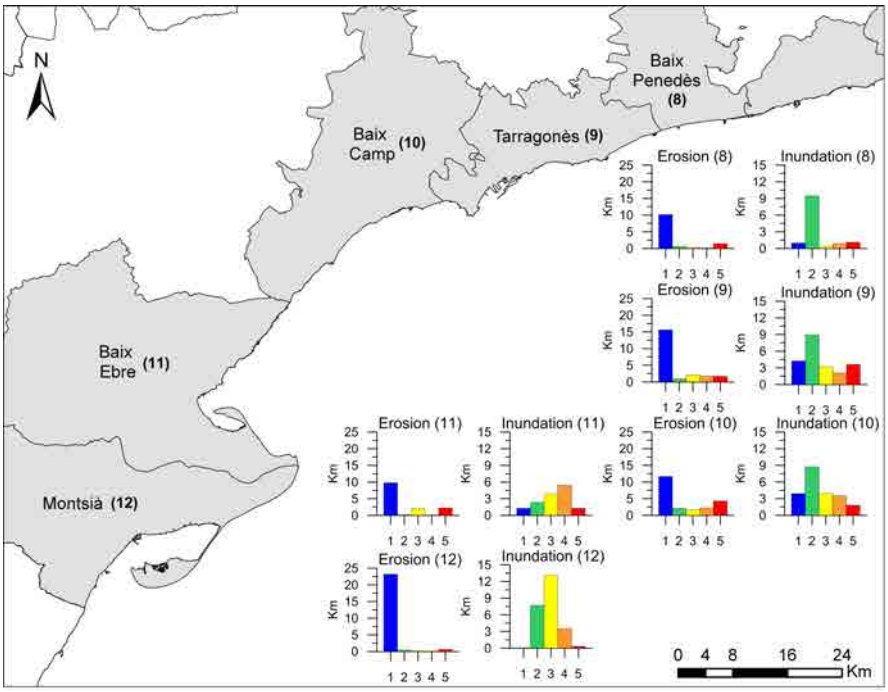

Figure 4.35: Length of coastline per *comarca* corresponding to each category of vulnerability to storm-induced erosion and inundation for a 50-yr return period. Results referred to the *comarcas* located within Tarragona province. Vulnerability categories range from 1 (very low) to 5 (very high)

Table 4.8: Percentage of coastline per *comarca* classified as high (H) or very high (VH) vulnerable to storm-induced erosion and inundation. Tr= 50 years.

Comarca	length (km)	%H+VH Erosion	%H+VH Inundation
Alt Empordà (1)	21.98	61.68	42.11
Baix Empordà (2)	19.51	41.58	24.97
La Selva (3)	7.63	30.46	30.53
Maresme (4)	39.01	32.60	48.26
Barcelonès (5)	13.09	30.37	22.37
Baix Llobregat (6)	11.03	0	33.05
Garraf (7)	10.63	52.71	12.99
Baix Penedès (8)	12.81	13.03	15.50
Tarragonès (9)	22.14	15.66	25.85
Baix Camp (10)	21.99	29.80	24.39
Baix Ebre (11)	14.17	15.68	47.30
Montsià (12)	24.65	2.91	15.57

To better explore such spatial variability, Figure 4.38 presents the results of erosion vulnerability obtained for the central and northern parts of Maresme (4) considering two different beach widths: (i) the average (inshore line) and (ii) the minimum (offshore line). As it can be observed, vulnerability increases significantly from the first one to the second. In general, when going over the coast from north to south, all beaches that precede a port or marina result little vulnerable to erosion, opposite to what happens to beaches located immediately after the same structure. This is explained by the direction of the main longshore sediment transport (LST), which goes from NE to SW, turning the structures that have been built along the coast into sediment traps that interfere with the natural sediment supply of beaches around them.

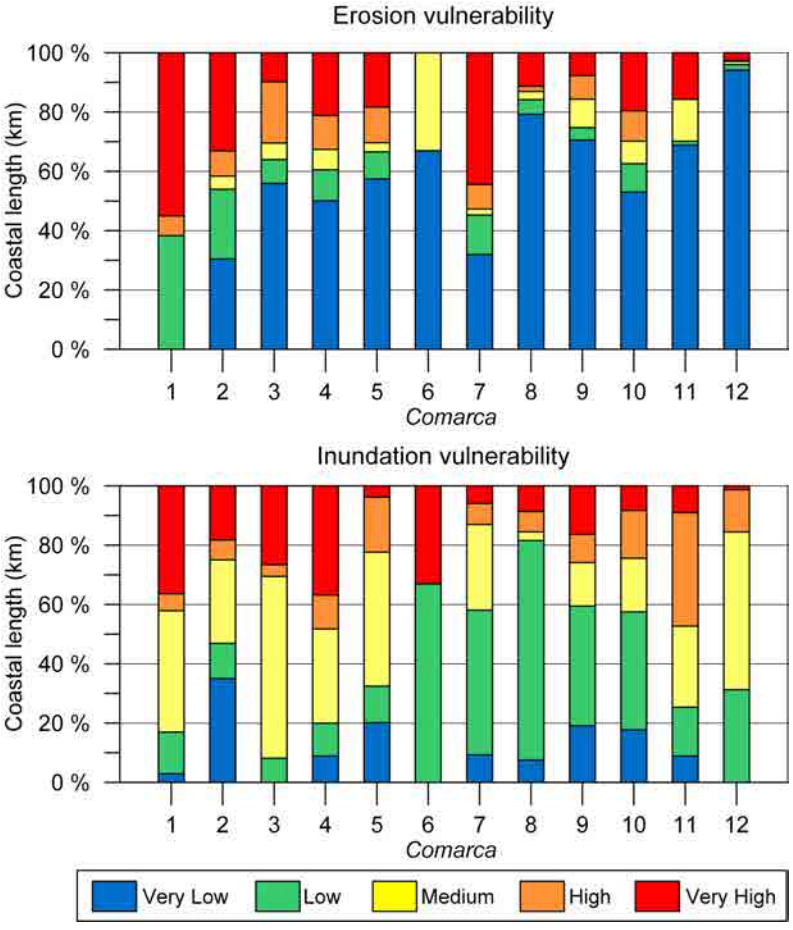

Figure 4.36: Percentage of coastline per *comarca* corresponding to each category of vulnerability to storm-induced erosion and inundation for a 50-yr return period.

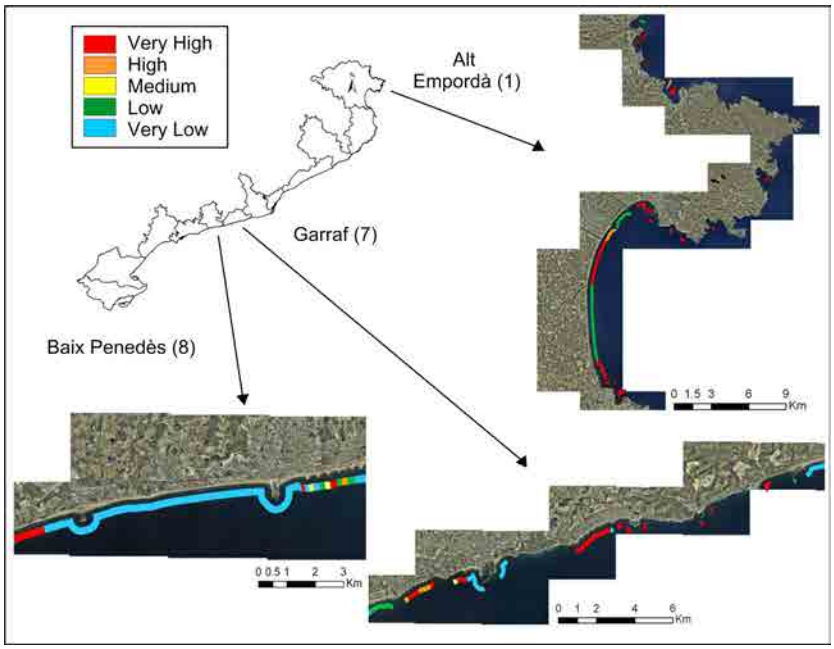

Figure 4.37: Spatial representation of erosion vulnerability results obtained for each beach within three coastal *comarcas*. Tr= 50 years.

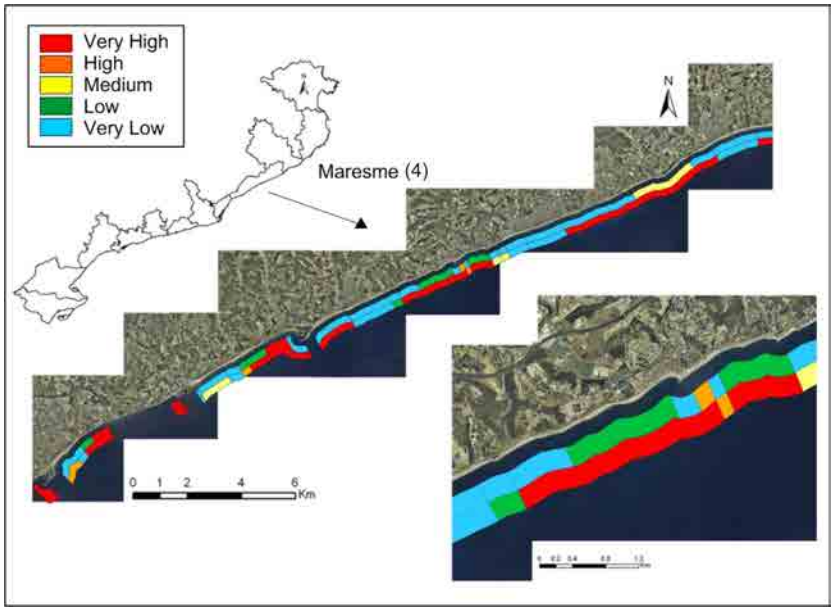

Figure 4.38: Spatial representation of erosion vulnerability results obtained for each beach within Maresme (4). Comparison of results obtained considering the averaged beach with (inshore line) and the minimum beach width (offshore line). Tr= 50 years.

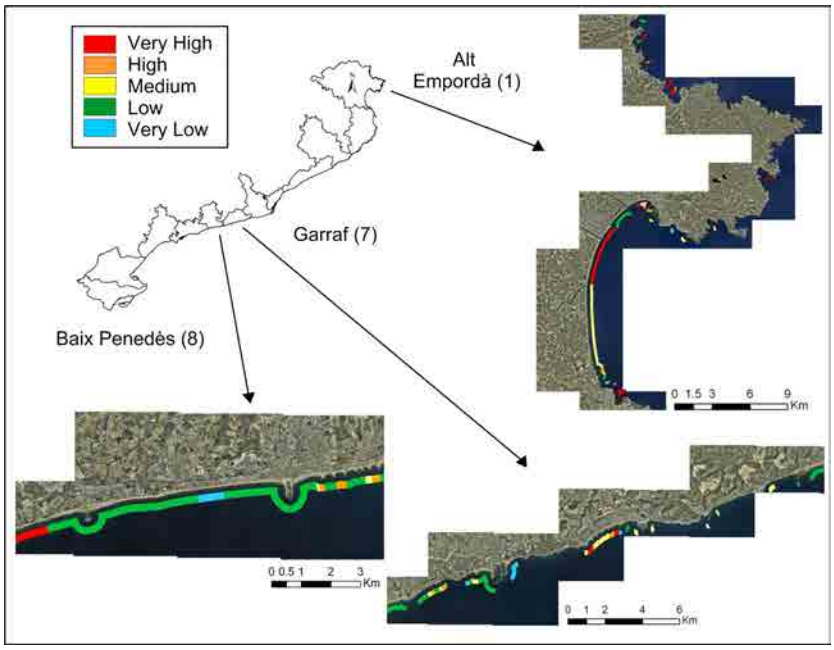

Figure 4.39: Spatial representation of inundation vulnerability results obtained for each beach within three coastal *comarcas*. Tr= 50 years.

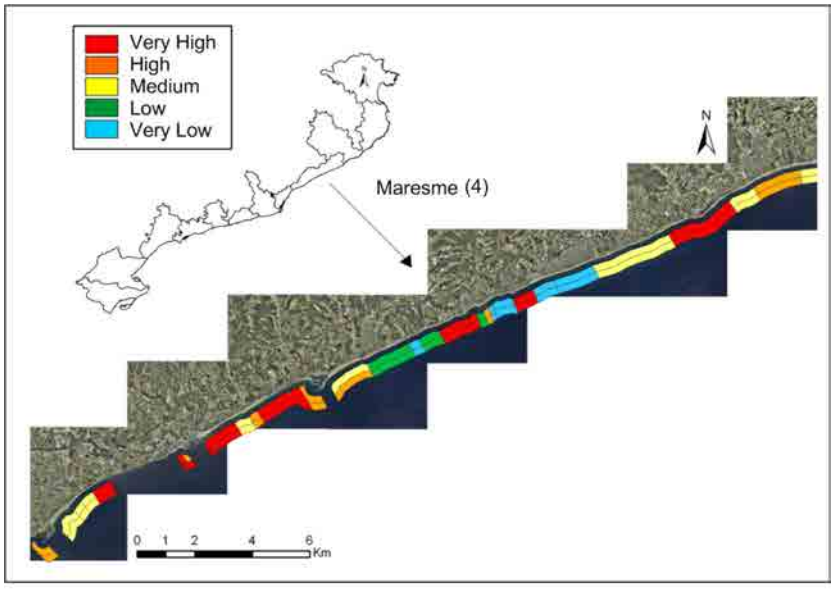

Figure 4.40: Spatial representation of inundation vulnerability results obtained for each beach within Maresme (4). Comparison of results obtained with (inshore line) and without considering the run-up (offshore line). Tr= 50 years.

The spatial representation of inundation vulnerability at beach scale considering the same *comarcas* than in the case of erosion is shown in Figure 4.39. As it can be observed, in this case Alt Empordà (1) and Garraf (7) present higher spatial variability than Baix Penedès (8). Compared to erosion, Alt Empordà (1) and Baix Penedès (8) remain ones of the most and least vulnerable *comarcas* respectively, whereas Garraf (7) is clearly less vulnerable to inundation than to erosion.

Finally, inundation vulnerability corresponding to Maresme (4) is shown in Figure 4.40. Again, two results are presented: (i) with (inshore line) and (ii) without considering the run-up (offshore line). No significant differences between both results are appreciated within this *comarca*, except for one beach that goes from high to very high vulnerable.

4.6 Validation[†]

In order to validate the proposed methodology, the magnitude of the storm-induced hazards (erosion and inundation) has been compared to storm-induced damage along the Catalan coast.

Due to the lack of existing systematic quantitative information on coastal damage, an alternative source has been used to obtain such information. In this approach, we assume that press can be used as a proxy-data source to obtain information about frequency and risk magnitude (e.g. Llasat et al., 2009). In this sense, we have used the quantification of storm-induced damage in the study area obtained through a systematic analysis of La Vanguardia newspaper from 1881 to 2008 (Jiménez et al., 2012). As shown in Table 4.9, damages were classified in 4 main classes: destruction, erosion, inundation and sand accumulation. Following the criteria described in this table, each event was classified on a three-class scale (maximum, medium and low). As a result, a damage value for each location and an overall damage value were obtained for each event. Finally, all values quantified during a given year were added to produce an annual overall storm-induced damage value.

Due to the regional-scale spatially-integrated approach adopted, in this case only the climatic forcing contribution (i.e. storm wave properties) was retained to determine storm-induced erosion and inundation intensity. As a result, the parameter used

[†]This section is based on Jiménez, J.A., Sancho, A., Bosom, E., Valdemoro, H.I., Guillén, J. and Galofré, J. (2012): Storm-induced damages along the Catalan coast (NW Mediterranean) during the period 1958-2008. Geomoprhology, 143-144:24-33.

Table 4.9: Description of the qualitative scale for storm-induced damage. Numbers between brackets indicate the quantitative value assigned to each class. Source: Jiménez et al. (2012).

Type of damage	Maximum (5)	Medium (3)	Low (1)
Erosion	"meters of erosion" or "beach completely disappeared"	"some erosion" without details	"some" loss of sand
Inundation	Houses, streets roads	promenade	beach
Sand accumulation	landward of the promenade	at the promenade	before the promenade and accumulation of other objects
Destruction	Infrastructure	damage but unspecified	beach furniture

to characterize the storm-induced inundation potential, IN, is given by:

$$IN = H_s^{1/2} T_p \tag{4.7}$$

This indicator results from retaining only the part that corresponds to wave contribution of the run-up equation (see Equation 4.2). Similarly, the parameter used to characterize the storm-induced erosion potential, ER, resulted from retaining the wave contribution of the erosion potential equation (see Equation 4.1), and is given by:

$$ER = (H_s/T_p)^{1/2} \tau \tag{4.8}$$

Figure 4.41 shows the relationship between the overall damage and inundation and erosion hazards for the period 1958-2008, calculated from reconstructed wave series (see section 4.2.2). As it can be observed, an exponential dependence of damage with storm-induced inundation and erosion has been found. The importance of this dependence increases for the period 1990-2008, during which a combination of the largest storms together with the full development of the coast occur.

Results also reveal that storm-induced damage has increased at a rate of about 40% per decade during the last 50 years (1958-2008). However, the main climatic forcing – storm-induced hazards – does not show any significant trend during this period, which should indicate that damage must be affected and/or controlled by other factors. One of them could be the existence of a bias in the information due to: (i) an increasing awareness of weather, climate and natural hazards in media over

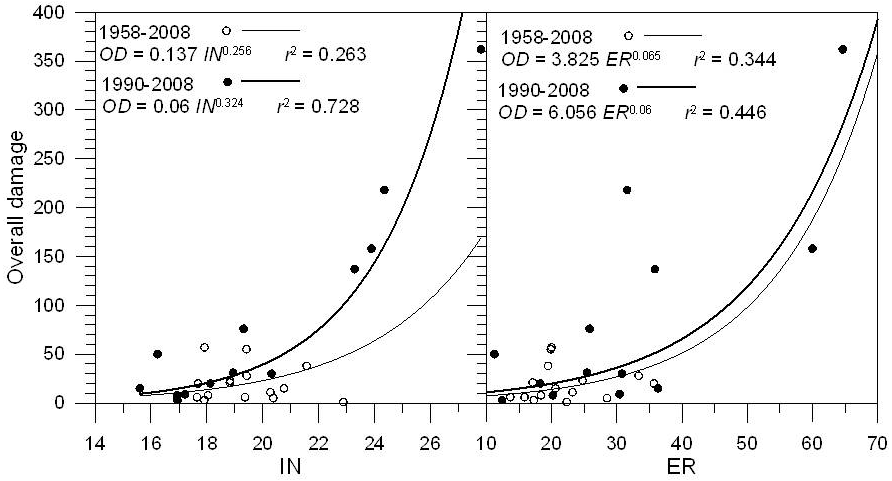

Figure 4.41: Damages vs. inundation and erosion hazards (left and right respectively). Source: Jiménez et al. (2012).

recent decades and, (ii) an increase of values (coastal uses and resources) affected by storm impacts through time. Referring to the last one, it has to be considered that the Catalan coast has experienced huge development during the second half of the 20^{th} century due to the tourism boom and the worldwide observed concentration of population in coastal areas. Furthermore, the more or less generalized coastline retreat observed along the Catalan coast over the last two decades (CIIRC, 2010) might also lead to an increase of the damages, as the values at risk will be more exposed to storm-induced hazards due to a major failure of the protection function of the beach.

In addition to these "local conclusions", the most important general conclusion is that the two proposed indicators of storm-induced hazards (erosion and inundation) behave as good proxies of coastal damage. In consequence, they can be used as good indicators of coastal vulnerability.

Chapter 5

Vulnerability to storms at different time scales

5.1 Introduction

The previously presented vulnerability assessment to storms along the Catalan coast (see chapter 4) has been obtained for current conditions. Nevertheless, beach characteristics will vary along time due to acting coastal processes, leading to changes in vulnerability even under a no-changing wave climate. For this reason, it is clear that the use of a vulnerability assessment framework to make decisions on coastal planning for the near future requires to include the potential influence of such processes. Thus, in this chapter, the developed vulnerability framework is extended by including the contribution of the main coastal processes acting at different scales that can modify the coastal geomorphology. To do so, two different time scales are considered: (i) medium and (ii) long-term. In this work, longshore sediment transport gradients (LST) and relative sea-level rise (RSLR) have been selected as the two main coastal agents acting at these time scales respectively. To characterize the effects of these agents, three processes have been taken into account: (i) medium-term erosion/accretion (ii) erosion due to RSLR and (iii) inundation due to RSLR. Although these processes do not affect the magnitude of the storm-induced hazards, they can lead to important changes on beach morphology, which will modify the ability of the coast to cope with the impact of storms along time and, as a result, they should also affect vulnerability.

Since these processes act at different beach scales, their contribution to future storm vulnerability will vary depending on the selected time projection for the analysis. Furthermore, although their effects should be cumulative because they occur simultaneously in nature, it is interesting to isolate their effects and to evaluate which of them results more relevant to storm vulnerability at different time scales.

The medium-term contribution (LST) has been considered through shoreline evolution rates, whereas different subsidence and sea-level rates have been used to assess long-term erosion and inundation due to RSLR.

Unless otherwise specified, the results of vulnerability to storms presented in this chapter are associated to a 50-yr return period.

In order to include real measurements of changes in coastal morphology due to natural and anthropogenic causes into the assessment, periodical updates of the beach characteristics database must be performed.

5.2 Medium-term contribution to storm-induced vulnerability

5.2.1 Introduction

In this study, LST has been selected as the main agent affecting the Catalan coast at medium-term scale (years to decades). It determines local beach sediment volume changes and, as a consequence, shoreline evolution. The development of coastal structures such as ports and marinas, can produce longshore gradients in transport rates, directly affecting beach stability and, in consequence, changing beach morphology and potentially affecting the beach resilience.

Instead of calculating this component from the theoretical standpoint, this has been directly derived from existing data. Thus, shoreline evolution rates obtained along the Catalan coast during the period 1995-2010 have been used. This period corresponds to conditions once major coastal modifications were already implemented and, in consequence, they could be considered as representative of the evolution conditions provided no new modifications are performed. These rates are an update of previous CIIRC (2010) estimates, by Jiménez and Valdemoro (2013) and, since they have been calculated by means of linear regression, they should represent medium-

term trends. Taking this into account, we can hypothesize that, due to the characteristics of the Catalan coast, they are mainly induced by longshore sediment transport gradients.

Considering that inundation vulnerability to storms is measured in terms of differences in the vertical dimension (berm height and water level), and that coastal evolution rates mainly reflect beach width changes, we have assumed that, when assessed independently, LST only interferes with vulnerability to storm-induced erosion. However, it has to be taken into account that significant changes in beach width may control the amount of floodwater entering the hinterland, specially in wide beaches. To account for this contribution, a numerical model considering overtopping and wave/bore propagation overland should be used at local scale for the identified hotspots.

This section is divided into two main parts: the characterisation of the beach medium-term evolution considering shoreline evolution rates and the analysis of the variations in vulnerability to storm-induced erosion considering the effects of medium-term erosion and accretion at different time scales.

5.2.2 Medium-term beach evolution

Shoreline evolution rates along the Catalan coast calculated from 1995 to 2010 show that most of the coastline present an erosive behaviour (Jiménez and Valdemoro, 2013). Table 5.1 shows the number of beaches, length and percentage of coastline corresponding to each evolution trend: erosion, accretion and equilibrium. It also shows the average and maximum erosion and accretion rates. As observed, about 77% of the coastline is classified as erosive. On the other side, 22% of the coast is classified as accretive, indicating that medium-term contribution to storm vulnerability will not be negative in all cases.

With respect to the maximum erosion and accretion rates (-22.47 m/yr in front of 7.31 m/yr respectively), they reflect two very extreme situations. The first one corresponds to a beach located immediately adjacent to the Ebre river mouth, subject to a strong reshaping process (see e.g. Jiménez et al., 1997b), whereas the second one is located upcoast of a marina that interrupts the littoral drift in the central coast.

Figure 5.1 shows the length of coastline subject to each shoreline evolution trend at province scale. Note that, in all cases, the total length occupied by erosive beaches is larger than the one occupied by beaches that are subject to accretion. The largest

Table 5.1: Shoreline evolution analysis of the study area for the period 1995-2010. Total coastal length: 218.65 km.

	Erosion	Accretion	Equilibrium
Num. beaches	259	80	9
Km	168.22	48.72	1.71
% Km coastline	76.94	22.28	0.78
Average rate (m/yr)	-0.99	0.87	–
Max. rate (m/yr)	-22.47	7.31	–

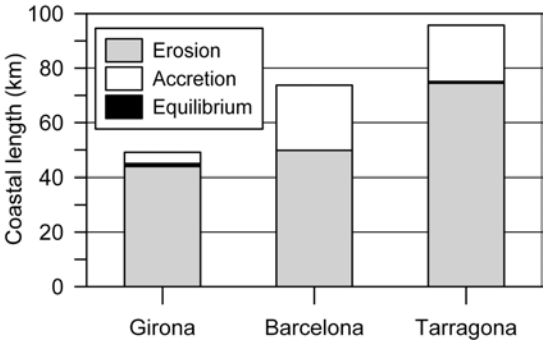

Figure 5.1: Coastal length of each province subject to erosion, accretion and equilibrium rates. Results obtained under baseline conditions (2010).

length of beach in equilibrium is found in the northernmost province (Girona). This is due to the fact that the aforementioned embayed beaches are mainly found in rocky coasts. At the same time, this province also presents the smallest length of beach subject to erosion (around 44 km in front of 50 km and 74 km in Barcelona and Tarragona respectively), although it represents 89% of its sedimentary coastline. It has to be considered that this coast is the most indented, being rock and cliffs the most representative length.

The percentage of coastline subject to each evolution trend analysed at *comarca* scale is shown in Table 5.2. According to this, La Selva (3), located in the North, presents the highest percentage of erosive coastline (98.1%), whereas Garraf (7), in the central coast, shows the highest percentage of coastline subject to accretion (58.2%). As observed, beaches in equilibrium are only present in 4 *comarcas*, mainly located within the northern province and always corresponding to very low percentages of coastline.

To integrate coastline evolution into the vulnerability assessment, shoreline evolution rates have been used to project future beach widths based on current/baseline

Table 5.2: Percentage of coastline per *comarca* subject to erosion, accretion and equilibrium rates. Results obtained under baseline conditions (2010).

Comarca	% Eros. (km)	% Acc. (km)	% Eq. (km)	Length (km)
Alt Empordà (1)	92.5	4.3	3.2	21.98
Baix Empordà (2)	82.5	15.9	1.8	19.51
La Selva (3)	98.1	1.2	0.7	7.63
Maresme (4)	71.7	28.3	0	39.01
Barcelonès (5)	86.2	13.8	0	13.09
Baix Llobregat (6)	55.7	44.3	0	11.03
Garraf (7)	41.8	58.2	0	10.63
Baix Penedès (8)	80.4	19.6	0	12.81
Tarragonès (9)	77.6	22.4	0	22.14
Baix Camp (10)	71.1	26.2	2.8	21.99
Baix Ebre (11)	97.3	2.7	0	14.17
Montsià (12)	71.4	28.6	0	24.65

conditions (2010) and for different time scales (5, 10, 25, and 50 years). Essentially, this is a simple empirical evolution model which is valid on the assumption that forcing conditions driving such behaviour will not suffer any significant change. As a consequence, beach width projections considering longer time periods than the used in the analysis (15-25 years) should be carefully considered.

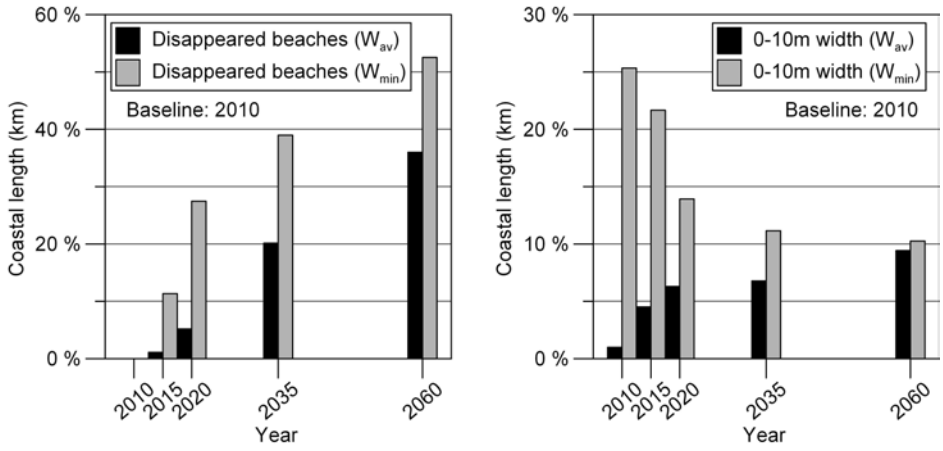

Figure 5.2: Percentage of coastline corresponding to disappeared and less than 10-meter wide beaches. Results obtained considering LST contribution and two different beach width measurements (average and minimum). Total coastal length: 218.65 km.

Figure 5.2 shows the percentage of studied coastline corresponding to disappeared and less than 10-meter wide beaches at different time scales. As it can be observed, results obtained using the current average beach width (black) are distinguished from

those obtained using the minimum (grey). Whilst the first one represents the beaches that should disappear, the second one is useful to identify beaches that do not necessarily disappear but contain very sensitive spots (a part of the beach would be fully eroded). The fact that a beach disappears means that its vulnerability to storm impacts turns immediately into very high, since no protection to face erosion and inundation exists.

As expected, results show an increasing number of disappeared beaches through time, being higher when the minimum beach width is considered. In terms of coastal extension, results obtained for the 25-yr projection (2035) considering the average beach width indicate that 20% of the coast (44 km) corresponds to beaches that will potentially disappear. With respect to the number of beaches with less than 10-meter wide, it does not necessarily have to increase along time projections, since some of them will eventually disappear from one projection to another. Despite the fact that from now on results will only refer to those obtained using the average beach width, differences between them and the ones obtained using the minimum beach wide should be taken into account when it comes to their interpretation.

5.2.3 Erosion vulnerability

Once beach width projections have been obtained, they are used as an indicator of the ability of the coast to cope with the impact of the storm, replacing current average beach width (W_{av}) in equation 4.4. Thus, in this case the intermediate variable equation used to calculate vulnerability can be defined as:

$$EV = \Delta x/(W_{av} + \Delta x_{LST}) \tag{5.1}$$

in which Δx_{LST} represents the beach evolution due to LST associated to a specific time projection.

The use of equation 5.1 leads to new values of the intermediate variable in comparison to the ones obtained when assessing vulnerability under current conditions. However, the thresholds of the vulnerability function remain equal because we are considering the same process (storm-induced erosion) as well as the same beach function (protection). Therefore, the vulnerability of the same beach should vary at different time projections. An example of these changes for a specific central coast beach is presented in Figure 5.3. Here it can be observed how vulnerability ranges from very low, when it is assessed under baseline conditions (2010), to low, medium, high and

very high, when 5-yr, 10-yr, 25-yr and 50-yr beach width projections are considered.

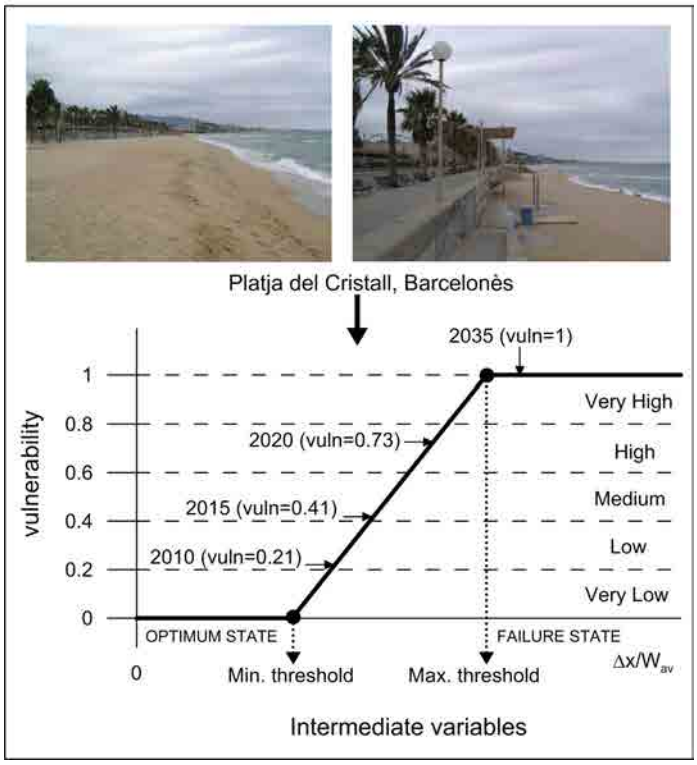

Figure 5.3: Differences in vulnerability to storm-induced erosion along different time scales due to LST contribution. Results obtained considering a 50-yr return period at Platja del Cristall (central coast).

Final vulnerability to storm-induced erosion for a 50-yr return period considering LST contribution is shown in Figure 5.4. Results are presented in terms of the number and total length of the beaches corresponding to each vulnerability category at different time scales. As it can be observed, an increase of vulnerability along time is clearly detected in both cases, reaching 58% of the coastline classified into the two worst categories at the 25-yr projection, which represents 127 km of coast and 68% of the beaches. This percentage increases up to 64% when the 50-yr projection is considered, corresponding to 159 km of coast and 70% of the beaches. Results also show a more or less constant increase in vulnerability through time until the 25-year projection (2035), slowing down significantly from this point onwards.

With respect to coastal sectors, the largest increase in vulnerability to storm-induced erosion due to LST contribution is observed in the southernmost one, were

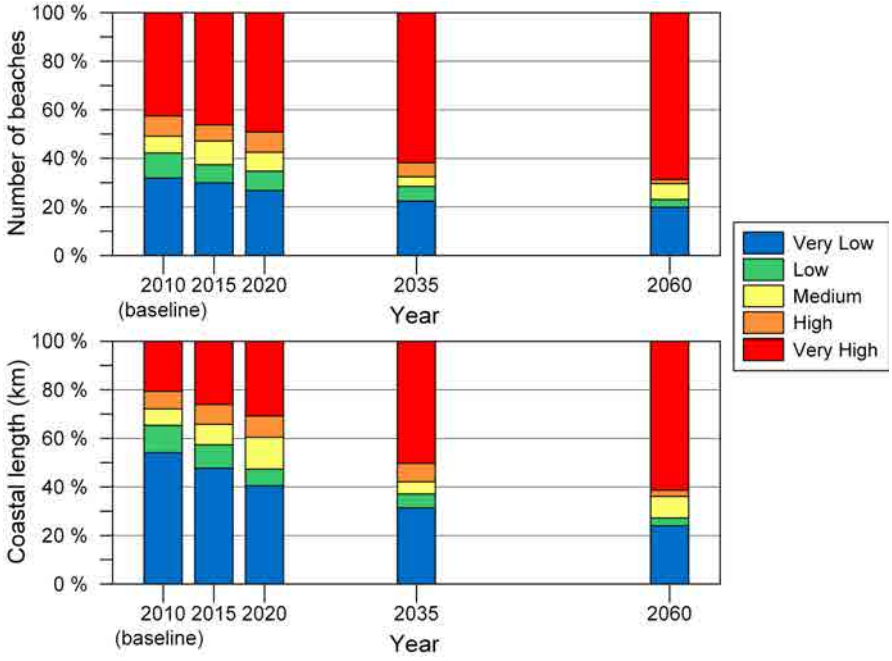

Figure 5.4: Percentage of beaches and coastline corresponding to each category of vulnerability to storm-induced erosion for a 50-yr return period. Considered contribution: LST. Total number of beaches: 348.

the percentage of coastline classified as high or very high vulnerable ranges from 9% at the baseline to 29%, 34% and 62% for the 5-yr, 10-yr and 25-yr projections respectively. Despite this, the two northernmost sectors remain, as at the baseline, the most vulnerable for all the considered projections. Due to the existence of positive shoreline evolution rates (accretion), a decrease in vulnerability is observed in sector IV at the 5-yr and 10-yr projections.

Results does not reveal any specific beach type as the most sensitive to changes in erosion vulnerability due to LST contribution. Instead, different beach types are affected. The most dissipative beach type (4) presents the largest increase in total length of coastline classified as high or very high vulnerable to erosion, although it is also the most common one in the study area. In relative terms, an important increase in vulnerability is also observed for some intermediate to reflective beach types (5 and 7), while types 6 and 1 remain the most vulnerable at all the projections.

Figure 5.5 shows the percentage of coastline corresponding to the two worst vulnerability categories at different time scales, considering 10-yr, 25-yr, 50-yr and 100-yr return periods. As expected, such percentage increases as the return period does so.

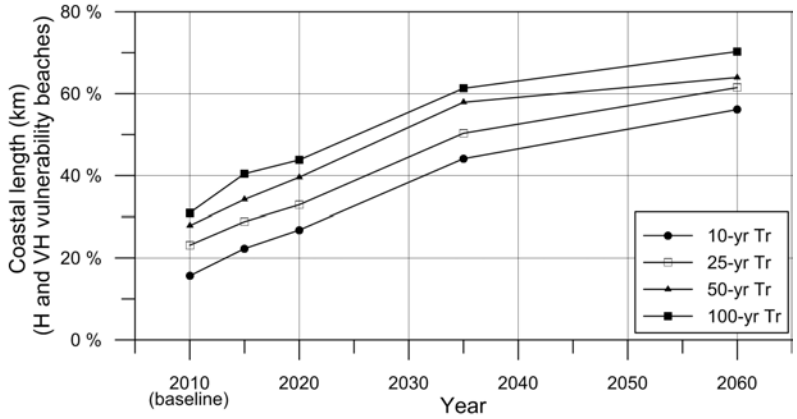

Figure 5.5: Percentage of coastline classified as high (H) or very high (VH) vulnerable to storm-induced erosion for different return periods. Considered contribution: LST. Total coastal length: 218.65 km.

In general terms, a similar behaviour is observed in all cases, although differences between return periods slightly decrease through time, highlighting the weight of LST contribution. When the 25-yr projection is considered, results already indicate that more than 40% of the coastline falls into high and very high vulnerability categories, independently of the selected return period.

Vulnerability results have also been interpreted taking into account different administrative scales of the study area. In this sense, Figure 5.6 shows the percentage of coastline classified into the two worst vulnerability categories for each coastal province. As it can be observed, Girona departs as the most vulnerable province compared to the other ones, maintaining this difference along all the projections. On the other side, Tarragona departs as the lowest vulnerable and experiences the largest increase in vulnerability, until reaching a similar percentage of high and very high vulnerable coastline than the one found in Barcelona at the 10-yr, 25-yr and 50-yr projections. This highlights the important role of medium-term erosion in the southern area of the Catalan coast and coincides with the previously presented shoreline evolution assessment, which indicates that the two largest erosion rates correspond to beaches located in the Ebre delta.

Table 5.3 shows the total length of coastline classified as high or very high vulnerable to storm-induced erosion for each *comarca*, considering different time projections. These results strongly agree with those obtained at sector and province scale, indicating that the northernmost area of the Catalan coast (Alt Empordà (1)) remains always as the most vulnerable, whilst the largest increase in vulnerability is found

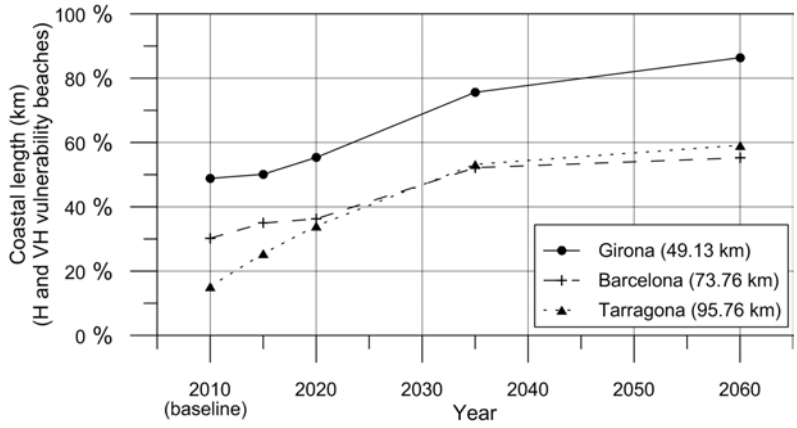

Figure 5.6: Percentage of coastline per province classified as high (H) or very high (VH) vulnerable to storm-induced erosion for a 50-yr return period. Considered contribution: LST.

at the southernmost part (Baix Ebre (11) and Montsià (12)). On the opposite, a decrease in vulnerability is observed at some or all the projections in Barcelonès (5) and Garraf (7) (central and southern *comarcas* respectively). As a conclusion, results obtained for the 25-yr and 50-yr projections suggest a shift of location of the lowest vulnerable *comarcas* from south to central coast with respect to the baseline, as a consequence of LST contribution. With the exception of Garraf (7), this shift does not correspond to a decrease in vulnerability at central *comarcas*, but to a significant increase at the southernmost ones.

Table 5.3: Length of coastline per *comarca* classified as high (H) or very high (VH) vulnerable to storm-induced erosion for a 50-yr return period. Considered contribution: LST.

	Km of H and VH vulnerability					
Comarca	2010	2015	2020	2035	2060	Length (km)
Alt Empordà (1)	13.56	13.56	13.56	19.76	21.53	21.98
Baix Empordà (2)	8.11	8.42	8.42	12.07	15.08	19.51
La Selva (3)	2.32	2.64	5.20	5.31	5.83	7.63
Maresme (4)	12.72	17.32	18.03	24.87	27.19	39.01
Barcelonès (5)	3.97	3.55	3.61	5.11	5.11	13.09
Baix Llobregat (6)	0	0	0	3.65	3.65	11.03
Garraf (7)	5.60	4.90	5.11	4.86	4.79	10.63
Baix Penedès (8)	1.67	1.83	3.85	6.87	7.54	12.81
Tarragonès (9)	3.47	4.48	8.30	9.64	11.36	22.14
Baix Camp (10)	6.55	6.27	6.69	8.39	11.30	21.99
Baix Ebre (11)	2.22	6.70	8.71	10.25	10.36	14.17
Montsià (12)	0.72	5.08	5.08	15.81	16.11	24.65

Results obtained considering current conditions and the 10-yr projection are presented using GIS format at beach scale for Alt Empordà(1), Garraf (4) and Baix Ebre (11) (see Figure 5.7). The first one shows no variation in vulnerability between baseline and the 10-yr projection. In contrast, the second and third one present the largest decrease and increase respectively. This type of representation permits to specifically identify which beaches present changes in vulnerability, as well as to compare their physical characteristics.

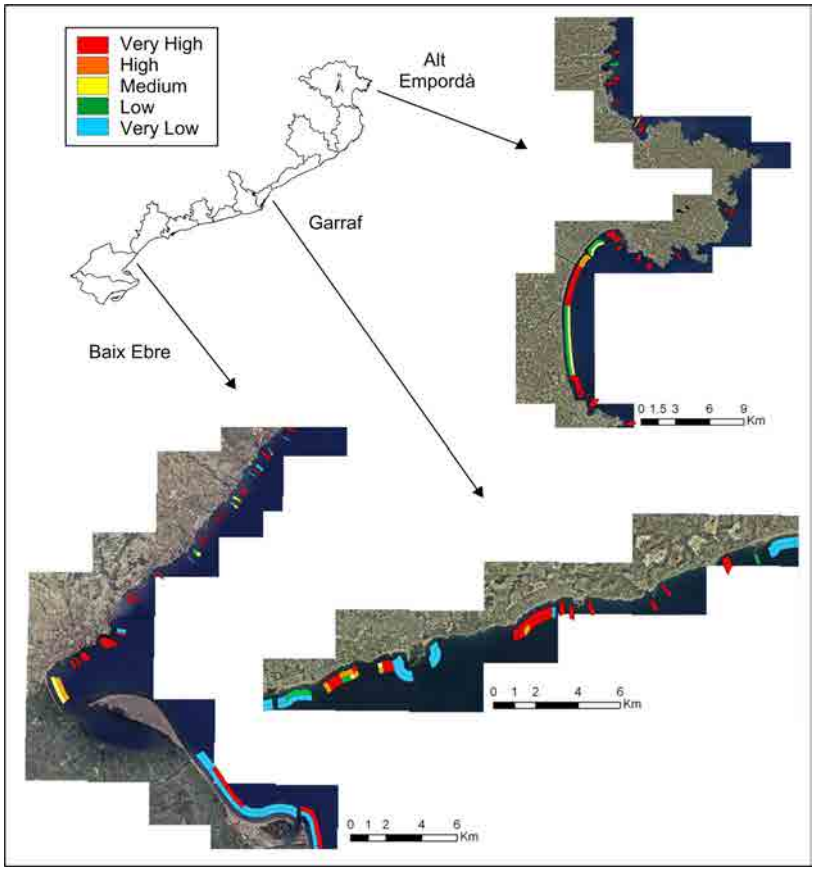

Figure 5.7: Spatial representation of vulnerability to storm-induced erosion for three coastal *comarcas*. Comparison between baseline vulnerability (inshore line, 2010) and the 10-yr projection considering LST contribution (offshore line, 2020). Results relative to a 50-yr return period.

5.3 Long-term contribution to storm-induced vulnerability *

5.3.1 Introduction

A lot of effort during the last decades has been put into assessing the wide range of impacts that climate change can potentially produce to coastal systems as well as its implications (e.g. Pernetta and Elder, 1992; Scavia et al., 2002; Nicholls and Cazenave, 2010; Nicholls et al., 2011). As the Fourth IPCC Assessment Report (AR4) reveals (Nicholls et al., 2007), hazards related to climate and sea level are affecting coasts worldwide and these areas will very likely be exposed to increasing risks. Therefore, it is relevant to develop coastal vulnerability assessment frameworks that allow the consideration of climate change effects, in order to increase its accuracy.

When referring to storms, coastal vulnerability can be modified by alterations in climate drivers such as sea-level and climate storminess (intensity and frequency). Whereas sea-level variations can affect the adaptation ability of the coast in front of storms by reducing the available beach width, changes in wave climate or storminess due to climate change would modify the magnitude of the impact and, as a consequence, vulnerability as well.

With respect to future storm characteristics in our latitudes (extra-tropical), some discrepancies exist among studies due to the use of different methodologies and approaches (Ulbrich et al., 2009). One of the changes that several studies suggest is a poleward shift of mid-latitudes storm tracks (Meehl et al., 2007). However, as a consequence of different definitions of "extreme" storms, some studies have obtained inconsistent results with respect to storm intensity changes for the same hemisphere (Ulbrich et al., 2009). For the Mediterranean region, although numerous authors suggest a decrease in the number of cyclones, as the variability in different study results suggest, it is still uncertain if future cyclones will be more or less intense (see e.g. Trigo et al., 2000; Lionello et al., 2002; Anagnostopoulou et al., 2006; Pinto et al., 2007; Nissen et al., 2010).

On the other side, wave climate under future scenarios has also been assessed during the last decades. To that effect, many studies have been performed at global scale

*This section is largely based on Bosom et al. (2014): RSLR-induced increase of vulnerability to storms along the Catalan coast (NW Mediterranean) (*presented at EGU 2014, manuscript in preparation*).

(e.g. Caires et al., 2006; Wang and Swail, 2006; Wang et al., 2008; Mori et al., 2010), identifying specific areas were wave climate has already increased or is expected to do so under future greenhouse emission scenarios. Regarding the Mediterranean region, some authors have reported a general decreasing trend of the mean significant wave height (Lionello and Sanna, 2005; Lionello et al., 2008; Casas-Prat and Sierra, 2013). However, a higher variability of results regarding extreme wave climate projections has been found for different models (Casas-Prat and Sierra, 2013).

Considering the lack of agreement regarding the definition of final climatic scenarios to quantify storminess and wave climate changes under the effects of climate change, in this study erosion and inundation due to relative sea-level rise are considered the main long-term scale processes occurring within the study area that can affect storm-induced vulnerability.

In terms of future sea-level, several projections have been obtained using different approaches and methodologies at global scale (see e.g. Rahmstorf, 2007; Grinsted and Jevrejeva, 2009; Vermeer and Rahmstorf, 2009). Still, the uncertainty associated to their results remains high, specifically if sea-level rise acceleration is considered (Church and White, 2006). In terms or regional assessments, numerous estimates of sea-level trends during the last decades have been obtained for the Mediterranean region (see e.g. Tsimplis and Baker, 2000; Fenoglio-Marc, 2002; Marcos and Tsimplis, 2008; Calafat and Jordà, 2011), although results are not always comparable because of the application of different methods, approaches and/or temporal and spatial scales. Within this context, one of the most commonly accepted approach is the one presented by the IPCC^{4th}Assessment Report, in which different sea-level rates are estimated based on the description of several greenhouse future scenarios at global scale (Meehl et al., 2007).

In this work, different subsidence and sea-level rise scenarios are used to quantify the effects of RSLR-induced erosion and inundation on the Catalan beaches to subsequently assess how these changes affect storm-induced erosion and inundation vulnerability (separately). In any case, the developed methodology easily allows changes in the inputs of wave climate —in case they can be quantified— without needing to modify it.

Within this context, the next subsection presents an assessment of the beach long-term evolution taking into account RSLR, followed by an analysis of the variations in storm-induced erosion and inundation vulnerability as a consequence of RSLR contribution.

5.3.2 Long-term beach evolution

One of the most used models to predict beach response to an increase of sea level is the Bruun Rule (Bruun, 1962). This simple model developed for sandy coasts assumes the existence of an equilibrium beach profile as a response to its exposure to a wave climate. Under these conditions, an increase in sea-level induces a landward and upward translation of the beach profile in order to reach its equilibrium shape according to the new mean sea-level (see Figure 5.8). Although this assumption implies no variation in beach width, beach elevation and water depth within the active profile, limiting conditions as the available accommodation space (and consequent sediment budget) may alter the response of the profile, preventing it from reaching the expected configuration. As a consequence, changes in beach width and berm height may occur, affecting storm-induced erosion and inundation vulnerability.

This model has been widely applied to many coastal areas in order to estimate RSLR-related cross-shore profile changes. Nevertheless, its use entails some limitations that have to be contemplated (e.g. Cooper and Pilkey, 2004; Davidson-Arnott, 2005) and, unless in the case of absence of littoral transport gradients and presence of sediment sources/sinks, it is not recommended for local scale assessments in which precise quantitative estimations are needed (Stive et al., 2009). Bearing in mind the Bruun rule limitations, Ranasinghe et al. (2011) recently proposed a probabilistic model to estimate coastal recession due to sea-level rise (PCR model). However, this model has adopted several simplifying assumptions that need to be carefully considered.

Due to the lack of a generally accepted morphological model to predict RSLR-induced coastal erosion, in this work it is characterised by applying the Bruun rule at a regional scale following the expression:

$$\Delta x_{RSLR} = s\frac{L}{B_{max} + d} = s\frac{1}{sl} \tag{5.2}$$

where Δx_{RSLR} is the expected beach retreat, s is the relative sea-level rise, L is the active profile width, B_{max} is the maximum berm height (beach elevation), d corresponds to the closure depth (see Figure 5.8) and sl is the active profile slope. As mentioned in Chapter 3, instead of selecting a specific closure depth (d), the active profile slope (sl) has been measured from the shoreline to 10 m depth, since active depth along the Catalan coast is comprised within this zone.

Adopting the general assumptions described by the Bruun rule, and taking into

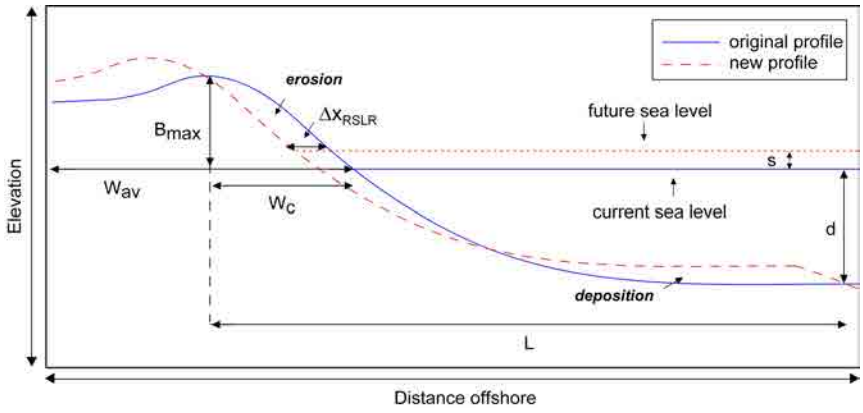

Figure 5.8: Diagram of the variables considered to characterize RSLR effects on the coastal systems according to the Bruun rule.

account that most of the beaches of the Catalan coast are backed by rigid boundaries that limit their landward migration, RSLR contribution should always cause changes in beach width. On the opposite, changes in beach elevation as a consequence of RSLR are only expected in some cases. As the ability of the system to respond to such forcing is limited by the available accommodation space, which can decrease along time due to beach retreat, is therefore acceptable to assume that a critical width is required for the beach to maintain its elevation. In this work, the definition of the critical beach width is proposed as the distance between the maximum elevation of the beach (Bmax) and the shoreline, described as:

$$W_c = \left(\frac{B_{max}}{tan\beta} \right) \tag{5.3}$$

where W_c (see Figure 5.8) is the critical beach width, B_{max} is the maximum berm height and $tan\beta$ is the beach-face slope. It is assumed that this width is the minimum necessary for the beach to maintain the actual profile, considered here as the equilibrium state. According to this assumption, the beach profile will adjust to RSLR as predicted by the Bruun rule as long as the projected (average) beach width does not decreases below the critical beach width (W_c). Otherwise, the lack of accommodation space will prevent the beach from maintaining its elevation.

Because inundation vulnerability is estimated in terms of the maximum beach elevation with respect to the run-up level, the concept of critical beach width becomes crucial to evaluate RSLR effects on stom-induced inundation vulnerability. Otherwise, no effects should be expected.

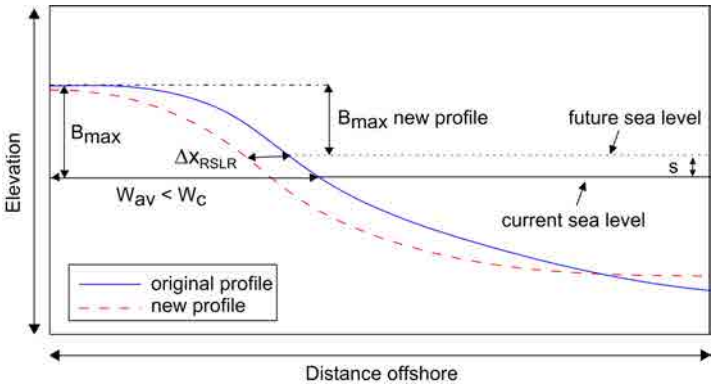

Figure 5.9: Diagram of the variables considered to characterize a decrease of beach elevation due to RSLR effects according to the Bruun rule.

The critical beach width has been calculated for each beach using profile data that was gathered during several field campaigns in 2008 (CIIRC, 2010). As a result, an average critical width of 16 meters has been found for the Catalan coast. A deeper assessment reveals that, under current conditions, the average beach width equals the critical width in 16% of the studied beaches. Consequently, 16% of the coastline will potentially turn unable to respond according to the Bruun rule model if any beach retreat occurs.

To characterise beach evolution due to RSLR, 8 different scenarios (see Figure 3.3 in Chapter 3) are considered for different time projections (5, 10, 25 and 50 years). The low, medium and high RSLR scenarios correspond to the IPCC sea-level estimates (Meehl et al., 2007) of 1.8, 3.8 and 5.9 mm/yr respectively, whereas the worst scenario corresponds to the Vermeer and Rahmstorf (2009) estimate of 13 mm/yr. At the same time, 5 subsidence areas have been considered in this study (see Table 3.4). Because the Ebre delta is the most important one, a representative subsidence value of 3 mm/yr is applied to the beaches corresponding to this zone, in front of the 1.5 mm/yr considered for the rest and considerably smaller subsidence area. As a result, beach width projections under different RSLR scenarios (with and without including subsidence) and time scales have been obtained.

Unless specified otherwise, presented results always refer to the scenarios including subsidence. Besides this, the medium scenario (3.8 mm/yr + subsidence) has been selected as the representative for general results such as vulnerability maps and other figures in which only one RSLR scenario is included. However, results obtained taking into account other scenarios are also compared when relevant.

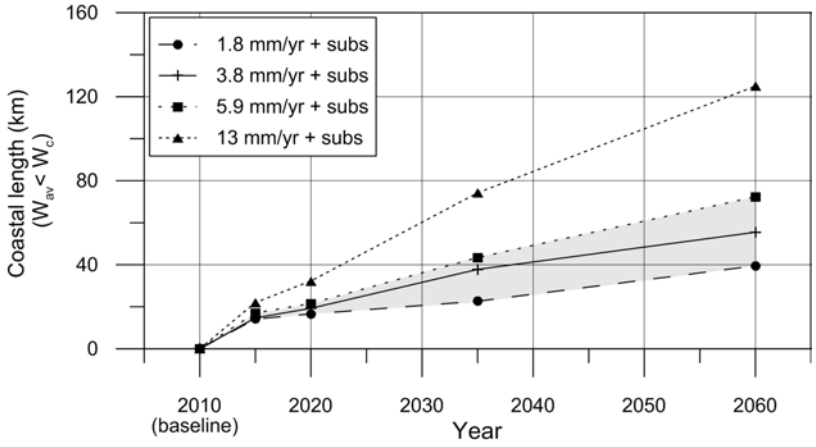

Figure 5.10: Length of coastline corresponding to beaches with width less than the critical value ($W_{av} < W_c$). Considered contribution: RSLR. Total coastal length: 218.65 km.

Figure 5.10 shows the total coastal length corresponding to beaches that, according to its width, will not potentially be able to maintain its elevation in response to RSLR. Although in all cases it increases along time, results obtained for the worst scenario are, as expected, considerably higher than the ones obtained for the IPCC scenarios. Note that these values include the length of those beaches that will potentially disappear (see Figure 5.11) which, in the case of the high and worst scenarios, contributes to more than 50% of the results when the longer time projections are considered.

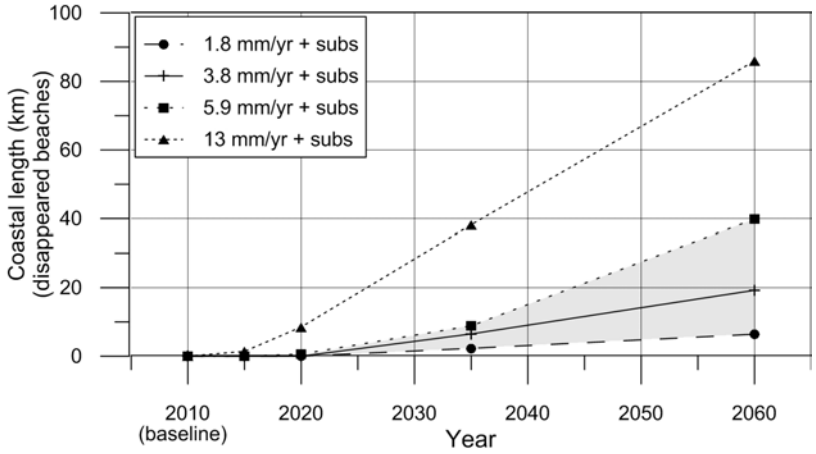

Figure 5.11: Length of coastline corresponding to beaches that will potentially disappear due to RSLR contribution. Total coastal length: 218.65 km.

Figure 5.11 presents the length of coastline corresponding to beaches that will potentially disappear under the contribution of different RSLR scenarios at different time scales. As it can be observed, results show a large variability among scenarios. If only the low, medium and high scenarios are considered, the total length of disappeared beaches ranges from 6 km to 40 km at the 50-yr projection, which corresponds to 3% and 18% of the coastline respectively. As expected, the values obtained for the worst scenario are significantly higher. Furthermore, none or very few beaches disappear for the IPCC scenarios at the 5-yr and 10-yr projections, which indicates that the effects of RSLR-induced processes can be generally detected at longer time scales than those caused by LST, clearly agreeing with the initial time scale classification.

As mentioned before, these results are based on the premise that the beaches are limited by hard structures that impede their landward migration in response to RSLR. Although this is the most frequent situation in the Catalan beaches, it has to be highlighted that there might be some areas, such as the Ebre delta and other low-lying natural areas, in which the lack of limiting structures would permit beaches to migrate landward and maintain their width and elevation.

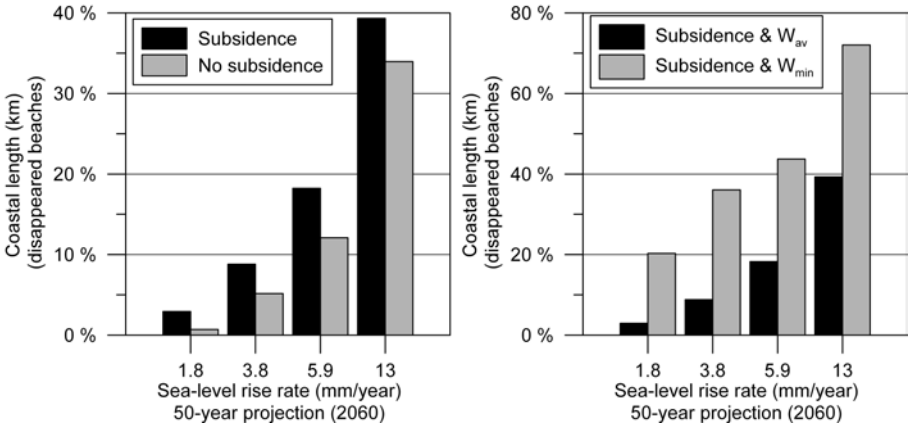

Figure 5.12: Percentage of coastline corresponding to beaches that will potentially disappear at the 50-yr projection due to RSLR contribution. Left plot: results obtained with and without considering subsidence rates. Right plot: results obtained considering average and minimum beach widths. Baseline: 2010. Total coastal length: 218.65 km.

Vulnerability results are generally presented considering the average beach width (W_{av}) and the RSLR scenarios with subsidence. However, it is interesting to assess differences between these results and the ones obtained considering the minimum beach width (W_{min}) and without accounting for subsidence. In this sense, Figure 5.12 shows the percentage of coastline corresponding to beaches that will potentially disap-

pear due to RSLR contribution at the 50-yr projection, calculated with and without considering subsidence (left) and using different beach widths (right). As expected, this value is larger when subsidence (left) and minimum beach width (W_{min})(right) are considered, although differences in the first case are always lower than the ones obtained for the second case. Again, it has to be mentioned that, more than to characterise the general evolution of the beach, results obtained using the minimum beach width (W_{min}) permit to identify beaches with important stability problems related to very specific spots/stretches.

In any case, it has to be considered that the inclusion of subsidence only affects low-lying areas where this process is relevant. Moreover, since these areas are usually characterized by having very mild profiles, its effect (shoreline retreat) will be very significant.

5.3.3 Erosion vulnerability

As in the case of LST, to calculate vulnerability to storm-induced erosion considering RSLR contribution, projected beach widths replace the current one (W_{av}) in equation 4.4, in such a way that the intermediate variable is defined as:

$$EV = \Delta x/(W_{av} + \Delta x_{RSLR}) \tag{5.4}$$

in which Δx_{RSLR} represents the beach retreat due to the effect of a particular RSLR scenario associated to a specific time projection, previously obtained using Equation 5.2. The values of this new intermediate variable are fit into the originally described erosion vulnerability function (see Table 4.5) in order to obtain vulnerability values for each beach.

Erosion vulnerability results at global scale associated to a 50-yr return period and considering RSLR contribution are shown in Figure 5.13. As observed, differences among scenarios increase along time, reaching a maximum of between 90 km and 124 km of coastline classified as high or very high vulnerable at the 50-yr projection when the low and high scenarios are considered (41% and 57% of the total coastline respectively). In the case of the worst scenario, this value increases up to 178 km (81% of the coastline).

From this point and for the rest of the section, erosion vulnerability results are presented considering the contribution of the medium RSLR scenario (3.8 mm/yr + subsidence). Figure 5.14 shows the percentage of coastline corresponding to each

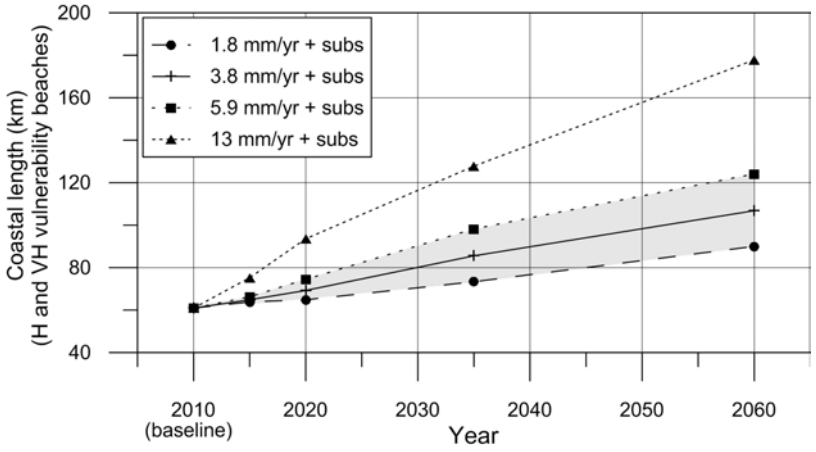

Figure 5.13: Length of coastline classified as high (H) or very high (VH) vulnerable to storm-induced erosion for a 50-yr return period. Considered contribution: RSLR. Total coastal length: 218.65 km.

erosion vulnerability category. Despite the fact that vulnerability increases along time projections, significant changes in relation to the baseline can be better appreciated from 2035 onward (25-yr projection). More precisely, the percentage of high and very high vulnerable coastline ranges from 28% at the baseline to 32%, 39% and 49% at the 10-yr, 25-yr and 50-yr projections respectively.

Results obtained under the same conditions reveal sector VI as the one presenting the largest increase in vulnerability, with around 25 km of coastline becoming high or very high vulnerable to erosion in 50 years (2060 horizon), opposite to sectors I and II, where this value decreases below 1 km. However, the percentage of high and very high vulnerable coastline at the 50-yr projection is quite similar in all cases (54%, 59% and 67% for sectors I, II and VI respectively), because the northernmost sector results already very vulnerable under current conditions.

With respect to the different beach types, the largest increase in vulnerability between baseline and the 50-yr projection is obtained for type 4, representative of the most dissipative beaches and also the most frequent one. An important increase in terms of percentage of coastline becoming high or very high vulnerable is also found for type 8, corresponding to an intermediate category with the second lowest representative values of grain size and beach-face slope. These results, together with the ones assessed at sector scale, highlight that RSLR contribution to erosion vulnerability also depends on beach morphology, being dissipative beaches clearly the most affected, since they have the mildest slope and thus, suffer the largest induced erosion.

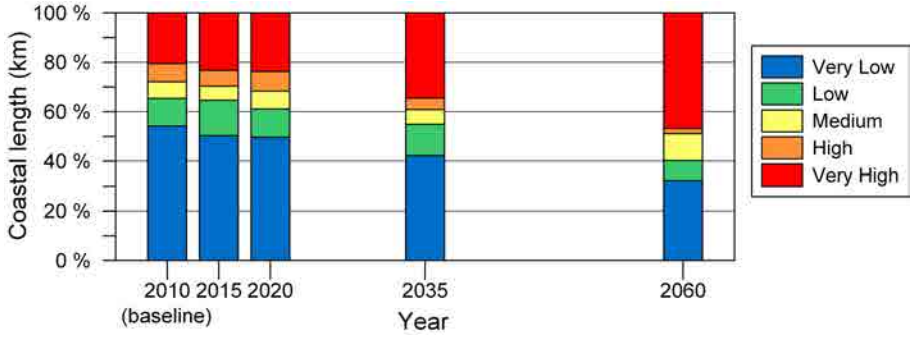

Figure 5.14: Percentage of coastline corresponding to each category of vulnerability storm-induced erosion for a 50-yr return period. Considered contribution: medium RSLR scenario (3.8 mm/yr + subsidence). Total coastal length: 218.65 km.

RSLR contribution to vulnerability to storm-induced erosion has also been analysed for hazards associated to different return periods (see Figure 5.15). As expected, the percentage of coastline corresponding to the two worst vulnerability categories increases as the return period does so. In terms of magnitude, when the medium RSLR scenario is considered, vulnerability increases similarly in all cases, with between 21% and 27% of the coastline becoming high or very high vulnerable to erosion between baseline and the 50-yr projection. As in the case of LST, differences in vulnerability among return periods are slightly higher at the baseline than for the 50-yr projection.

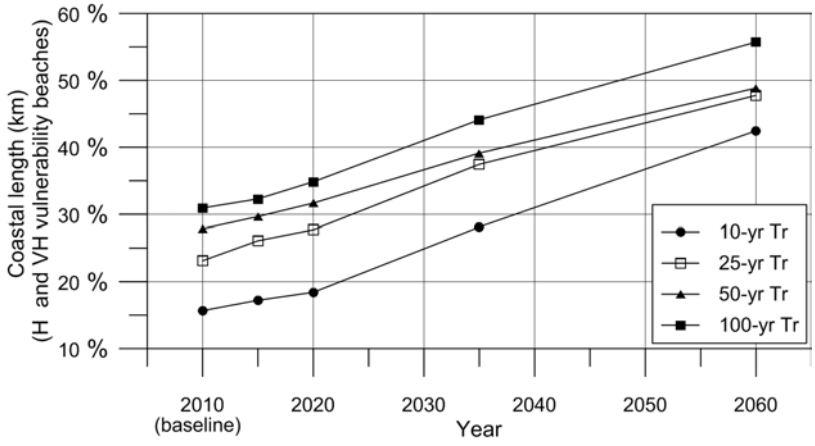

Figure 5.15: Percentage of coastline classified as high (H) or very high (VH) vulnerable to storm-induced erosion for different return periods. Considered contribution: medium RSLR scenario (3.8 mm/yr plus subsidence). Total coastal length: 218.65 km.

Figure 5.16 presents the erosion vulnerability results grouped by provinces. Despite the fact that each province departs from different vulnerability levels at the

baseline, they tend to converge, ending with similar percentages of coastline classified into the two worst vulnerability categories (52%, 47% and 48% from north to south). As it can be observed, Girona is always the most vulnerable province, showing an almost insignificant increase in vulnerability along time. On the opposite, Tarragona stands out as the coastal province showing the largest increase in vulnerability with respect to baseline conditions.

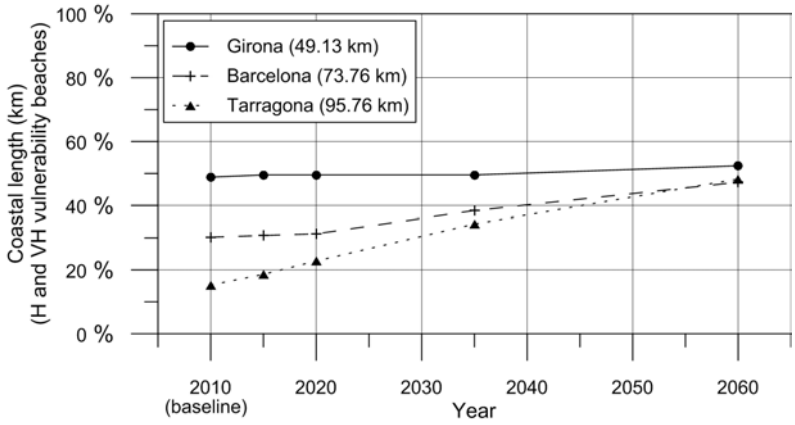

Figure 5.16: Length of coastline per province classified as high (H) or very high (VH) vulnerable to storm-induced erosion for a 50-yr return period. Considered contribution: medium RSLR scenario (3.8 mm/yr + subsidence).

Table 5.4 shows the total length of coastline occupied by high and very high vulnerable beaches at *comarca* scale. Results highlight again the southernmost part of the Catalan coast as the most sensitive to the effects of RSLR in terms of vulnerability to storm-induced erosion. To be more precise, the largest increase in vulnerability is detected at the two southernmost *comarcas* (Baix Ebre (11) and Monstià (12)) which, when evaluated in relative terms, start as the lowest vulnerable at the baseline to become two of the most vulnerable at the 50-yr projection. This is mainly due to the fact that the southern part of the coast, corresponding to the Ebre delta, is characterised by dissipative beaches with very mild profile slopes which, as mentioned before, enhances RSLR-induced beach retreat. In addition to this, RSLR also includes a significant contribution of subsidence in this area.

Figure 5.17 shows the percentage of coastline corresponding to each vulnerability category at the 50-yr projection. This approach allows a more comprehensive assessment of differences between *comarcas*. Although the two most vulnerable at the baseline, Alt Empordà (1) and Garraf (7), experience very low and moderate increases in vulnerability to erosion due to RSLR respectively, they are, together with

Table 5.4: Length of coastline per *comarca* classified as high (H) or very high (VH) vulnerable to storm-induced erosion for a 50-yr return period. Considered contribution: medium RSLR scenario (3.8 mm/yr + subsidence).

	Km of H and VH vulnerability					
Comarca	2010	2015	2020	2035	2060	Length (km)
Alt Empordà (1)	13.56	13.56	13.56	13.56	14.01	21.98
Baix Empordà (2)	8.11	8.14	8.14	8.14	8.99	19.51
La Selva (3)	2.32	2.64	2.64	2.64	2.75	7.63
Maresme (4)	12.72	12.72	12.89	14.52	19.31	39.01
Barcelonès (5)	3.97	4.38	4.38	4.38	4.66	13.09
Baix Llobregat (6)	0.00	0.00	0.00	3.65	3.65	11.03
Garraf (7)	5.60	5.60	5.81	5.81	7.23	10.63
Baix Penedès (8)	1.67	1.67	1.83	2.66	2.88	12.81
Tarragonès (9)	3.47	4.21	4.21	5.22	5.67	22.14
Baix Camp (10)	6.55	6.85	7.71	8.37	9.56	21.99
Baix Ebre (11)	2.22	4.11	7.08	7.20	11.48	14.17
Montsià (12)	0.72	0.99	0.99	9.42	16.62	24.65

Baix Ebre (11) and Monstià (12), two of the most vulnerable at the 50-yr projection. As observed, central *comarcas* are the ones that present the highest percentages of coastline corresponding to very low vulnerable beaches.

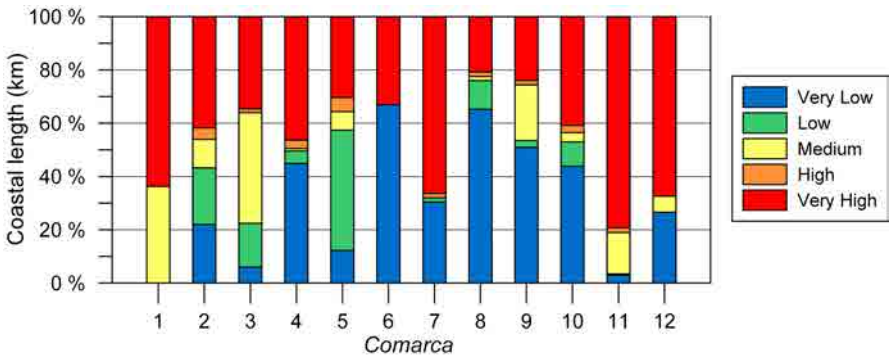

Figure 5.17: Percentage of coastline per *comarca* corresponding to each category of vulnerability to storm-induced erosion for a 50-yr return period and a 50-yr projection. Considered contribution: medium RSLR scenario (3.8 mm/yr + subsidence).

Lastly, Figure 5.18 compares vulnerability to storm-induced erosion at beach scale between baseline and the 50-yr projection in Alt Emporà (1) and Baix Ebre (11). Although they are two of the most vulnerable *comarcas* at the 50-yr projection, they present the lowest and highest variations of vulnerability with respect to current conditions, with a percentage of high and very high vulnerable coastline ranging from 62% to 64% and from 13% to 65% respectively. Again, the significant increase in

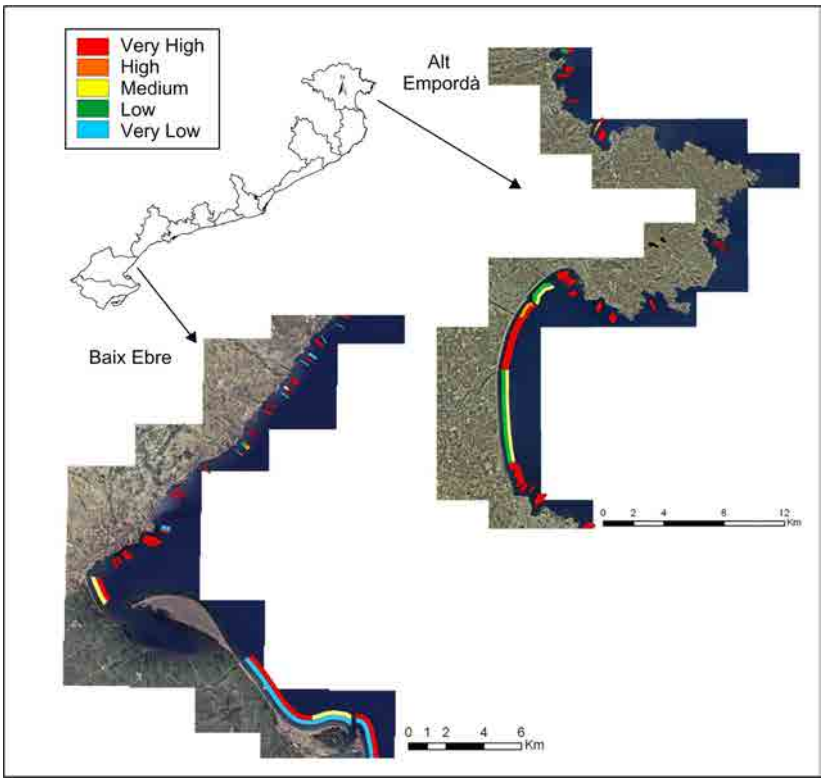

Figure 5.18: Spatial representation of vulnerability to storm-induced erosion for two coastal *comarcas*. Comparison between baseline vulnerability (inshore line, 2010) and the 50-yr projection considering a RSLR scenario of 3.8 mm/yr plus subsidence (offshore line, 2060). Results relative to a 50-yr return period.

erosion vulnerability in the case of Baix Ebre (11) is due to the fact that it combines very mild slopes with important subsidence rates, which contributes to intensify beach retreat due to RSLR.

5.3.4 Inundation vulnerability

As mentioned before, if the beach width obtained after considering RSLR-induced erosion is equal or higher than the before defined critical beach width (W_c) (see equation 5.3), we assume that the accommodation space is enough for the beach to maintain its profile elevation. As vulnerability is defined in terms of the vertical elevation of the beach with respect to run-up elevation, no variations in vulnerability to storm-induced inundation are expected under these conditions. Thus, the intermediate variable remains equal than the one described in equation 4.5. The contrary

occurs if the final beach width is lower than the critical beach width (W_c), in which case the beach can not maintain its elevation and the new intermediate variable is defined as:

$$IV = Ru/(B_{max} - s) \tag{5.5}$$

where Ru is the run-up elevation associated to a determined return period in meters, B_{max} is the maximum berm height and s is the value of RSLR at a specific time projection (see Figure 5.9).

Despite the large number of beaches that potentially disappear or present widths less than the critical value as a consequence of RSLR, the increase in vulnerability to storm-induced inundation due to this agent contribution is lower than in the case of erosion. As it can be observed in Figure 5.19, the coastal length corresponding to the beaches that fall into the two worst inundation vulnerability categories increases from 67 km at the baseline to 9km and 102 km at the 50-year projection when the low and high RSLR scenarios are considered respectively.

As in the previous section, the vulnerability results presented in the following lines are referred to the ones obtained considering the contribution of the medium RSLR scenario with subsidence rates.

Figure 5.20 shows the percentage of coastline corresponding to each inundation vulnerability category for a 50-yr return period at different time scales. Results show no variations in vulnerability for the two first projections compared to the baseline and very little variations when the 25-yr projection is considered. As observed, around 9% of the coastline becomes high or very high vulnerable to inundation between the baseline and the 50-yr projection. In general, the increase in vulnerability to inundation due to RSLR contribution is significantly lower than the one obtained for erosion and it is only perceptible at longer projections, when the cumulative effects of erosion affect the critical beach width. Besides this, inundation results indicate a more heterogeneous classification of the coastline with respect to all vulnerability categories.

Results interpreted at sector scale suggest that, as in the case of erosion, the largest increases in vulnerability to storm-induced inundation due to RSLR contribution are found in the southern areas of the Catalan coast. If baseline results are compared to those obtained for the 50-yr projection, the largest increase in vulnerability is detected in sector VI, where 35% of the coastline becomes high or very high vulnerable to storm-induced inundation due to RSLR contribution in 50 years (2060). Opposite to this, sector III, in the central coast, shows the lowest increase in vulnerability with only

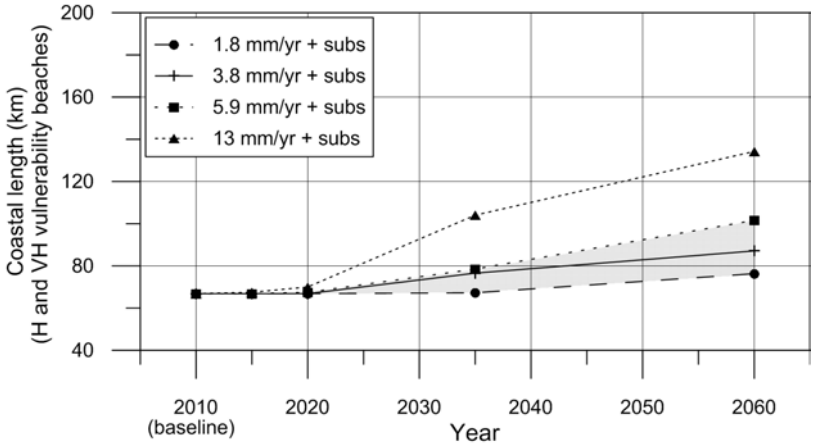

Figure 5.19: Length of coastline classified as high (H) or very high (VH) vulnerable to storm-induced inundation for a 50-yr return period. Considered contribution: RSLR. Total coastal length: 218.65 km.

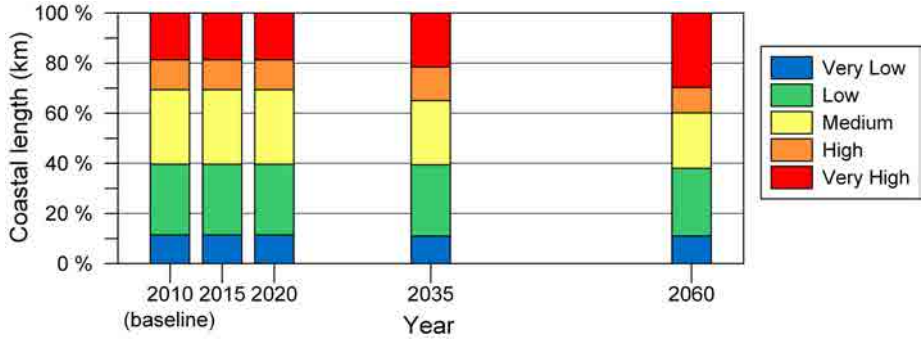

Figure 5.20: Percentage of coastline corresponding to each category of vulnerability to storm-induced inundation for a 50-yr return period. Considered contribution: medium RSLR scenario (3.8 mm/yr + subsidence). Total coastal length: 218.65 km.

0.3% of its coastline becoming high or very high vulnerable within the same period.

These results are logical considering that the southern areas, predominated by dissipative beaches with very mild slopes and subject to important subsidence rates, are extremely sensitive to RSLR-induced beach retreat. As a consequence, the same beaches are also prone to become unable to maintain its critical width and, consequently, more affected by changes in beach elevation due to RSLR-induced inundation. This explains the fact that dissipative beaches (type 4) are also the most affected by RSLR in terms of inundation vulnerability. On the contrary, no variations in coastal vulnerability due to RSLR is detected for beach types 1 and 5, both representing reflective beaches. However, these results have to be carefully interpreted because

all the beaches classified into types 1 and 5, mainly characterised by high beach-face slopes and, consequently, higher run-up magnitudes, already result very vulnerable at the baseline.

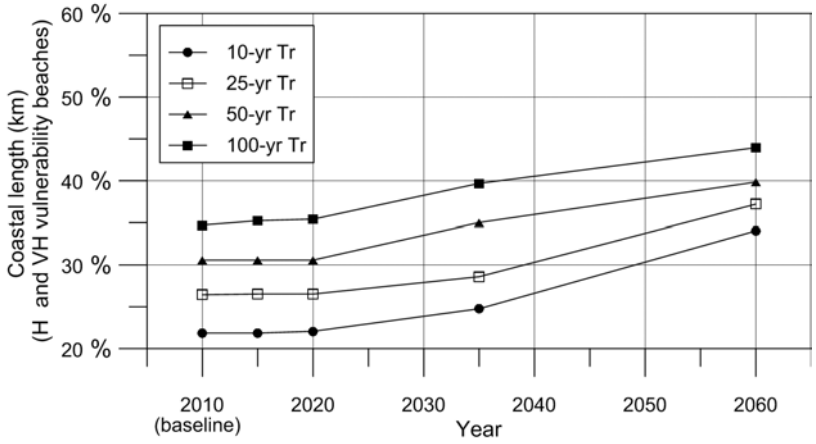

Figure 5.21: Percentage of coastline classified as high (H) or very high (VH) vulnerable to storm-induced inundation for different return periods. Considered contribution: medium RSLR scenario (3.8 mm/yr + subsidence). Total coastal length: 218.65 km

Figure 5.21 shows the percentage of coastline corresponding to high and very high vulnerable beaches for different return periods and time projections. Results reveal a very similar behaviour among return periods, although differences between them tend to decrease along time due to RSLR contribution. As expected, vulnerability increases as the return period does so. In all cases variations in vulnerability for the 5-yr and 10-yr projections are little significant with respect to the baseline. As observed, the percentage of coastline classified into the two worst categories at the 50-yr projection ranges from 34% to 44% for the 10-yr and 100-yr return period respectively.

Figure 5.22 presents inundation vulnerability results for each province. Here it can be observed how the largest increase in vulnerability occurs in the southernmost province, whereas RSLR contribution results almost imperceptible in Barcelona and Girona. The highest percentage of high and very high vulnerable coastline at the 50-yr projection is found in Tarragona (42%), yet it is very similar to the one found in Barcelona (41%). Again, vulnerability increments result significantly lower than in the case of erosion.

The same results at *comarca* scale are presented in Table 5.5. As it can be observed, the southernmost *comarca* is clearly the most affected by RSLR, with 53% of its coastline becoming high or very high vulnerable to storm-induced inundation

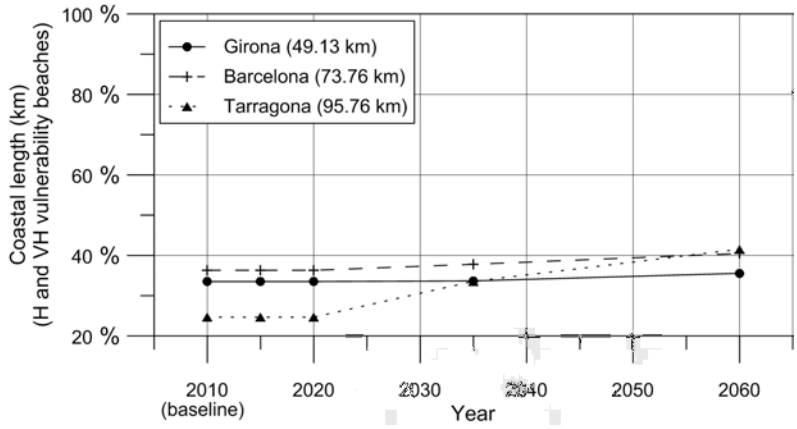

Figure 5.22: Length of coastline per province classified as high (H) or very high (VH) vulnerable to storm-induced inundation for a 50-yr return period. Considered contribution: medium RSLR scenario (3.8 mm/yr + subsidence).

at the 50-yr projection with respect to the baseline. An important increase in vulnerability is also observed in Garraf (7) and Baix Ebre (11), located in the central and southern coast respectively although, opposite than in the case of erosion, the last one is already one of the most vulnerable at the baseline. Despite the fact that Maresme (4) and Baix Llobregat (6), located in the central coast, present no variations in vulnerability to storm-induced inundation due to RSLR contribution when the medium RSLR scenario is considered, the first one is always one of the most vulnerable *comarcas* independently of the projection.

Table 5.5: Length of coastline per *comarca* classified as high (H) or very high (VH) vulnerable to storm-induced inundation for a 50-yr return period. Considered contribution: medium RSLR scenario (3.8 mm/yr + subsidence).

	Km of H and VH vulnerability					
Comarca	2010	2015	2020	2035	2060	Length (km)
Alt Empordà (1)	9.26	9.26	9.26	9.26	9.94	21.98
Baix Empordà (2)	4.87	4.87	4.87	4.95	5.07	19.51
La Selva (3)	2.33	2.33	2.33	2.33	2.46	7.63
Maresme (4)	18.83	18.83	18.83	18.83	18.83	39.01
Barcelonès (5)	2.93	2.93	2.93	2.93	3.43	13.09
Baix Llobregat (6)	3.65	3.65	3.65	3.65	3.65	11.03
Garraf (7)	1.38	1.38	1.38	2.48	3.95	10.63
Baix Penedès (8)	1.99	1.99	1.99	1.99	2.11	12.81
Tarragonès (9)	5.72	5.72	5.72	5.72	6.04	22.14
Baix Camp (10)	5.36	5.36	5.36	5.36	5.84	21.99
Baix Ebre (11)	6.70	6.70	6.70	7.27	8.86	14.17
Montsià (12)	3.84	3.84	3.84	11.80	16.94	24.65

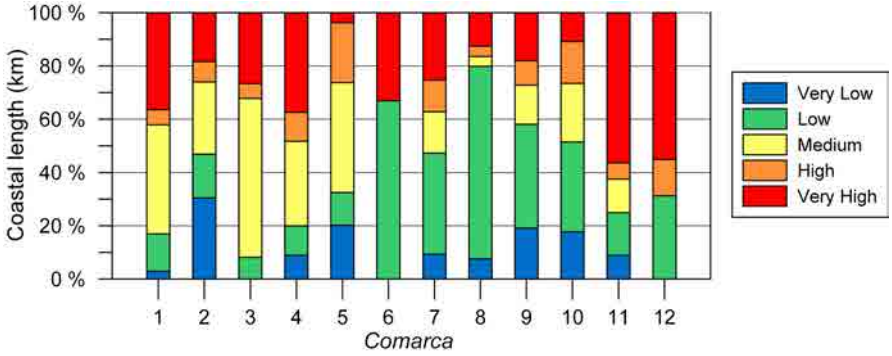

Figure 5.23: Percentage of coastline per *comarca* corresponding to each category of vulnerability to storm-induced inundation for a 50-yr return period and a 50-yr projection. Considered contribution: medium RSLR scenario (3.8 mm/yr + subsidence).

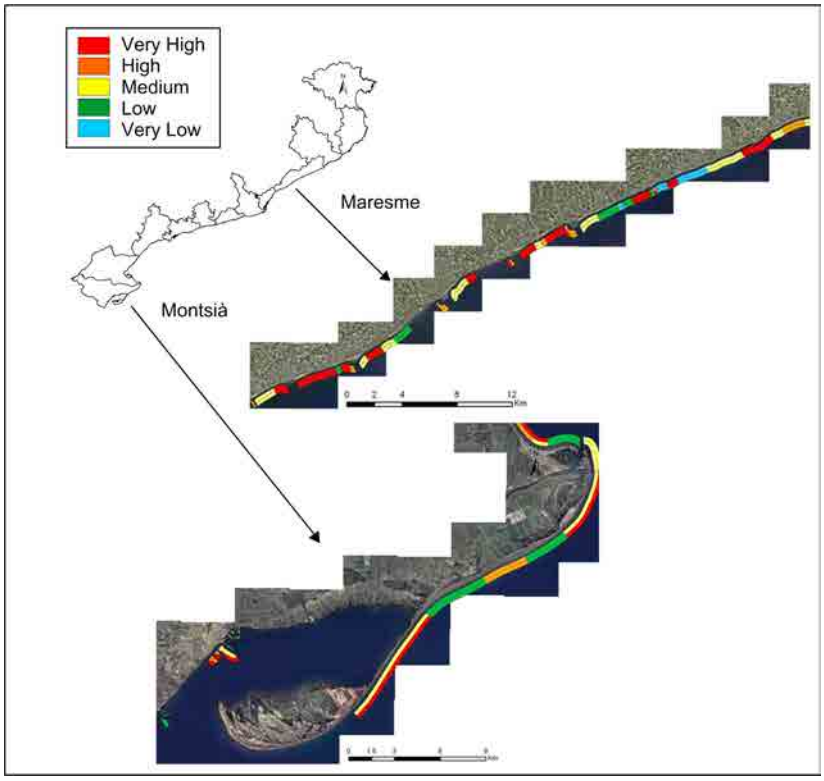

Figure 5.24: Spatial representation of vulnerability to storm-induced inundation for two *comarcas*. Comparison between baseline vulnerability (inshore line, 2010) and the 50-yr projection considering a RSLR scenario of 3.8 mm/yr plus subsidence (offshore, 2060). Results relative to a 50-yr return period.

Differences among *comarcas* with respect to the distribution of all the vulnerability categories at the 2060 horizon are shown in Figure 5.23. In agreement with previous results, the two southernmost *comarcas* stand out as the most vulnerable to storm-induced inundation. This is due, in part, to the combination of very mild slopes, fine sediment and large subsidence rates, which contributes to increase RSLR-induced erosion and, in consequence, RSLR-inundation. At the same time, the characteristic low profiles of this area also reduce the ability of the coast to cope with storm-induced inundation. Besides this, Maresme (4) and Alt Empordà (1) also present significant vulnerability, not as a result of RSLR contribution, but already at the baseline.

Figure 5.24 shows inundation results at beach scale considering the two *comarcas* that present minor and major changes in vulnerability at the 50-yr projection with respect to current conditions. Although no variations in any beach are detected in the case of Maresme (4), it can be observed how baseline vulnerability is already important, with very few beaches classified into low and very low categories. On the other hand, an important increase in vulnerability to storm-induced inundation can be observed in Montsià (12) as a consequence of RSLR contribution.

5.4 Integrated vulnerability

Once the contribution of RSLR and LST to storm-induced vulnerability is assessed separately, they are integrated to assess the overall vulnerability to storms in the Catalan coast.

Final vulnerability results are presented following the same structure that in previous sections. First, an analysis of the beach evolution considering the integrated effects of LST and RSLR-induced processes is performed. This is done to quantify the potential variations in the resilience of the beach at selected time projections. After this, erosion and inundation vulnerability is assessed and interpreted considering different spatial and temporal scales.

5.4.1 Beach evolution at multiple time scales

Although LST and RSLR-induced changes in beach morphology verify at different main time scales, they are cumulative. This means that when they are integrated over a given time period, their contribution is added to obtain the final beach morphology. The resulting beach width projections are considered as an indicator of the future

ability of the coast to cope with storm-impacts, assuming no variations in shoreline evolution and RSLR rates at the time scale of the analysis.

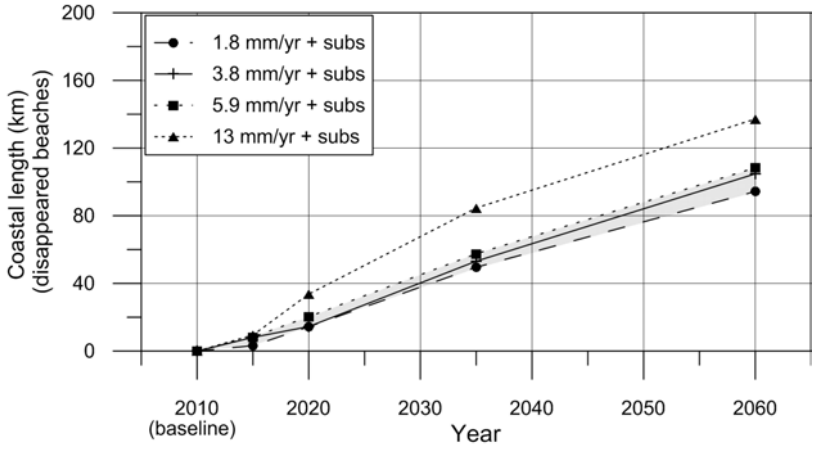

Figure 5.25: Length of coastline corresponding to disappeared beaches due to the integrated effects of LST and RSLR. Total coastal length: 218.65 km.

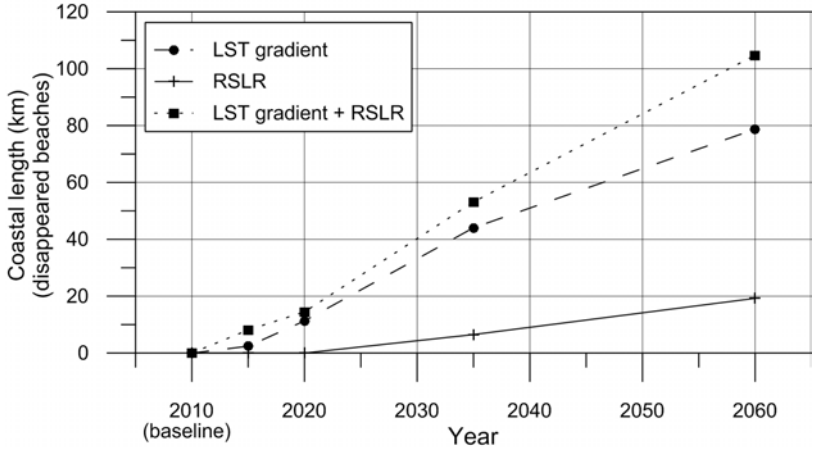

Figure 5.26: Coastal length corresponding to disappeared beaches. Considered contributions: (i) LST, (ii) medium RSLR scenario (3.8 mm/yr + subsidence) and (ii) both of them. Total coastal length: 218.65 km.

As it was previously showed for each component, one of the direct consequences of their effects is the potential disappearance of beaches. Figure 5.25 shows the total length of coastline corresponding to beaches that will potentially disappear due to the integrated effects of LST and RSLR. As before, this should correspond to the worst case scenario, in which beaches are backed by rigid boundaries and, in consequence,

without accommodation space.

When the 50-yr projection is considered, all scenarios result in more than 90 km of disappeared beaches (about 41% of the total coastline). Due to the weight of LST contribution, differences among scenarios are lower than when only RSLR is considered (see Figure 5.11). In addition to this, the coastal length corresponding to beaches that will potentially disappear results much larger in this case.

The different contribution of each component to beach disappearance is shown in Figure 5.26. In this specific case, the medium RSLR scenario is considered. As it can be seen, the main contribution is due to LST, which clearly dominates from relative short term scales. Furthermore, the fact that the total length of disappeared beaches is similar to the addition of both contributions suggest that each process affects different types of beach. In this sense, and as mentioned before, dissipative beaches are clearly the most affected by RSLR-induced beach retreat, whereas the LST contribution is, in general, independent of the beach type.

5.4.2 Erosion vulnerability

The results of vulnerability to storm-induced erosion obtained integrating the effects of LST and RSLR are presented in this section. Unless otherwise specified, RSLR contribution corresponds to the medium scenario with subsidence.

Figure 5.27 shows the length of coastline classified into the two worst categories of vulnerability to storm-induced erosion associated to a 50-yr return period and considering the contribution of 4 different RSLR scenarios. As it can be observed, the magnitudes associated to the worst scenario are significantly higher than the ones obtained for the other ones. However, if compared with the results obtained when RSLR contribution is assessed independently, differences among scenarios are much lower due to LST contribution (see Figure 5.13). Integrated results indicate that, independently of the selected scenario, a minimum of 101 km of the studied coastline will potentially be high or very high vulnerable to storm-induced erosion at the 10-yr projection (2020), which corresponds to more than 46% of the coastline. When the 50-yr projection is considered, these values increase to 160 km and 73% of the coast.

Figure 5.28 shows the total length of high and very high vulnerable beaches obtained with and without integrating LST and RSLR contributions. As expected, when both contributions are assessed separately, vulnerability is higher in the case of LST, since shoreline evolution rates at this scale are significantly larger than those

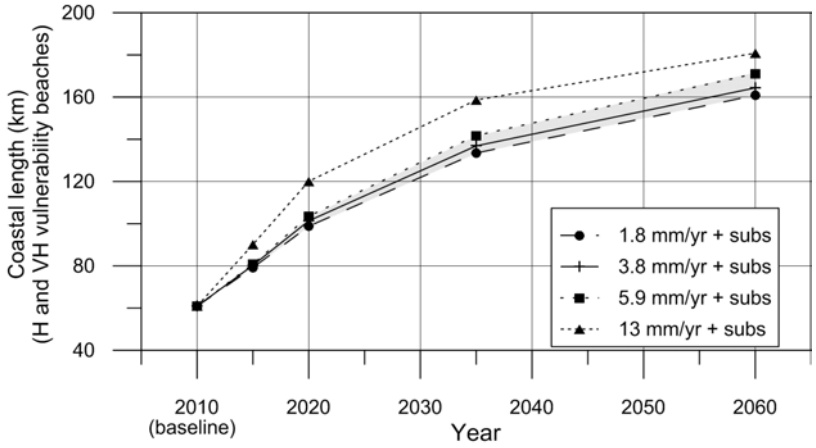

Figure 5.27: Length of coastline classified as high (H) or very high (VH) vulnerable to storm-induced erosion for a 50-yr return period. Considered contributions: LST and RSLR. Total coastal length: 218.65 km.

RLSR-induced. Opposite to what happens in the case of disappeared beaches, integrated vulnerability results do not correspond to the addition of the two processes contribution. This can be explained by the complexity of the concept of vulnerability, which involves the relation of multiple variables. As a consequence, integrated erosion vulnerability values result from the synergy of both processes.

The percentage of coastline corresponding to each category of vulnerability obtained considering both contributions is shown in Figure 5.29. Results reveal the two most extreme vulnerability categories as the dominant ones, reaching a maximum at the 50-yr projection, in which the remaining categories are almost non-existent. The largest increase in the percentage of coastline that falls into to the two worst vulnerability categories occurs between the 10-yr and 25-yr projections, ranging from 38% to 60% (an increase of 0.9% per year).

Results show that the percentage of high and very high vulnerable coastline exceeds 50% in all sectors at the 50-yr projection. Although the northernmost sector results the most vulnerable at the 25-yr and 50-yr projections, the largest increase in vulnerability is found at sector VI, which is subject to important beach retreat caused not only by RSLR, but also by the background erosion detected at some of the largest beaches of the Ebre delta. With respect to beach types, the increase in vulnerability cannot be solely explained by changes in one specific beach type, which stresses again the combined contribution of both processes.

Integrated erosion vulnerability evaluated considering different return periods is

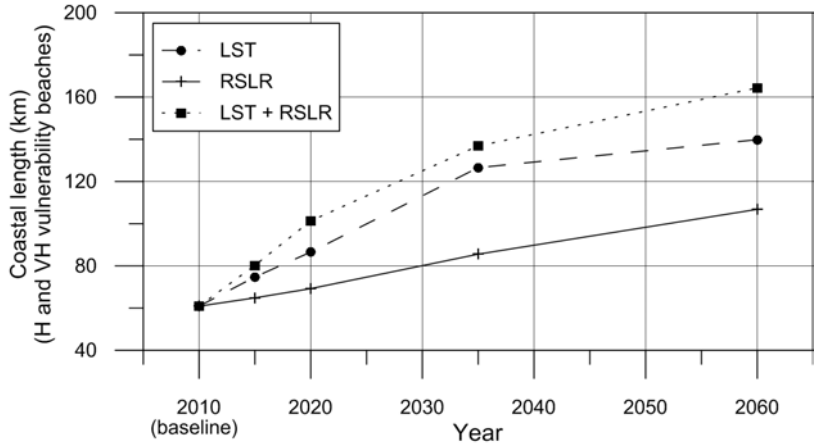

Figure 5.28: Comparison of the coastal length corresponding to high (H) and very high (VH) vulnerable beaches to storm-induced erosion for a 50-yr return period. Considered contributions: (i) LST, (ii) medium RSLR scenario (3.8 mm/yr + subsidence) and (ii) both of them. Total coastal length: 218.65 km.

shown in Figure 5.30. As observed, the total length of high and very high vulnerable coastline for the different return periods tends to attain an asymptotic value for time projections exceeding 50-yr. This will serve to stress the role of background erosion in controlling the long-term behaviour of coastal vulnerability to storms. Thus, independently of the return period, more than 50% and 70% of the coastline becomes high and very high vulnerable to storm-induced erosion at the 25-yr and 50-yr projections respectively.

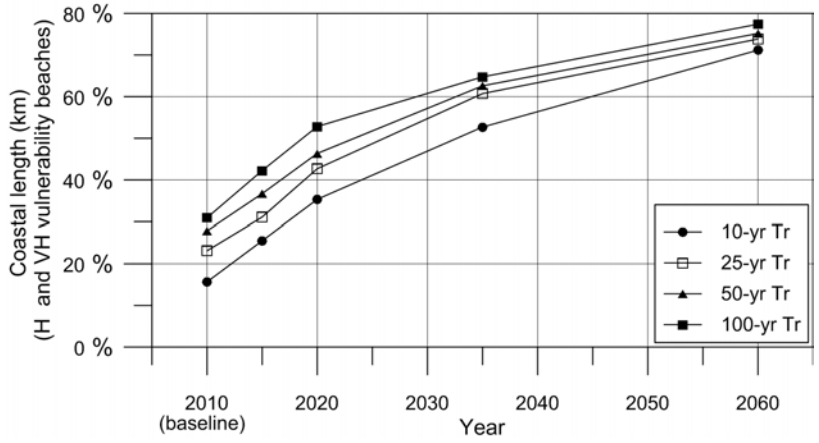

Figure 5.30: Percentage of coastline classified as high (H) or very high (VH) vulnerable to storm-induced erosion for different return periods. Considered contributions: LST and the medium RSLR scenario (3.8 mm/yr + subsidence). Total coastal length: 218.65 km.

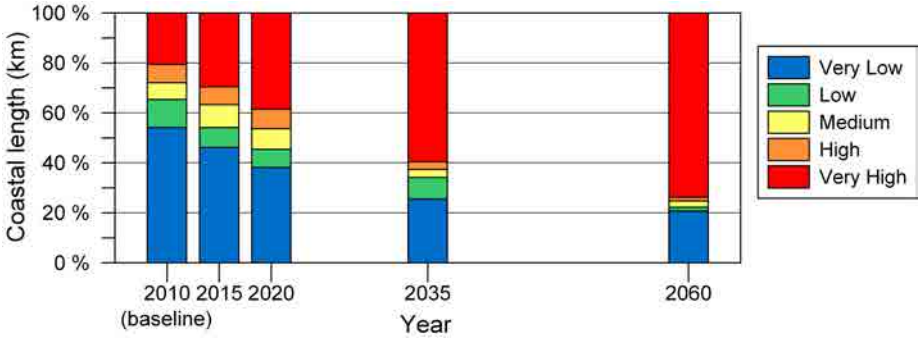

Figure 5.29: Percentage of coastline corresponding to each category of vulnerability to storm-induced erosion for a 50-yr return period. Considered contributions: LST and the medium RSLR scenario (3.8 mm/yr + subsidence). Total coastal length: 218.65 km.

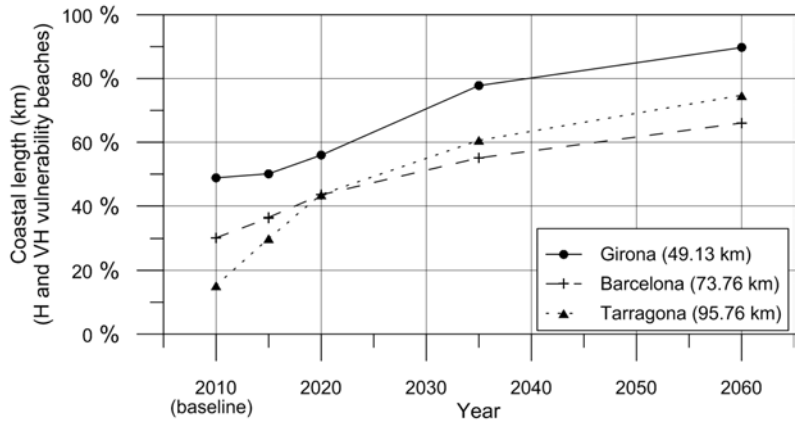

Figure 5.31: Percentage of coastline per province classified as high (H) or very high (VH) vulnerable to storm-induced erosion for a 50.yr return period. Considered contributions: LST and the medium RSLR scenario (3.8 mm/yr + subsidence).

Erosion results expressed at province scale are shown in Figure 5.31. It can be observed how, independently of the time scale, the northern province (Girona) is the most vulnerable to erosion. In spite of this, and coinciding with the results obtained at sector scale, Tarragona presents the largest increase in vulnerability.

Table 5.6 shows the coastal length corresponding to high and very high vulnerable beaches for each *comarca* at different time scales. In general, results indicate that from the 10-yr projection onward, the most vulnerable *comarcas* are located at the northern and southern parts of the Catalan coast. Two clear examples of this are Alt Empordà (1) and Baix Ebre (11), in which the percentage of coastline corresponding to the two worst vulnerability categories reaches 100% and 99.6% respectively at the

50-yr projection. However, the largest increase in vulnerability occurs at the southern *comarcas*, mainly because of the combination of very mild slopes and the location of the most important subsidence area, which enhances RSLR-induced erosion, together with some of the most important medium-term erosion rates. On the other hand, a decrease in vulnerability at earlier projections as a consequence of LST effects is observed in Barcelonès (5) and Garraf (7). When compared to the results obtained when only LST contribution is considered (see Table 5.3), the vulnerability of Garraf (7) decreases for the three first time projections, instead of for all of them, highlighting again the long-term contribution of RSLR to the overall vulnerability.

Table 5.6: Length of coastline per *Comarca* classified as high (H) or very high (VH) vulnerable to storm-induced erosion for a 50-yr return period. Considered contributions: LST and the medium RSLR scenario (3.8 mm/yr + subsidence).

	Km of H and VH vulnerability					
Comarca	2010	2015	2020	2035	2060	Length (km)
Alt Empordà (1)	13.56	13.56	13.56	20.21	21.98	21.98
Baix Empordà (2)	8.11	8.42	8.62	12.07	15.20	19.51
La Selva (3)	2.32	2.64	5.31	5.92	6.89	7.63
Maresme (4)	12.72	18.02	19.33	26.32	28.83	39.01
Barcelonès (5)	3.97	3.55	4.01	5.38	9.85	13.09
Baix Llobregat (6)	0	0	3.65	3.65	3.65	11.03
Garraf (7)	5.60	5.31	5.11	5.28	6.39	10.63
Baix Penedès (8)	1.67	1.83	4.03	6.87	9.33	12.81
Tarragonès (9)	3.47	5.67	8.30	11.36	15.13	22.14
Baix Camp (10)	6.55	7.26	6.69	12.64	14.91	21.99
Baix Ebre (11)	2.22	8.59	8.89	10.25	14.11	14.17
Montsià (12)	0.72	5.43	13.86	16.92	18.11	24.65

Differences in erosion vulnerability among *comarcas* for the 50-yr projection are shown in Figure 5.32. Here it can be easily observed how more than 50% of the coastline of all the *comarcas* becomes very high vulnerable to storm-induced erosion, with the exception of Baix Llobregat (6). Furthermore, the two extreme vulnerability categories are the most important ones in all cases (very high and very low).

Results represented at beach scale for the two *comarcas* that show the largest and lowest increase in vulnerability at the 50-yr projection with respect to the baseline are presented in Figure 5.33. In the case of Garraf (7), this scale of representation permits to specifically identify which beaches present a decrease in vulnerability. With respect to Baix Ebre (11), it can be observed how the beaches located in the Ebre delta change from very low to very high vulnerability in 50 years.

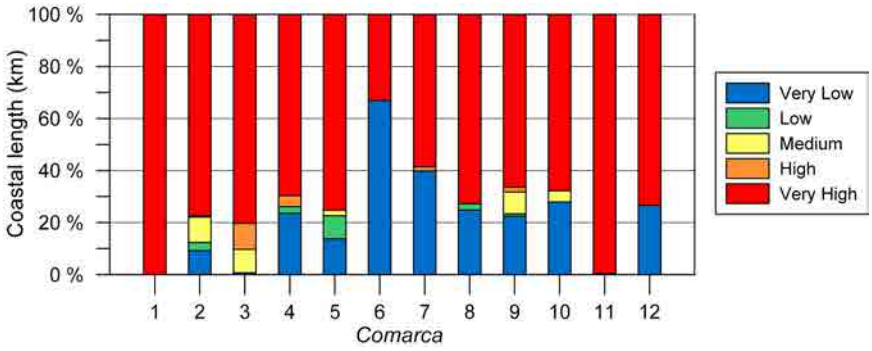

Figure 5.32: Percentage of coastline per *comarca* corresponding to each category of vulnerability to storm-induced erosion for a 50-yr return period and a 50-yr projection. Considered contributions: LST and the medium RSLR scenario (3.8 mm/yr + subsidence).

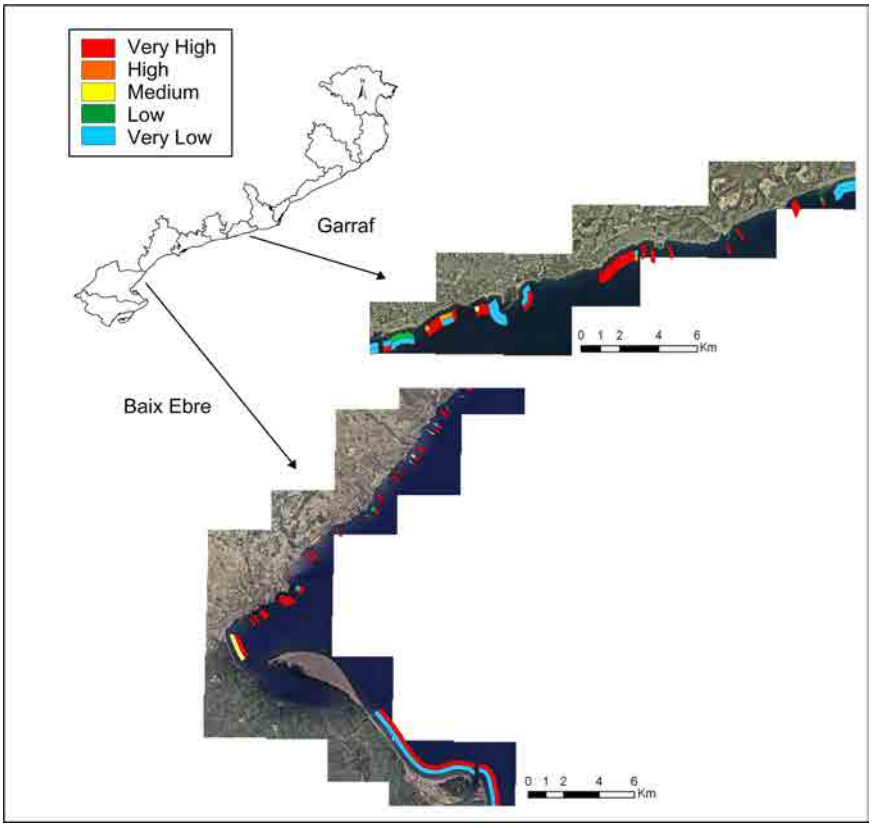

Figure 5.33: Spatial representation of vulnerability to storm-induced erosion for two *comarcas*. Comparison between baseline vulnerability (inshore line, 2010) and the 50-yr projection considering LST and a RSLR of 3.8 mm/yr plus subsidence (offshore line, 2060). Results relative to a 50-yr return period.

Lastly, Figure 5.34 shows differences in vulnerability among current conditions and the 10-yr projection at beach scale for Barcelonès (5). Apart from being one of the *comarcas* that shows a lower increase in vulnerability at this time horizon (2020), a large spatial variability in terms of vulnerability categories can be observed.

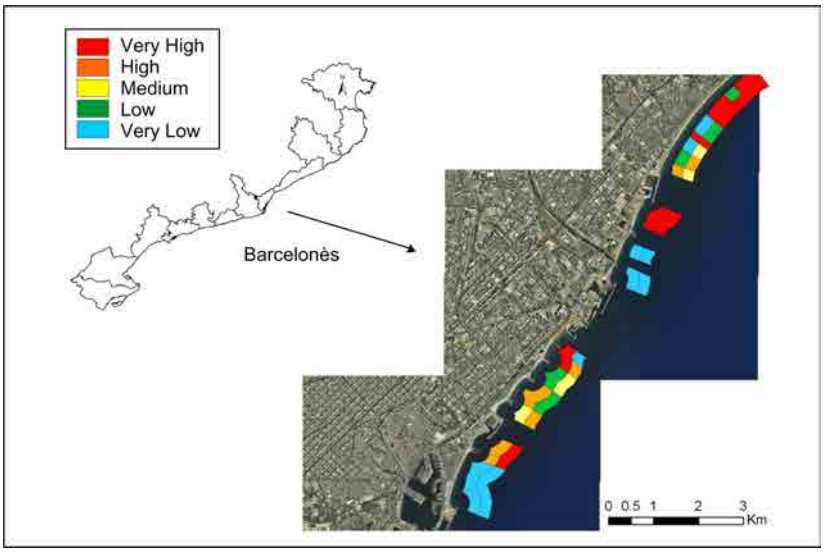

Figure 5.34: Spatial representation of vulnerability to storm-induced erosion for the Barcelonès *comarca*. Comparison between current/baseline vulnerability (inshore line, 2010) and a 10-yr projection considering shoreline evolution rates and a RSLR of 3.8 mm/yr plus subsidence (offshore line, 2060). Results relative to a 50-yr return period.

5.4.3 Inundation vulnerability

Final results of vulnerability to storm-induced inundation obtained integrating LST and RSLR contributions are presented in this section. In this work we have assumed that LST does not directly affect storm-induced inundation vulnerability because the vertical elevation of the beach remains constant. Nevertheless, the final beach width considers beach retreat caused by the effect of both processes, in such a way that the number of beaches which width is less than the critical value may differ from the obtained when only RSLR is considered. As in the case of erosion, results considering both contributions refer, in the case of RSLR, to the medium scenario.

Figure 5.35 shows the coastal length corresponding to beaches with widths less than the critical value, which, as observed again, does not necessarily increases along time. If we compare these results with the ones obtained when only RSLR is accounted

for (see Figure 5.36), a decrease in the length of coastline associated to beaches that will not potentially maintain its elevation can be observed at the final projection, as well as a more rapid increase at earlier projections (5-yr and 10-yr). Besides this, final integrated results show much lower differences among RSLR scenarios (see Figure 5.10).

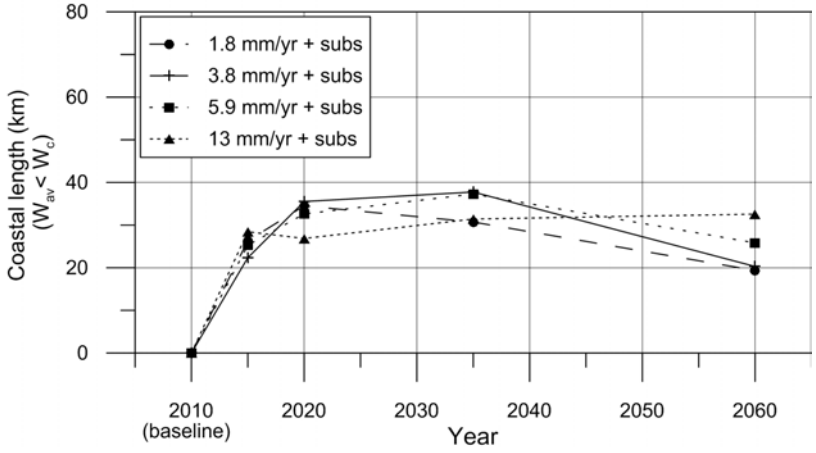

Figure 5.35: Length of coastline corresponding to beaches with width less than the critical width ($W_{av} < W_c$), due to LST and RSLR contributions. Total coastal length: 218.65 km.

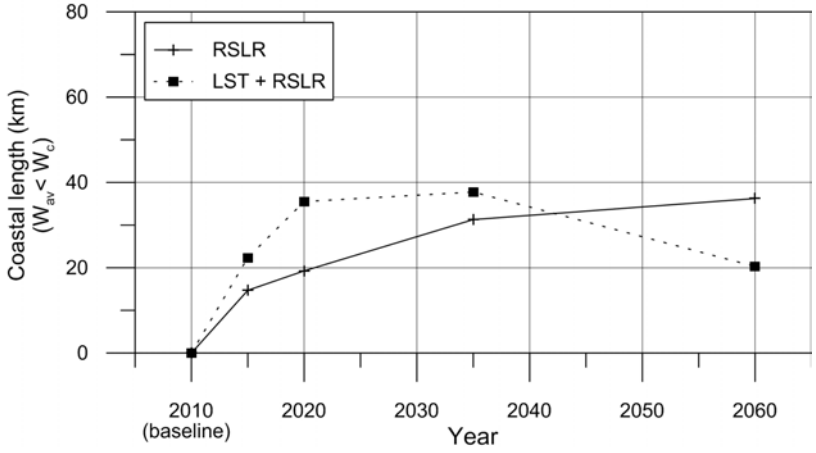

Figure 5.36: Length of coastline corresponding to beaches with width less than the critical value ($W_{av} < W_c$). Considered contributions: (i) the medium RSLR scenario (3.8 mm/yr + subsidence) and (ii) LST and the medium RSLR scenario. Total coastal length: 218.65 km.

The total length of high and very high vulnerable beaches to storm-induced inundation once LST and RSLR effects are integrated is shown in Figure 5.37. As it can be observed, if the 10-yr projection is considered, a minimum of 74 km (34%) of the coastline falls into the two worst vulnerability categories. These values increase up to 134 km and 60% when the 50-yr projection is accounted for. As a consequence of LST contribution, these results show a major increase in vulnerability and minor differences between RSLR scenarios, compared to those obtained when only RSLR contribution is considered (see Figure 5.19). The comparison between results with and without integrating both components is shown in Figure 5.38. The coastal length corresponding to high and very high vulnerable beaches at the 50-yr projection is much higher when both components are considered, revealing an important contribution of erosion due to LST to final inundation vulnerability, which appears to be already noticeable at early projections.

Figure 5.39 presents the evolution of vulnerability to storm-induced inundation through time. Even when LST-induced erosion is considered, the effects of RSLR are noticed at long-term scales, which is proven by the very little significant increase in vulnerability obtained for the 5-yr and 10-yr projections. On the contrary, if differences between the 50-yr projection and baseline are taken into account, the percentage of coastline corresponding to the two worst vulnerability categories ranges from 31% to 67%. Furthermore, these results stress out that vulnerability categories are more heterogeneously distributed than in the case of erosion, being medium and low categories the most important at baseline, 5-yr and 10-yr projections.

The same results interpreted at sector scale point at sector VI as the one in which the largest increase in vulnerability occurs at the 50-yr projection with respect to the baseline. The main difference between these results and the ones obtained when only RSLR contribution is considered resides in the magnitude of vulnerability variations, as sector VI appears to be the one presenting the largest increase in both cases, as well as the most vulnerable at the final projection. However, as a result of LST contribution, integrated results also show important increases in vulnerability for the rest of coastal sectors.

Opposite to what can be observed in the case of erosion, inundation vulnerability cannot decrease through time. This is mainly due to the fact that in this work it is defined in terms of the maximum vertical elevation of the beach, which we assume remains constant even if the total beach width increases under accretive shoreline conditions. The formulation of inundation vulnerability in terms of elevation implies that, as long as the beach width does not decrease below the critical value (W_c), no

variations in vulnerability will occur. However, in the case of using floodwater or overtopping entering in the hinterland to define the inundation magnitude, vulnerability should decrease as beach width gets wider.

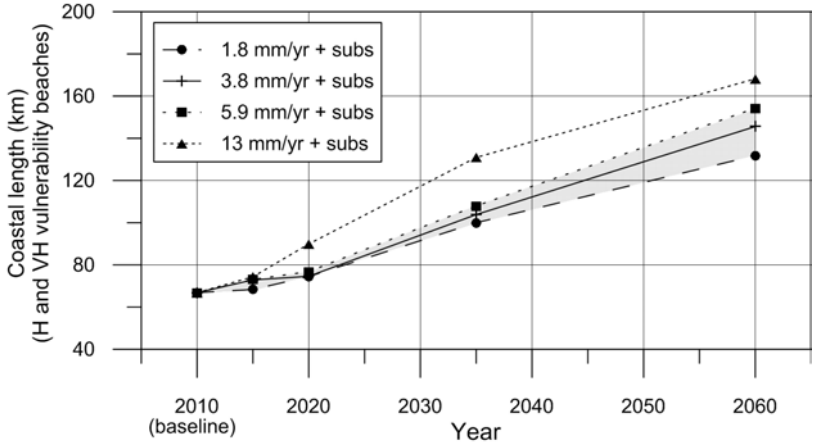

Figure 5.37: Percentage of coastline classified as high (H) or very high (VH) vulnerable to storm-induced inundation for a 50-yr return period. Considered contributions: LST and RSLR. Total coastal length: 218.65 km.

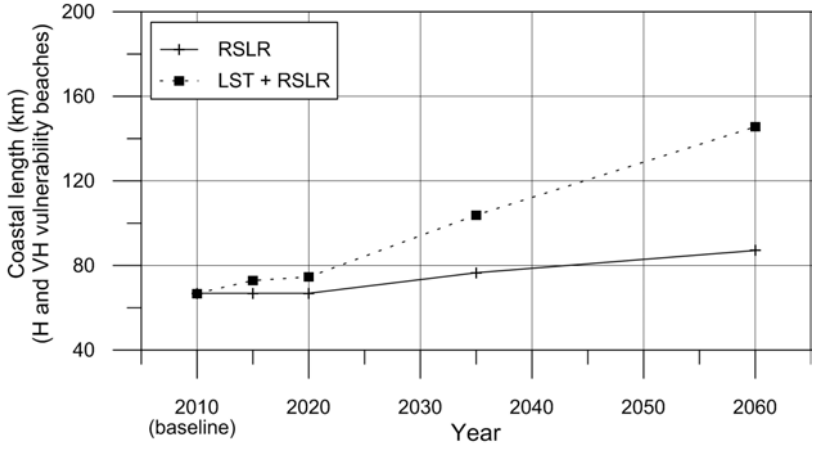

Figure 5.38: Length of coastline classified as high (H) or very high (VH) vulnerable to storm-induced inundation for a 50-yr return period. Considered contributions: (i) the medium RSLR scenario (3.8 mm/yr + subsidence) and (ii) LST and the medium RSLR scenario. Total coastal length: 218.65 km.

Results obtained for the 50-yr projection reveal that beach types 4 and 8 are the

ones in which the largest increases in vulnerability are detected. As mentioned before, the first one represents the most dissipative conditions. The second one corresponds to intermediate conditions, yet it is characterized by presenting the second lowest representative values of grain size and beach-face slope. In spite of this, other beach types representative of intermediate and reflective beaches (6, 3 and 7) also present important increases in vulnerability. These results support, once again, the conclusion that RSLR contribution preferentially targets dissipative beaches, characteristic of low-lying areas such as the Ebre delta, while LST contribution does not depend on the beach type.

Final vulnerability to storm-induced inundation has been also assessed for different return periods. As it can be observed in Figure 5.40, results obtained for the 50-yr projection suggest that, when RSLR and LST contributions are integrated, more than 60% of the studied coastline becomes high or very high vulnerable to storm-induced inundation, independently of the selected return period. Similarly to what happens when only RSLR is considered, differences between return periods at the baseline are higher than at the 50-yr projection.

Figure 5.41 shows the percentage of coastline classified into the two worst inundation vulnerability categories for each province at different time scales. As it can be seen, the most significant increase in vulnerability is clearly detected in Tarragona. This province results the most affected by RSLR, as it is mainly composed of dissipative beaches with very mild slopes and comprises the most significant subsidence areas. Furthermore, not only a major beach retreat due to RSLR is observed in these southernmost areas, but they are also characterized by very low profiles, which enhances their vulnerability to inundation. However, a significant increase in vulnerability is also observed in the other provinces at the 25-yr and 50-yr projections, with at least 40% and 60% of the their coastline classified into the two worst categories respectively, which highlights the uniform contribution of LST.

The coastal length corresponding to high and very high vulnerable beaches for each *comarca* at different time scales is shown in Table 5.7. As it can be observed, Maresme (4), in the central coast, and Baix Ebre (11), in the South, are two of the most vulnerable *comarcas* at the baseline and for all the time projections. Even though the largest increase in vulnerability evaluated at the 50-yr projection with respect to the baseline is found in Baix Ebre (11), the contribution of LST leads to important increases in vulnerability at the rest of *comarcas*.

Opposite to what happens when RSLR contribution is assessed independently,

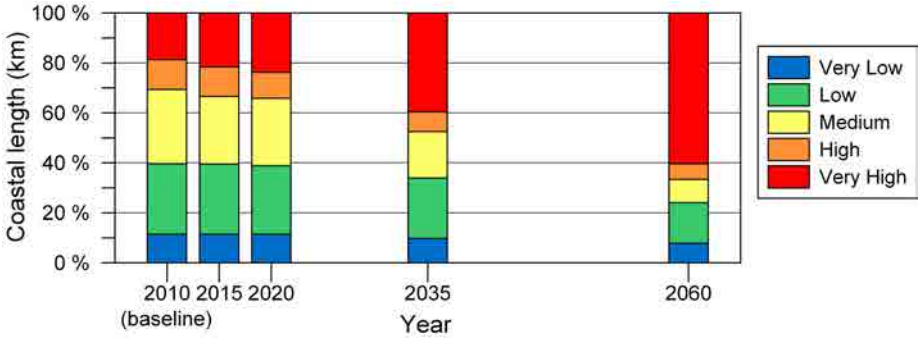

Figure 5.39: Percentage of coastline corresponding to each category of vulnerability to storm-induced inundation for a 50-yr return period. Considered contributions: LST and the medium RSLR scenario (3.8 mm/yr + subsidence). Total coastal length: 218.65 km.

in this case the southernmost *comarcas* already present increases in vulnerability at the 5-yr and 10-yr projections respectively, due to LST contribution, which accelerates inundation vulnerability in the areas most affected by RSLR. Moreover, in this case increases in vulnerability are not only focussed on the southern *comarcas*, being Maresme (4) a clear example of it.

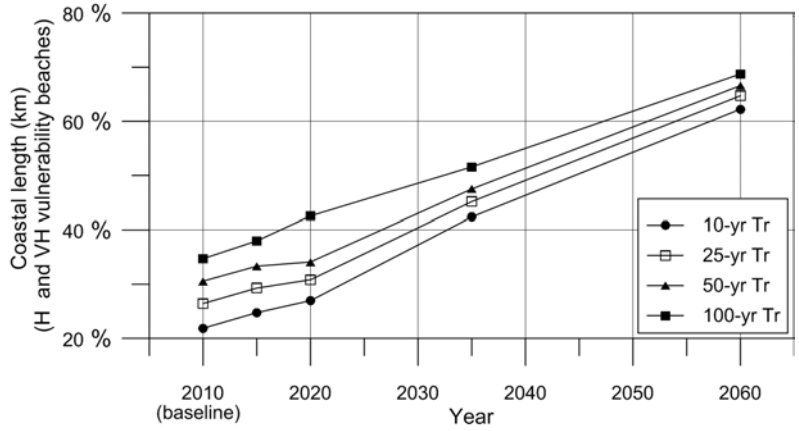

Figure 5.40: Percentage of coastline classified as high (H) or very high (VH) vulnerable to storm-induced inundation for different return periods. Considered contributions: LST and the medium RSLR scenario (3.8 mm/yr + subsidence). Total coastal length: 218.65 km.

Differences among *comarcas* in the percentage of coastline corresponding to each vulnerability category at the 50-yr projection are presented in Figure 5.42. In general, the most vulnerable *comarcas* are located at the southern and northern extremes of the Catalan coast, whereas the central area results less vulnerable. Moreover, and opposed to what erosion results indicate, intermediate vulnerability categories such

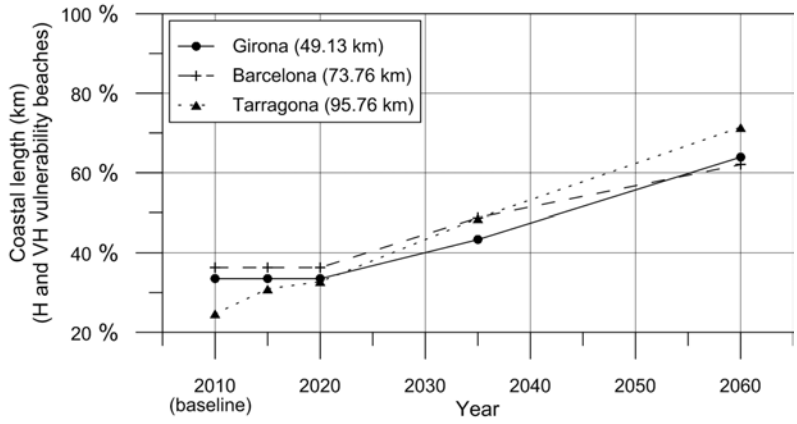

Figure 5.41: Length of coastline per province classified as high (H) and very high (VH) vulnerable to storm-induced inundation for a 50-yr return period. Considered contributions: LST and the medium RSLR scenario (3.8 mm/yr + subsidence).

as medium and very low remain still important.

Table 5.7: Length of coastline per *comarca* classified as high (H) or very high (VH) vulnerable to storm-induced inundation for a 50-yr return period. Considered contributions: LST and the medium RSLR scenario (3.8 mm/yr + subsidence)

	Km of H and VH vulnerability					
Comarca	2010	2015	2020	2035	2060	Length (km)
Alt Empordà (1)	9.26	9.26	9.26	9.94	17.71	21.98
Baix Empordà (2)	4.87	4.87	4.87	6.45	8.18	19.51
La Selva (3)	2.33	2.33	2.33	4.89	5.52	7.63
Maresme (4)	18.83	18.83	18.83	24.96	31.70	39.01
Barcelonès (5)	2.93	2.93	2.93	3.72	5.31	13.09
Baix Llobregat (6)	3.65	3.65	3.65	3.65	3.65	11.03
Garraf (7)	1.38	1.38	1.38	3.66	5.10	10.63
Baix Penedès (8)	1.99	1.99	2.11	3.70	7.84	12.81
Tarragonès (9)	5.72	5.72	6.97	7.76	14.31	22.14
Baix Camp (10)	5.36	5.44	5.79	5.96	12.34	21.99
Baix Ebre (11)	6.70	8.21	8.21	9.98	13.92	14.17
Montsià (12)	3.84	8.28	8.28	19.16	20.01	24.65

The lowest and largest increases in the percentage of coastline classified as high and very high vulnerable at the 50-yr projection with respect to the baseline are found in Baix Empordà (2) and Montsià (12) respectively. Figure 5.43 shows inundation vulnerability at beach scale for these two *comarcas*, in such a way that beaches that present variations can be specifically identified. As observed, almost all the southern

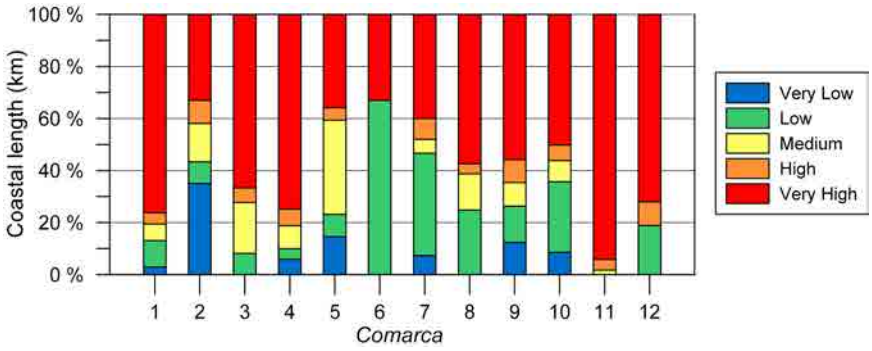

Figure 5.42: Percentage of coastline per *comarca* corresponding to each category of vulnerability to storm-induced inundation for a 50-yr return period and a 50-yr projection. Considered contributions: LST and the medium RSLR scenario (3.8 mm/yr + subsidence).

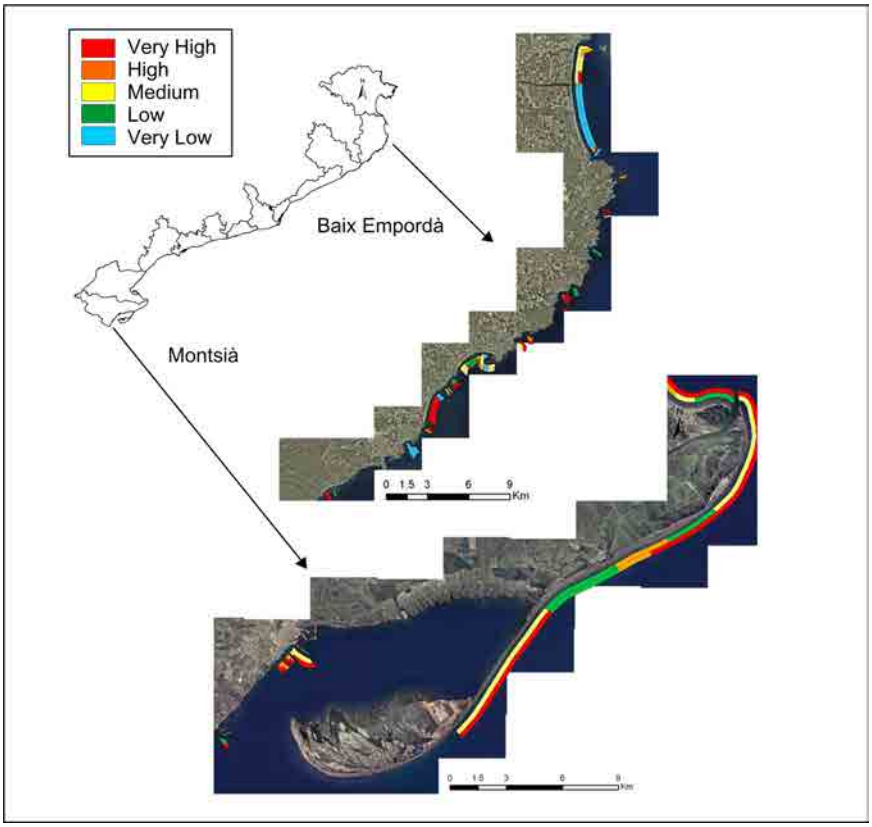

Figure 5.43: Spatial representation of vulnerability to storm-induced inundation for two *comarcas*. Comparison between baseline vulnerability (inshore line, 2010) and the 50-yr projection considering LST and a RSR of 3.8 mm/yr plus subsidence (offshore line, 2016). Results relative to a 50-yr return period.

part of the Ebre delta becomes very high vulnerable to storm-induced inundation, opposite to what happens in Baix Empordà (2), where only very few beaches show an increase in vulnerability.

Finally, these results agree with those obtained by Jiménez et al. (2012), which indicate an increase of the damages caused by storms in the Catalan coast during the last decades, due, among others, to the effect of background erosion. The results obtained in this work suggest a continuation/increase of such trend.

Chapter 6

Summary and Conclusions

In this work a methodology to assess coastal vulnerability to storms at different time scales has been developed and applied at regional scale to the Catalan coast (NW Mediterranean). Due to this, main conclusions are presented in two sections, covering both aspects separately.

6.1 Coastal vulnerability assessment methodology

The developed methodology permits to quantitatively assess storm-induced erosion and inundation vulnerability separately. To do so, the magnitude of the hazards is balanced with the beach capacity to cope with them. In this sense, a combination of variables defining the climatic forcing together with beach geomorphology is used to characterise the hazards intensity, whereas the resilience of the beach is only considered a function of its geomorphology (beach width and elevation for erosion and inundation respectively).

A parametric model specific for the Catalan coast has been used to determine storm-induced erosion magnitude. Such parametrization is derived from a numerical model that predicts cross-shore sediment transport (SBEACH) and a beach profile erosion predictor (JA). With respect to storm-induced inundation, it is generally caused by a combination of high water levels (storm surges and high tides) and wave action (run-up). However, the magnitude of the storm surges is much lower than the wave-induced component in the study zone. As a consequence, the run-up value at

the storm peak has been used to characterise inundation magnitude.

Aiming to obtain an objective assessment of vulnerability at large spatial and temporal scales, the proposed methodology is based on a probabilistic approach in which the storm-induced hazard magnitude is obtained for a probability of occurrence instead of for a determined storm event. As a result, the spatial variability in the storm climate is properly considered and, then, vulnerability values associated to the same probability of occurrence can be compared along the coast.

In order to become a useful planning tool, any method as the presented in this work should permit to assess future vulnerability. Thus, a methodology to take into account medium and long-term variations of storm-induced vulnerability has also been proposed by considering the effects induced by other acting processes. Here, erosion/accretion due to longshore sediment transport (LST) gradients and erosion and inundation due to relative sea-level rise (RSLR) have been selected as the main medium and long-term processes acting in the study area. With respect to LST contribution, it has been characterised by means of shoreline evolution rates assuming that, due to the characteristics of the study area, they are mainly induced by LST gradients. On the other hand, RSLR contribution has been defined for different sea-level and subsidence rates.

These coastal processes will essentially affect the resilience of the beach, as they will modify the beach morphology and, in consequence, its ability to cope with erosion and inundation. However, forcing conditions might also suffer long-term variations that, although they are not relevant for the study area, could be easily included by modifying the probabilistic distribution of the hazards.

The method has been optimized to its application at large spatial scales by reducing the necessary data and calculations. This has been done by defining different coastal sectors with homogeneous wave conditions and classifying the existing beaches within 8 categories (according to its sediment size and slope). As a result, the hazards are calculated for different combinations of coastal sectors and beach types instead of for each beach. In spite of this, as vulnerability is assessed considering the adaptation ability of each beach in front of such hazards, results are obtained at local scale.

This kind of analysis requires vulnerability to be updated as beaches evolve. Otherwise, estimations would not represent realistic conditions. Thus, the implementation of a coastal monitoring plan to complement the method is strongly recommended. Furthermore, a local validation of the methodology is also suggested before its application. For such purpose, a damage database should be built.

The versatility of the proposed method allows, not only to easily update information on process magnitudes and beach characteristics if necessary, but also to apply it to other coastal areas.

Lastly, a georeferenced database that contains information on beach morphology and vulnerability has been created. As a result, vulnerability can be easily combined with other territorial information, such as land use, to identify coastal uses and resources at risk. This should support coastal managers to make informed decisions for managing coastal disasters.

6.2 Vulnerability to storms in the Catalan coast

The proposed methodology has been applied to 219 km along the coast of Catalonia (NW Mediterranean). In general, a large variability in hazards intensity is observed along the coast even within the same sector, which highlights the important contribution of beach geomorphology. Furthermore, because beach characteristics directly determine the local capacity to cope with the hazards, such contribution results even larger when vulnerability is assessed.

Results for a 50-yr return period based on current conditions indicate a similar order of magnitude of storm-induced erosion and inundation vulnerability along the Catalan coast, with 28% and 31% of the coastline corresponding to high and very high vulnerable beaches respectively. When LST and the medium RSLR scenario are considered, a slightly higher increase in vulnerability along different time projections is detected in the case of erosion. As a result, 63% and 48% of the coastline results high or very high vulnerable at the 25-yr projection for erosion and inundation respectively, increasing up to 75% and 66% at the 50-yr projection. In general, inundation results present a more heterogeneous classification, whereas the two most extreme vulnerability categories are always the most frequent in the case of erosion.

Results also suggest that, depending on the selected RSLR scenario, between 20% and 40% of the coastline will potentially disappear under the integrated effects of LST and RSLR in only 25 years (2035 horizon).

As it can be observed in Figure 6.1, vulnerability interpreted at sector scale reveals sectors I and II as the most vulnerable to storm-induced erosion at the baseline. This is mainly due to the fact that these sectors are characterised by an intense storm climate. On the other side, the combination of moderate to intense storm climate

and steep beach slopes, which lead to higher run-up values, turns sectors II and III into the most vulnerable to inundation. However, it is important to stress out that vulnerability might have been overestimated in the northern sector because of the presence of embayed beaches, which configuration and orientation would prevent them from the action of eastern storms (generally the most important). This would be specially relevant in the case of erosion, where important differences in the hazard magnitudes between sector I and the other ones have been detected.

Changes in vulnerability due to the contribution of RSLR are generally detected at longer time scales and result lower than those obtained when only LST is accounted (see Figure 6.1). As expected, RSLR contribution is significantly higher in the southern part of the Catalan coast, where dissipative beaches with very mild slopes lead to larger RSLR-induced beach erosion. Besides this, the Ebre delta, located in this area, is potentially subject to important subsidence rates that contribute to increase erosion. With respect to LST, its contribution does not seem to depend on the beach type.

Although the developed methodology assumes that the vertical elevation of the beach can only be modified by RSLR, the effects of this agent depend on the projected beach width, which is modified as much by RSLR as by LST. Thus, important differences in inundation vulnerability between integrated results and those obtained considering only RSLR can be observed (see Figure 6.1).

Vulnerability has also been interpreted considering different administrative units. Under current conditions, the two *comarcas* that present a major percentage of coastline classified as high and very high vulnerable to erosion are located in the northern and central parts of the study area (Alt Empordà (1) and Garraf (7)). When LST and the medium RSLR scenario contributions are considered, the largest increase in vulnerability with respect to the baseline is found in the southernmost *comarcas*. As a result, Baix Ebre (11), which is subject to important beach erosion due to LST and RSLR, becomes, together with Alt Empordà (1) and La Selva (3), one of the most vulnerable at the 25-yr and 50-yr projections.

Although shoreline evolution rates indicate that 77% of the Catalan coast is erosive at the baseline (Jiménez and Valdemoro, 2013), a decrease in vulnerability to storm-induced erosion will occur in those areas where accretion is the dominant medium-term process. However, such decrease could not be detected at long-term due to RSLR-contribution.

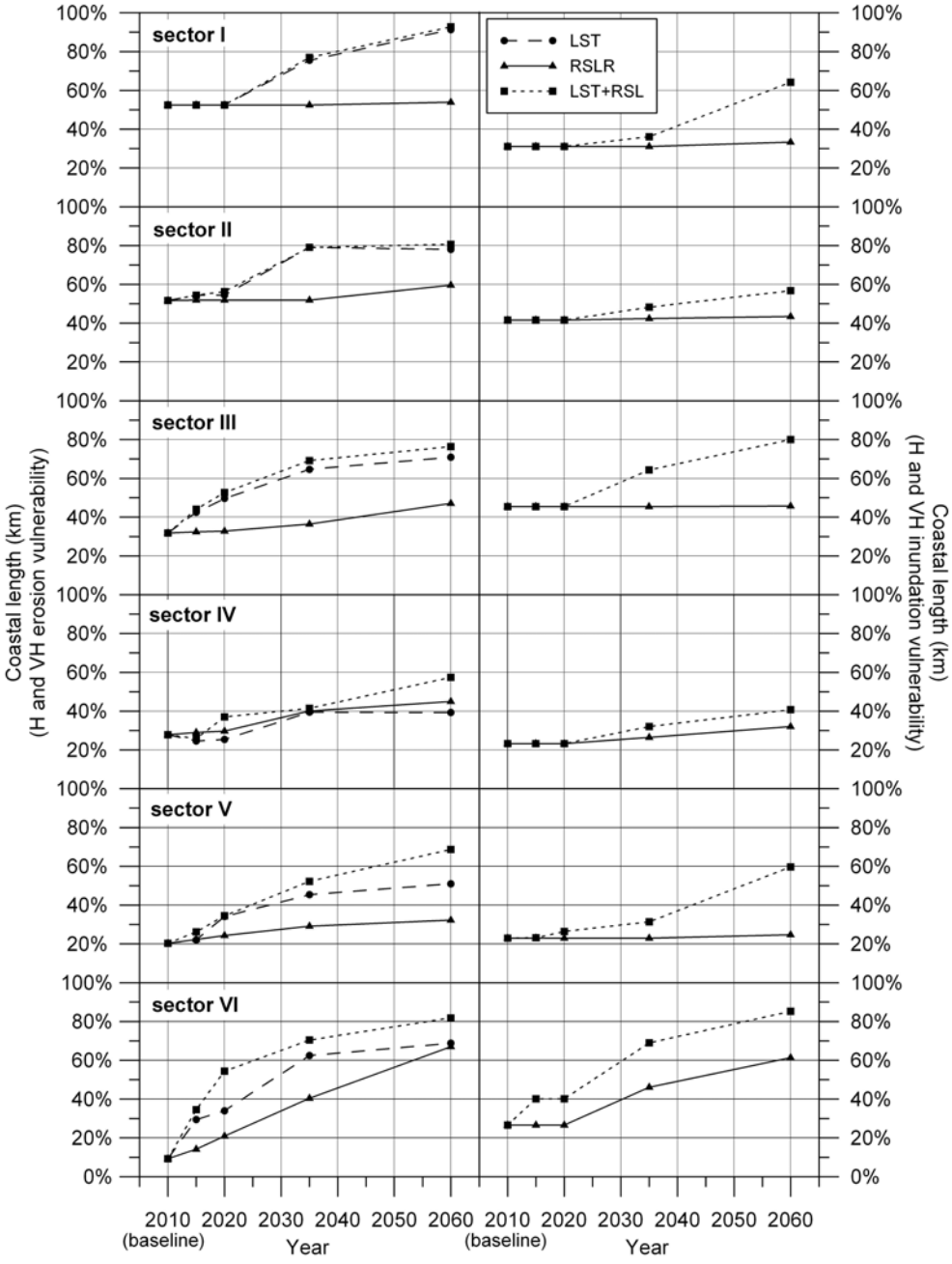

Figure 6.1: Percentage of coastline corresponding to high (H) and very high (VH) vulnerable beaches for each hazard and coastal sector at different time scales. Results obtained for a 50-yr return period considering separately the contribution of: (i) LST, (ii) a RSLR scenario of 3.8 mm/yr plus subsidence and (iii) the integration of both of them. Sectors I to VI located from North to South of the Catalan coast (see Figure 3.3).

With respect to inundation, Maresme (4) and Baix Ebre (11), located in the central and southern parts of the coast respectively, are two of the most vulnerable *comarcas* under current conditions and at any time projection. In the first case, vulnerability is mainly caused by high run-up magnitudes, which result from the combination of moderate to intense storm climate with steep beach profiles. Opposite to this, the second one is characterised by very dissipative beaches in which the low elevation of the profile becomes the main source of vulnerability. The largest increase in inundation vulnerability with respect to the baseline it is always found in the southernmost *comarca* (Montsià (12)), which results the most vulnerable at the 25-yr projection and one of the most vulnerable at the 50-yr projection. Furthermore, and contrary to what happens when only RSLR is considered, some variations in vulnerability are detected at the 5-yr and 10-yr projections in the southernmost *comarcas*, highlighting the contribution of LST to integrated inundation vulnerability.

Finally, Figures 6.2, 6.3 and 6.4 show detailed vulnerability maps corresponding to the 25-yr projection for Girona, Barcelona and Tarragona provinces respectively. These maps permit to differentiate the coastal stretches that correspond to each vulnerability category at *comarca* and municipality scale.

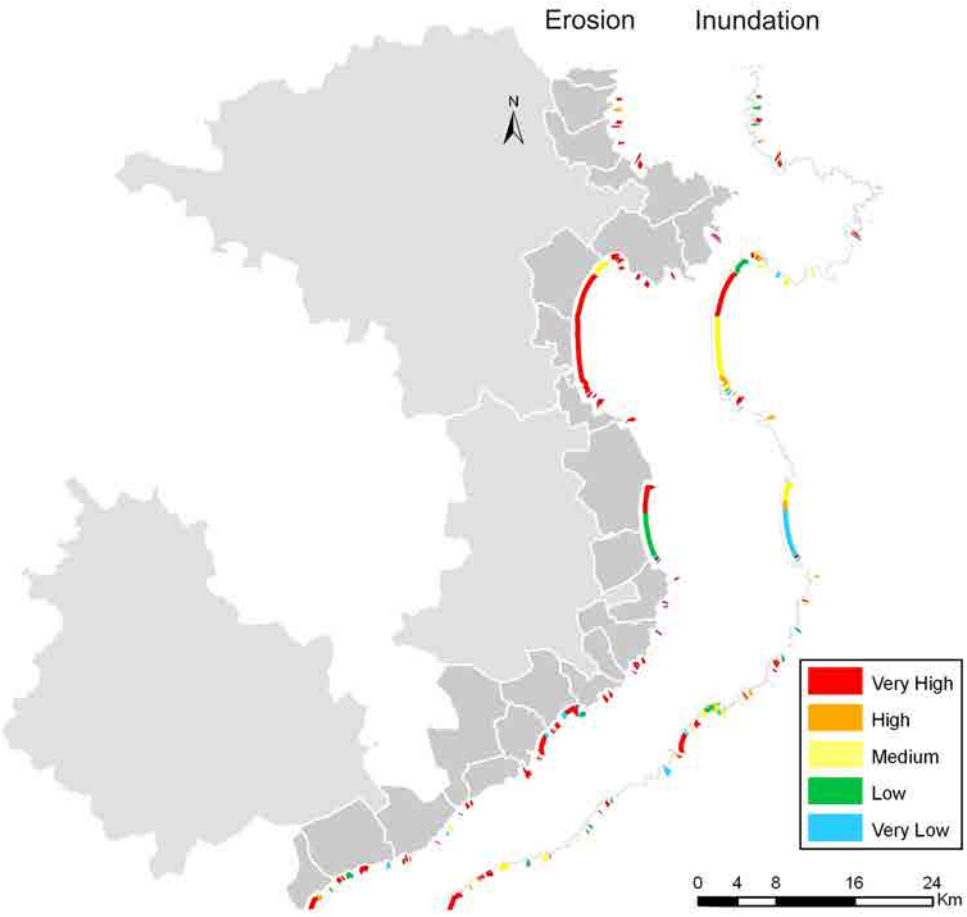

Figure 6.2: Vulnerability to storm-induced erosion and inundation of Girona province for the 25-yr projection (2035). Tr=50 years. Considered contributions: LST and the medium RSLR scenario (3.8 mm/yr + subsidence). Coastal *comarcas* and municipalities in light and dark grey respectively.

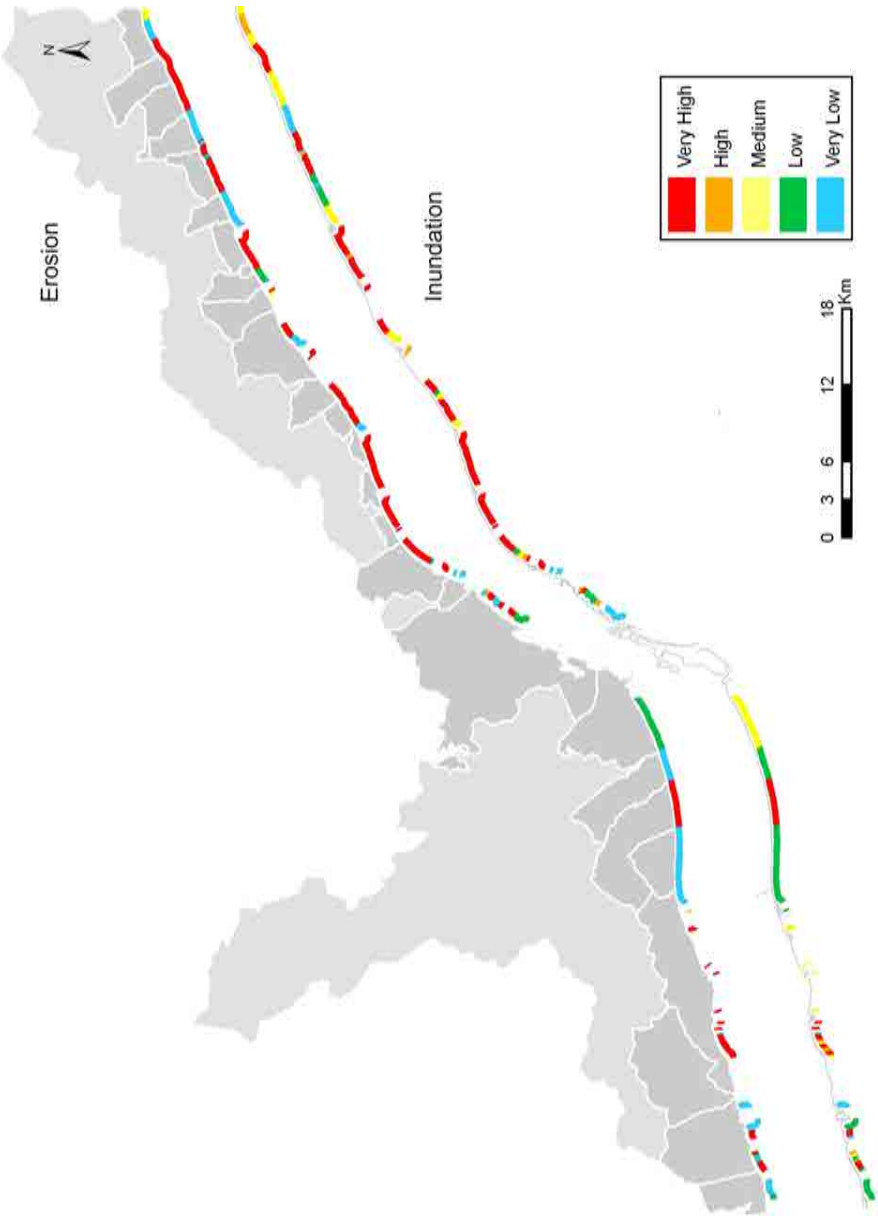

Figure 6.3: Vulnerability to storm-induced erosion and inundation of Barcelona province for the 25-yr projection (2035). Tr=50 years. Considered contributions: LST and the medium RSLR scenario (3.8 mm/yr + subsidence). Coastal *comarcas* and municipalities in light and dark grey respectively.

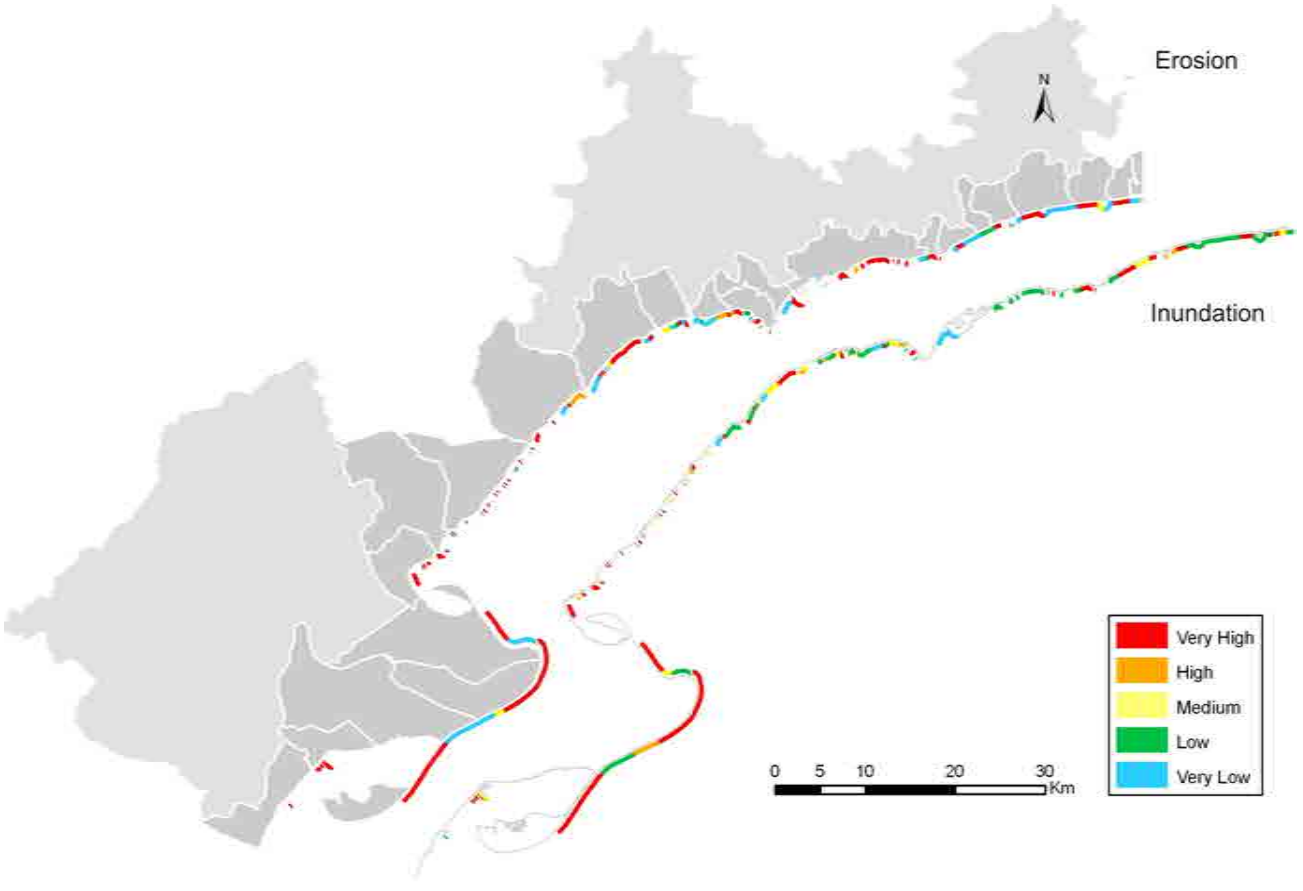

Figure 6.4: Vulnerability to storm-induced erosion and inundation of Tarragona province for the 25-yr projection (2035). Tr=50 years. Considered contributions: LST and the medium RSLR scenario (3.8 mm/yr + subsidence). Coastal *comarcas* and municipalities in light and dark grey respectively.

6.3 Further work

During the development of this work, different challenges that could complement and/or improve the proposed methodology as well as the obtained results have been identified:

1. To assess the magnitude of inundation in terms of flow, such as by means of the overtopping, instead of only considering the vertical elevation of the beach.
2. To take into account directionality (storms – beach orientation) to assess hazard magnitude.
3. To create a proper database to make a further "objective" calibration of the proposed indicators.
4. To combine vulnerability results with other spatial information, such as land use and socio-economic aspects, to evaluate coastal risk induced by storm events.
5. Finally, it could be of interest to integrate the erosion and inundation vulnerability indexes into a total storm vulnerability index that takes into account the contribution of both hazards to define the final vulnerability categories.

Bibliography

Abascal, A. J., Castanedo, S., and Medina, R. (2010). GOS, un reanálisis de marea meteorológica de 60 años de lata resolución para el sur de Europa. In *I Encuentro Oceanografía Física Española*, Barcelona, España.

Abuodha, P. a. O. and Woodroffe, C. D. (2010). Assessing vulnerability to sea-level rise using a coastal sensitivity index: a case study from Southeast Australia. *Journal of Coastal Conservation*, 14(3):189–205.

Alcántara-Araya, I. (2002). Geomorphology, natural hazards, vulnerability and prevention of natural disasters in developing countries. *Geomorphology*, 47:107–124.

Alves, F. L., Coelho, C., Coelho, C. D., and Pinto, P. (2011). Modelling coastal vulnerabilities - Tool for decision support system at inter-municipality level. *Journal of Coastal Research*, SI 64:966–970.

Anagnostopoulou, C., Tolika, K., Flocas, H., and Maheras, P. (2006). Cyclones in the Mediterranean region: present and future climate scenarios derived from a general circulation model (HadAM3P). *Advances in Geosciences*, 7:9–14.

Anfuso, G. and Martínez Del Pozo, J. A. (2009). Assessment of coastal vulnerability through the use of GIS tools in South Sicily (Italy). *Environmental management*, 43(3):533–45.

Bolaños, R., Sanchez-Arcilla, A., and Cateura, J. (2007). Evaluation of two atmospheric models for windwave modelling in the NW Mediterranean. *Journal of Marine Systems*, 65:336–353.

Borgman, L. (1963). Risk criteria. *Journal of Waterway, Port, Coastal and Ocean Engineering- ASCE*, 89,(WW3):1–35.

Boruff, B. J., Emrich, C., and Cutter, S. L. (2005). Erosion hazard vulnerability of US coastal counties. *Journal of Coastal Research*, 21(5):932–942.

Bosom, E. and Jiménez, J. A. (2010). Storm-induced coastal hazard assessment at regional scale: application to Catalonia (NW Mediterranean). *Advances in Geosciences*, 8:1–5.

Bosom, E. and Jiménez, J. a. (2011). Probabilistic coastal vulnerability assessment to storms at regional scale application to Catalan beaches (NW Mediterranean). *Natural Hazards and Earth System Science*, 11(2):475–484.

Bosom, E., Jiménez, J. A., and Nicholls, R. J. (2014). RSLR-induced increase of vulnerability to storm along the Cataln coast (NW Mediterranean). *In preparation.*

Brooks, N. (2003). Vulnerability, risk and adaptation: A conceptual framework. Working paper 38:1–16.

Bruun, P. (1962). Sea-level rise as a cause of shore erosion. *Proceedings of the American Society of Civil Engineers. Journal of the Waterways and Harbors Division*, 88:117–130.

CADS (2005). Informe sobre levolució de lestat del medi ambient a Catalunya: Litoral, biodiversitat i sol i territori 2. Technical report, Consell Assessor per al Desenvolupament Sostenible, Generalitat de Catalunya, Barcelona.

CADS (2008). RISKCAT: Els riscos naturals a Catalunya. Informe executiu. Technical report, Consell Assessor per al Desenvolupament Sostenible, Generalitat de Catalunya, Barcelona.

Caires, S., Swail, R., and Wang, X. L. (2006). Projection and analysis of extreme wave climate. *Journal of Climate*, 19:5581–5605.

Calafat, F. M. and Jordà, G. (2011). A Mediterranean sea level reconstruction (1950 - 2008) with error budget estimates. *Global and Planetary Change*, 79:118–133.

Casas-Prat, M. and Sierra, J. P. (2013). Projected future wave climate in the NW Mediterranean Sea. *Journal of Geophysical Research: Oceans*, 118(7):3548–3568.

Cavaleri, L. and Bertotti, L. (2004). Accuracy of the modelled wind and wave fields in enclosed seas. *Tellus*, 56A(2):167–175.

CEPAL (2012). Efectos del cambio climático en la costa de América Latina y el Caribe: Vulnerabilidad y exposición. Technical report, Comisión Económica para América Latina y el Caribe, Santiago de Chile.

Church, J. A. and White, N. J. (2006). A 20th century acceleration in global sea-level rise. *Geophysical Research Letters*, 33, L01602.

CIIRC (2010). Estat de la zona costanera a Catalunya. Technical report, Centre Internacional d'Investigació dels Recursos Costaners, Barcelona.

Coles, S. (2001). *An introduction to statistical modeling of extreme values*. Springer, London, UK.

Cooper, J. A. G. and Pilkey, O. H. (2004). Sea-level rise and shoreline retreat: time to abandon the Bruun Rule. *Global and Planetary Change*, 43:157–171.

Davidson-Arnott, R. G. D. (2005). Conceptual model of the effects of sea level rise on sandy coasts. *Journal of Coastal Research*, 21(6):1166–1172.

De Pippo, T., Donadio, C., Pennetta, M., Petrosino, C., Terlizzi, F., and Valente, A. (2008). Coastal hazard assessment and mapping in Northern Campania, Italy. *Geomorphology*, 97:451–466.

Dean, R. (1973). Heuristic models of sand transport in the surf zone. In *Proceedings of the 1st Australian Conference on Coastal Engineering, 1973: Engineering Dynamics of the Coastal Zone, Sydney*, pp. 208–214, Sydney. Institution of Engineers.

Di Paola, G. D., Iglesias, J., Rodríguez, G., Benassai, G., Aucelli, P., and Pappone, G. (2011). Estimating coastal vulnerability in a meso-tidal beach by means of quantitative and semi-quantitative methodologies. *Journal of Coastal Research*, SI 61:303–308.

Divoky, D. and Mcdougal, W. G. (2006). Response-based coastal flood analysis. In *Proceedings of the 30th International Conference on Coastal Engineering, San Diego, USA)*, pp. 5291–5301, San Diego, USA. ASCE.

Doherty, K., Folley, M., Doherty, R., and Whittaker, T. (2011). Extreme value analysis of wave energy converters. In *Proceedings of the Twenty-first International Offshore and Polar Engineering Conference*, pp. 557–564, Mawi, USA.

Domínguez, L., Anfuso, G., and Gracia, F. (2005). Vulnerability assessment of a retreating coast in SW Spain. *Environmental Geology*, 47(8):1037–1044.

Duro, J. A. and Rodríguez, D. (2011). Estimació del PIB turístic per Catalunya , marques i comarques. Technical report, Direcci General de Turisme, Generalitat de Catalunya.

Fenoglio-Marc, L. (2002). Long-term sea level change in the Mediterranean Sea from multi-satellite altimetry and tide gauges. *Physics and Chemistry of the Earth*, 27:1419–1431.

Furlan, A., Bonotto, D. M., and Gumiere, S. J. (2011). Development of environmental and natural vulnerability maps for Brazilian coastal at São Sebastião in São Paulo State. *Environmental Earth Sciences*, 64(3):659–669.

Füssel, H.-M. (2007). Vulnerability: a generally applicable conceptual framework for climate change research. *Global Environmental Change*, 17(2):155–167.

Füssel, H.-M. and Klein, R. J. T. (2006). Climate change vulnerability assessments: an evolution of conceptual thinking. *Climatic Change*, 75(3):301–329.

Gaddis, E. B., Miles, B., Morse, S., and Lewis, D. (2007). Full-cost accounting of coastal disasters in the United States: Implications for planning and preparedness. *Ecological Economics*, 63(2-3):307–318.

García-Mora, M. R., Gallego-Fernández, J. B., and García-Novo, F. (2000). Plant diversity as a suitable tool for coastal dune vulnerability assessment. *Journal of coastal research*, 16(4):990–995.

García-Mora, M. R., Gallego-Fernández, J B Williams, A. T., and Garcia-Novo, F. (2001). A coastal dune vulnerability classification. A case study of the SW Iberian Peninsula. *Journal of Coastal Research*, 17(4):802–811.

Generalitat de Catalunya (2012). Catalunya Turística en Xifres 2012. Technical report, Direcció General de Turisme. Departament d'Empresa i Ocupació.

GIOC (2004). Impactos en la costa española por efecto del cambio climático (Grupo de Ingeniería Oceanográfica y de Costas, Universidad de Cantabria). Technical report, Oficina Española de Cambio Climático (Ministerio de Medio Ambiente).

Godschalk, D. R., Brower, D. J., and Beatley, T. (1989). *Catastrophic coastal storms, hazard mitigation and development management*. Duke University Press, Durham, USA.

Gornitz, V. (1991). Global coastal hazards from future sea level rise. *Palaeogeography, Palaeoclimatology, Palaeoecology*, 89(4):379–398.

Gornitz, V., Beaty, T. W., and Daniels, R. C. (1997). A coastal hazards data base for the US West Coast. Technical report, Oak Ridge National Laboratory.

Gornitz, V., Daniels, R. C., White, T. W., and Birdwell, K. R. (1994). The development of a coastal risk assessment database for the U.S. southeast: Erosion and inundation from sea-level rise. *Journal of Coastal Research*, SI 12:327–338.

Gouldby, B. and Samuels, P. (2005). Language of Risk, project definitions. FLOODSITE. Project report T32-04-01.

Green, C. and McFadden, L. (2007). Coastal vulnerability as discourse about meanings and values. *Journal of Risk Research*, 10(8):1027–1045.

Grinsted, A. Moore, J. and Jevrejeva, S. (2009). Reconstructing sea level from paleo and projected temperatures 200 to 2100AD. *Climate Dynamics*, 34:4611–472.

Guedes Soares, C., Weisse, R., Carretero, J. C., and Alvarez, E. (2002). A 40 years hindcast of wind, sea level and waves in european waters. In *Proceedings of the 21st international Conference on Offshore Mechanics and Arctic Engineering*, pp. 669–675, Oslo, Norway.

Gutierrez, B. T., Plant, N. G., and Thieler, E. R. (2011). A bayesian network to predict coastal vulnerability to sea level rise. *Journal of Geophysical Research*, 116, F202009.

Harvey, N. and Woodroffe, C. D. (2008). Australian approaches to coastal vulnerability assessment. *Sustainability Science*, 3(1):67–87.

Hinkel, J. (2005). DIVA: an iterative method for building modular integrated models. *Advances in Geosciences*, 4:45–50.

Hinkel, J. and Klein, R. J. (2009). Integrating knowledge to assess coastal vulnerability to sea-level rise: The development of the DIVA tool. *Global Environmental Change*, 19(3):384–395.

Hinkel, J. and Klein, R. J. T. (2007). Integrating knowledge for assessing coastal vulnerability to climate change. In McFadden, L., Nicholls, R. J., and Penning-Rowsell, E. C. (editors), *Managing Coastal Vulnerability: An Integrated Approach*. Elsevier Science, Amsterdam, The Netherlands.

Ibáñez, C., Canicio, A., Day, J. W., and Curcó, A. (1997). Morphologic development, relative sea level rise and sustainable management of water and sediment in the Ebre Delta, Spain. *Journal of Coastal Conservation*, 3:191–202.

Ibáñez, C., Sharpe, P. J., Day, J. W., Day, J. N., and Prat, N. (2010). Vertical accretion and relative sea level rise in the Ebro delta wetlands (Catalonia, Spain). *Wetlands*, 30:979–988.

IDESCAT (2014). Anuari Estadístic de Catalunya, 2013. Institut d'Estadística de Catalunya. Generalitat de Catalunya. URL: http://www.idescat.cat/pub/?id=aec (accessed February 26th 2014).

IPCC CZMS (1992). Global climate change and the rising challenge of the sea. Report of the Coastal Zone Management Subgroup, Response Strategies Working Group

of the Intergovernmental Panel on Climate Change, Ministry of Transport, Public Works and Water Management, The Hague, The Netherlands.

Jiménez, J. A., Ciavola, P., Balouin, Y., Armaroli, C., Bosom, E., Gervais, M., and Ferrara, U. (2009). Geomorphic coastal vulnerability to storms in microtidal fetch-limited environments: application to NW Mediterranean & N Adriatic Seas. *Journal of Coastal Research*, (56):1641–1645.

Jiménez, J. A. and Madsen, O. S. (2003). A simple formula to estimate settling velocity of natural sediments. *Journal of Waterway, Port, Coastal and Ocean Engineering*, 129(2):70–78.

Jiménez, J. A., Sánchez-Arcilla, A., and Stive, M. J. F. (1993). Discussion on prediction of storm/normal beach profiles. *Journal of Waterway, Port, Coastal and Ocean Engineering*, 19(4):466–468.

Jiménez, J. A., Sánchez-Arcilla, A., and Valdemoro, H. I. (1997a). Predicción de los cambios en el perfil de playa utilizando parámetros adimensionales sencillos. *Revista de Obras Públicas*, 3362:29–39.

Jiménez, J. A., Sánchez-Arcilla, A., Valdemoro, H. I., Gracia, V., and Nieto, F. (1997b). Processes reshaping the Ebro delta. *Marine Geology*, 144(97):59–79.

Jiménez, J. a., Sancho-García, A., Bosom, E., Valdemoro, H. I., and Guillén, J. (2012). Storm-induced damages along the Catalan Coast (NW Mediterranean) during the period 1958-2008. *Geomorphology*, 143-144:24–33.

Jiménez, J. A. and Valdemoro, H. I. (2013). Playas a lo largo de la costa catalana: ¿un recurso sostenible? In *XII Jornadas Españolas de Ingeniería de Costas y Puertos*, Cartagena, Spain.

Judge, E. K., Overton, M. F., and Fisher, J. S. (2003). Vulnerability indicators for coastal dunes. *Journal of Waterway Port Coastal and Ocean Engineering*, 129(6):270–278.

Khouakhi, A., Snoussi, M., Niazi, S., and Raji, O. (2013). Vulnerability assessment of Al Hoceima bay (Moroccan Mediterranean coast): a coastal management tool to reduce potential impacts of sea-level rise and storm surges. *Journal of Coastal Research*, SI 65:968–973.

Klein, R. J. T., Nicholls, R. J., and Mimura, N. (1999). Coastal adaptation to climate change: Can the IPCC technical guidelines be applied? *Mitigation and Adaptation Strategies for Global Change*, 4:239–252.

Larson, M. and Kraus, N. C. (1989). SBEACH: Numerical model for simulating storm-induced beach change. Report 1: Empirical foundation and model development. Technical Report CERC-89-9, US Army Corps of Engineers, Vicksburg.

Lionello, P., Cogo, S., Galati, M., and Sanna, A. (2008). The Mediterranean surface wave climate inferred from future scenario simulations. *Global and Planetary Change*, 63(2-3):152–162.

Lionello, P., Dalan, F., and Elvini, E. (2002). Cyclones in the Mediterranean region: the present and the doubled CO_2 climate scenarios. *Climate Research*, 22:147–159.

Lionello, P. and Sanna, A. (2005). Mediterranean wave climate variability and its links with NAO and Indian Monsoon. *Climate Dynamics*, 25(6):611–623.

Llasat, M. C., Llasat-Botija, M., and López (2009). A press database on natural risks and its application in the study of floods in Northeastern Spain. *Natural Hazards and Earth System Science*, 9:2049–2061.

Mahendra, R. S., Mohanty, P. C., Bisoyi, H., Kumar, T. S., and Nayak, S. (2011). Assessment and management of coastal multi-hazard vulnerability along the CuddaloreVillupuram, East coast of India, using geospatial techniques. *Ocean & Coastal Management*, 54(4):302–311.

Málvarez García, G., Pollard, J., and Domínguez, R. (2000). Origins, management and measurement of Stress on the coast of Southern Spain. *Coastal Management*, 28:215–234.

Marcos, M. and Tsimplis, M. N. (2008). Coastal sea level trends in Southern Europe. *Geophysical Journal International*, 175:70–82.

Martínez, M., Intralawan, A., Vázquez, G., Pérez-Maqueo, O., Sutton, P., and Landgrave, R. (2007). The coasts of our world: Ecological, economic and social importance. *Ecological Economics*, 63(2-3):254–272.

Martins, V. N., Pires, R., and Cabral, P. (2012). Modelling of coastal vulnerability in the stretch between the beaches of Porto de Mós and Falésia, Algarve (Portugal). *Journal of Coastal Conservation*, 16(4):503–510.

McFadden, L. and Green, C. (2007). Defining 'vulnerability': conflicts, complexities and implications for Coastal Zone Management. *Journal of Coastal Research*, SI 50:120–124.

McFadden, L., Nicholls, R. J., and Penning-Rowsell, E. (2007). *Managing coastal vulnerability*. Elsevier, 262 pp.

Meehl, G. A., Stoker, T. F., Collins, W. D., Friedlingstein, P., Gaye, A. T., Gregory, J. M., Kitoh, A., Knutti, R., Murphy, J. M., Noda, A., Raper, S. C. B., Watterson, I. G., Weaver, A. J., and Zhao, Z.-C. (2007). Global climate projections. In Solomon, S., Qin, D., Manning, M., Chen, Z., Marquis, M., Averyt, K. B., Tignor, M., and Miller, H. L. (editors), *Climate Change 2007: The Physical Science Basis.*, pp. 747–845. Cambridge University Press, UK and New York.

Mendoza, E. T. (2008). *Coastal vulnerability to storms in the Catalan Coast.* PhD thesis, Universitat Politècnica de Catalunya.

Mendoza, E. T. and Jiménez, J. A. (2006). Storm-induced beach erosion potential on the Catalonian coast. *Journal of Coastal Research*, SI 48:81–88.

Mendoza, E. T. and Jiménez, J. A. (2008). Vulnerability assessment to coastal storms at a regional scale. In *Proceedings of the 31st Int.ernational Conference on Coastal Engineering, ASCE*, Hamburg, Germany.

Mendoza, E. T. and Jiménez, J. A. (2009). Regional geomorphic vulnerability analysis to storms for Catalan beaches. In *Proceedings of the Institution of Civil Enginers.* Maritime Engineering 162(3):127-135.

Mendoza, E. T., Jimenez, J. A., and Mateo, J. (2011). A coastal storms intensity scale for the Catalan sea (NW Mediterranean). *Natural Hazards and Earth System Science*, 11(9):2453–2462.

Meur-Férec, C., Deboudt, P., and Morel, V. (2008). Coastal risks in France: an integrated method for evaluating vulnerability. *Journal of Coastal Research*, 24:178–189.

Mori, N., Yasuda, T., Mase, H., Tom, T., and Oku, Y. (2010). Projection of extreme wave climate change under global warming. *Hydrological Research Letters*, 4:15–19.

Morton, R. A. (2002). Factors controlling storm impacts on coastal barriers and beaches – A preliminary basis for near real-time forecasting. *Journal of Coastal Research*, 18(3):486–501.

Nicholls, R., Wong, P., Burkett, V., Codignotto, J., Hay, J., McLean, R., Ragoonaden, S., and Woodroffe, C. (2007). Coastal systems and low-lying areas . In Parry, M., Canziani, O., Palutikof, J., van der Linden, P., and Hanson, C. (editors), *Climate Change 2007: Impacts, Adaptation and Vulnerability. Contribution of Working Group II to the Fourth Assessment Report of the Intergovernmental Panel on Climate Change*, pp. 315–356. Cambridge University Press, Cambridge, UK.

Nicholls, R. J. and Cazenave, A. (2010). Sea-level rise and its impact on coastal zones. *Science*, 328(5985):1517–20.

Nicholls, R. J., Marinova, N., Lowe, J. A., Brown, S., Vellinga, P., de Gusmão, D., Hinkel, J., and Tol, R. S. J. (2011). Sea-level rise and its possible impacts given a 'beyond 4C world' in the twenty-first century. *Philosophical transactions of the Royal Society A: Mathematical, physical and engineering sciences*, 369(369):161–181.

Nissen, K. M., Leckebusch, G. C., Pinto, J. G., Renggli, D., Ulbrich, S., and Ulbrich, U. (2010). Cyclones causing wind storms in the Mediterranean: characteristics, trends and links to large-scale patterns. *Natural Hazards and Earth System Science*, 10(7):1379–1391.

Pérez-Maqueo, O., Intralawan, A., and Martínez, M. (2007). Coastal disasters from the perspective of ecological economics. *Ecological Economics*, 63(2-3):273–284.

Pernetta, J. C. and Elder, D. L. (1992). Climate, sea level rise and the coastal zone: management and planning for global changes. *Ocean & Coastal Management*, 18:113–160.

Pethick, J. S. and Crooks, S. (2000). Development of a coastal vulnerability index: a geomorphological perspective. *Environmental Conservation*, 27(4):359–367.

Pinto, J. G., Ulbrich, U., Leckebusch, G., Spangehl, T., Reyers, M., and Zacharias, S. (2007). Changes in storm track and cyclone activity in three SRES ensemble experiments with the ECHAM5 / MPI-OM1 GCM. *Climate Dynamics*, 29:195–210.

Ponce de León, S. and Guedes Soares, C. (2008). Sensitivity of wave model predictions to wind fields in the Western Mediterranean sea. *Coastal Engineering*, 55(11):920–929.

Prinos, P. and Sanchez-Arcilla, A. (2008). Analysis of riverine and coastal extremes. The FLOODsite approach. *Journal of Hydraulic Research*, volume 46, supplement 2 (Special Issue).

Rahmstorf, S. (2007). A semi-empirical approach to projecting future sea-level rise. *Science*, 315(5810):368–70.

Ramieri, E., Hartley, A., Barbanti, A., Santos, F. D., Laihonen, P., Marinova, N., and Santini, M. (2011). Methods for assessing coastal vulnerability to climate change. Technical paper 1/2011, European Environment Agency. European Topic Centre on Climate Change Impacts, Vulnerability and Adaptation, Bologna, Italy.

Ranasinghe, R., Callaghan, D., and Stive, M. J. F. (2011). Estimating coastal recession due to sea level rise: beyond the Bruun rule. *Climatic Change*, 110(3-4):561–574.

Rangel-Buitrago, N. and Anfuso, G. (2009). Assessment of coastal vulnerability in la guajira peninsula, colombian caribbean sea. *Journal of Coastal Research*, SI 56:792–796.

Reguero, B., Menéndez, M., Méndez, F., Mínguez, R., and Losada, I. (2012). A Global Ocean Wave (GOW) calibrated reanalysis from 1948 onwards. *Coastal Engineering*, 65:38–55.

Sahin, O. and Mohamed, S. (2013). Coastal vulnerability to sea-level rise: a spatial-temporal assessment framework. *Natural Hazards*, 70(1):395–414.

Sallenger, A. H. (2000). Storm-impact scale for barrier islands. *Journal of Coastal Research*, 16(3):890–895.

Sanchez-Arcilla, A., Jimenez, J. A., and Valdemoro, H. I. (1998). The ebro delta: Morphodynamics and vulnerability. *Journal of Coastal Research*, 14(3):754–772.

Santos, M., Río, L., and Benavente, J. (2013). GIS-based approach to the assessment of coastal vulnerability to storms. Case study in the Bay of Cádiz (Andalusia, Spain). *Journal of Coastal Research*, SI 65:826–831.

Sardá, R., Avila, C., and Mora, J. (2005). A methodological approach to be used in integrated coastal zone management processes: the case of the Catalan Coast (Catalonia, Spain). *Estuarine, Coastal and Shelf Science*, 62(3):427–439.

Scavia, D., Field, J. C., Boesch, D. F., Buddemeier, R. W., Burkett, V., Cayan, D. R., Fogarty, M., Harwell, M. A., Howarth, R. W., Mason, C., Denise, J., Royer, T. C., Sallenger, A. H., and Titus, J. G. (2002). Climate change impacts on U.S. coastal and marine ecosystems. *Estuaries*, 25(2):149–164.

Shchepetkin, A. F. and McWilliams, J. C. (2005). The regional oceanic modeling system (ROMS): a split-explicit, free-surface, topography-following-coordinate oceanic model. *Ocean Modelling*, 9(4):347–404.

Small, C. and Nicholls, R. J. (2003). A global analysis of human settlement in coastal zones. *Journal of Coastal Research*, 19(3):584–599.

Sornoza, L., Arasa, A., Maestro, A., Rees, J. G., and Hernandez-Molina, F. J. (1998). Architectural stacking patterns of the Ebro delta controlled by Holocene

high-frequency eustatic fluctuations, delta-lobe switching and subsidence processes. *Sedimentary Geology*, 117(1-2):11–32.

Stive, M. J., Ranasinghe, R., and Cowell, P. (2009). Sea level rise and coastal erosion. In Kim, Y. (editor), *Handbook of coastal and ocean engineering*, pp. 1023–1038. World Scientific.

Stockdon, H. F., Doran, K. S., and Sallenger, A. H. (2009). Extraction of lidar-based dune-crest elevations for use in examining the vulnerability of beaches to inundation during hurricanes. *Journal of Coastal Research*, SI 53:59–65.

Stockdon, H. F., Holman, R. A., Howd, P. A., and Sallenger, A. H. (2006). Empirical parameterization of setup, swash, and runup. *Coastal Engineering*, 53(7):573–588.

Thieler, E. R. and Hammar-Klose, E. S. (1999). National assessment of coastal vulnerability to sea-level rise, U.S. Atlantic coast. Open-file report 99-593, U.S. Geological Survey.

Thieler, E. R. and Hammar-Klose, E. S. (2000a). National assessment of coastal vulnerability to sea-level rise, U.S. Gulf of Mexico coast. Open-file report 00-179, U.S. Geological Survey.

Thieler, E. R. and Hammar-Klose, E. S. (2000b). National assessment of coastal vulnerability to sea-level rise: U.S. Pacific coast. Open-file report 00-178, U.S. Geological Survey.

Tolman, H. L. (2002). User manual and system documentation of WaveWatch-III version 2.22. Technical note, NOAA/NWS/NCEP/MMAB (Available at: http://polar.wwb.noaa.gov/mmab/papers/tn222/MMAB_222.pdf).

Torresan, S., Critto, A., Rizzi, J., and Marcomini, A. (2012). Assessment of coastal vulnerability to climate change hazards at the regional scale: the case study of the North Adriatic Sea. *Natural Hazards and Earth System Science*, 12(7):2347–2368.

Trigo, I. F., Davies, T. D., and Bigg, G. R. (2000). Decline in Mediterranean rainfall caused by weakening of Mediterranean cyclones. *Geophysical Research Letters*, 27(18):2913–2916.

Tsimplis, M. N. and Baker, F. (2000). Sea level drop in the mediterranean sea: An indicator of deep water salinity and temperature changes? *Geophysical Research Letters*, 27(12):1731–1734.

Ulbrich, U., Leckebusch, G. C., and Pinto, J. G. (2009). Extra-tropical cyclones in the present and future climate: a review. *Theoretical and Applied Climatology*, 96(1-2):117–131.

United Nations (UN) Atlas of the Oceans (2010). Human Settlements on the Coast. URL: http://www.oceansatlas.org (Uses > Human Settlements on the Coast) (accessed February 5th 2014.

Van der Meer, J. W. and Janseen, W. (1995). Wave run-up and wave overtopping at dikes. In Kobayashi, N. and Demirbilek, Z. (editors), *Wave forces on inclined and vertical wall structures*, pp. 1–27. ASCE.

Vermeer, M. and Rahmstorf, S. (2009). Global sea level linked to global temperature. *Proceedings of the national Academy of Sciences*, 106(51):21527–21532.

Vickery, P. J., Lin, J., Skerlj, P. F., Jr, L. A. T., and Huang, K. (2006a). HAZUS-MH Hurricane model methodology.I: Hurricane hazard, terrain, and wind load modeling. *Natural Hazards Review*, 7(2):82–93.

Vickery, P. J., Skerlj, P. F., Lin, J., Jr, L. A. T., Young, M. A., and Lavelle, F. M. (2006b). HAZUS-MH Hurricane Model Methodology.II: Damage and loss estimation. *Natural Hazards Review*, 7(2):94–103.

WAMDI Group (1988). The WAM Model – A third generation ocean wave prediction model. *Journal of Phisical Oceanography*, 18:1775–1810.

Wang, X. L. and Swail, V. R. (2006). Climate change signal and uncertainty in projections of ocean wave heights. *Climate Dynamics*, 26(2-3):109–126.

Wang, X. L., Swail, V. R., Zwiers, F. W., Zhang, X., and Feng, Y. (2008). Detection of external influence on trends of atmospheric storminess and Northern oceans wave heights. *Climate Dynamics*, 32(2-3):189–203.

Wise, R. S., Smith, S. J., and Larson, M. (1996). SBEACH: Numerical model for simulating storm-induced beach change. Report 4: Cross-shore transport under random waves and model validation with SUPERTANK field data. Technical Report CERC-89-9, US Army Corp of Engineers, Vicksburg.

Youssef, A. M., Pradhan, B., Gaber, A. F. D., and Buchroithner, M. F. (2009). Geomorphological hazard analysis along the Egyptian Red Sea coast between Safaga and Quseir. *Natural Hazards and Earth System Science*, 9:751–766.

Appendix A: Vulnerability maps

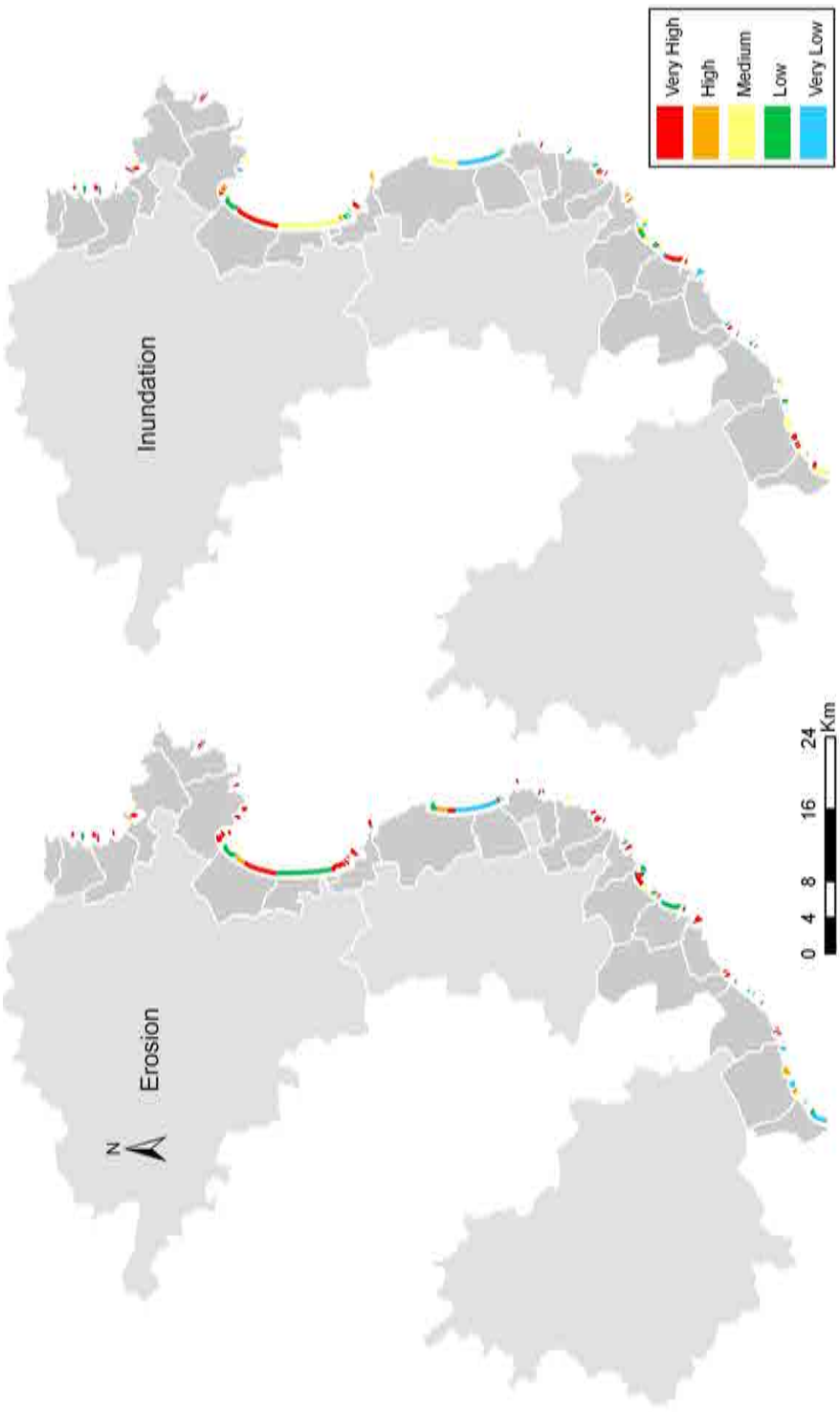

Figure A.1: Maps of vulnerability to storm-induced erosion and inundation of Girona province under current conditions (2010). Tr=50 years. Coastal *comarcas* in light grey, coastal municipalities in dark grey.

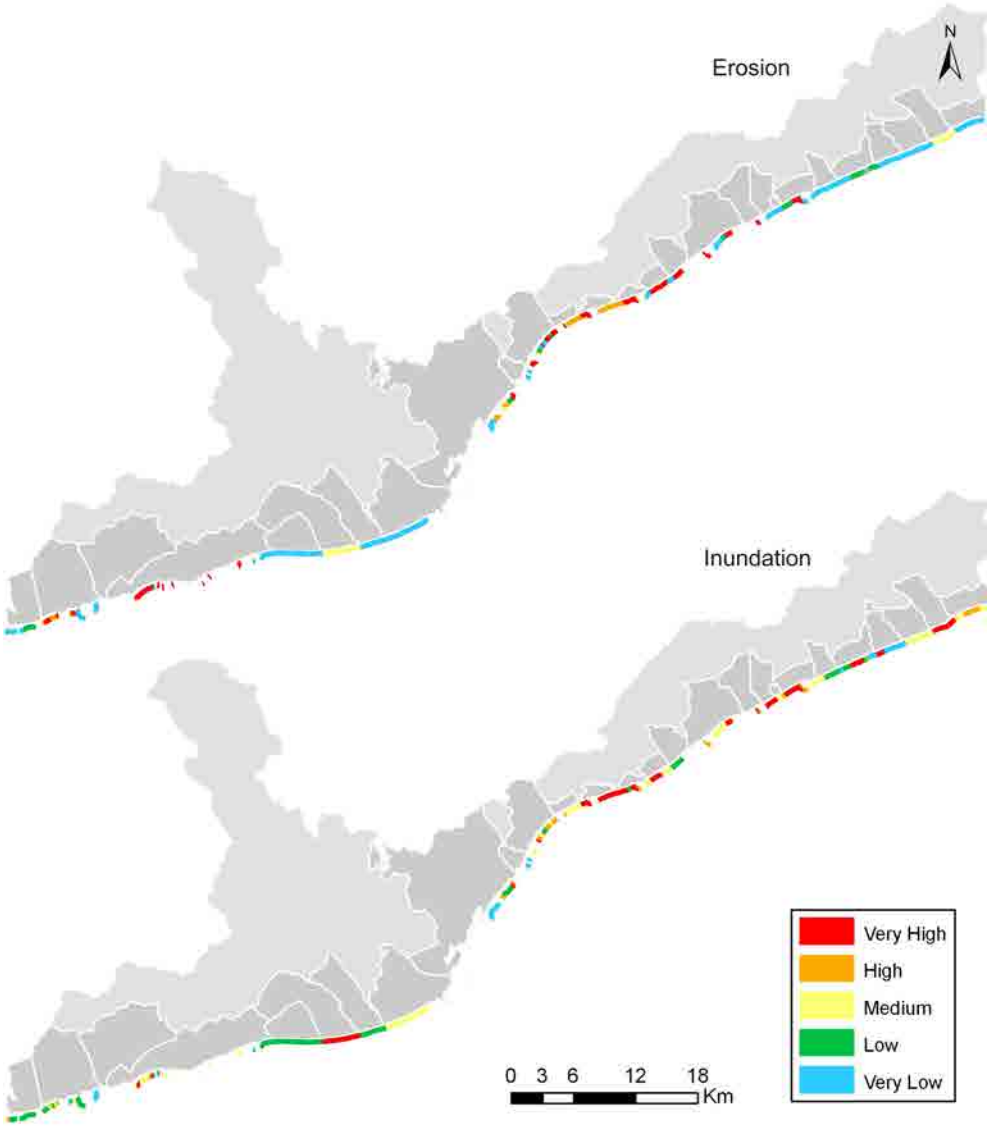

Figure A.2: Maps of vulnerability to storm-induced erosion and inundation of Barcelona province under current conditions (2010). Tr=50 years. Coastal *comarcas* in light grey, coastal municipalities in dark grey.

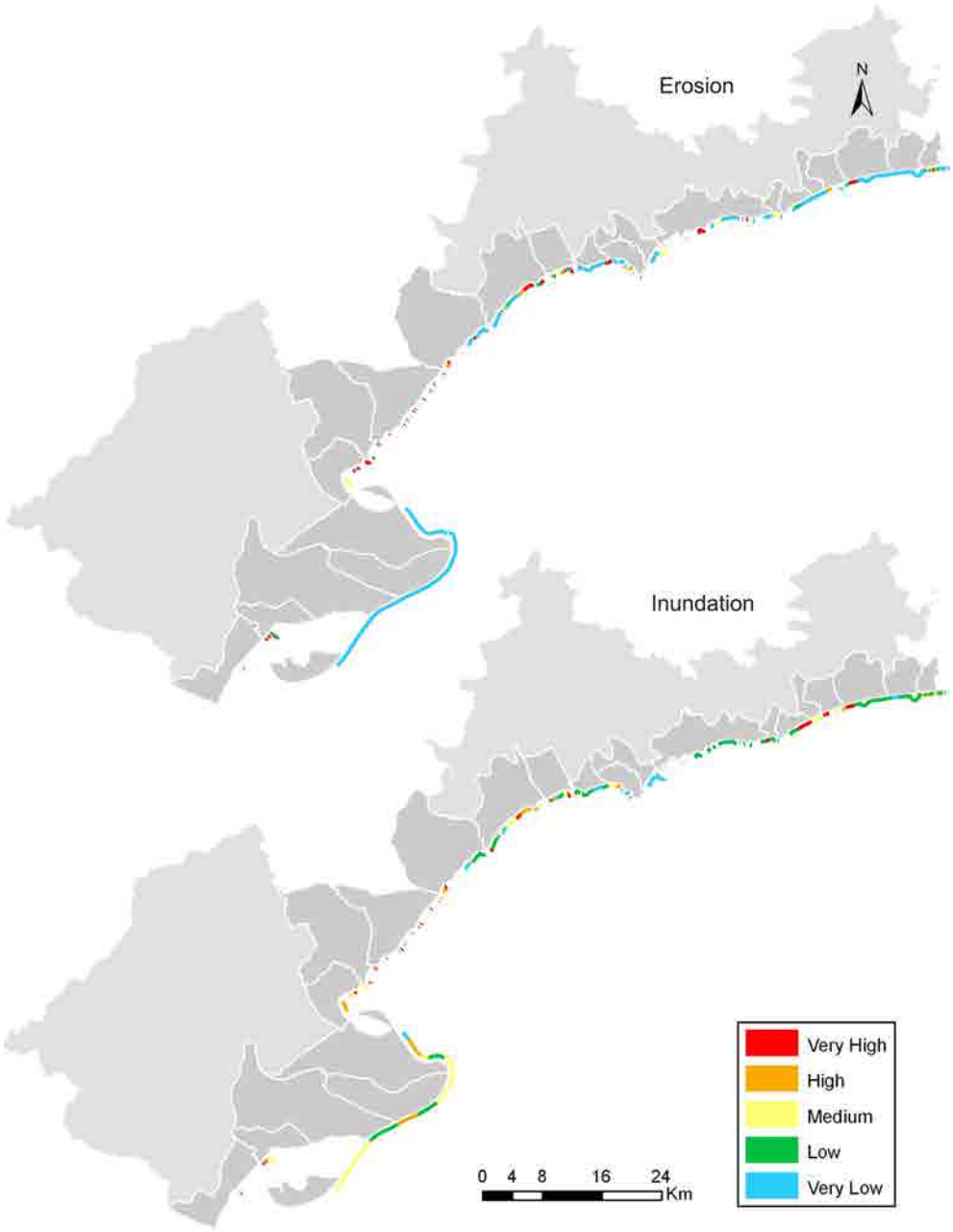

Figure A.3: Maps of vulnerability to storm-induced erosion and inundation of Tarragona province under current conditions (2010). Tr=50years. Coastal *comarcas* in light grey, coastal municipalities in dark grey.

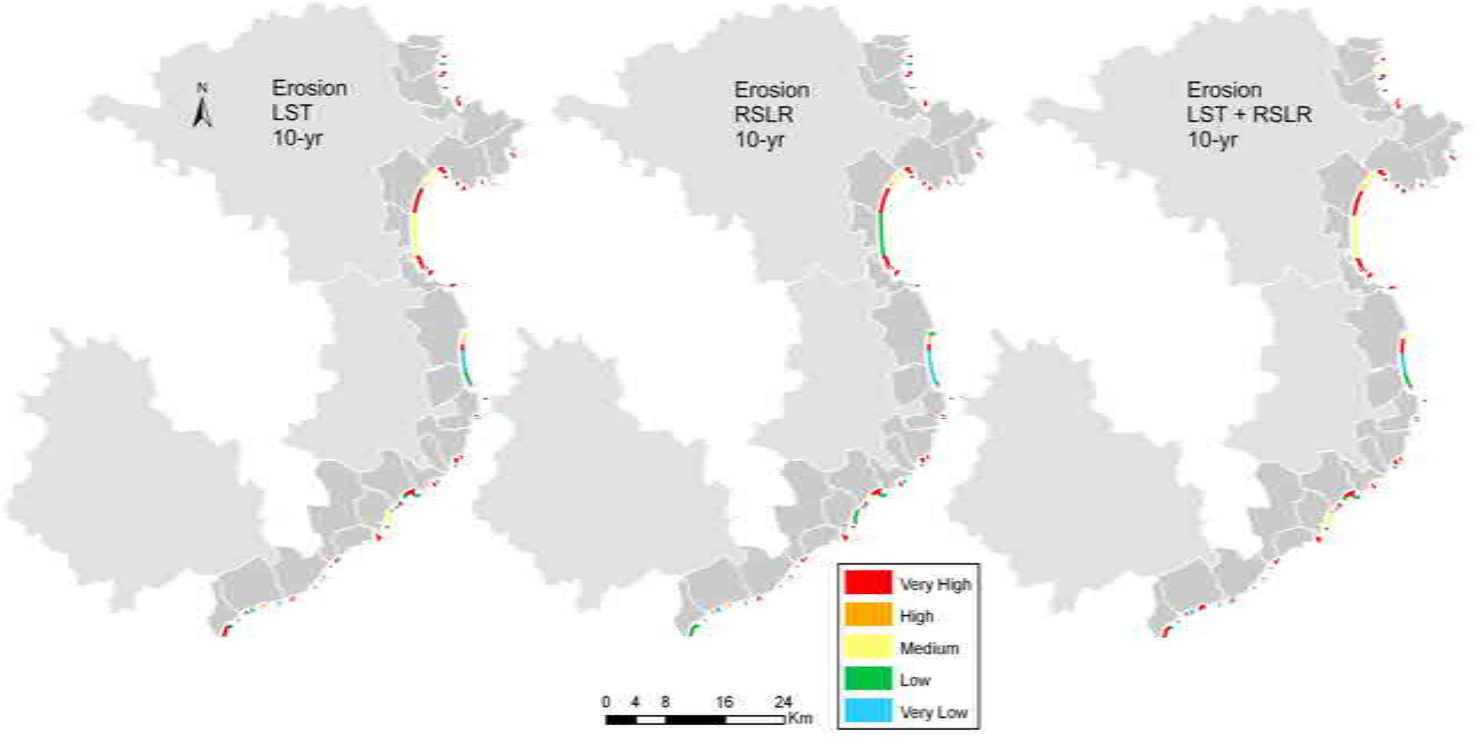

Figure A.4: Maps of vulnerability to storm-induced erosion of Girona province for the 10-year projection with respect to the baseline (2010). Top: LST contribution. Middle: RSLR contribution. Bottom: LST and RSLR integrated contribution. Tr=50 years. Coastal *comarcas* in light grey, coastal municipalities in dark grey.

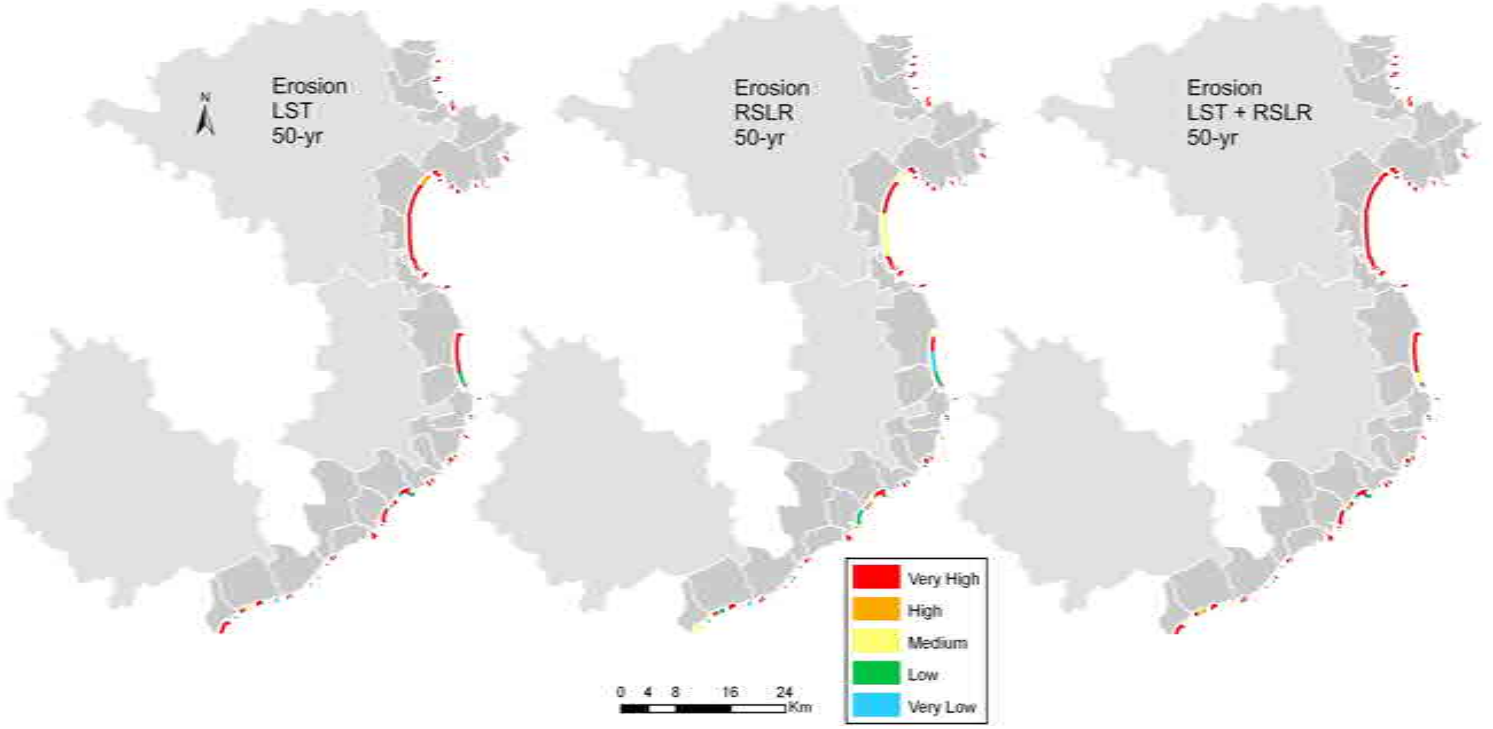

Figure A.5: Maps of vulnerability to storm-induced erosion of Girona province for the 50-year projection with respect to the baseline (2010). Top: LST contribution. Middle: RSLR contribution. Bottom: LST and RSLR integrated contribution. Tr=50 years. Coastal *comarcas* in light grey, coastal municipalities in dark grey.

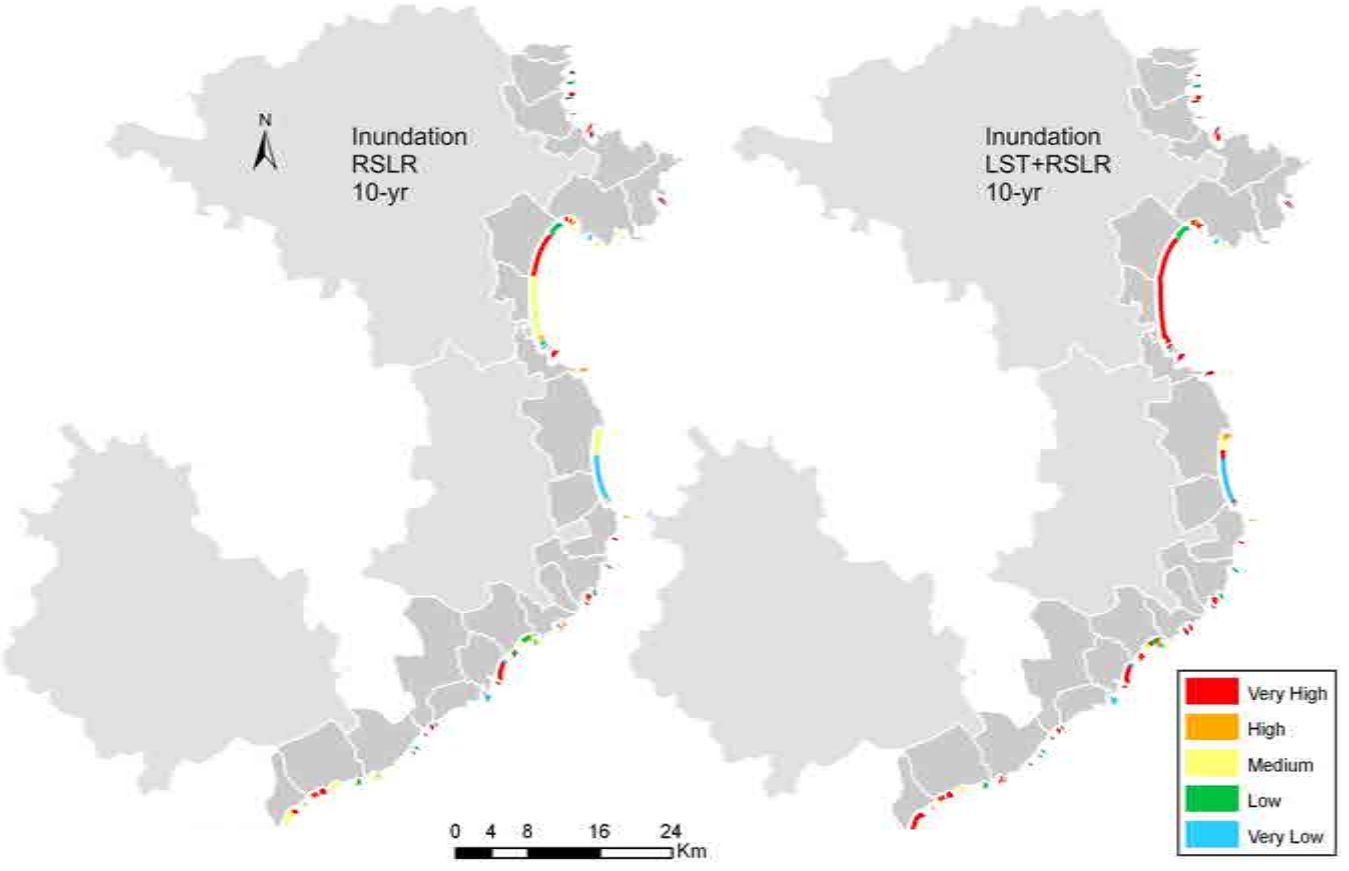

Figure A.6: Maps of vulnerability to storm-induced inundation of Girona province for the 10-year projection with respect to the baseline (2010). Top: RSLR contribution. Bottom: LST and RSLR integrated contribution. Tr=50 years. Coastal *comarcas* in light grey, coastal municipalities in dark grey.

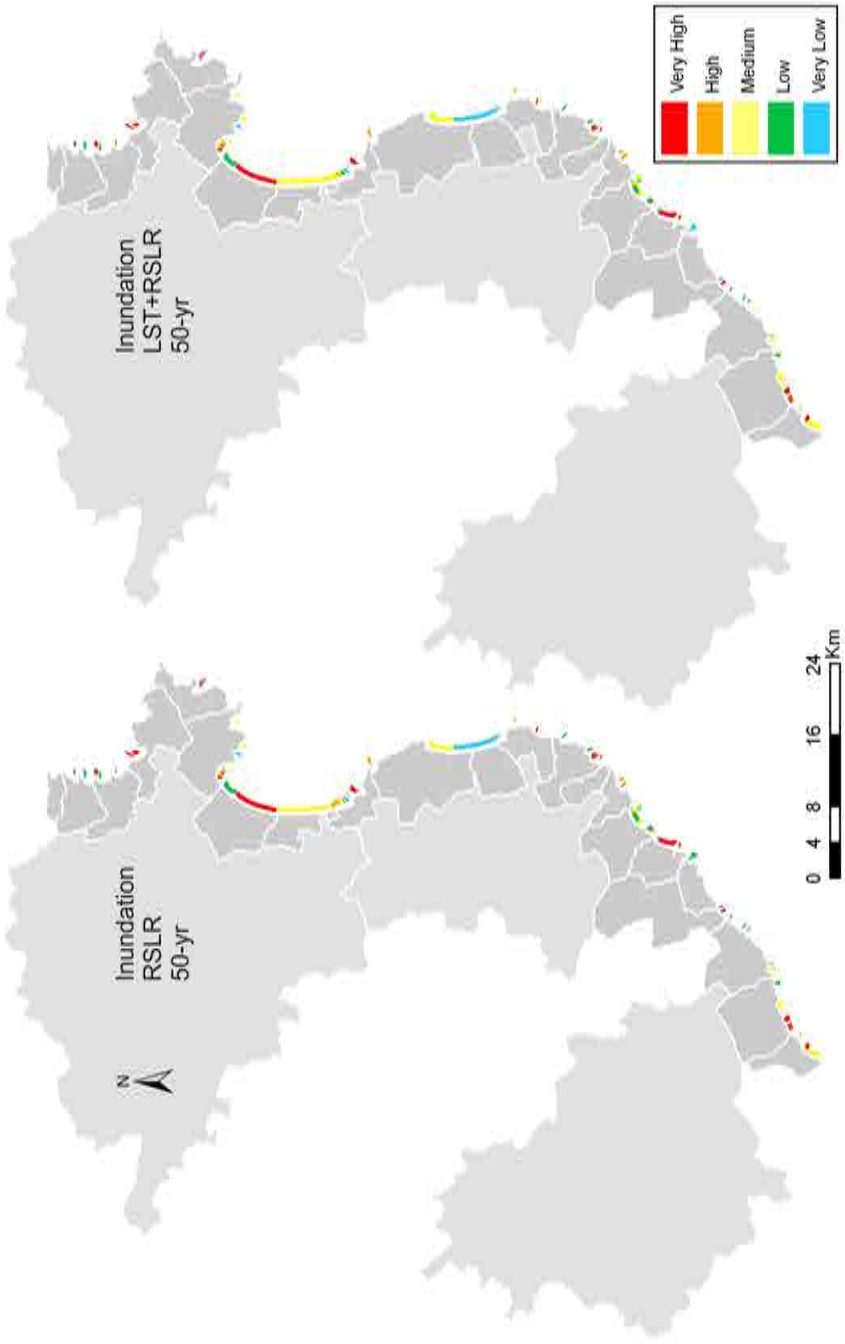

Figure A.7: Maps of vulnerability to storm-induced inundation of Girona province for the 50-year projection with respect to the baseline (2010). Top: RSLR contribution. Bottom: LST and RSLR integrated contribution. Tr=50 years. Coastal *comarcas* in light grey, coastal municipalities in dark grey.

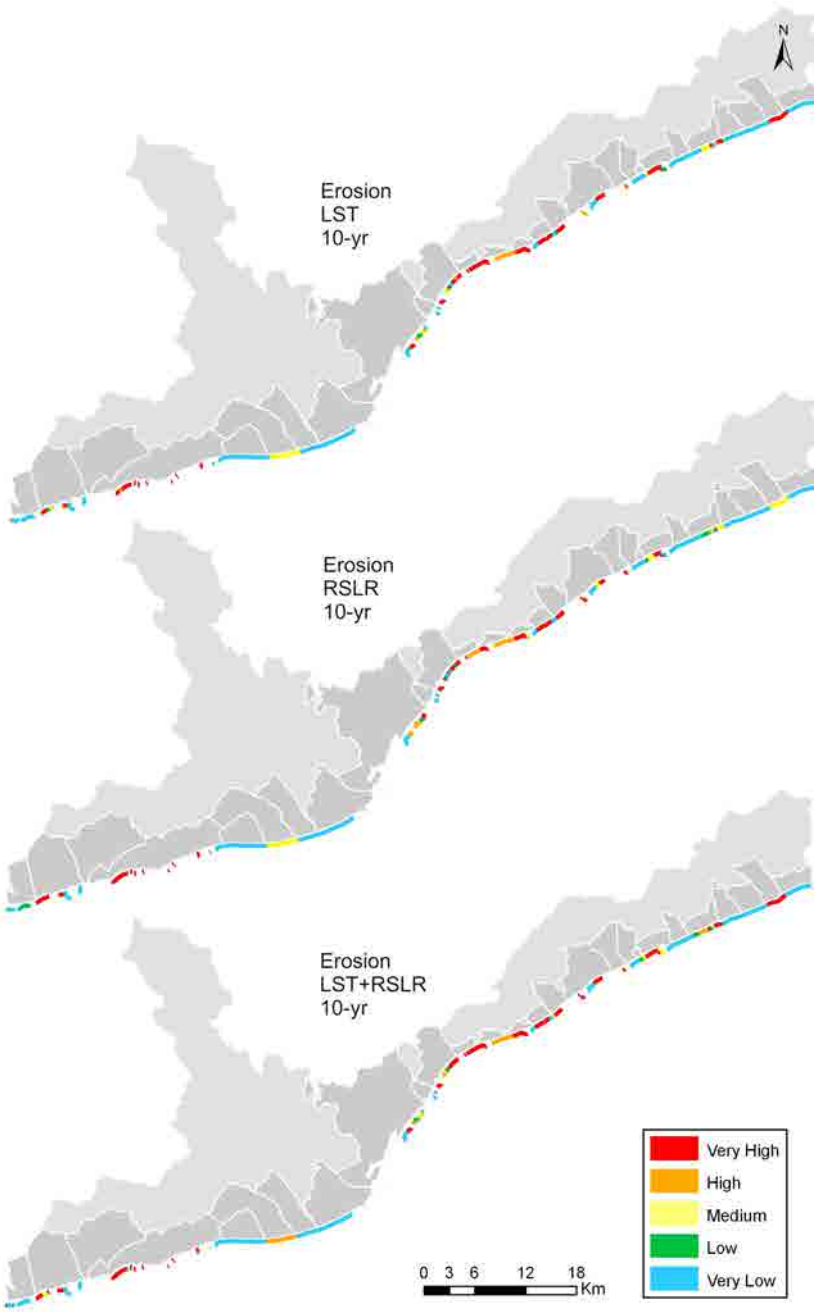

Figure A.8: Maps of vulnerability to storm-induced erosion of Barcelona province for the 10-year projection with respect to the baseline (2010). Top: LST contribution. Middle: RSLR contribution. Bottom: LST and RSLR integrated contribution. Tr=50 years. Coastal *comarcas* in light grey, coastal municipalities in dark grey.

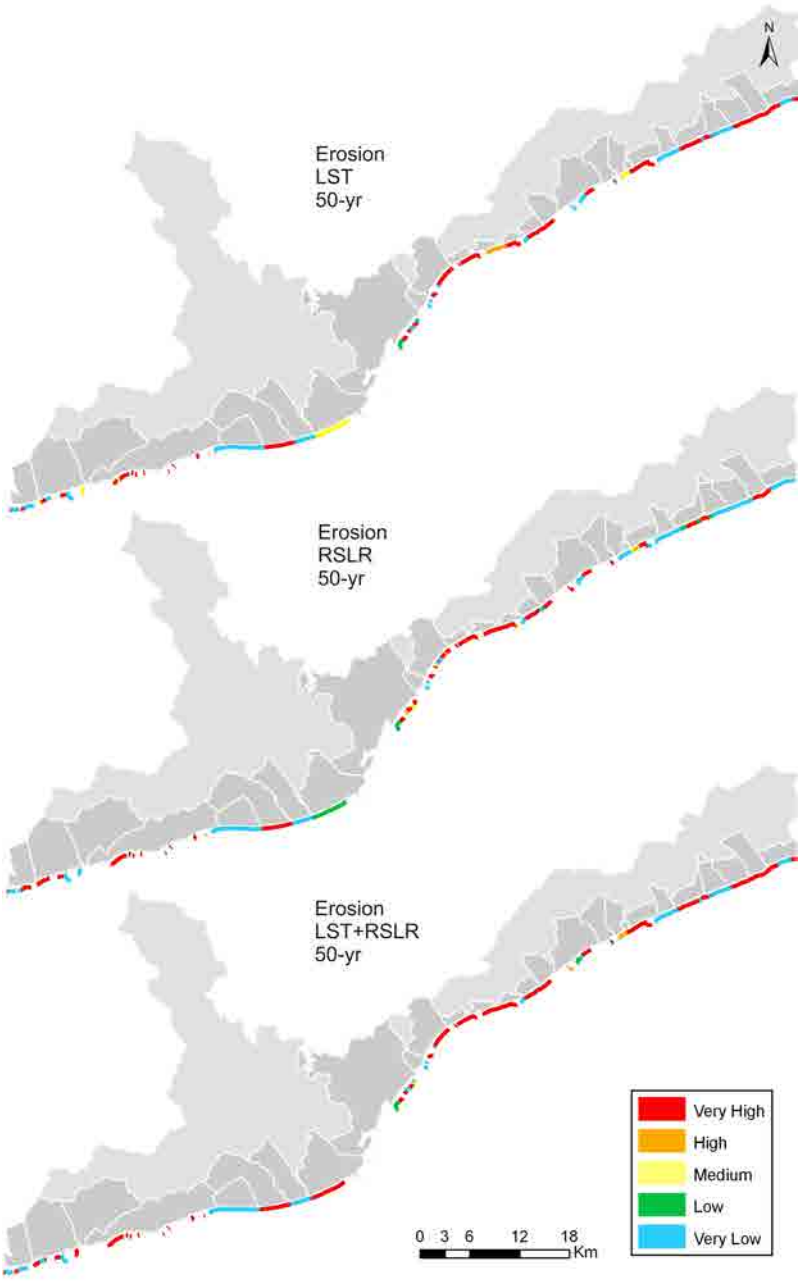

Figure A.9: Maps of vulnerability to storm-induced erosion of Barcelona province for the 50-year projection with respect to the baseline (2010). Top: LST contribution. Middle: RSLR contribution. Bottom: LST and RSLR integrated contribution. Tr=50 years. Coastal *comarcas* in light grey, coastal municipalities in dark grey.

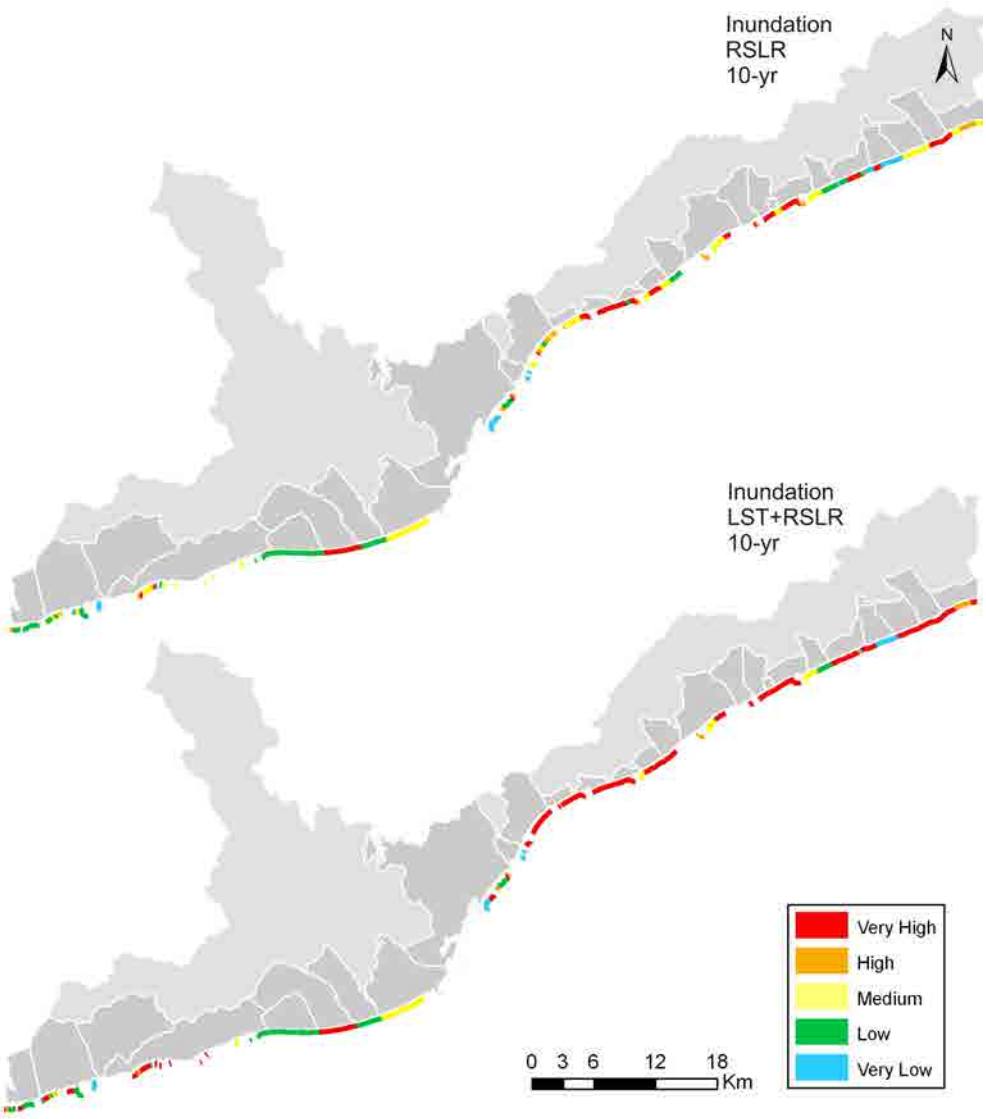

Figure A.10: Maps of vulnerability to storm-induced inundation of Barcelona province for the 10-year projection with respect to the baseline (2010). Top: RSLR contribution. Bottom: LST and RSLR integrated contribution. Tr=50 years. Coastal *comarcas* in light grey, coastal municipalities in dark grey.

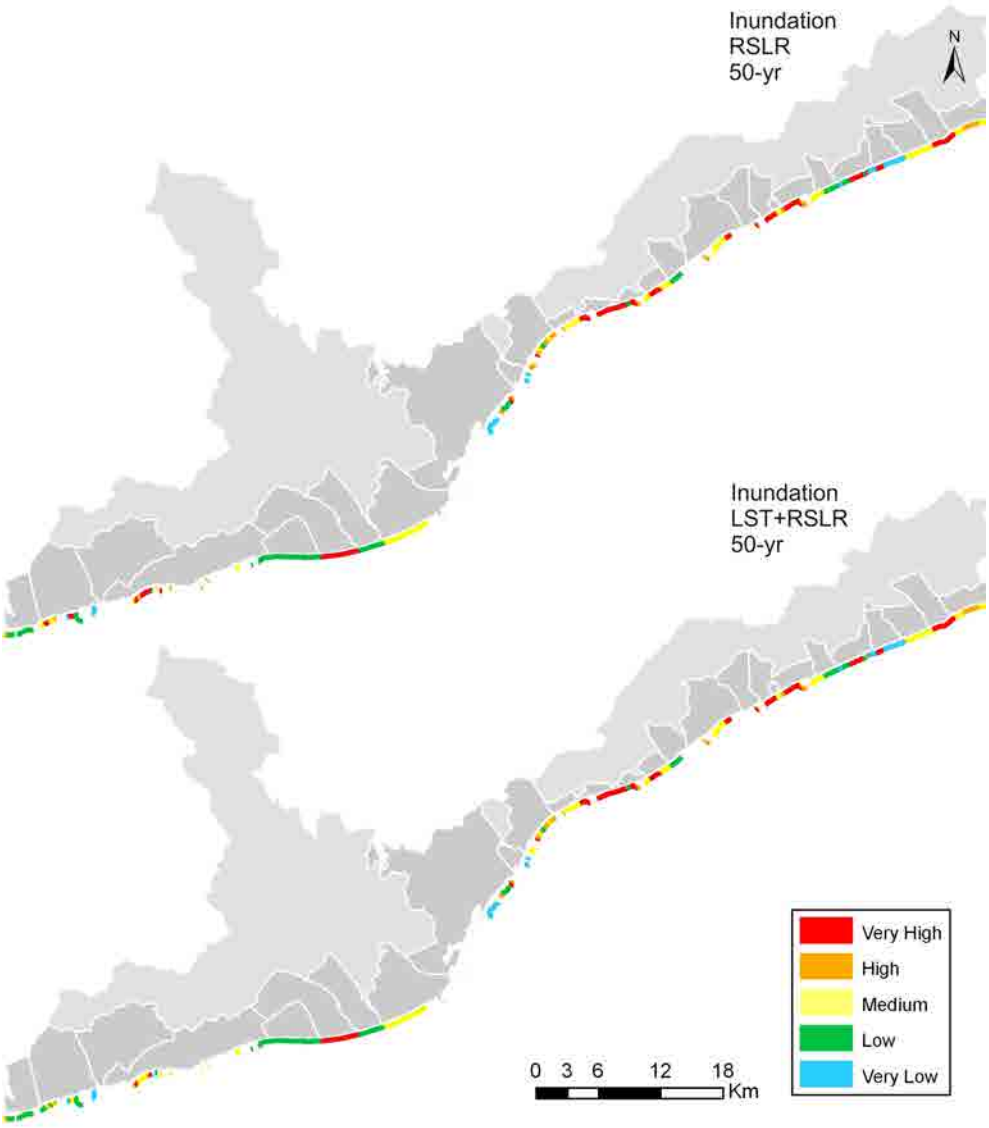

Figure A.11: Maps of vulnerability to storm-induced inundation of Barcelona province for the 50-year projection with respect to the baseline (2010). Top: RSLR contribution. Bottom: LST and RSLR integrated contribution. Tr=50 years. Coastal *comarcas* in light grey, coastal municipalities in dark grey.

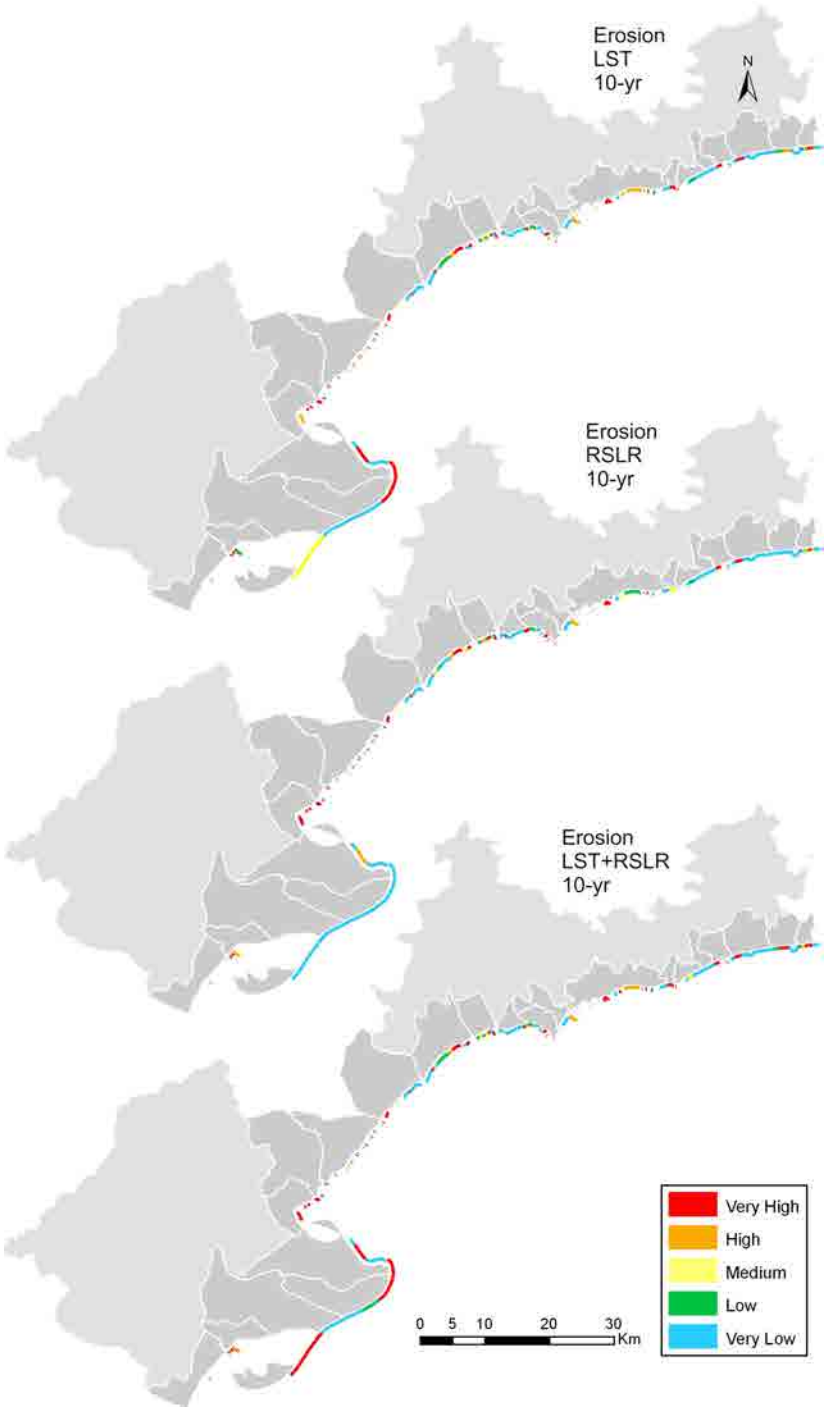

Figure A.12: Maps of vulnerability to storm-induced erosion of Tarragona province for the 10-year projection with respect to the baseline (2010). Top: LST contribution. Middle: RSLR contribution. Bottom: LST and RSLR integrated contribution. Tr=50 years. Coastal *comarcas* in light grey, coastal municipalities in dark grey.

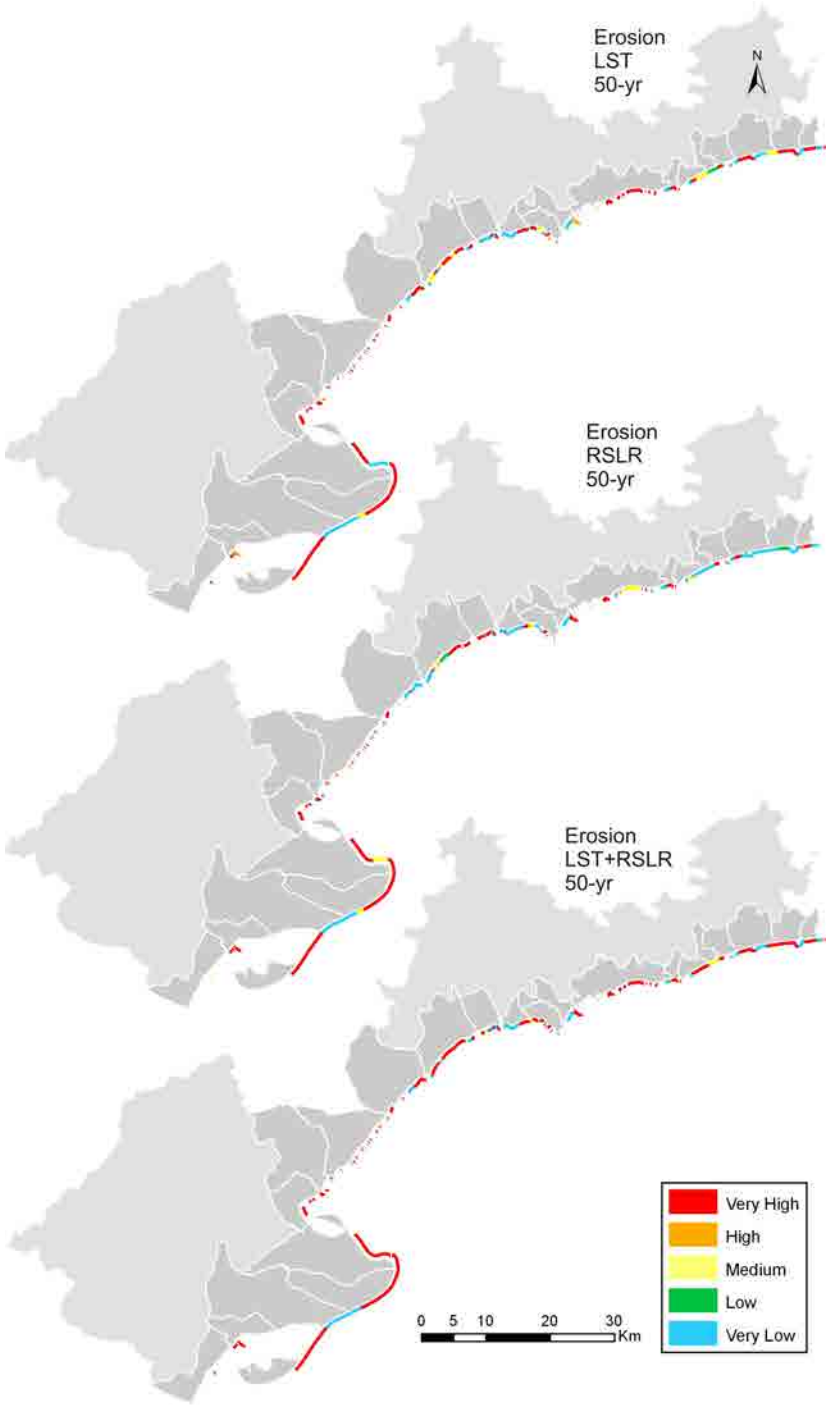

Figure A.13: Maps of vulnerability to storm-induced erosion of Tarragona province for the 50-year projection with respect to the baseline (2010). Top: LST contribution. Middle: RSLR contribution. Bottom: LST and RSLR integrated contribution. Tr=50 years. Coastal *comarcas* in light grey, coastal municipalities in dark grey.

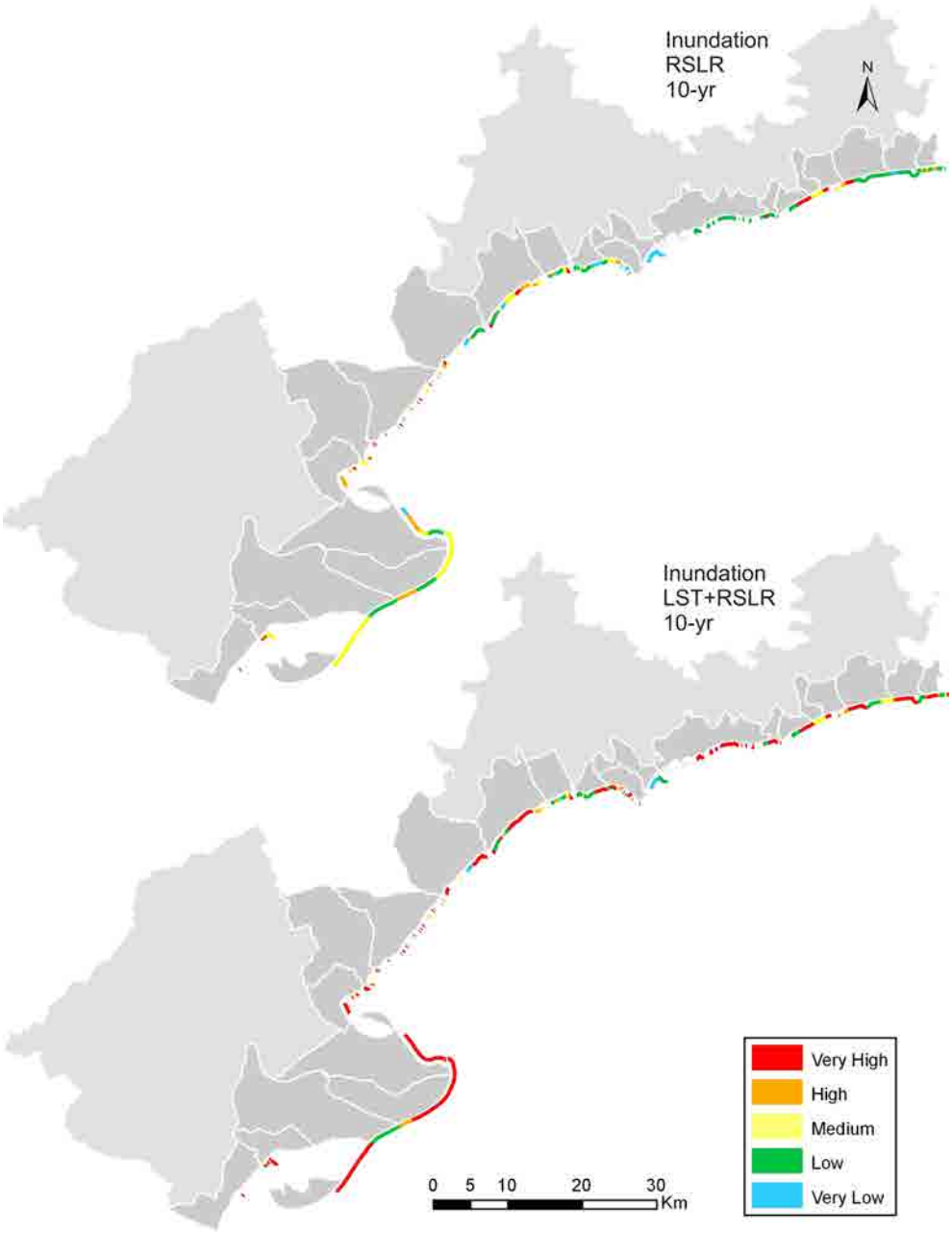

Figure A.14: Maps of vulnerability to storm-induced inundation of Tarragona province for the 10-year projection with respect to the baseline (2010). Top: RSLR contribution. Bottom: LST and RSLR integrated contribution. Tr=50 years. Coastal *comarcas* in light grey, coastal municipalities in dark grey.

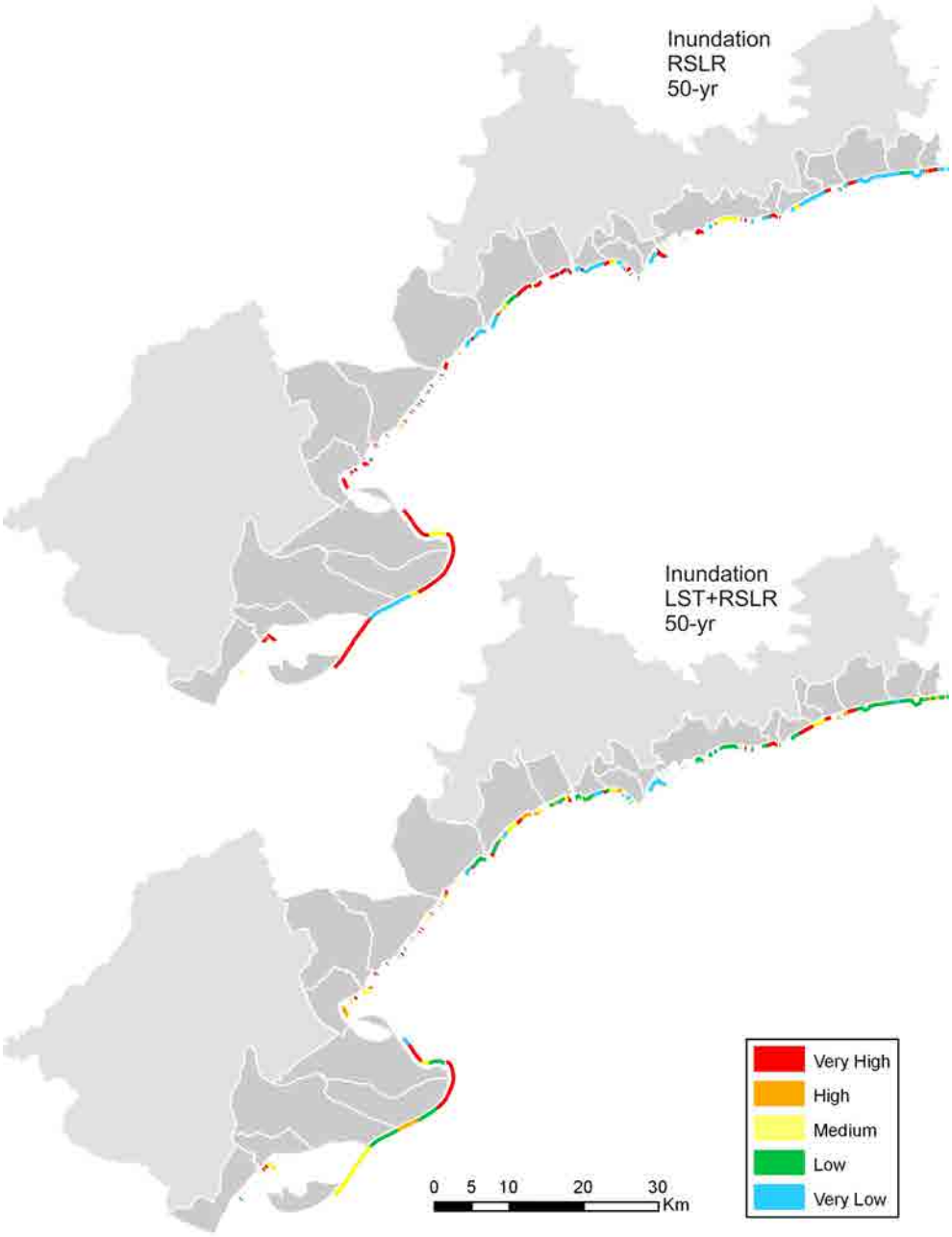

Figure A.15: Maps of vulnerability to storm-induced inundation of Tarragona province for the 50-year projection with respect to the baseline (2010). Top: RSLR contribution. Bottom: LST and RSLR integrated contribution. Tr=50 years. Coastal *comarcas* in light grey, coastal municipalities in dark grey.

Appendix B: GOW calibration

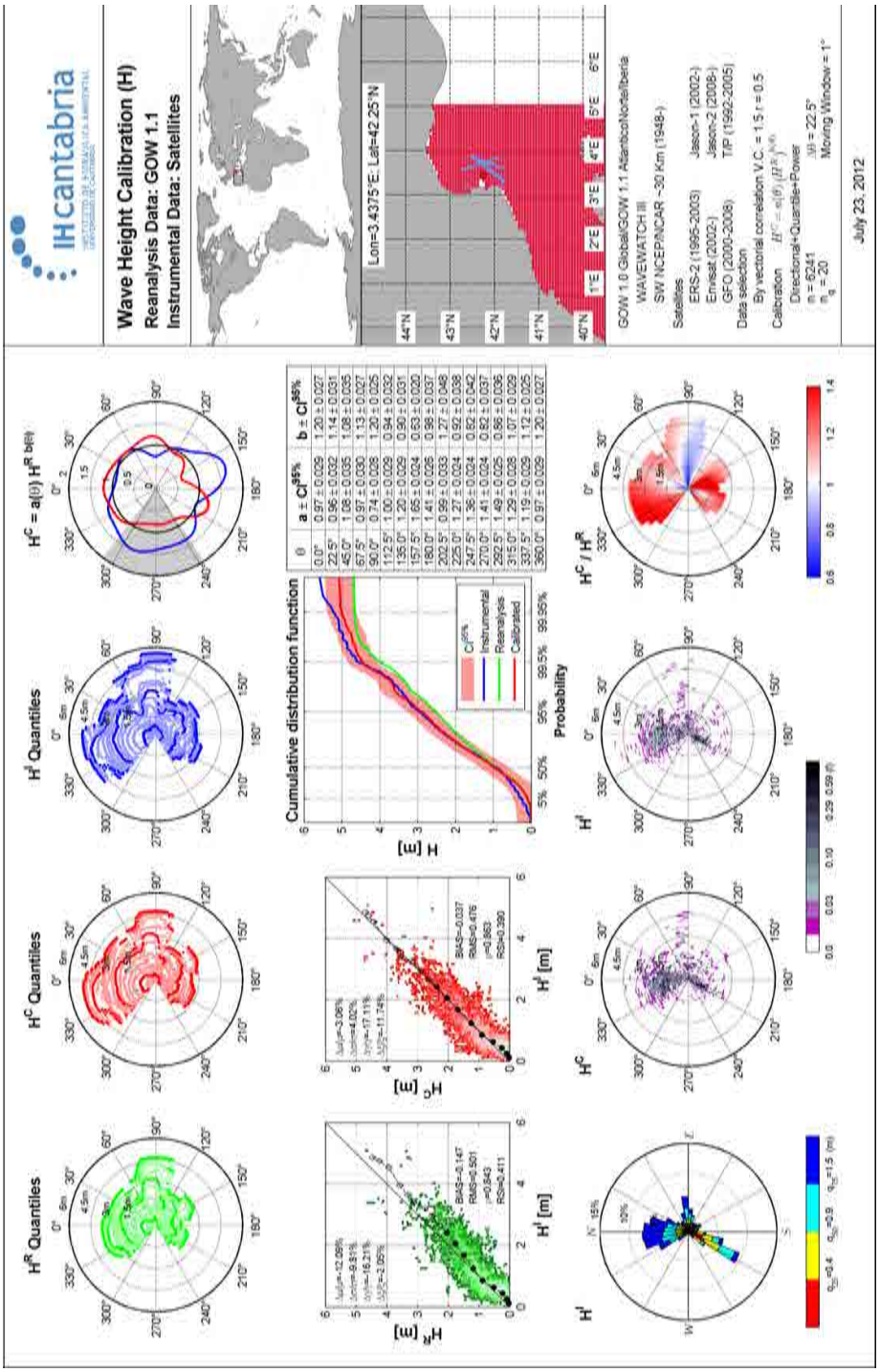

Figure B.1: Brief summary of the calibration of GOW data using satellite altimetry data. Node: Roses/Sector I.

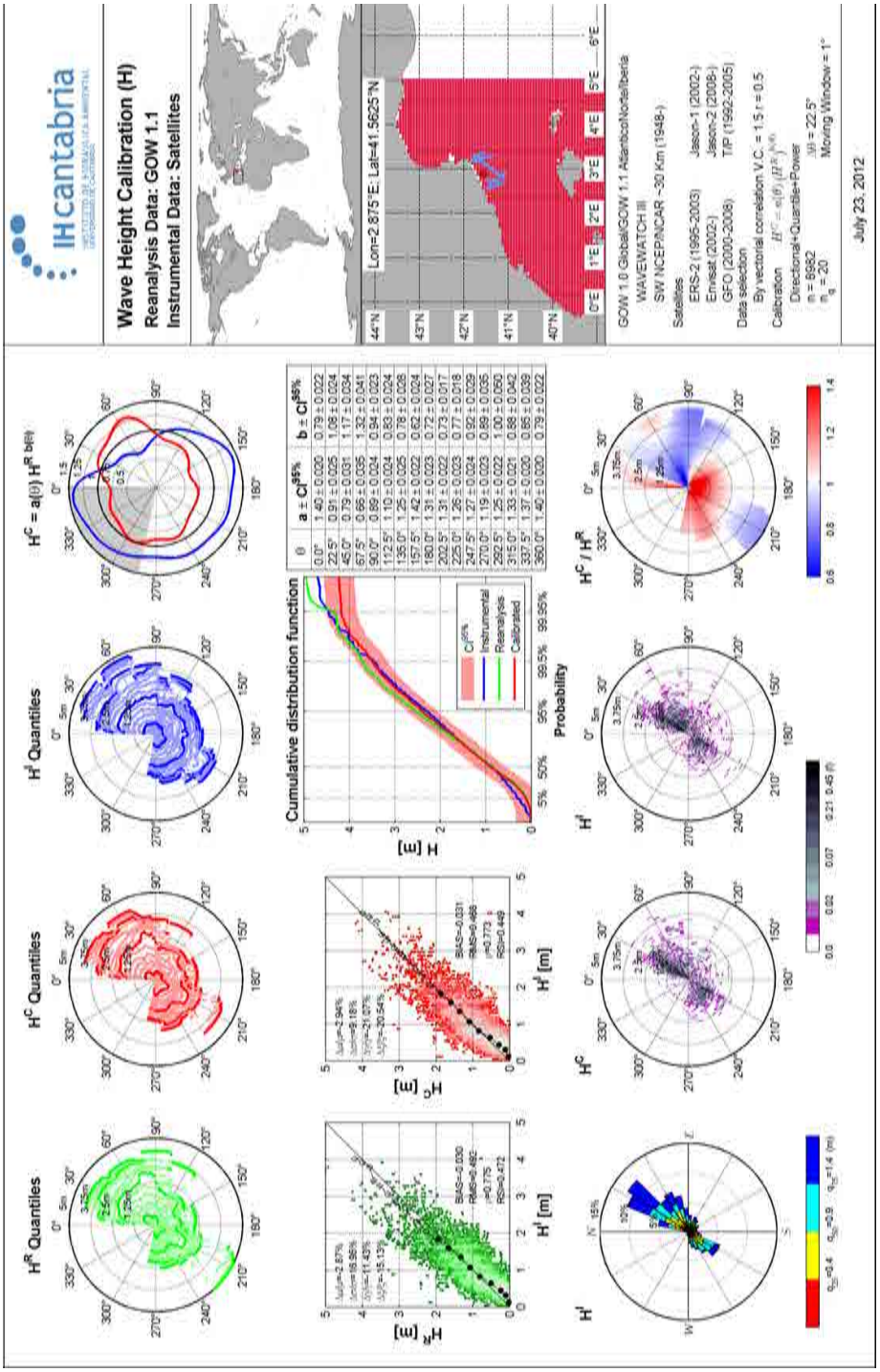

Figure B.2: Brief summary of the calibration of GOW data using satellite altimetry data. Node: Tordera/Sector III.

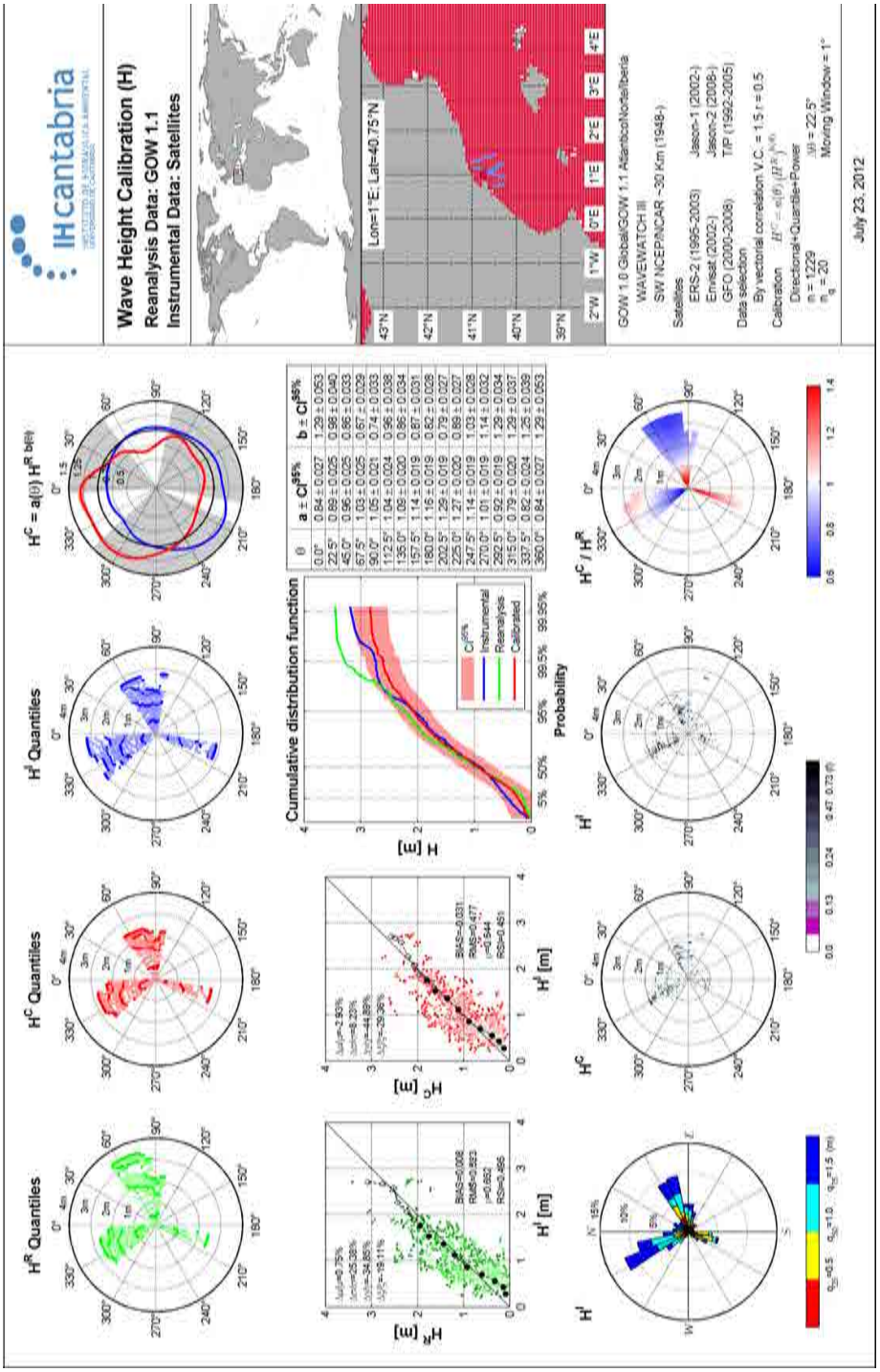

θ	a ± CI^95%	b ± CI^95%
0.0°	0.84 ± 0.027	1.29 ± 0.053
22.5°	0.89 ± 0.025	0.98 ± 0.040
45.0°	0.96 ± 0.025	0.86 ± 0.033
67.5°	1.03 ± 0.025	0.67 ± 0.029
90.0°	1.05 ± 0.021	0.74 ± 0.033
112.5°	1.04 ± 0.024	0.96 ± 0.038
135.0°	1.09 ± 0.020	0.86 ± 0.034
157.5°	1.14 ± 0.019	0.87 ± 0.031
180.0°	1.16 ± 0.019	0.82 ± 0.028
202.5°	1.29 ± 0.019	0.79 ± 0.027
225.0°	1.27 ± 0.020	0.89 ± 0.027
247.5°	1.14 ± 0.019	1.03 ± 0.028
270.0°	1.01 ± 0.019	1.14 ± 0.032
292.5°	0.92 ± 0.019	1.29 ± 0.034
315.0°	0.79 ± 0.020	1.29 ± 0.037
337.5°	0.82 ± 0.024	1.25 ± 0.039
360.0°	0.84 ± 0.027	1.29 ± 0.053

Figure B.3: Brief summary of the calibration of GOW data using satellite altimetry data. Node: Ebre/Sector VI.

Appendix C: Scientific contributions

Participation in seminars and congresses

- **Bosom, E. and Jiménez, J.A. (2009):** Spatial and temporal variations in storm related coastal hazards in the Catalan coast. Proceedings of the 4th International Short Conference on Applied Coastal Research (SCACR), Barcelona, June 2009, 219-229. *Oral presentation (speaker) and proceedings contribution.*

- **Bosom, E. and Jiménez, J.A. (2009):** A robust methodology for regional-scale analysis of storm-induced coastal hazards. 11th Plinius Conference on Mediterranean Storms, Barcelona, September 2009. *Oral presentation (speaker).*

- **Bosom, E. (2009):** Análisis de procesos costeros inducidos por temporales a escala regional. Seminario de Geología, Morfodinámica y Gestión Costera. Investigaciones actuales y futuras. Instituto de Ciencias del Mar, CMIMA, CSIC, Barcelona, October 2009. *Oral presentation (speaker).*

- **Bosom, E. and Jiménez, J.A. (2010):** Storm-induced coastal hazard assessment at regional scale: Application to Catalonia (NW Mediterranean). Adv. Geosci., 26, 8387, 2010 (special publication as proceedings of the 11th Plinius Conference on Mediterranean Storms, Barcelona, September 2009). *Proceedings contribution.*

- **Bosom, E. and Jiménez, J.A. (2010):** Coastal storms hazard and vulnerability assessments at a regional scale. A tool for ICZM. International Conference on Coastal Conservation and Management in the Atlantic and Mediterranean, Estoril, April 2010. *Oral presentation (speaker).* .

- **Bosom, E. and Jiménez, J.A. (2011):** Coastal Vulnerability Assessment to Storm Impacts. Application to the Catalan Coast. Jornadas sobre nuevas tecnologías aplicadas al estudio de riesgos naturales en la costa. Investigaciones actuales y perspectivas, Santander, August 2011. *Poster contribution.*

- **Bosom, E. y Jiménez, J.A. (2011):** Evaluación probabilística de la vulnerabilidad costera al impacto de temporales. Aplicación al litoral Catalán. Libro de ponencias de las XI Jornadas Españolas de Costas y Puertos, Las Palmas de Gran Canaria, Spain, May 2011, 176-185. *Oral presentation (speaker) and proceedings contribution.*

- **Bosom, E. and Jiménez, J.A. (2013):** Metodología para la evaluación de la vulnerabilidad costera al impacto de temporales. Aplicación al litoral Catalán. 5º taller de trabajo de la Red Temática de Colaboración: Ingeniería Aplicada

al Diagnóstico de Riesgos Hidrometeorológicos, Fluviales y Costeros, Tampico, Mexico, June 2013. *Oral presentation (speaker).*

- **Bosom, E., Jiménez, J.A. and Nicholls, R.J. (2014):** RSLR-induced increase of vulnerability to storms along the Catalan coast (NW Mediterranean). European Geosciences Union General Assembly 2014, Vienna, Austria, April May 2014. *Oral presentation (speaker).*

- **Jiménez, J.A., Valdemoro, H.I., Solé, F., Mendoza, E. T., Gracia, V., Bosom, E. and Sánchez-Arcilla, A. (2009):** Evaluación de la vulnerabilidad costera a diferentes procesos. Una aproximación multiescalar. X Jornadas Españolas de Costas y Puertos, Santander, May 2009. *Oral presentation*

- **Jiménez, J.A., Sancho, A., Bosom, E., Valdemoro, H.I., Guillén, J. and Galofré, J. (2010):** Validation of vulnerability assessment to storms at the Catalan coast (NW Mediterranean) during the last 50 years. 32nd Coastal Engineering Conference, ASCE, Shanghai, China, June-July 2010. *Oral presentation.*

- **Jiménez, J.A., Valdemoro, H.I., Bosom, E. and Gracia, V. (2011):** Storm-induced coastal hazards in the Ebro delta (NW Mediterranean). Proceedings of the Coastal Sediments 2011, World Scientific Press, Miami, USA, 1332-1345. *Oral presentation and proceedings contribution.*

- **Jiménez, J.A., Bosom, E. and Valdemoro, H.I. (2013):** Coastal vulnerability to storm impacts at different time scales. Encuentro Internacional de Manejo del Riesgo por Inundaciones. Instituto de Ingeniería (UNAM), México DF, January 2013. *Oral presentation*

Contributions to scientific journals and books

- **Bosom, E. and Jiménez, J.A. (2011):** Probabilistic Coastal vulnerability assessment to storms at regional scale - application to Catalan beaches (NW Mediterranean). Natural Hazards and Earth System Sciences, 11, 475484.

- **Bosom, E., Jiménez, J.A. and Nicholls, R.J. (2014):** RSLR-induced increase of vulnerability to storms along the Catalan coast (NW Mediterranean) (in preparation).

- **Jiménez, J.A., Ciavola, P., Balouin, Y., Armaroli, C., Bosom, E. and Gervais, M. (2009):** Geomorphic coastal vulnerability to storms in microtidal fetch-limited environments: application to NW Mediterranean & N Adriatic Seas. Journal of Coastal Research, SI 56 1641-1645.
- **Jiménez, J. A. and Bosom, E. (2009):** Section 12: Spain-Catalan Coast (pp 94-106). In: MICORE Review of Climate Change Impacts on Store Occurrence (Deliverable 1.4). Edited by Ferreira, O., Vousdoukas, M. and Ciavola, P. Developed within the Workpackage 1 of the MICORE European project.
- **Jiménez, J.A., Sancho, A., Bosom, E., Valdemoro, H.I., Guillén, J. and Galofré, J. (2012):** Storm-induced damages along the Catalan coast (NW Mediterranean) during the period 1958-2008. Geomorphology, 143-144, 2433.
- **Jiménez, J.A., Ballesteros, C., Valdemoro, H.I., Bosom, E., Oltra, A., Nicholls, R.J. and Sánchez-Arcilla, A. (2014)** Impact of high-end scenarios of SLR on a Mediterranean hotspot: the Catalan coast. Regional Environmental Change (in preparation).

International research stays

- **US Geological Survey St. Petersburg Science Center**
  Florida, EEUU
  Period: From September 2nd to December 3rd, 2010
  Host researcher: Dr. Asbury H. Sallenger, director of the Hurricane and Extreme Storm Impact Group.
  Objective: To improve, develop and apply techniques to evaluate coastal vulnerability to extreme storms in sedimentary coasts.

- **School of Civil Engineering and the Environment**
  University of Southampton, United Kingdom
  Period: From January 9th to April 13th, 2012
  Host researcher: Professor Robert J. Nicholls
  Objective: To become familiar with the techniques to evaluate vulnerability at large scale, the selection of climatic scenarios and the downscaling techniques at regional scale.